Vascular and Immune Changes Underlying the Detrimental Short-Term Effects of High-Fat, High-Calorie, Diets

Devin Kenneth Clarke

School of Psychology

University of Sussex

Submitted for the degree of

Doctor of Philosophy

September 2019

Declaration

I hereby declare that this thesis has not been and will not be submitted in whole or in part to another University for the award of any other degree.

Signature:

Devin Kenneth Clarke

UNIVERSITY OF SUSSEX

DEVIN KENNETH CLARKE

Submitted for the degree of

DOCTOR OF PHILOSOPHY

VASCULAR AND IMMUNE CHANGES UNDERLYING THE DETRIMENTAL SHORT-TERM EFFECTS OF HIGH-FAT, HIGH-CALORIE, DIETS

SUMMARY

Evidence suggests that diets high in fat and calories (HFD) can induce detrimental hippocampal-specific behavioural effects starting after as little as 24 hours on the diet. Such a rapid and region-specific cognitive impact is unexpected given the brain is largely insulated from rapid peripheral changes by the blood-brain barrier (BBB). Understanding why this occurs will not only add valuable insight into how influential diets are on our brains, but could also help explain why the hippocampus appears to be one of the regions most sensitive to damage in a myriad of disease states, most prominently in Alzheimer's Disease.

To investigate this I compared mice fed a HFD to those fed a control diet at numerous timepoints, and looked for changes in animal behaviour, microglial and immune responses in the brain, and changes in the brain's blood supply. The techniques used to do this included behavioural tests, tissue immunostaining, antibody arrays, cranial window implantations, and confocal and two photon microscopy. I compared the measures between timepoints, diets, and brain regions - the hippocampus, cortex, and hypothalamus - to identify which of these measures appeared to change in a hippocampal-specific manner.

Results showed that HFD feeding disrupts the relationship between increased neural efficiency and cognitive performance in the hippocampus, with this perhaps driving early hippocampus-specific impairment. This disruption may be related to changes occurring in the vasculature, where HFD-induced capillary bed structural changes increase the resistance to blood flow. Short-term HFD feeding also led to an increased density of microglial cells. This, and the capillary bed changes, were not region-specific, and my results suggest that these were likely translated to hippocampus-specific cognitive deficits due to the impoverished relationship between vascular support and neuronal metabolism in the hippocampus.

Acknowledgements

First and foremost my thanks go to Catherine, my supervisor, for all the support, kind words, and inspiration you have provided over what have been some of the most challenging years of my life. At the start of this journey I didn't fully appreciate just how important having a supervisor who is not only a mentor and a leader, but also a friend (and fellow karaoke lover), would be. I couldn't have asked for a better guide.

I also feel privileged to have been part of the fantastic group of scientists that Catherine has assembled. It's special to find friends that are so supportive and inspirational, but also so much fun. I wouldn't trade my time in this lab for anything, and I know I am lucky to have had such great people around me. Katie, you never failed to make me laugh and are always willing to share interesting facts. Having your support an arm's length away in these final months have made them far easier to get through, and given me moments of laughter that I desperately needed. Orla, I will always cherish your enthusiasm, kindness, laughter, and our mutual love of a milky coffee. Though it was exhausting, lab-parenting project students with you is one of my favourite PhD memories. Kira, I'm so grateful to have had your guidance, whether that be for programming advice or what to make for dinner. I've thoroughly enjoyed having you by my side, chatting about football, grabbing treats from the co-op, or stealing a bowl from your assortment of crockery. Laura, since you joined the lab I've wondered how we ever managed without you. A significant part of this thesis wouldn't have been possible without the work you do, and Monday mornings are always brighter after hearing about your adorable feline companions. Finally, Dori, your arrival in the lab broadened our horizons and I'm so fortunate to know someone who I am always learning from, in more ways than one. Without you we wouldn't have the Sinterklaas tradition, or the fantastic poems to go with it. I'm proud to have been on the same programme as you. To all of you, thank you for making my time in the lab such a joy, and for joining the Hall lab in the first place, otherwise I would never have had the privilege of knowing you.

To those at Sussex Neuroscience, particularly those who founded and run the PhD programme without which I would not have these years to cherish, thank you. Not only for funding my

research, or giving me the chance to take part in international conferences and training opportunities, but also for allowing me to be part of such a great community. I still remember my interview fondly, and was so impressed by the people I met that day, an impression that has only grown over time. I would also like to thank the Ancillary Unit staff, without your support none of my project would have been possible. To Roger, formerly of the Centre for Advanced Microscopy, your guidance started me down this long, fluorescently-illuminated road, for which I am grateful.

To Ruth, you have been a fantastic help throughout my time at Sussex, from helping me settle in to looking after me once I did. For doing it all with such kindness, thank you. To Hans, my second supervisor, joint meetings with you and Catherine were always stimulating, and usually entertaining. Without you I wouldn't have had the basis for such a fascinating project to pursue. To Sarah, my assessor, I always enjoyed our annual review meetings, and the enthusiasm you had for my research and my future helped to revive me when I needed it.

To my rotation project supervisors, Jenny and Keith. Thank you for letting me work with you. Without the experience I had in both your labs, and the people I met, my PhD journey would never have been so enjoyable, or satisfying. I have taken my first steps in the world of scientific publishing thanks to you, Jenny, and Keith, without your help I wouldn't have earned the scholarship that allowed me to chance to do so. Thank you both.

I must also thank the first friends I ever made in Brighton. Rich, Sofia, Leonie, and Ana. When I consider how lucky I have been to have had such a fantastic supervisor, lab, and university to work in, it seems almost excessive that my programme contemporaries are so wonderful as well. I have such fond memories of our first year lunches together, adventures on weekend (and weekday) evenings, and trips to Amsterdam and Lisbon. You made starting a new life in a new place much more enjoyable than I dared hope. Rich, my fellow flapjack enthusiast, our chats on the bridge, in the sunshine, were highlights of this last year. Ana, you have been not only a great flatmate, but a fantastic friend. I'm very lucky to have met someone that I could share all the highs and lows of the last four years with, and I don't know how I would have managed without you in this final year especially. Thank you for reigniting my passion for Harry Potter, something I never would have guessed would be a part of the thesis writing experience.

Lastly, I have to thank my incredible parents, Graham and Gaelene. Thank you for all the opportunities you have given me through hard work and sacrifice. I would never have been able to complete this PhD without your unending love and support, and though I know I can never repay you, I can make the most of what you have given me. This achievement is as much mine as it is yours.

Contents

List of Tables

List of Figures

List of Abbreviations

Adora2a Adenosine Receptor 2A

AgRP Agouti-Related Peptide

ARC Arcuate Nucleus

ATP Adenosine Triphosphate

AUC Area Under the Curve

BBB Blood-Brain Barrier

BCA Bicinchoninic Acid

BDNF Brain-Derived Neurotrohpic Factor

BrdU Bromodeoxyuridine

CA1 Hippocampal Cornu Ammonis 1

CBF Cerebral Blood Flow

CCR2 Chemokine Receptor Type 2

$CMRO_2$ Cerebral Metabolic Rate of Oxygen Consumption

CMS Compound Motility Score

CNS Central Nervous System

COX-1 Cyclooxygenase 1

CPA $CMRO_2$ Peak Aligned

CVO Circumventricular Organ

Cx3CR1 C-X3-C Motif Chemokine Receptor 1

EI Extension Index

FITC Fluorescein Isothiocyanate

GFP Green Fluorescent Protein

GLUT1 Glucose Transporter 1

HbO Oxygenated Haemoglobin

HbR Deoxygenated Haemoglobin

HbT Total Haemoglobin

HFD High Fat Diet

i.p. Intraperitoneal

IgG Immunoglobulin G

II Instability Index

IKBKB Inhibitor of Nuclear Factor Kappa B Kinase Subunit Beta

IKBKE Inhibitor of Nuclear Factor Kappa B Kinase Subunit Epsilon

IL-1 Interleukin 1

IL-1β Interleukin 1 Beta

IL-6 Interleukin 6

ISD Inter-Soma Distance

LMM Linear Mixed Model

LPS Lipopolysaccharide

LTP Long-Term Potentiation

m Minimum Value

MI Motility Index

NaF Sodium Fluorescein

NFκB Nuclear Factor Kappa-Light-Chain-Enhancer of Activated B Cells

NG2 Neuron-Glial Antigen 2

NI Novelty Index

NOCR Novel Object-Context Recognition

NPY Neuropeptide Y

NRF2 Nuclear Factor Erythroid 2-Related Factor 2

p Peak Value

PBS Phosphate Buffered Saline

PC1 First Principal Component

PCA Principle Component Analysis

PFA Paraformaldehyde

POMC Pro-Opiomelanocortin

PUFA Polyunsaturated Fatty Acid

RI Retraction Index

ROC Receiver Operating Characteristic

ROI Region of Interest

ROS Reactive Oxygen Species

SFA Saturated Fatty Acid

SI Stability Index

SO_2 Oxygen Saturation

SOCS3 Suppressor of Cytokine Signalling 3

t2m Time to Minimum Value

t2o Time to Onset

t2p Time to Peak Value

t2r Time to Offset

TCA Target Cell Area

TLR4 Toll-like Recetor 4

TNF-α Tumour Necrosis Factor Alpha

TrkB Tropomyosin Receptor Kinase B

V1 Primary Visual Cortex

VEGF Vascular Endothelial Growth Factor

ZO-1 Zonula Occludens-1

Chapter 1

Introduction

Modern life in many countries is linked to low levels of physical activity, and when coupled with the easy availability of energy dense, cheap, palatable foods, can lead to an energy imbalance. This isn't exclusively down to poor dietary choices, as these foods can alter the brain in ways that affect not only decision making processes but also energy homeostasis mechanisms, promoting the further intake of calories in a positive feedback cycle. Such a relationship can promote the development of obesity, which is a major risk factor for a host of diseases (type 2 diabetes, coronary heart disease, depression, dementia, cancer, and all causes of death; Pi-Sunyer et al. 1998; Bhaskaran et al. 2014; Xu et al. 2011; Luppino et al. 2010) and is on the rise. In the United Kingdom, over 50% of the population is projected to be obese by 2050 (compared to 23% in 2004) with the cost to the National Health Service of treating obesity and its consequences in the same year predicted to rise to £6.5 billion from £1 billion in 2007. Over the same period the wider cost to society is expected to grow from £15.8 billion to £49.9 billion (Butland et al., 2007). Obesity is also linked to cognitive impairment that long precedes dementia onset. Higher body mass index values are associated with deficits in memory and executive functioning in otherwise healthy young adults, and being obese at any two of early adulthood, early midlife, and late midlife stages, is associated with impaired memory and executive function after adjusting for age and education (obesity and cognitive impairment reviewed in Miller and Spencer 2014). These deficits could be linked to obesity associated changes in the brain's vasculature or the promotion of neuroinflammation.

Obesity is a risk factor for cardiovascular and microvascular disease and is linked to endothelial dysfunction and the development of atherosclerosis. The microcirculation is critical in nutrient exchange and oxygen supply, and obesity-associated microvascular dysfunction likely contributes to the development of microvascular dementia. In the brain, changes in the microvasculature could impair neurovascular coupling - the link between neuronal activity and blood supply

- and thus lead to vascular cognitive impairment. Given that in the brain there is no perivascular adipose tissue, obesity induced vascular changes are likely to result from changes in neuronal/glial metabolic activity, haemodynamic changes, or from the influence of circulating factors (obesity and the microcirculation reviewed in Sorop et al. 2017). With regards to inflammation, this has been described as 'metainflammation' in obesity owing to its tonic, low-grade, multi-organ nature. Inflammation occurs in the pancreatic islets, adipose tissue, liver, skeletal muscle, and the brain, in the obese state (Lumeng and Saltiel, 2011). Neuroinflammation has been linked to the development of obesity following a switch to a diet high in saturated fat and calories (HFD) in rodents (Valdearcos et al., 2017) and has been implicated in obesity and HFD-associated cognitive impairment (Miller and Spencer, 2014)

Animal models of diet-induced obesity are typically associated with HFD feeding, where switching rodents to diets where either 45% or 60% of the total calories are derived from fat promotes the development of obesity, which typically occurs faster on 60% diets. This is in comparison to normal rodent diets that are roughly 10% fat. The composition of the diets used in HFD studies sometimes varies quite significantly, with sucrose content and the profile of fatty acids differing (the use of HFDs in the study of obesity discussed in Speakman 2019). Generally however rodent HFDs are enriched in saturated fatty acids (SFAs) and these diets show surprisingly rapid effects on the brain, with cognitive impairment appearing after only 24 hours (McLean et al., 2018) and hypothalamic inflammation being detected at the same timepoint (Thaler et al., 2012). The fact that these changes occur so rapidly in spite of the fact that the brain is largely protected from changes in the periphery and circulation by the blood-brain barrier (BBB) is particularly interesting. It is important to note that a typical obesogenic diet in humans consists not only of high levels of dietary fat, but also refined carbohydrates and sugars. Though the use of a HFD, rather than a high fat and sugar, or high sugar, diet, is more common in rodent research, evidence suggests that all three are capable of inducing cognitive impairments (Abbott et al., 2019).

The rapid central effects of HFD feeding in rodents suggests that dietary components themselves may have direct effects on the brain. This certainly seems to be the case in the hypothalamus, a brain region with an integral role in energy homeostasis, where SFAs are shuttled after consumption and drive microglial activation (Valdearcos et al., 2014). In doing so, SFA feeding drives increased food intake in a microglia-mediated manner (Valdearcos et al., 2017). SFAs likely enter the hypothalamus through the median eminence, a circumventricular organ (CVO) that allows the sampling of blood content (Rodríguez et al., 2010). CVOs consist of fenestrated capillaries that have fewer tight junctions between endothelial cells and are therefore more permeable (Bennett et al. 2009 in Haddad-Tóvolli et al. 2017). Here SFA activation of microglia is

likely via toll-like receptor 4 signalling (TLR4; Milanski et al. 2009), and this promotes not only inflammation but also microglia-dependent neuronal injury (Valdearcos et al., 2014). Short-term HFD feeding is associated with a number of hypothalamic changes that tip the balance in favour of energy intake, where 48-hours of HFD exposure increases the firing rate of hypothalamic orexigenic (appetite stimulating) agouti-related peptide / neuropeptide Y (AgRP/NPY) neurons (Wei et al., 2015), and 24 hours of HFD leads to an increase in the mRNA levels of inflammatory markers such as the proinflammatory cytokines interleukin 6 (IL-6) and tumour necrosis factor alpha (TNF-α). After 3 days there are increases in the mRNA levels of SOCS3 (suppressor of cytokine signalling 3), which regulates cytokine signalling, and components of the NFκB (nuclear factor kappa-light-chain-enhancer of activated B cells) pathway IKBKB and IKBKE (inhibitor of nuclear factor kappa B kinase subunits beta and epsilon; Thaler et al. 2012). The upregulation of SOCS3 and IKBKB/IKBKE promotes leptin and insulin signalling resistance, blunting the central response to satiety signalling from the gut, a key component of diet induced obesity (reviewed in Velloso and Schwartz 2011).

Dietary components likely also play a role in non-hypothalamic routes of obesogenesis. As reviewed in Berthoud et al. (2011) obesity is associated with changes in both energy homeostasis and reward functions (i.e. 'liking' and 'wanting'). Whether addiction-like behaviour can be driven by repeated exposure to palatable food is still under debate, but evidence for sucrose-associated addiction-like behaviour exists. In rodent models, repeated access to sucrose leads to sucrose bingeing, cross-sensitization to amphetamine-induced locomotor activity, withdrawal symptoms - such as increased anxiety and depression (Avena et al., 2008) - and a reduced reinforcing efficacy of normal foods (Cottone et al., 2008). These changes are associated with an upregulation of dopamine release (Avena et al., 2008) and dopamine transporter expression (Bello et al., 2003), as well as changes in the availability of dopamine receptors D1 and D2 in the nucleus accumbens (Avena et al., 2008; Bello et al., 2002). Evidence for drug-addiction-like changes is weaker for non-sweet palatable foods that are typically high in fat, but intermittent corn oil access in rats can stimulate dopamine release in the nucleus accumbens (Liang et al., 2006).

Another brain region implicated in the development of obesity is the hippocampus. Much like the HFD-induced positive-feedback cycle that links hypothalamic energy homeostasis to food intake, evidence suggests that hippocampal deficits promote dysfunctional control of appetite and eating behaviour. It is suggested that diets disrupts the role of the hippocampus in determining when to start and end meals, promoting overeating, and furthering hippocampal disruption in a vicious cycle (Hargrave et al. 2016 in Yeomans 2017). Indeed, communication between the hippocampus and hypothalamus has been suggested to be important in the inhib-

ition of food intake (Sweeney and Yang, 2015). In humans medial temporal lobe damage impairs the use of interoceptive information regarding hunger and satiety, whilst in rats, temporary hippocampal inactivation leads to increased food intake and weight gain (reviewed in Davidson et al. 2019). Interestingly, HFD-induced cognitive deficits in rodents appear to be hippocampus-specific, at least with short-term feeding. McLean et al. (2018) report deficits on tasks that are hippocampus-specific over 2 weeks of dietary manipulation, whilst Kanoski and Davidson (2010) demonstrated hippocampus-specific cognitive deficits following 72 hours of feeding in rats, though cognitive impairment on hippocampus-independent tasks appeared after 30 days. In general rodents tested on hippocampus-specific behavioural tests, such as object-place-context (Langston and Wood, 2010) and object-place recognition, show impairments following HFD treatment (Valladolid-Acebes et al., 2013; Heyward et al., 2012), in contrast to other behavioural paradigms that involve more distributed neural networks or non-hippocampal learning where the effects of dietary treatment are far more inconsistent (reviewed in Cordner and Tamashiro 2015). In humans, though not looking at hippocampal-dependent memory, both five and seven days of a HFD impaired cognitive function in healthy subjects, suggesting that rapid dietary effects on cognition occur in humans as well. With regards to hippocampus-specific effects, subjects with a higher dietary fat and sugar intake were suggested to be impaired on hippocampal-dependent, but not frontal-dependent, cognitive tests. However to date it appears no studies exist in humans that have used short-term HFD interventions to assess hippocampus-dependent cognitive changes (effect of high fat and high sugar diets on cognition reviewed in Yeomans 2017).

The mechanisms driving early hippocampus-specific cognitive impairments resulting from a HFD are still unclear. In contrast to the strong evidence that the rapid dietary effects seen in the hypothalamus result from the postprandial influx of SFAs into the region (Valdearcos et al., 2014), the hippocampus lacks a close association with any CVO and is therefore more protected from changes in circulating factors (such as SFAs). Numerous alternative mechanisms have been proposed to mediate the early hippocampus-specific effects of diet reported, and these can be broadly categorised into vascular or inflammation related, where besides direct associations with HFD induced cognitive deficits (vascular changes; Tucsek et al. 2014b, hippocampal inflammation; Liu et al. 2014; Thirumangalakudi et al. 2008; Pistell et al. 2010), vascular and inflammatory changes are capable of mediating the other proposed mechanisms such as leptin and insulin resistance (McLean et al., 2018), oxidative stress, BBB impairment, changes in brain-derived neurotrophic factor (BDNF) levels (Cordner and Tamashiro, 2015), deficits in neurovascular coupling (Sorop et al., 2017), and pericyte dysfunction (Gomez-Smith et al., 2018). However, no studies have looked at region-specific changes across multiple proposed mechanisms at timepoints relevant

to the early hippocampal deficits, making it difficult to ascertain what exactly drives the rapid, hippocampus-specific, cognitive deficits associated with HFD feeding. My PhD aimed to address this by looking at changes in vascular and immune response in the brain following short-term HFD feeding across the hippocampus, cortex, and hypothalamus. The goals of this were to further our understanding of how HFDs drive obesity through their effects on the hippocampus, and to shed light on why the hippocampus appears to be particularly susceptible to various pathologies.

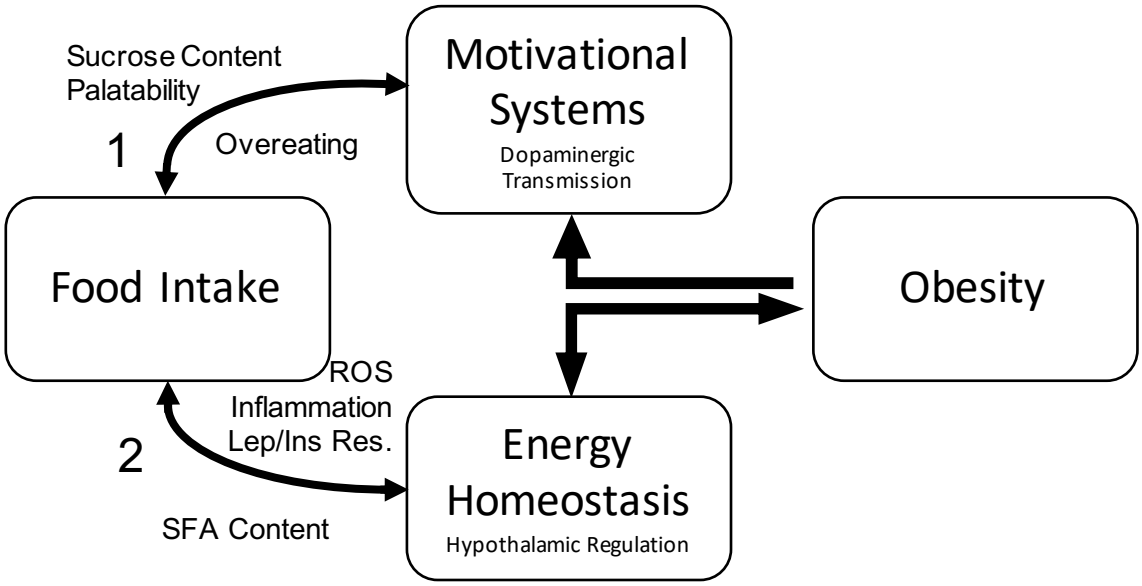

Figure 1.1: Metabolic and Motivational Regulation of Food Intake. The metabolic and motivational changes induced by the intake of high calorie, highly palatable foods, are regulated by hypothalamic homeostatic functions and dopaminergic neurotransmission respectively. **1.** Palatable foods can stimulate reward functions, and in doing so, promote excessive food intake. **2.** Similarly, dietary components such as saturated fatty acids (SFAs) can promote inflammation and leptin and insulin signalling resistance (Lep/Ins Res.), which along with oxidative stress (ROS; reactive oxygen species), can alter the mechanisms responsible for energy homeostasis driving a positive feedback cycle that promotes the development of obesity. The obese state also influences both metabolic and motivational processes. Figure adapted from Berthoud et al. (2011).

1.1 Inflammation-Related Mechanisms of HFD-Induced Cognitive Deficits

Obesity and HFD exposure are strongly associated with inflammatory responses. Inflammation is typically a coordinated response to harmful stimuli that is intended to return the system to baseline levels, and is part of the innate immune system. It is initiated by immune cells that are resident in the damaged tissue and recognise damage signals that are either associated with pathogens or injury to the host itself. In acute inflammatory responses the detection of these signals leads to

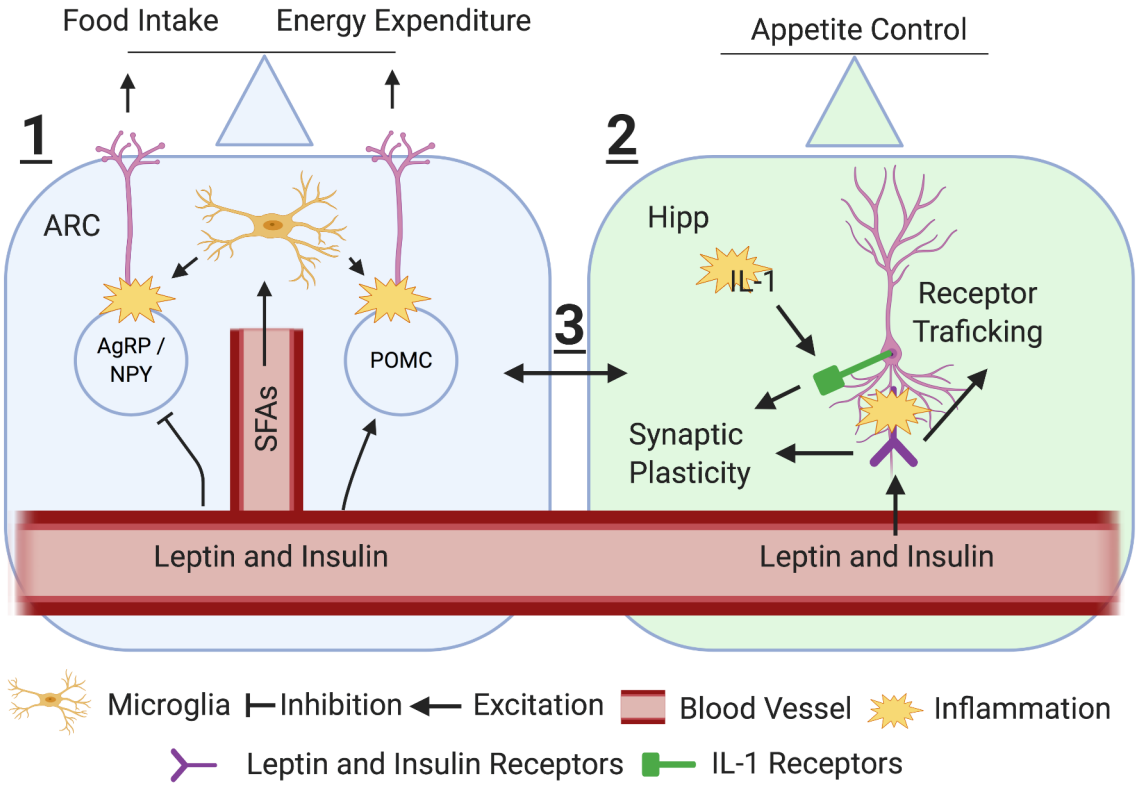

Figure 1.2: Hypothalamic and Hippocampal Regulation of Energy Homeostasis. 1. The balance of activity between AgRP/NPY and POMC neuronal populations in the hypothalamus contributes to the control of energy homeostasis, where increased activity in the former generally promotes food intake, whilst in the latter this promotes energy expenditure. Leptin and insulin can cross the BBB into the hypothalamus, where leptin inhibits and promotes AgRP/NPY and POMC activity respectively. HFD feeding promotes the entry of SFAs into the ARC, where they stimulate microglial activation and inflammation that can impair neuronal leptin and insulin signalling, tipping the energy homeostasis balance in favour of food intake. **2.** The hippocampus plays a role in the regulation of appetite control and the use of interoceptive satiety information. Here, leptin and insulin signalling modulate receptor trafficking and synaptic plasticity via neuronal receptors. HFD induced inflammation leads to resistance to leptin and insulin signalling, impairing these processes, and disrupts the physiological action of hippocampal IL-1, which under normal conditions promotes synaptic plasticity. **3.** Communication between the hippocampus and hypothalamus is important for the appropriate inhibition of food intake. Figure created with BioRender.com.

the generation of signalling molecules, such as inflammatory cytokines, which promote increased blood flow to the region and the infiltration of circulating leukocytes. This aids in removal of the initial cause of the inflammation, the clearance of necrotic cells, and the promotion of tissue repair. Inflammatory changes can however be damaging to the tissue itself, a particular problem in conditions associated with chronic inflammation, such as obesity, where chronic, low-grade, widespread, inflammation is reported. Obesity is associated with increases in the levels of circulating cytokines and acute phase proteins, leukocyte recruitment to inflamed tissues, and the generation

of reparative tissue responses (reviewed in Lumeng and Saltiel 2011). Obesity-associated inflammation may well underlie the cognitive deficits reported, as inflammation has been proposed to promote cognitive dysfunction and the development of dementias, with observational studies in humans showing a consistent relationship between inflammatory markers and dementia or cognitive impairment (Gorelick, 2010). Metabolic syndrome, which can be defined as a grouping of disorders including abdominal obesity, hypertriglyceridaemia, low high-density lipoprotein levels, hypertension, and hyperglycaemia (Yaffe et al., 2004), is associated with dementias and cognitive impairment (Gorelick, 2010), with this primarily seen in those with high levels of inflammation (Yaffe et al., 2004). Indeed, in HFD rodent models cognitive deficits have been linked to elevated levels of inflammatory cytokines (Liu et al., 2014; Thirumangalakudi et al., 2008; Pistell et al., 2010).

In order for inflammation to alter neuronal processes it has to have an impact on the brain. Microglia are the brain's resident immune cells, and they play important roles in brain development, plasticity, and immune surveillance. In a physiological state they monitor synapses, remove apoptotic debris, and play a role in synaptic pruning, using highly motile processes to survey their local environment thereby permitting a rapid response to any changes (Norden and Godbout, 2013). Upon inflammatory activation they become proliferative and multiply (Kettenmann et al., 2011), as well as altering their morphology (typically from a ramified to an amoeboid shape during strong inflammatory responses), and producing inflammatory cytokines (Hanisch and Kettenmann, 2007). Their activation though is not a binary process, with different stimuli eliciting different microglial reactions. An example of this is microglial priming, where primed microglia show signs of activation such as proliferation (priming reviewed in Li et al. 2018) though with less distinct morphological changes (they remain highly ramified despite showing larger and less-round somata than resting cells; Torres-Platas et al. 2014) and do not produce inflammatory cytokines (Perry and Holmes 2014 cited by Hoogland et al. 2018). They also show an elevated degree of cytokine production in response to a secondary inflammatory stimulus (microglial priming reviewed in Perry and Holmes 2014), and microglial priming occurs both in ageing and neurodegenerative diseases (reviewed in Tay et al. 2017; Norden and Godbout 2013; Perry and Holmes 2014).

The peripheral inflammation associated with obesity and HFD feeding could drive neuroinflammation through inflammation of primary afferent nerves in the periphery, the activation of microglial cells situated at CVOs, the transport of peripheral cytokines by transporters situated on the BBB, or the activation of interleukin 1 (IL-1) receptors on perivascular macrophages and endothelial cells in brain venules (reviewed in Dantzer et al. 2008). Conversely, neuroinflammation can also be facilitated by the breakdown of the BBB leading to the entry of plasma-derived

factors and toxins such as fibrinogen (Ryu and McLarnon, 2009) that can promote inflammation, or through the direct action of dietary components such as SFAs (Valdearcos et al., 2014) on microglial signalling (Milanski et al., 2009). With regards to hippocampus-specific effects, HFD induced cognitive deficits could be mediated in part through receptors for IL-1 that are enriched in the hippocampus (reviewed in Parnet et al. 2002) and IL-1β, along with other proinflammatory cytokines, has been shown to impair hippocampal-dependent learning and long-term potentiation (LTP; Lynch 2015), and contextual (Barrientos et al., 2002) and spatial (Goshen et al., 2007) memory. Though basal IL-1 levels are required for hippocampal-dependent memory, any deviation from the physiological range has detrimental effects (Goshen et al., 2007).

Regarding the fact that HFD induced hippocampus-specific cognitive impairment occurs rapidly after switching diets, it is important to consider the timecourse of inflammatory changes. Within the brain inflammation appears to occur earliest in the hypothalamus, where 24 and 72 hours of HFD feeding induced elevations in the mRNA of proinflammatory cytokines and the density of microglia respectively (Thaler et al., 2012). Hypothalamic inflammation seems to be followed by the hippocampus, where one week of HFD supplemented with fructose syrup led to astrocytic activation along with evidence of microglial morphological changes (Calvo-Ochoa et al., 2014). In the cortex no signs of inflammation, as assessed by changes in the levels of proinflammatory cytokine mRNA, were detected after a week of HFD (Guillemot-Legris et al., 2016), though Denver et al. (2018) report an increased cortical microglial density after 18 days. Whilst these results suggest that hippocampal inflammation doesn't occur early enough to coincide with rapid cognitive changes (that are reported after only 24 hours; McLean et al. 2018), no studies have looked at hippocampal inflammatory changes prior to one week of HFD feeding so it still remains a strong possibility.

1.1.1 Leptin and Insulin Resistance

Besides these proposed direct effects on hippocampal processing, inflammation may also impair cognition by promoting resistance to both insulin and leptin signalling. Leptin and insulin receptors are highly expressed in the hippocampus, and evidence suggests that they play a role in hippocampal-dependent learning and memory, perhaps by regulating synaptic plasticity and receptor trafficking (briefly reviewed in Cordner and Tamashiro 2015).

Leptin was initially identified as an important player in weight gain when Ingalls et al. (1950) described a mutant mouse strain associated with severe obesity. This mutation was later found to be associated with the leptin gene (*ob*; Zhang et al. 1994). Leptin is a hormone produced

predominantly by adipose tissue and whose levels in the circulation reflects total adipose mass (Weigle et al., 1997). Increases in leptin are associated with reductions in appetite and decreased body weight (Morioka et al., 2016), and though it is too large to cross the BBB by diffusion, it likely enters the brain via an adjustable, saturable transport system associated with transcellular receptors (Maness et al. 2000 cited in Gruzdeva et al. 2019). Once in the brain, leptin acts on the hypothalamic arcuate nucleus (ARC), where both AgRP/NPY and pro-opiomelanocortin (POMC) neurons express leptin receptors (Gautron and Elmquist, 2011). Here it promotes the production of appetite suppressing neuropeptides and weight-reducing α-melanocytostimulating hormone in POMC neurons, whilst in AgRP/NPY neurons, leptin inhibits the production of appetite-stimulating AgRP and NPY (reviewed in Zhou and Rui 2013; Myers et al. 2008).

Insulin is secreted by pancreatic beta cells during periods of nutrient uptake and inhibits the output of glucose by the liver whilst promoting its transport into skeletal muscle and adipose tissue. It can cross the BBB and has receptors in the hypothalamus (Havrankova et al., 1978) where its direct administration inhibits food intake (Hatfield et al., 1974). Deletion of the insulin receptor in neurons increases body fat mass (Bruning et al., 2000), and resistance to the blood glucose lowering effects of insulin (Reaven, 2005) is pervasive in obesity and precedes the development of type 2 diabetes, which along with hyperinsulinaemia, is a risk factor for weight gain in children and adolescents (Kolb et al., 2018). However, the anorexigenic (appetite suppressing) effects of insulin are not always replicated (Jessen et al., 2010), and when administered peripherally insulin increases food intake. The uncertainty regarding the role of insulin in appetite and weight regulation suggests that it plays a minor role in comparison to leptin, though the two are likely involved in neuronal cross-talk given that leptin signalling is enhanced if insulin is also present (Carvalheira et al., 2001). However, there is evidence that the two act on distinct populations of neurons with insulin hyperpolarising, and leptin depolarising, a subset of POMC cells (Williams et al., 2010). These results highlight the fact that despite some potential mechanistic overlap and similarity of function, leptin and insulin still appear capable of differential effects on energy homeostasis.

Diet-induced obesity is associated with impaired responses to leptin throughout the brain (Morabito et al., 2017) and three days of HFD in rats is sufficient to induce both central insulin resistance, which is associated with greater caloric intake (Clegg et al., 2011), and an attenuation of leptin-driven changes in feeding behaviour (Wang et al., 2001). This is likely the result of inflammation, given that the intracerebroventricular administration of a low dose of proinflammatory tumour necrosis factor alpha (TNF-α) induces insulin and leptin resistance and shifts neurotransmitter expression to an obesity-like pattern (Romanatto et al. 2007 cited in Velloso and Schwartz

2011). Hypothalamic insulin resistance induced after only 72 hours of HFD feeding (Thaler et al., 2012) is thought to be the result of the inflammation-driven upregulation of SOCS3 and the serine kinase IKK (Zhang et al., 2008). Inflammation-induced insulin and leptin resistance could be mediated by signalling through TLR4 on microglia, whose activation by SFAs can result in leptin resistance (Milanski et al., 2009). Similar HFD-induced changes in leptin signalling have been reported in the hippocampus by Mainardi et al. (2017), and though they did not look into the presence of concurrent inflammation, work by Calvo-Ochoa et al. (2014) demonstrated the presence of low levels of hippocampal inflammation and changes in hippocampal insulin signalling following 7 days of HFD feeding. Therefore, inflammation-induced leptin and insulin signalling resistance in the hippocampus could play a role in the observed hippocampus-dependent cognitive deficits, and may also promote dysfunctional regulation of eating behaviour that leads to weight gain.

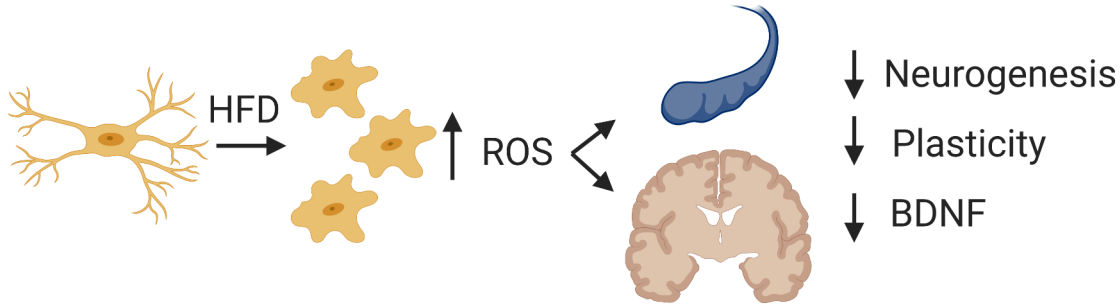

Figure 1.3: HFD-Induced Inflammation Promotes Oxidative Stress. HFD feeding promotes the activation of microglia, stimulating their proliferation and phenotypic shift from a ramified towards an amoeboid morphology. Activated microglia act as sources of ROS, promoting oxidative stress. HFD-induced oxidative stress has been detected in both the hippocampus and cortex, and is associated with an impairment in hippocampal neurogenesis, neuronal plasticity, and a downregulation of BDNF expression. Figure created with BioRender.com.

1.1.2 Oxidative Stress

Oxidative stress is an imbalance in the production of reactive oxygen species (ROS) and antioxidant defences. It can lead to lipid peroxidation and protein damage, where the former is associated with changes in cell membrane fluidity, permeability, potential, and can ultimately lead to membrane rupture, and the latter involves protein changes such as the addition of carbonyl groups, or protein cross-linking or fragmentation (oxidative stress reviewed in Betteridge 2000). While ROS generation can be driven by the oxidative metabolism of glucose (Du et al., 2000), activated microglia can also act as sources of ROS (reviewed in Lull and Block 2010) and inflammation is closely linked with oxidative stress (as reviewed in Mittal et al. 2014; Biswas 2016). Oxidative

stress can impair hippocampal learning and memory, which is related to changes in neurogenesis and spine density (Huang et al., 2015). The degree of neurogenesis in the dentate gyrus also seems to correlate negatively with levels of IL-1β, IL-1, and TNF-α (Boehme et al. 2014 cited in Borsini et al. 2015). HFD feeding increases the levels of oxidative stress in the hippocampus, which coincides with deficits in spatial memory (Xia et al., 2015; Kishi et al., 2015; Liu et al., 2014; Molteni et al., 2004; Cui et al., 2012) though this is not region specific given HFD-induced oxidative stress has also been detected in the cortex (Liu et al., 2014). These cognitive effects are attenuated by anti-oxidant treatment (Xia et al., 2015; Liu et al., 2014; Cui et al., 2012).

Besides ROS derived from activated microglia, Morrison et al. (2010) provide evidence that HFD decreases the signalling of nuclear factor erythroid 2-related factor 2 (NRF2), a major regulator of antioxidant responses, which suggests this is partly responsible for the observed oxidative stress and cognitive impairment. It is also likely that elevated blood glucose levels associated with HFD feeding, seen after only a week (Winzell and Ahren, 2004), accelerate glucose oxidative metabolism and in doing so elevate the production of ROS (Du et al. 2000; seen in diabetes; Shah et al. 2013). For this to be the case, circulating hyperglycaemia would have to translate into elevated glucose levels in the brain, a process mediated by glucose transporter 1 (GLUT1), the main glucose transporter expressed on endothelial cells in the BBB (Vannucci et al., 1998). GLUT1 expression is changed to maintain normoglycaemia in the brain (during fasting-associated hypoglycaemia; Fuente-Martiń et al. 2012) so the hyperglycaemic state associated with HFD feeding would be expected to decrease its expression levels. Indeed, this occurs as expected, though the decrease is only transient and rather than maintaining brain glucose availability, is associated with a reduction of cerebral glucose levels (Jais et al., 2016). This suggests that HFD-induced hyperglycaemia is not responsible for the reported increases in oxidative stress in the brain (at least not within the first 3 weeks), but provides evidence of HFD-driven dysfunction in brain glucose regulation. Reduced GLUT1 levels are associated with neuronal dysfunction and degeneration and BBB integrity is mediated by GLUT1 (Winkler et al., 2015), indicating that the transient reduction reported by Jais et al. (2016) may have long-lasting implications for neural processing.

Oxidative stress can also impact BDNF levels during HFD feeding. BDNF modulates synaptic plasticity and its levels are decreased by HFD in both the hippocampus (Kishi et al., 2015; Molteni et al., 2004; Camer et al., 2015) and cortex (Kaczmarczyk et al., 2013; Pistell et al., 2010; Camer et al., 2015). A reduction in BDNF signalling, induced either by HFD feeding (Camer et al., 2015; Kaczmarczyk et al., 2013; Pistell et al., 2010) or antagonism of the BDNF receptor tropomyosin receptor kinase B (TrkB; Kishi et al. 2015), is associated with cognitive impairments. This could be related to a loss of dendritic spines (Granholm et al., 2008; Arnold et al., 2014) that has been

reported following HFD feeding, and changes in synapsin 1 and CREB, modulators of learning and memory, correlate with HFD-induced reductions in hippocampal BDNF levels (Molteni et al., 2004). A study by Wu et al. (2004a) showed that the HFD-induced decrease in BDNF levels was associated with oxidative stress and could be rescued through treatment with the anti-oxidant vitamin E, implicating oxidative stress as the mediator of BDNF level changes. Oxidative stress could reduce BDNF by diminishing the activity of activator protein-1 and CREB, or impairing NMDA function (Wu et al., 2004a). Reductions in NMDA receptor binding densities are correlated with reduced BDNF levels in the prefrontal cortex, but not the hippocampus, following HFD feeding (Camer et al., 2015). Inflammation can also affect BDNF expression, where the intraperitoneal injection of proinflammatory stimuli such as IL-1β or lipopolysaccharide (LPS) decreases BDNF mRNA levels in the hippocampus (Lapchak et al., 1993) and protein levels in the hippocampus and cortex (Guan and Fang, 2006), though this is likely partially mediated by inflammation-driven oxidative stress.

1.1.3 Summary

In summary, HFD-induced inflammation could influence cognition through a number of mechanisms. Inflammatory cytokines are involved in supporting hippocampal-dependent learning and LTP (Goshen et al., 2007), though when present in non-physiological levels can impair these processes (reviewed in Lynch 2015). Inflammation can also induce neuronal resistance to both leptin and insulin signalling, two pathways that likely influence hippocampal cognition through the modulation of synaptic plasticity and receptor trafficking (briefly reviewed in Cordner and Tamashiro 2015). Finally, oxidative stress has been linked to cognitive deficits in a number of HFD studies, and has also been implicated in the HFD-induced reduction of BDNF levels, a neurotrophin involved in modulating synaptic plasticity. Oxidative stress can be driven by inflammation.

With regards to the rapid hippocampus-specific deficits observed by McLean et al. (2018) and Kanoski and Davidson (2010), HFD induced oxidative stress has been reported in both the hippocampus and cortex, with the latter reported after only a week (Kaczmarczyk et al., 2013), and in contrast to the hippocampus-specific enrichment of leptin (Scott et al., 2009) and IL-1 receptors (reviewed in Parnet et al. 2002), insulin receptors are highly expressed in both regions (Havrankova et al., 1978). Therefore, if inflammation-related changes in insulin signalling and oxidative stress are related to the hippocampus-specific cognitive deficits, they must demonstrate hippocampus-specific effects. In contrast, global inflammation could drive hippocampus-specific changes given the hippocampal enrichment of the IL-1 and leptin receptors.

Overall, studies suggest that HFD-induced inflammation occurs in a region and time-specific manner, though studies that compare inflammation between regions in a single model are rare. The only study so far, to my knowledge, that has directly compared early changes in cortical and hippocampal inflammation is Denver et al. (2018). They showed that HFD elevated microglial densities in both the dentate gyrus and cortex after 18 days of feeding, which, given that HFD-induced cognitive deficits remain hippocampus-specific for 30 days (Kanoski and Davidson, 2010), suggests global inflammation has greater effects on hippocampal versus cortical processing. However, Denver et al. (2018) did not assess hippocampus-specific cognition, instead using more cortically-dependent novel object recognition and Morris water maze tests (HFD and its effects on behaviour reviewed in Cordner and Tamashiro 2015). As such, a direct relation between early global inflammation and hippocampus-specific deficits in behaviour during HFD feeding has yet to be made.

1.2 Vascular Mechanisms of HFD-Induced Cognitive Deficits

Other possible mechanisms involved in HFD-induced cognitive deficits relate to the vasculature. As stated previously, obesity is a risk factor for cardiovascular and microvascular disease and is linked to endothelial dysfunction and the development of atherosclerosis. The main role of the vasculature in the brain is to supply oxygen and nutrients and remove carbon dioxide and metabolic waste products, where dysfunction in this network disrupts its ability to support neuronal metabolism and contributes to the development cerebromicrovascular disease (microvasculature reviewed in Sorop et al. 2017). Blood supply for the brain comes from the internal carotid arteries and the vertebral arteries, which branch and combine to form the cerebral arteries, the basilar artery, and the circle of Willis, which likely improves the chances of brain regions continuing to be supplied with blood in the event of a major artery becoming occluded. Neurons are more sensitive to oxygen deprivation than other cell types, so any interruption in the supply of oxygen or glucose leads to significant damage (Purves et al., 2001). Arteries and arterioles that supply neurons penetrate into the parenchyma and form a network of capillaries, with individual neurons generally within 20 µm of a capillary. Brain vessels are composed of endothelial cells connected via tight and adherens junctions which limit paracellular transport into the brain, though other cell types are also intimately associated with brain vessels. Astrocytes attach end-feet to microvessels that facilitate their role in transporting oxygen and glucose to neurons by regulating local blood flow, with a similar role also existing for pericytes and vascular smooth muscle cells, vascular mural cells that wrap around vessels and through their contraction also regulate changes in flow (brain microvessels described in Kolinko et al. 2014). Activity-dependent changes in the blood supply in the

brain are mediated by neurovascular coupling, the mechanism whereby local changes in neuronal activity are coupled to regional changes in blood flow. This occurs in capillaries, and precapillary arterioles, via interactions and metabolic signalling between neurons, astrocytes, pericytes, and endothelial cells, with evidence suggesting the initial change in flow occurs in capillaries before propagating upstream to arterioles (Fouda et al., 2019; Sweeney et al., 2018).

In recent years evidence regarding the importance of vascular changes in various pathologies, such as Alzheimer's Disease (reviewed in de la Torre 2002) and ageing (briefly summarised in Le Couteur and Lakatta 2010) has accumulated. Reductions in cerebral blood flow (CBF) are reported in both vascular cognitive impairment and Alzheimer's disease, and many vascular risk factors are also risk factors for these conditions. Increases in the measures of small vessel disease in the brain precede cognitive decline, and dementias are widely associated with vascular dysfunction and neurovascular uncoupling (the disruption of the relationship between neuronal activity and changes in blood flow; Fouda et al. 2019). In obesity human subjects show reduced levels of blood flow in the brain, impaired vascular responses to vasoactive molecules, and indices of cerebral microvascular disease (such as microbleeds) are more common (Sorop et al., 2017). Obesity-associated reductions in blood flow correlate with memory impairment (Birdsill et al., 2013). In animal models both reductions (Estato et al., 2017; Obadia et al., 2017; Tucsek et al., 2014b) and increases (Yamamoto et al., 2019; Yi et al., 2012) in microvascular density have been observed. A common feature is that regardless of direction, changes in vascular density are associated with cognitive deficits (Tucsek et al., 2014b; Coucha et al., 2019). HFD associated reductions in vascular diameter have also been reported (He et al., 2016; Constantinescu et al., 2011), as have reductions in CBF in HFD fed rats (Glaser et al., 2012; Obadia et al., 2017). With regards to neurovascular coupling, rodent HFD feeding is associated with a reduction in the vascular response to neuronal activity (Tucsek et al., 2014b; Li et al., 2013) and there is strong evidence of impairment in vasodilatory capacity in models of obesity (Chantler et al., 2015; Phillips et al., 2005; Schwaninger et al., 2003) and HFD feeding (Obadia et al., 2017). However, studies that have looked at region-specific, and early, changes in vascular structure and function in response to a HFD are notably lacking, making it difficult to evaluate their contribution to the rapid hippocampus-specific cognitive impairments reported.

1.2.1 Blood-Brain Barrier Disruption

The BBB is a specialised barrier that essentially isolates the CNS from the rest of the body. It is formed of specialised endothelial cells (Wolburg and Lippoldt, 2002) with tight junction pro-

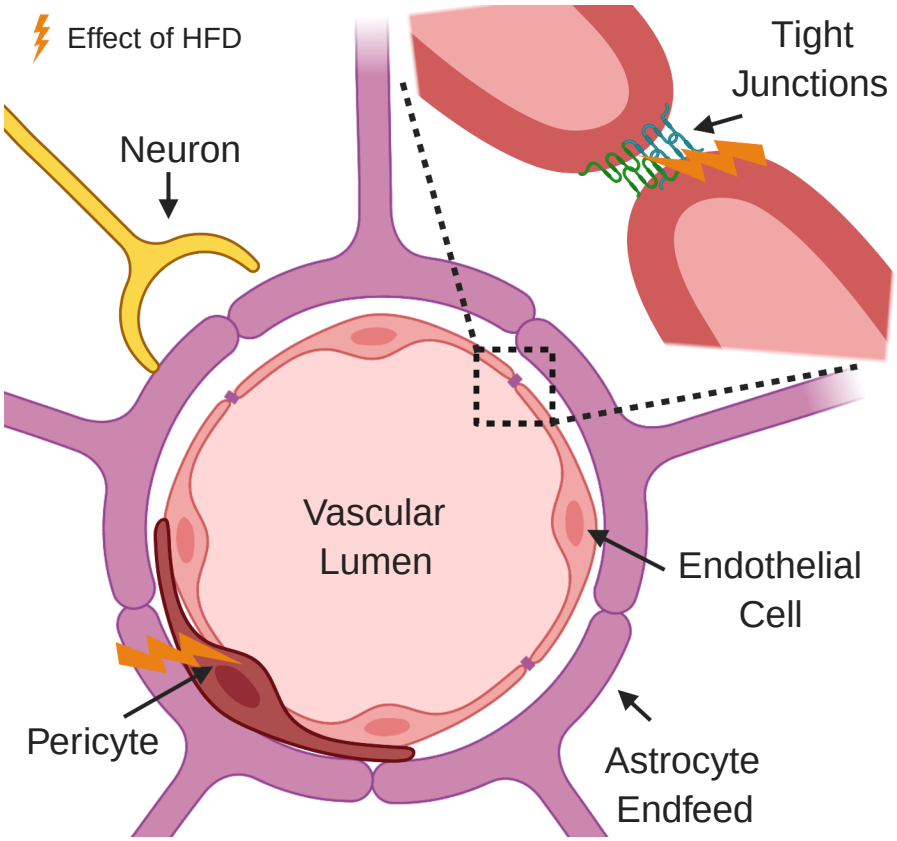

Figure 1.4: The Blood-Brain Barrier. The BBB is a specialised barrier that limits the movement of molecules between the brain parenchyma and the vasculature. It consists of endothelial cells connected by specialised tight junctions, which inhibit the paracellular movement of molecules. Pericytes sit on the abluminal surface of the vasculature, and play important roles in the regulation of blood flow, capillary support, and BBB integrity. Astrocytic endfeet form an additional component of the BBB. HFD feeding can reduce BBB integrity by diminishing the expression of tight junctions, and has been shown to reduce pericyte coverage of the vasculature. Figure adapted from Aday et al. (2016) and created with BioRender.com.

teins, such as occludin and the claudins, being the main structures involved in barrier integrity (Huber et al., 2001). Paracellular transport between endothelial cells is restricted by the presence of these tight junction proteins, whilst transocytosis at the BBB is reduced relative to the periphery and is associated with a reduction in the number of endocytic vesicles. Alterations in the integrity of the BBB are associated with cognitive decline (Nation et al., 2019) and decreased BBB integrity can be both a cause and consequence of CNS pathologies (Hawkins and Davis, 2005). Disruption in the BBB has been linked to the hippocampus-specific cognitive deficits associated with HFD feeding (Cordner and Tamashiro, 2015; Davidson et al., 2019), where BBB breakdown in a hippocampus-specific manner could permit the entry of a number of plasma-derived factors that typically generate neurotoxic products and can compromise synaptic and neuronal functions (Zlokovic, 2008), including proinflammatory circulating factors such as plasma derived immunoglobulin G (IgG), thrombin, and fibrinogen (Tucsek et al., 2014a; Carreño-Müller et al., 2003;

Davalos et al., 2012).

Reports of HFD induced BBB breakdown are widespread (Davidson et al., 2012; Chang et al., 2014; Pallebage-Gamarallage et al., 2012; Elahy et al., 2015) and seen across a variety of different tracers and markers of integrity (e.g. endogenous IgG and albumin leakage, entry of sodium fluorescein (NaF) and radio-labelled sucrose) with this breakdown linked to cognitive impairment (Kanoski et al., 2010; Davidson et al., 2012, 2013). These changes also appear to be region and time-specific. Hippocampus-specific BBB leakage has been reported in genetically obese and HFD fed rats (Yoo et al., 2016; Kanoski et al., 2010; Davidson et al., 2012) consistent with reports of decreases in the levels of claudin-5 and occludin in the hippocampus (Yamamoto et al., 2019) but not parietal cortex (Li et al., 2016) after 16 weeks of HFD feeding. At the same timepoint Salameh et al. (2019) showed that HFD elevated levels of radio-labelled sucrose in the hippocampus and hypothalamus, but not at the whole brain level, whilst radio-labelled albumin was elevated at the whole brain level and hypothalamus but not the hippocampus. These results suggest that HFD induced reductions in BBB integrity could indeed be hippocampus-specific, but that this may also depend on relative permeability to the molecules in question. For example, when looking either exclusively at the hippocampus or across the entire brain, only the hippocampus was permeable to sucrose ($\sim$342.3Da). In contrast, the hippocampus showed no entry of the larger albumin molecule, which was otherwise detected at the whole brain level($\sim$69kDa; molecular sizes from Saunders et al. 2015). The route of entry likely mediates this effect, where HFD could affect trans- or paracellular transport systems differentially. Salameh et al. (2019) make the point that both sucrose and albumin can cross the BBB using either route, and that there is no method to clearly distinguish between these two.

The mechanism linking HFD feeding to BBB breakdown seems most likely to be oxidative stress. The protective effect of nicotine on HFD induced BBB breakdown has been suggested to relate to its anti-oxidant activity (Elahy et al., 2015) and anti-oxidants prevented SFA associated BBB breakdown whilst decreasing levels of central inflammation (Takechi et al., 2013). Resveratrol, which also has antioxidant activity, attenuates HFD induced BBB disruption (Chang et al., 2014) though this may also relate to the resveratrol-mediated reductions in the levels of total cholesterol and low density lipoproteins, as well as the promotion of cytoskeletal polymerisation and adenosine triphosphate (ATP) synthesis in cerebrovascular endothelial cells (Chang et al., 2014). Finally, antagonism of the endothelial adenosine receptor 2a (Adora2a) prevented HFD induced BBB breakdown (Yamamoto et al., 2019). Adora2a is upregulated in brain microvessels following 16 weeks of HFD feeding, and is suggested to promote BBB leakage by eliciting NFκB mediated down-regulation of tight junction proteins (Yamamoto et al., 2019).

Whilst there is evidence that changes in the BBB could be hippocampus-specific, the time-course of these are important if they are to be related to cognitive effects. In what appears to be the only study that looks at BBB changes within the first week of HFD feeding, Rijnsburger et al. (2019) noted no increase in the permeability of the hypothalamic BBB to Evans blue dye, nor any changes in the expression levels of the tight junction proteins zonula occludens-1 (ZO-1), claudin-5, and occludin. Evans blue is widely stated to bind to plasma albumin (Saunders et al., 2015), and so these results may indicate an absence of large-scale BBB disruption following a week of dietary manipulation. However, Saunders et al. (2015) make the case that there are plenty of issues surrounding the use and interpretation of Evans blue for the assessment of BBB integrity, so these results should be viewed cautiously. Regardless, Rijnsburger et al. (2019) provide an assessment of BBB integrity at what appears to be the earliest documented timepoint in HFD studies, and though their Evans blue result should be viewed cautiously, the fact they detect no hypothalamic changes in tight junction protein levels suggests an absence of HFD induced changes in paracellular transport across the BBB. Again, however, it is important to consider that HFD induced BBB disruption may be both time and region specific, so extrapolating these results to the hippocampus should be done with caution.

Besides reductions in integrity, HFD feeding is also associated with impairments in receptor mediated transport across the BBB. HFD reduces brain endothelial cell insulin uptake (Gray et al., 2017) suggesting it may do so at the BBB *in vivo*, and HFD-induced impairments in the transport of leptin into brain appear after 6 weeks (Schuster et al., 2018). The latter can be induced by elevated circulating triglyceride levels (Banks et al., 2004). The degree of BBB leptin uptake correlates negatively with adiposity levels and appears to develop alongside obesity, where even modest weight reduction can improve it (Banks and Farrell, 2003), making it unlikely that impaired BBB transport of leptin plays a role in the early stages of HFD feeding.

1.2.2 Pericyte Dysfunction

Pericytes are vascular mural cells that are a key cellular component of the BBB and sit on the abluminal surface of microvessels. They are embedded in a common basement membrane with endothelial cells, and wrap their processes around the endothelium (Trost et al., 2016). In areas where a basement membrane is absent, they make direct contact with endothelial cells (Winkler et al., 2011). Reductions in pericyte coverage correlate with increased rates of both para- and transcellular transport across the BBB, which are related to decreases in the expression of tight and adherens junction proteins (Haddad-Tóvolli et al., 2017). Pericytic coverage of the vasculature is

reduced by HFD (Yamamoto et al., 2019; Tucsek et al., 2014b) but treatment with an Adora2a antagonist not only attenuated this effect, it also reduced the degree of HFD-induced BBB breakdown. Whilst Adora2a is expressed on both endothelial cells and pericytes, these results indicate that HFD-induced BBB disruption could be mediated by dietary effects on pericytes (Yamamoto et al., 2019). These effects could be related to oxidative stress, an insult that pericytes seem particularly susceptible to. Hyperglycaemia associated oxidative stress induces cerebral pericyte death through apoptosis *in vitro* (Shah et al., 2013), whilst in a mouse model of diabetes treatment with an anti-oxidant prevented the loss of pericytes (Price et al., 2012). Though not observed directly, these results indicate that oxidative-stress induced pericyte dysfunction could lead to BBB breakdown during HFD feeding, and in doing so may trigger further downstream detrimental effects. If this were to occur in a region-specific manner, pericyte dysfunction might be a key driver of hippocampus-specific dietary effects.

Besides a role in maintaining the BBB, pericytes are also key players in the regulation of blood flow (Hall et al., 2014) and preserving cerebral circulation. Pericyte dysfunction has been implicated in a number of CNS pathologies such as stroke, where their constriction and subsequent death contributes to the no-reflow phenomenon, reducing blood flow and likely contributing to continuing neuronal damage, and in diabetes, where retinal pericyte loss, which can cause local oedema, occurs early in disease progression due to inhibited endothelial to pericyte communication. Finally, pericyte loss coincides with a loss of BBB function in Alzheimer's Disease (reviewed in Cheng et al. 2018). Changes in vascular densities reported in HFD models (reductions; Estato et al. 2017; Obadia et al. 2017; Tucsek et al. 2014b, increases; Yamamoto et al. 2019; Yi et al. 2012) have been associated with cognitive deficits (Tucsek et al., 2014b; Coucha et al., 2019) and pericytes play key roles in both the formation of new blood vessels (in part through the Ephrin-B2 signalling pathway; Sweeney et al. 2016) and support of existing vessels, where their loss or aberrant constriction in hypertension has been linked to the development of cerebral capillary loss (reviewed in Hirunpattarasilp et al. 2019). Inhibition of pericyte Ephrin-B2 prevented the aberrant neovascularisation reported by Coucha et al. (2019), whilst the loss of vessels observed by Tucsek et al. (2014b) was suggested to relate to the loss of pericytes they observed. Pericyte loss, and associated capillary rarefaction, have been proposed to be mediated by mechanical and oxidative stress (briefly reviewed in Hirunpattarasilp et al. 2019). Oxidative stress in ischaemia induces aberrant pericyte constriction (Yemisci et al., 2009), and given that HFD feeding has been reported to reduce blood flow and perfusion in HFD fed rats (Glaser et al., 2012; Obadia et al., 2017), its possible that such a mechanism is also at play.

HFD induced disruptions in neurovascular coupling (Tucsek et al., 2014b; Li et al., 2013) are

thought to lead to cognitive deficits (Sorop et al., 2017), and pericytes have been implicated in this (Gomez-Smith et al., 2018) as well, given the role they play in regulating blood flow (Hall et al., 2014). Whilst pericytes sit on capillaries and have protruding cell bodies with thin longitudinal processes, they reflect an end of a spectrum of vascular mural cells that begins with the coverage of arteries and arterioles by smooth muscle cells, which have a ring shaped morphology (pericytes reviewed in Armulik et al. 2011). Bridging the gap between smooth muscle cells and pericytes are cells with features of both. Though smooth muscle cells are generally acknowledged as contractile, the role of pericytes in controlling cerebral blood flow has been controversial. This partly relates to a lack of agreement on how to define the transitional cell types (Grant et al., 2019), an important distinction given that they likely have different physiological roles, with evidence strongly supporting a contractile role for ensheathing pericytes (located on proximal branches of penetrating arteriole offshoots; Hill et al. 2015; Fernández-Klett et al. 2010) whilst for capillary pericytes this is a more inconsistent finding (in support: Hall et al. 2014; Peppiatt et al. 2006; Kisler et al. 2017, against: Fernández-Klett et al. 2010; Wei et al. 2016; Hill et al. 2015). Studies investigating the effect of HFD feeding on pericyte function are lacking, but given the potential heterogeneity of function between pericyte subtypes, this is an important factor that must be considered in future work.

1.2.3 Basal Hippocampal Susceptibility

Pericyte-related or not, disruptions in hippocampal neurovascular coupling and vascular supply seem promising candidates for the mechanisms driving HFD induced cognitive deficits. However, the increased susceptibility of the hippocampus to damage or pathology such as hypoxia (Ng et al., 1989), Alzheimer's Disease, and ageing (reviewed in Fjell et al. 2014), suggests that it may be the hippocampus itself, rather than any region-specific dietary effects, that are responsible for hippocampus-specific changes. Evidence indicates that the enhanced susceptibility of the hippocampus to early damage relates to its paucity of vascular support relative to other brain regions such as the neocortex. This is supported by findings that consistently demonstrate a lower vessel density in the hippocampus relative to cortex (Wu et al., 2004b; Patt et al., 1997; Zeller et al., 1997) which seems to be the case across frontal (Bohn et al., 2016; Klein et al., 1986), visual, and auditory cortices (Klein et al., 1986). Regional vessel density and local blood flow, as well as glucose utilisation, are correlated (Klein et al., 1986), so one might expect this to be matched by a relatively lower level of neuronal energy demand in the hippocampus. However, it appears that its metabolic demands are at least similar to, if not greater than, those in the cortex. Neuronal density is reduced in the parietal and visual cortices relative to hippocampal CA1 (reviewed in

Keller et al. 2018), and both the uptake and utilisation of glucose is seen at similar levels in the hippocampus and the cortex (Kleinridders et al., 2018; Zeller et al., 1997). This would suggest that the hippocampus shows a degree of uncoupling between energy demand and supply relative to other brain areas, and this may explain its enhanced susceptibility to the early effects of numerous brain pathologies including HFD feeding.

1.2.4 Summary

HFD feeding is associated with dysfunctional changes in the ability of the vasculature to support neuronal activity both in a functional and structural capacity. However, no studies have investigated the extent of HFD-induced vascular changes at early timepoints, nor directly compared them between regions in a single model, so how they might relate to early hippocampus-specific cognitive changes is unclear. Region-specific BBB disruption has also been proposed to explain cognitive changes, where HFD induced decreases in BBB integrity appear to be dependent on the duration of manipulation, brain region, and route of entry into the brain. Again, no studies so far have compared early changes between regions. Pericytes are affected by long-term HFD feeding (Tucsek et al., 2014b; Yamamoto et al., 2019) and given their involvement in numerous aspects of vascular physiology (functional and structural regulation of the capillary bed, maintenance of BBB integrity), any dietary effects they suffer could have a widespread impact. Once more however, early dietary effects in pericytes have not been investigated. Finally, the possibility that global dietary effects are translated into hippocampus-specific changes thanks to its relatively worse level vascular support is apparent from the literature, though no studies have yet directly compared all of vascular structure, function, and neuronal metabolism, between the hippocampus and cortex.

1.3 Aims and Hypotheses

So far no studies exist that have compared some of the numerous mechanisms proposed to mediate the hippocampal cognitive impairment observed in short-term HFD feeding across multiple brain regions, despite the fact that such work is necessary in order to determine what is driving these rapid region-specific cognitive changes. The aim of my PhD was to address this, and to evaluate hypotheses regarding whether inflammatory and vascular changes show region and time-specific responses to a HFD. In my first experimental chapter I describe immunofluorescence imaging studies I undertook in mice fed a HFD for 2 weeks. Here I imaged the hypothalamus, hippocampus, and cortex, evaluating diet-induced changes in vascular structure, BBB integrity, pericyte coverage, and microglial activation (assessed by their density and morphology), with the aim of

establishing whether the suggested mechanisms were affected in a global or region-specific manner at a timepoint relevant to hippocampus-specific cognitive impairment. In the second and third experimental chapters I describe *in vivo* timecourse imaging studies conducted in awake, behaving mice where data were collected from both the hippocampus and cortex over an 8 week HFD feeding protocol. In addition, the mice in these chapters were tested on a hippocampus-specific behavioural task so that their performance could be correlated with *in vivo* data.

The second experimental chapter discusses my investigation of changes in microglial activation *in vivo*, using changes in their morphology as an index of this. The aims of this were to evaluate whether neuroinflammatory responses to HFD occur in both a time and region-specific manner, to test a hypothesis based on work in the first experimental chapter that suggested HFD might prime, rather than overtly activate, microglial cells, and to see if microglial activation correlated with hippocampus-specific cognition. In my final experimental chapter I describe my investigation of changes in blood flow, oxygenation, and neurovascular coupling *in vivo*. The aims of this were to evaluate whether HFD induced changes in these measures showed region or time-specific patterns, to test hypotheses regarding the lack of vascular support in the hippocampus and whether vascular structural changes detected in my immunofluorescence data correlated with changes in blood flow and vascular function *in vivo*, and to investigate if hippocampus-specific cognition correlated with any of the measures taken.

Chapter 2

Methods

2.1 Animals

Animal procedures were carried out in accordance with the guidelines of the UK Animals (Scientific Procedures) Act 1986. Mice were housed individually in a temperature controlled room (22 +/- 2°C) with a 12 hour light/dark cycle. Mice of varied age and both sexes were used. Body weight was monitored daily.

All mice used were bred on a C57BL/6J background. Reporter mutations used were NG2DsRedBAC (NG2: Neuron-Glial Antigen 2; Zhu et al. 2008) and Cx3CR1-GFP (Cx3CR1: C-X3-C motif chemokine receptor 1; Jung et al. 2000). NG2-DsRed positive mice constitutively express the fluorescent DsRed protein under the NG2 promoter, which labels vascular mural cells (pericytes and vascular smooth muscle cells) as well as oligodendrocyte precursor cells, though these can be distinguished morphologically and by their position in the parenchyma. Cx3CR1-GFP expression labels microglial cells, as well as circulating monocytes and subsets of natural killer and T cells (Imai et al., 1997). All mice with this mutation were heterozygotes. The Cx3CR1-GFP mutation involves the knockout of one allele of the Cx3CR1 gene, and its complete knockdown of is associated with impairments in cognition and synaptic plasticity (Rogers et al., 2011), as well as changes in the metabolic impact of HFD feeding (Shah et al., 2015).

2.2 Dietary Manipulations

Animals had *ad libitum* access to water and either a HFD or control diet. For all experiments (except one of the three immunofluorescence studies) the same combination of diets were used. The single study differed because it was the initial pilot immunofluorescence experiment, and was

conducted using diets purchased by the lab prior to my arrival. Following this study new diets supplemented with the anthelmintic Fenbendazole were sourced as at the time animals throughout the animal unit were undergoing pinworm treatment. These Fenbendazole diets were then used throughout all other work. These diets consisted of a HFD composed of 45% calories from fat (4.72kcal/g, Research Diets D12451-150FBZ) and a control diet that contained 10% calories from fat (3.84kcal/g, Research Diets D12450H-150FBZ). In **Chapter 3** the single immunofluorescent pilot study that differed used a HFD composed of 45% calories from fat (4.56kcal/g, Special Diet Services 824018) and a control diet containing 11.5% calories from fat (3.9kcal/g, OpenSource Diets D10001). Where diets differed in an analysis this was included as a factor. The percentage of calories derived from protein, carbohydrate, and fat sources for each diet are presented in **Table 2.1**. The ingredients in each diet as a percent of total weight are presented in **Table 2.2**. Diets composed of 45% rather than 60% (the other commonly used HFD percentage) of total calories from fat were used given that prior to my project this fat percentage was shown to be associated with hippocampus-specific cognitive impairments after two weeks of feeding in unpublished work by my lab. In addition, 45% represents a less severe distortion of dietary fat content relative to control diets and is therefore arguably a better model of obesogenic diets in humans (Speakman, 2019).

Fenbendazole was chosen as the anthelmintic given its lack of documented interactions and large margin of safety (Pritchett and Johnston, 2002). In a comparison of standard rodent chow to that supplemented with Fenbendazole, no difference in eating behaviour or weight gain was detected, though rats did show preference for the standard chow (Vento et al., 2008). The drug did also not affect the incidence or onset of diabetes in non-obese diabetic mice (Franke and Shirwan, 2006). It was also shown to have no effect on behavioural tests involving the relationship between a stimulus and food (Keen et al., 2005). However, there is some evidence that it promotes more severe detrimental effects when LPS is injected into the striatum (Hunter et al., 2007) and other studies suggest it has a degree of influence on immune responses (Yu et al., 2014; Villar et al., 2007; Ramp et al., 2010) though at baseline this appears to not be the case (Cray et al., 2008).

2.3 Novel Object-Context Recognition Task

In order to evaluate hippocampus-specific cognition a novel object-context recognition (NOCR) task was used. This task is a modified version of the novel object recognition paradigm, which measures the proportion of time an animal spends with novel rather than familiar objects given that cognitively intact animals show preferences for novelty. Though the novel object task in-

	D12451-150FBZ High Fat Diet	D12450H-150FBZ Control Diet	824018 Pilot High Fat Diet	D10001 Pilot Control Diet
Percent of calories from fat	45%	10%	45%	11.5%
Percent of calories from carbohydrates	35%	70%	35%	67.7%
Percent of calories from protein	20%	20%	20%	20.8%
Calorie density (kcal/g)	4.72	3.84	4.56	3.90

Table 2.1: Diet Calories Percentages. Table demonstrating the percentage of calories derived from fats, carbohydrates, and proteins, in the experimental diets. Codes indicate the diet model number. Pilot indicates the diets used in the first immunofluorescence study.

volves hippocampal processing, the prefrontal and perirhinal cortices are also involved. Given that tasks that rely on distributed processing (in comparison to those that depend more exclusively on the hippocampus) show inconsistent dietary effects (HFD behaviour studies reviewed in Cordner and Tamashiro 2015), and my primary interest was in investigating the mechanisms underlying hippocampus-specific cognitive impairment following HFD feeding, I opted to use a modified version of the novel object task that measures novel object-context recognition. In this version animals are exposed to two distinct contexts associated with discrete pairs of objects. On testing day one object is swapped between pairs so that each context contains an object that though familiar, is novel in that particular context. Object-context recognition is more closely associated with hippocampal cognition than simple novel object recognition, given that permanent hippocampal lesions impair novel object-context, but not novel object, recognition (Mumby et al., 2002). The hippocampus-specific nature of the NOCR task is supported by work demonstrating that long-term object-context memory is reduced by the infusion of a protein synthesis inhibitor into the hippocampus, but not the perirhinal or insular cortices, or the amygdala (Balderas et al., 2008). NOCR impairment has been seen following only 48 hours of HFD feeding, with other hippocampus-specific tasks showing deficits after a single day (McLean et al., 2018). The same study showed no evidence of impaired novel object recognition over two weeks of dietary manipulation, highlighting the existence of rapidly-induced, hippocampus-specific, cognitive impairment associated with HFD feeding previously demonstrated by Kanoski and Davidson (2010). Previous unpublished work within my lab has shown a deficit in NOCR performance in mice fed a 45% HFD for two weeks.

NOCR behavioural analysis was carried out in arenas (35 x 35cm with 35 cm high walls). Two

% w/w	D12451-150FBZ High Fat Diet	D12450H-150FBZ Control Diet	824018 Pilot High Fat Diet	D10001 Pilot Control Diet
Casein	23.29%	18.94%	26.51%	20.00%
Choline Bitartate	0.23%	0.19%	0.30%	0.20%
L-Cystine	0.35%	0.28%	0.40%	-
DL-Methionine	-	-	-	0.30%
Lard	20.67%	1.89%	18.00%	-
Rice Starch	-	-	18.43%	-
Corn Starch	8.48%	42.83%	-	15.00%
Cellulose	5.82%	4.74%	6.16%	5.00%
Soya Oil	2.68%	2.37%	4.32%	-
Corn Oil	-	-	-	5.00%
Sucrose	20.12%	16.37%	20.34%	50.00%
Maltodextrin	11.65%	7.10%	-	-

Table 2.2: Diet Ingredients. The ingredients for each diet as a percentage of total weight according to the manufacturer's documentation. Codes indicate the diet model number. Pilot indicates the diets used in the first immunofluorescence study. Dashes indicate ingredients that were not present in the diet.

different contexts were used. Context 1 had a white floor and alternating white and black walls and was paired with an almond scent. Context 2 had a metal grid placed over the floor and had grey walls and was paired with a lemon scent. During all habituation, training, and testing stages, white noise was played to avoid the interference of any outside sound. Objects in each context were placed in the top left and bottom right corners of the arenas, 10cm from the nearest walls. The object pairs used were white salt shakers and Christmas tree baubles. These two pairs of objects were chosen as preliminary testing showed no difference in exploratory preference between them. Behavioural tasks were performed during the light phase and mice were placed in the center of the arenas.

On day 11 of dietary manipulation mice were habituated to the two contexts without objects. On days 12 and 13 mice were trained to associate the two contexts with their associated objects.

On day 14 mice were tested by placing them in each context with one object swapped between contexts, so that each context now contained an object that was novel but only in that context. The order of context exposure, object set paired with each context, odour association, and location of novel object placement on test day, were balanced across diet groups. Exposure to the contexts at all stages (habituation, training, and testing) occurred for 10 minutes in each context, with a 5 minute break in between exposures. During this break mice were returned to their home cages and the contexts were cleaned with ethanol to remove debris and any odour marking. Behavioural testing was performed on mice with hippocampal window implantations as well as naive mice. Unfortunately, mice with window implantations appeared distinct to naive mice, and the difference in colour and texture between HFD and control diets was clear. As such, performance of the behavioural protocol was not blind to surgical status or diet group.

Analysis of NOCR performance was done manually using videos taken on test day by logging the beginning and end time of each interaction mice had with the objects in their environment. Care was taken to ensure that only legitimate exploration of objects was recorded, and interactions where mice simply climbed on the objects were ignored. This analysis was done blind to dietary manipulation and object novelty, though not surgical status, by having a colleague rename and reorganise the recorded video files. NOCR performance was quantified by calculating a novelty index (NI) that represents the difference in time spent exploring the novel and familiar objects as a proportion of total exploration time;

$$\frac{N_t - F_t}{N_t + F_t}$$

where N_t represents the time spent exploring the novel object and F_t the familiar object.

2.4 Surgical Window Implantation Procedure

In vivo experiments were conducted in mice implanted with windows for imaging cortical V1 and hippocampal CA1. Mice were anaesthetized in an induction chamber with 4% isoflurane until their breathing rate reached $\sim$1.5Hz at which time the isoflurane percentage was decreased to 2% and the induction chamber was flushed for 4 seconds. The animals were then placed in a stereotactic frame and secured with a heat mount (Kopf). Reflexes were checked to ensure adequate anaesthesia levels before subcutaneous injections of 0.9% saline (400 µL), the opioid analgesic buprenorphine (1.2 µg, 0.3mg/ml, Vetergesic, Ceva), the anti-inflammatory steroid dexamethasone (120 µg, 2mg/ml, Dexadreson, MSD Animal Health), and the non-steroidal anti-inflammatory meloxicam (6.2 µg, 0.5mg/ml, Metacam, Boehringer Inglehim) were administered to reduce de-

hydration, post-operative pain, and inflammation, respectively. Temperature was maintained at 37°C throughout using a homeothermic blanket (PhysioSuite, Kent Scientific Corporation).

Hair over the skull was first trimmed using scissors, before the remaining hair was removed with hair removal cream (Veet, Reckitt Benckiser). The exposed skin was cleaned with saline and then sterilised with ethanol and iodopovidone (Betadine, Mundipharma). The skin and periosteum over the skull were cut away and removed with small spring scissors and forceps across the entire dorsal skull surface. During this process, any bleeding was minimised using absorption spears (Fine Science Tools). Following removal, the edges of the skin were sealed to the the skull with surgical cyanoacrylate (Vetbond, 3M) before surgical calipers and a pen were used to mark a 3mm circle overlaying the visual cortex or hippocampus. The skull, excluding the marked region, was then roughened using a scalpel to create overlapping scores in perpendicular directions to aid in cement and head plate adhesion, before being covered in surgical cyanoacrylate. The mouse was then tilted on the head mount so that the area marked for the craniotomy laid flat. The roughened area was covered with dental cement (Unifast TRAD, GC; previously mixed with black acrylic) and a stainless steel head plate (designed and built in the University of Sussex workshop) was placed over the (still wet) dental cement and left for a few minutes until dry.

Following this, a dental drill (OmniDrill 35, World Precision Instruments) was used to drill around the edges of the marked area alternating between 0.5, 0.7, and 1mm drill bits as necessary (diameter at the tip, Fine Science Tools) ensuring that regular breaks were taken and that the area was frequently moistened with saline to prevent overheating of the brain. The area surrounding this was also flattened. Once the skull was thin enough, the bone was moistened with saline for a final time and then lifted off with forceps and a microprobe. Gelfoam (Pfizer) was used to stop any bleeding of the brain. Once bleeding halted, forceps were used to remove the dura (if it hadn't been removed during the craniotomy).

For visual cortex surgeries, an optical window (made from two 3mm glass coverslips and a 5mm glass coverslip, Harvard Apparatus) was placed into the craniotomy and secured using a glass rod whilst absorption spears were used to dry the liquid surrounding the window. The edges of the glass window were then sealed to the skull, first with surgical cyanoacrylate, then with dental cement. For hippocampal surgeries, $\sim$1.5mm of cortex was aspirated (New Askir 30, CA-MI Srl) until the striations of the corpus callosum (just above CA1 hippocampus) were visualised (see Dombeck et al. 2010 for detailed protocol). A 3mm round stainless-steel cannula (2.4mm ID, 3mm OD, 1.5mm height, Coopers Needle Works Ltd) with a 3mm glass coverslip attached (Harvard Apparatus) was inserted into the craniotomy and secured. Finally, for both surgery types, 2 rubber rings were secured on top of the head plate with dental cement to allow for two-photon

imaging using a water-based objective. Mice were removed from the head mount attached to the isoflurane machine and placed into a heat box (37°C) to recover, before being singly-housed in a recovery cage. For three days following the surgery mice were given daily 10 µg doses of meloxicam mixed into wet food mash.

2.5 *In Vivo* Experimental Set-up

A week after surgery mice implanted with windows for *in vivo* imaging were moved into a reverse light/dark cycle so that imaging during the day would not disrupt their circadian rhythms. *In vivo* imaging sessions took place at least 3 weeks following the surgery to allow enough time for the majority of reactive gliosis to subside (astrocytic and microglial responses to the surgery subside within 30 and 7-10 days of V1 window surgery respectively; Holtmaat et al. 2009, and 20 days of CA1 window surgery; Gu et al. 2014). Mice were gradually habituated to the two photon setup to reduce not only the detrimental effect of excessive movement on image collection, but also chronic restraint stress, given chronic stress can influence microglial morphology (Hinwood et al., 2013). This typically took place during the 3 weeks following surgery. Mice were head-fixed underneath a two-photon microscope (Scientifica) atop of a free-moving polystyrene cylinder that allowed voluntarily running during imaging sessions. This was fitted with a rotary encoder (Kubler) to measure locomotion. A combined laser doppler flowmetry/haemoglobin spectroscopy probe (Oxy-CBF probe; VMS Oxy, Moor Instruments) was also available to record haemodynamic parameters. In front of the mice were two computer screens (Asus) that were dark during microglial data acquisition and displayed drifting gratings (PsychoPy; spatial frequency of 0.04 cycles per degree, temporal frequency of 2Hz, gratings angled at 315°, bars sized at 220 degrees of visual space at a 17cm distance from the mouse) when collecting Oxy-CBF probe recordings from V1 window mice. Immediately prior to most imaging sessions mice were intravenously injected with 2.5% (w/v) Texas Red Dextran (70kDa, neutral, Invitrogen) to label blood plasma and visualise the vasculature. This involved warming the mice in a heat box to 37°C for 10 minutes to dilate blood vessels and increase their accessibility in the tail, before restraining and injecting the dye into a tail vein using an insulin syringe (BD Microfine). Alternatively, vessels were labelled through subcutaneous injection of 2.5% (w/v) Texas Red Dextran (3kDa, neutral, Invitrogen). A schematic of the experimental setup is presented in **Figure 2.1**. *In vivo* imaging was conducted a day before the beginning of dietary manipulation (D-1), and then at 2, 4, and 6 hours, as well as 1, 3, 7, 10, 14, 21, 30, 35, 42, 49, and 56 days, after the onset of diet manipulation. Oxy-CBF probe recordings were not conducted at the 2, 4, and 6 hour timepoints given they temporarily bleached

fluorescent signal.

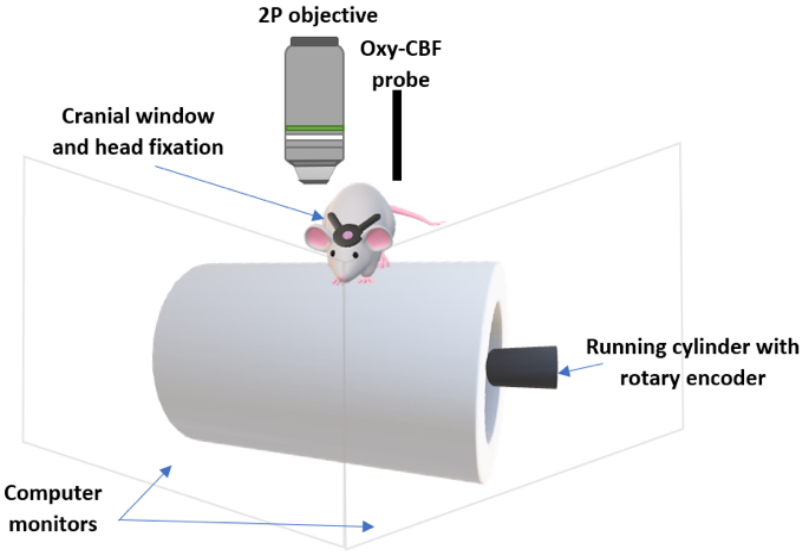

Figure 2.1: Experimental Setup Schematic.

2.6 Lipopolysaccharide-Induced Microglial Activation

Mice used for *in vivo* imaging were given intraperitoneal (i.p.) injections of LPS (O111:B4; Sigma-Aldrich) at a dosage of 4mg/kg in 0.9% saline to induce microglial activation at the end of imaging on the 56th day of dietary manipulation. 24 hours post-injection, two photon image stacks of microglia and Oxy-CBF probe recordings were collected. Microglia demonstrated profound morphological changes indicating an inflammatory response. Following imaging mice were culled using a terminal dose of i.p. sodium pentobarbital (Dolethal; Vétoquinol Ltd) at 120mg/kg (diluted to 10% in saline).

2.7 Statistical Analysis

Analysis was done using linear mixed models (LMM). Unlike ANOVAs, LMMs do not depend on limited assumptions about the variance-covariance matrix and can accommodate missing data, as well as allowing for the inclusion of different grouping configurations e.g. nested groups, partially crossed groups, and crossed groups. In an LMM variables are classified as fixed factors or random factors. Generally speaking, fixed factors are factors of experimental interest whilst random factors are factors that include a small sample of all possible levels e.g. subject ID or

animal number would typically be included as random factors. Random factors can have both random intercepts and random slopes specified, allowing for them to account for an interaction between the random factor and a fixed factor (see Magezi 2015 for its description of LMMs).

Data are reported as estimated marginal means +/- 1 standard error of the mean unless otherwise indicated. Estimated marginal means were extracted from the relevant LMM. The threshold for statistical significance was set at $p < 0.05$, with the threshold for a trend effect set at $p < 0.1$. All pairwise comparisons were done with a Bonferroni correction applied. All statistical analysis was done in R (R Core Team, 2013) in the RStudio environment (R Studio Team, 2015).

Chapter 3

Short-Term HFD-Induced Changes in Microglial and Vascular Function

3.1 Introduction

HFD feeding induces deficits in hippocampus-dependent cognition after only 24 hours (McLean et al., 2018) with impairments in hippocampus-independent non-spatial memory taking 30 days to appear (Kanoski and Davidson, 2010). The mechanisms responsible for this region-specific effect have yet to be established, with HFD either associated with unique hippocampal changes, or the elevated susceptibility of the hippocampus to damage (hypoxia; Ng et al. 1989, Alzheimer's Disease and ageing; reviewed in Fjell et al. 2014) translating global dietary effects into region-specific cognitive impairment. These deficits have been linked to both inflammatory and vascular changes. Inflammation could alter hippocampal processing either directly through the action of proinflammatory cytokines (Lynch, 2015; Barrientos et al., 2002; Goshen et al., 2007) or indirectly by inducing leptin and insulin resistance (briefly reviewed in Cordner and Tamashiro 2015) or promoting oxidative stress (microglia and oxidative stress reviewed in Lull and Block 2010). Others have suggested that changes in the vasculature such as a loss of BBB integrity (Cordner and Tamashiro, 2015), deficits in neurovascular coupling (Sorop et al., 2017), or pericyte dysfunction (Gomez-Smith et al., 2018), could mediate the effect of HFD on cognition. I evaluated the effect of short-term HFD-feeding on vascular and immune measures in the cortex, hippocampus, and hypothalamus, to assess their relative contributions to the reported early cognitive deficits and determine if they occurred in a region-specific or global manner. In addition, I tested mice on a hippocampus-specific test of cognitive function (NOCR) and correlated this with changes in hippocampal protein expression.

3.1.1 Hippocampus-Specific Novel Object-Context Recognition

Tests of hippocampal function run the gamut from the Morris water maze to conditioned inhibition tasks, though some require more distributed neural processing than others. To test hippocampus-specific cognition I opted to use a novel object-context recognition task. In this task animals are tested on their recognition of an object that is novel in a given context, but not novel outright. Whilst simple novel object recognition involves hippocampal, prefrontal and perirhinal cortical processing (novel object recognition briefly reviewed in Cordner and Tamashiro 2015), permanent hippocampal lesions impair novel object-context but not novel object recognition (Mumby et al., 2002). In addition, long-term object-context memory is reduced by the infusion of a protein synthesis inhibitor into the hippocampus, but not the perirhinal or insular cortices, or the amygdala (Balderas et al., 2008). McLean et al. (2018) report that HFDimpairs NOCR performance after only 48 hours of HFD feeding with other hippocampus-specific tasks showing deficits after 24 hours, though no impairment of simple novel object recognition was seen over the two weeks of the study.

3.1.2 Microglia and Inflammation

Neuroinflammation is associated with a decline in memory and has been linked to the cognitive deficits seen in overweight and obese individuals (reviewed in Miller and Spencer 2014). Microglia, the brain's resident immune cells, respond to damage and injury by proliferating and shifting their morphology from a resting, ramified phenotype, towards an amoeboid-like structure (Hanisch and Kettenmann, 2007). Their activation is usually accompanied by the production of cytokines, such as IL-1β and IL-6, which can disrupt the mechanisms involved in cognition and memory (Bellinger et al., 1995; Jankowsky and Patterson, 1999; Gemma and Bickford, 2007; Lynch, 2015). Activated microglia can also act as sources of ROS and promote oxidative stress (reviewed in Lull and Block 2010) which has been linked to impairments in hippocampal learning and memory. This may relate to changes in neurogenesis and spine density (Huang et al., 2015). Inflammation can also promote the development of leptin and insulin resistance (Romanatto et al., 2007) with their signalling pathways thought to be involved in hippocampal-dependent learning and memory (briefly reviewed in Cordner and Tamashiro 2015).

HFD feeding is associated with both central and peripheral inflammatory responses (reviewed in Lumeng and Saltiel 2011) where the former is driven either through the signalling of peripheral cytokines (Layé et al., 1994), the breakdown of the BBB and the entry of factors like IgG, thrombin, and fibrinogen that are proinflammatory (Tucsek et al., 2014a; Carreño-Müller et al.,

2003; Davalos et al., 2012), or, as appears to be the case in the hypothalamus, the stimulation of microglial TLR4 by SFAs (Milanski et al., 2009) that show postprandial influx into the region (Valdearcos et al., 2014). Changes in microglial morphology and density have been reported in the hypothalamus, hippocampus, and cortex, across a range of HFD studies (Thaler et al., 2012; Calvo-Ochoa et al., 2014; André et al., 2017; Zhou et al., 2018; Denver et al., 2018) and HFD-induced increases in the levels of proinflammatory cytokines have also been recorded (Liu et al., 2014; Thirumangalakudi et al., 2008; Pistell et al., 2010). However, there is also evidence for an absence of changes in cytokine levels (Kaczmarczyk et al., 2013) or microglial activation (Knight et al., 2014; Spencer et al., 2019; Baufeld et al., 2016; Bocarsly et al., 2015) within the first 8 weeks of HFD feeding.

3.1.3 The Blood-Brain Barrier

The BBB isolates the CNS from the rest of the body and is formed of specialised endothelial cells (Wolburg and Lippoldt, 2002) and tight junction proteins that are involved in barrier integrity (Huber et al., 2001). HFD-induced BBB breakdown has been associated with cognitive decline (Davidson et al., 2012; Kanoski et al., 2010) and is a hallmark of a number of CNS pathologies (reviewed in Hawkins and Davis 2005). The detection of endogenous IgG in the brain has been used to indicate BBB leakage (Saunders et al., 2015), and HFD-induced BBB breakdown has been seen to occur in number of studies (Davidson et al., 2012; Chang et al., 2014; Pallebage-Gamarallage et al., 2012; Elahy et al., 2015; Kanoski et al., 2010) with reports showing hippocampus-specific decreases in BBB integrity (Davidson et al., 2012; Kanoski et al., 2010) and reductions in the expression of tight junction proteins (hippocampus; Yamamoto et al. (2019); but not parietal cortex; Li et al. 2016).

Pericytes are vascular mural cells that not only regulate blood flow (Hall et al., 2014) but also maintain the integrity of the BBB. Reductions in their coverage of the vasculature correlate with increased rates of transport across the BBB and decreases in the expression of tight and adherens junction proteins (BBB reviewed in Haddad-Tóvolli et al. 2017). Models of pericyte deficiency clearly demonstrate the importance of pericytes in preventing neurodegeneration, with their loss promoting neuronal damage either through BBB disruption or leading to dysregulation of blood flow and the maintenance of normoxia (the role of pericytes in health and disease reviewed in Winkler et al. 2011). HFD feeding reduces their vascular coverage (Yamamoto et al., 2019; Tucsek et al., 2014b) and this correlates with the degree of cognitive impairment (Tucsek et al., 2014b).

GLUT1 plays a vital role in the transport of glucose into the brain and is situated at the BBB

(Vannucci et al., 1998) where it also plays a role in the maintenance of BBB integrity (Winkler et al., 2015). GLUT1 expression is altered to maintain constant levels of glucose availability (Fuente-Martiń et al., 2012) and it is sensitive to changes in oxygenation, with its levels increasing in response to hypoxia (Harik et al., 1996). GLUT1 expression is transiently decreased by HFD feeding, which correlates with a reduction in brain glucose levels (Jais et al., 2016). In a combined HFD and stroke model, this transient GLUT1 reduction was proposed to compromise tissue viability and lead to elevated levels of cell death following ischaemia (Haley et al., 2019), suggesting a HFD-induced and GLUT1-mediated increase in the susceptibility of neurons to damage could play a role in HFD-induced cognitive deficits.

3.1.4 Blood Supply and the Cerebrovasculature

Recent years have seen the importance of the vascular changes underlying pathologies such as Alzheimer's Disease (reviewed in de la Torre 2002) and ageing (briefly summarised in Le Couteur and Lakatta 2010) emphasised. Changes in the vasculature can impair the mechanisms that support neuronal metabolism through nutrient exchange and waste removal. HFD feeding has been shown to reduce vascular diameters (He et al., 2016; Constantinescu et al., 2011) and levels of blood flow (Glaser et al., 2012; Obadia et al., 2017), and though both increases and decreases in vascular density have been reported (decreases; Estato et al. 2017; Obadia et al. 2017; Tucsek et al. 2014b, increases; Yamamoto et al. 2019; Yi et al. 2012), they are both associated with cognitive impairment (Tucsek et al., 2014b; Coucha et al., 2019). Whilst the latter likely leads to cognitive impairment by reducing blood flow and metabolic support for neural signalling (Tucsek et al., 2014b), the former could be linked to unorganised, poorly perfused, leaky new vessels (as seen with upregulated vascular endothelial growth factor (VEGF) expression) that promote neuronal dysfunction (Coucha et al., 2019). HFD also impairs neurovascular coupling (Tucsek et al., 2014b; Li et al., 2013) and the ability of the vasculature to dilate in response to vasoactive signals (Obadia et al., 2017).

3.1.5 Aims, Hypotheses, and Experimental Approach

A number of mechanisms have been proposed to mediate the detrimental effect of HFD on cognition. However, few studies exist that have investigated these mechanisms at early enough timepoints in the hippocampus to be relevant to the rapid cognitive changes reported. As such, a significant gap in our understanding of the early effects of HFD feeding exists. Though Calvo-Ochoa et al. (2014) showed that HFD induces low levels of hippocampal inflammation after a

week of feeding, this is still too delayed to relate to the cognitive deficits seen after only 24 hours (McLean et al., 2018). Similarly, with regards to vascular changes, only GLUT1 expression has been evaluated within the first few days of dietary manipulation (Jais et al., 2016), with studies looking at changes in BBB integrity, pericyte coverage, and vascular structure and function within the first two weeks of dietary manipulation notably scarce or absent entirely. The earliest time at which BBB-related changes have been analysed appears to be one week, though this was limited to the hypothalamus (Rijnsburger et al., 2019).

I had multiple aims with the work presented in this chapter. The first was to investigate inflammatory and vascular changes that could be responsible for HFD-related cognitive impairment at an early timepoint in the hippocampus, in order to address the lack of studies that have looked at early hippocampal changes. Secondly, by investigating the hypothalamus, hippocampus, and cortex, I aimed to evaluate whether changes were taking place globally, or in a region-specific manner. In this way I could establish whether HFD-induced hippocampus-specific cognitive deficits were the result of hippocampus-specific dietary effects, or the translation of global effects into hippocampus-specific neuronal dysfunction owing to its enhanced susceptibility to pathology. Thirdly, I tested mice on the hippocampus-specific NOCR task with the aim of replicating previous unpublished work in may lab showing a deficit induced by HFD feeding, and correlating behavioural performance with protein levels from hippocampal lysates. Finally, I wanted to investigate if the reporter mutation I planned to use in future *in vivo* experiments (heterozygous Cx3CR1-GFP expression) influenced the effects of HFD feeding.

To achieve these aims I fed mice a HFD or control diet for two weeks. I chose the two week timepoint given this was the duration of feeding used in previous unpublished work from my group that showed a detrimental effect of HFD on NOCR, and this represents a time where cognitive impairments are still hippocampus-specific (Kanoski and Davidson (2010) suggests that HFD-induced cognitive impairments are hippocampus-specific for up to 30 days). This approach allowed me to investigate the relative importance of diet-induced inflammatory and vascular changes to early hippocampus-specific cognitive impairment. At the two week timepoint I tested mice on the NOCR task before using their hippocampal lysates to investigate correlations between behavioural performance and changes in the expression of a range of hippocampal proteins, including proinflammatory cytokines. In addition, I carried out post-mortem brain slice immunofluorescent analyses on three separate cohorts of mice to compare dietary effects between the cortex, hippocampus, and hypothalamus. Microglial activation, BBB integrity, pericyte coverage, GLUT1 expression, and capillary structure were quantified. Microglial activation was assessed by calculating their density and comparing their morphologies, and BBB integrity was determined by

measuring the levels of extravasated endogenous IgG. Pericyte coverage was quantified by measuring the distance between adjacent pericytes, and changes in the capillary bed were evaluated by measuring capillary density, radius, radius variance, and the proportion of capillary length perfused by a fluorescent gelatin perfusate. To address my final aim, I included a cohort of Cx3CR1-GFP heterozygotes in my immunofluorescence experiments.

3.2 Methods

3.2.1 Animals, Dietary Manipulation, and Experimental Approach

Details of animal genotypes, diets used, and behavioural testing, are presented in the main methods (**Chapter 2**). Results from two separate cohorts of mice are discussed in this chapter. Immunofluorescence data were collected from NG2-DsRed, and joint NG2-DsRed / Cx3CR1-GFP mutants. Where genotype differed in a given analysis it was included as a factor. The majority of data were collected from NG2-DsRed mice, with the joint NG2-DsRed / Cx3CR1-GFP mutants used in order to investigate the effect of the partial knockdown of the Cx3CR1 gene associated with the Cx3CR1-GFP mutation on responses to HFD feeding. This was important as the *in vivo* work described in the next two chapters is based on Cx3CR1-GFP mice, and prior to undertaking the *in vivo* work I wanted to investigate whether this mutation was associated with differential dietary effects.

Behavioural testing was conducted after I had completed my immunofluorescence experiments. This was done on a cohort of wild type C57BL/6J mice as well as Cx3CR1-GFP mutants that had received hippocampal window implantations and were being used for *in vivo* imaging experiments. To relate behavioural performance to protein expression data, behavioural analysis in this chapter was limited to 8 of the wild type mice that had hippocampal tissue collected for protein expression analysis. This involved excluding one wild type mouse from analysis, the details of which are in the statistical analysis section. Mice were given *ad libitum* access to water and either a HFD or control diet for two weeks and weighed daily, though the time of day at which weights were taken varied. Summary statistics of age, sex, and genotype split between the immunofluorescence and protein array / behavioural cohorts are displayed in **Table 3.1**. The issues regarding the use of mice varying in age, sex, and genotype, are described in the discussion.

	Protein Array / NOCR Cohort	Immunofluorescence Cohort
Genotype (Wild Type / NG2-DsRed / Cx3CR1-GFP)	8/0/0	0/44/18
Count (HFD)	8 (4)	62 (31)
Male : Female	5 : 3	27 : 35
Mean Age +/- SD (Weeks)	12.36 +/- 2.04	16.20 +/- 9.32

Table 3.1: Summary Statistics of Mice Used in Chapter 3. Statistics are presented split by cohort. **Genotype** indicates the number of mice of each genotype used, where Cx3CR1-GFP refers to joint NG2-DsReD/Cx3CR1-GFP mutants. **Count** indicates the total number of mice with those fed a HFD denoted in parentheses. **Male : Female** displays the ratio of male to female mice. **Age** represents age at the start of dietary manipulation, and is presented as the mean +/- 1 SD in units of weeks.

3.2.2 Immunofluorescence Protocol

For immunofluorescence imaging, at the end of the two weeks of dietary manipulation animals were i.p. injected with sodium pentobarbital (Dolethal; Vétoquinol Ltd) at 120mg/kg (diluted to 10% in saline). Once unresponsive to noxious stimuli, the chest cavity was opened and a needle was placed into the left ventricle. The right atrium was then cut before the animals were transcardially perfused with ice cold 0.1M phosphate buffer saline (PBS) for 5 minutes at a flow rate of 5ml/min (this flow rate was used for all perfusion steps).

Following the perfusion of ice cold PBS, animals were perfused with 75ml of ice cold 4% paraformaldehyde (PFA; Sigma-Aldrich) in 0.1 M PBS before this was switched to 10ml of PBS maintained at 30°C. This was followed by 15ml of a solution composed of 0.2% fluorescein isothiocyanate (FITC) conjugated albumin (Sigma-Aldrich) in 5% gelatine (Sigma-Aldrich) in PBS kept at 30°C. This was prepared according to the method in Lugo-Hernandez et al. (2017). Briefly, gelatin powder was dissolved in 0.1M PBS at 60°C, before the solution was cooled to 40°C with constant stirring. At this point the FITC-conjugated albumin was added before the solution was filtered through filter paper (GE Whatman) and stored at 30°C to prevent setting. After FITC-conjugated albumin perfusion, animals were placed head down on ice for 30 minutes to allow the gelatin solution to set. After setting brains were extracted and fixed in 4% PFA at 4°C overnight. Brains were then rinsed with PBS before being stored in a 30% sucrose and 0.1% sodium azide (Sigma-Aldrich) solution at 4°C for 48 hours. Coronal brain slices were then cut at 200 µm thickness using a vibrotome (Leica). This thickness was chosen to preserve the labelled vascular network within each slice.

All following steps were performed with gentle agitation with slices free-floating in 24 well plates. Slices were washed in PBS for three cycles at 10 minutes per cycle, before they were incubated in a blocking / permeabilisation solution (10% normal goat serum (Vector Laboratories), 0.05% Triton X-100 (Sigma-Aldrich), and 0.2M glycine (Sigma-Aldrich) in PBS) for 3 hours at room temperature. Following this, they were incubated with primary antibodies at appropriate dilutions in the blocking / permeabilisation solution overnight at room temperature before being washed in PBS for three cycles at 10 minutes per cycle. Incubation of slices with secondary antibodies diluted appropriately in PBS then took place at room temperature for 4 hours, before a final wash with PBS for three cycles at 10 minutes per cycle. Slices were mounted on slides (SuperFrost, Thermo Scientific) with coverslips (Menzel 24 x 60 mm 0.13 - 0.16mm, Thermo Scientific) using HardSet Vectashield (Vector Laboratories). Slides were modified with buffers made of 200 µm thick double sided tape (FiveSeasonStuff Limited) to minimise compression and distortion of the slices by coverslips.

Differences Between Immunofluorescence Studies

The immunofluorescence protocol for the first 14 mice analysed differed slightly. In this case, perfusion proceeded directly from ice cold PBS to FITC-conjugated albumin. Immediately after the gelatin had set, instead of incubating brains in PFA, they were extracted and sliced on the vibrotome prior to the slices being incubated free-floating in 500 µL of 4% PFA for 30 minutes before being washed three times for ten minutes per wash with PBS. At this point the slices were subjected to the same washing, blocking/permeabilisation, and antibody incubation steps. Additionally, the slides used for imaging did not have the 200 µm buffers. These methodological differences were accounted for in the statistical analysis of results.

The protocol also differed slightly for the NG2-DsRed/Cx3CR1-GFP mice, given the overlap in emission spectra between FITC and GFP. These mice had their brains collected and stored in PFA immediately after termination of the PFA perfusion step, and were not perfused with the FITC-conjugate solution.

3.2.3 Antibodies

Primary antibodies used were rabbit anti-Iba1 (1:1000, Synaptic Systems, 234 003; 1:500, WAKO, 019-19741), biotinylated horse anti-mouse IgG (1:500, Vector Laboratories, BA-2000), and rabbit anti-GLUT1 (1:500, Abcam, ab15309). Secondary antibodies used were goat anti-rabbit Alex Fluor 405, 647, 633 (1:1000, Invitrogen; A31556, A21245, A21071), and streptavidin Alexa Fluor

647 (1:500, Invitrogen, S32357).

3.2.4 Immunofluorescence Image Capture

All imaging was done blind to mouse identity and dietary manipulation. Images were taken using a 20X objective (HC PL APO CS2 20X/0.75, Leica Microsystems) on an inverted Leica SP8 TCS confocal microscope (Leica Microsystems). Continuous wave lasers with 405, 488, 561, and 633 nm excitation wavelengths were used. Images were collected using a 1024 x 1024 pixel matrix with line averaging of 16, and a depth of 8-bit. Images were collected in z-stacks with a z distance of 0.69 µm, and pixel sizes in the x and y directions of 0.57 µm. All image analysis was done using the Fiji distribution of ImageJ (Schindelin et al., 2012). Given results are presented as a combination of three separate immunofluorescence studies, different levels of laser power and photodetector gain were used. This was accounted for in the statistical analysis of results.

Three z-stacks were taken for each brain region (hippocampus, cortex, and hypothalamus) for each animal, with each region only being imaged a single time per slice. Generally, imaging and analysis was restricted to hippocampal CA1, cortical V1, and the hypothalamic ARC, though occasionally adjacent subregions were included.

Pericyte coverage was quantified in NG2-DsRed mice. Microglial density and morphology was quantified using Iba1 staining of slices, or through the endogenous expression of Cx3CR1-GFP. GLUT1 and IgG staining intensity were analysed in slices incubated with anti-GLUT1 and anti-mouse IgG antibodies. Vascular morphology was assessed in slices where vessels had been labelled through the perfusion of FITC-conjugated albumin.

3.2.5 Immunofluorescence Image Quantification

Image analysis was done blind to mouse identity and dietary manipulation. NG2-labelled pericytes were identified by their distinct morphology and association with blood vessels, and assessed using the criteria outlined in Grant et al. (2019). Pericyte coverage was quantified by measuring the inter-soma distance (ISD) between adjacent pericytes. This was only done for NG2 positive cells present on vessel branches that were two or more branches from penetrating arterioles in order to restrict analysis to the capillary bed. The ISD was calculated in composite z-stacks by tracing along vessels between pericyte cell bodies, and distance was calculated in 2D.

Vessel length and radius were calculated by taking maximum z projections of the composite z-stacks before thresholding the FITC signal manually. A region of interest (ROI) was then drawn

on the image to exclude vessels that were less than two branches away from penetrating arterioles. The length of FITC labelled vessels within the ROI was calculated by skeletonising the image, with the length of the skeleton taken as a measure of vessel length in 2D. To calculate vessel radius and vessel radius variance a Euclidean distance map of the image was computed and the associated skeleton was used as a ROI to measure the mean grey value and its standard deviation along the centre of the vessels in the Euclidean distance map. The grey value along the skeleton represents the 2D radius of the vessels.

Microglia were counted as Iba1 or Cx3CR1 labelled cells using the cell counter plugin in ImageJ, and microglial morphology was quantified by tracing microglial cells using the Simple Neurite Tracer plugin (Longair et al., 2011) for ImageJ. Microglial density was calculated by dividing the number of microglia by the volume of tissue analysed, whilst microglial morphology was quantified by measuring the number of processes at varying distances from the centre of the microglial soma. These values were binned by 1 µm.

GLUT1 and IgG staining intensity analyses were limited to vascular ROIs drawn using FITC signal as a mask. This was done as GLUT1 is vessel associated (Vannucci et al., 1998) and IgG staining was seen mainly on vessels. Mean intensity values were computed, before having the average mean grey value of no-primary stained control slices subtracted in an animal and region-specific manner. These background corrected values were then used in analysis.

FITC signal showed incomplete perfusion of the vascular bed, with segments of non-perfused vasculature situated between perfused areas. As such, 2D traces of these non-perfused segments were added on to the measure of vessel length obtained through FITC thresholding to calculate a total vessel length. The orientation of pericyte processes, as well as the use of z-stacks, enabled identification and tracing of these segments. Total vessel length was normalised to the volume of tissue analysed. The proportion of this total vessel length that was perfused was also computed.

The distribution of the proportion of total vessel length perfused showed more of a bimodal than normal distribution. To facilitate analysis of this data using logistic regression, perfusion proportions of less than 50% were classified as "low perfusion", whilst proportions greater than or equal to 50% were classified as "high perfusion".

3.2.6 Protein Profiler Array

Hippocampi were collected from wild type mice following the completion of NOCR behavioural testing and processed for use with the Mouse Cytokine Array C1000 kit (AAM-CYT-3, Ray Biotech). Briefly, brains were removed and hippocampi were dissected out following cervical dislo-

cation. These were weighed and then homogenised in homogenisation buffer composed of 0.1M PBS with 10 µg/ml of protease inhibitors (Protease Inhibitor Cocktail, Abcam, ab65621). After homogenisation, Triton X-100 was added to a final concentration of 1%, before samples were frozen at -80°C. Following this, samples were thawed, centrifuged at 10,000g for 5 minutes, and protein concentrations were quantified using a bicinchoninic acid (BCA) assay (Pierce BCA Protein Assay Kit, Life Technologies). The protein array was then performed according to the manufacturer's instructions and arrays were loaded with 500 µg of protein. Blot images were analysed in ImageJ, where the intensity of the signal for each spot had local background values subtracted. The background corrected values were then normalised to the value of the positive control spots on the same array. The assay, and image analysis, was performed blinded to mouse identity and dietary manipulation.

3.2.7 Statistical Analysis

As stated in the main methods chapter, all analyses were run using LMMs, and all plotted values represent the estimated marginal mean +/- 1 SEM derived from the appropriate LMM, unless otherwise indicated. Images were used as subjects in the analysis of the immunofluorescence data. Mice were used as subjects in the analysis of weight gain and behavioural data. Individual protein level readings were used as subjects in the protein array analysis. Where mice weren't used as subjects this was accounted for by including a random effect structure in the statistical model that grouped measurements by animal in the relevant LMMs.

For the analysis of weight changes, to control for differences in starting weight, the weight of mice as a proportion of their starting weight was compared over the two week dietary timecourse. Here fixed effects were specified as diet, day, and their interaction. Sex and age, and their full interactions with diet and day, were included. Random intercepts were included to account for different levels of dataset (i.e. immunofluorescence or protein array / behavioural cohorts), study (i.e. immunofluorescence study 1, 2, or 3), and animals within each study. An autoregressive order 1 model was included to account for the correlation in values between adjacent time points.

Analysis of immunofluorescence results was done using diet and region, and their interaction, as fixed effects. A random intercept for different studies, and animals nested within study, was included. In addition, a random slope for region was included to account for variation in the relationship between regions across studies and animals. A compound symmetry correlation structure was used to account for the repeated measures of different brain regions within an animal. Sex, age, and weight gain, and their interactions with diet, were included as factors. For measures

where mice differed by genotype or diet pairings, their main effects, and interactions with diet, were also included. Images were used as subjects in the analysis.

NOCR performance was analysed with diet as a fixed effect, and with the main effects of sex and age, and their interactions with diet, included. A random intercept for animal was included.

Changes in protein levels measured using the protein array were analysed by including diet, NOCR performance, and their interaction, as fixed effects. NOCR performance was included to investigate the relationship between protein expression levels and cognitive performance. A random intercept for animal was included. Given the number of proteins analysed (62) the p values of the effects of diet, NOCR performance, and their interaction, derived from the LMMs, were adjusted using the Bonferroni correction for multiple comparisons. Each protein array provided duplicate measurements of protein levels. Each replicate was used as a subject in the analysis.

After quantifying total vessel length, images where the proportion of this that was labelled (i.e. perfused) by FITC was less than 50% were classified as "low perfusion", with those showing greater than 50% perfusion classified as "high perfusion". This distribution was analysed using logistic regression. Diet, region, and their interaction, were included as fixed factors, as were the main effects of sex, age, and weight change. The predict function in R was used to calculate classification probabilities.

In order to reduce the dimensionality of the microglial morphology data, the approach taken in Heindl et al. (2018) was used. A principle component analysis (PCA) with centering and scaling of features was run on the morphology measurements. The first principal component, which by definition reflects the greatest level of variability in the data, was used as a single value reflecting a 'morphology index', and this was analysed with an LMM as in the immunofluorescence analysis description.

One animal was excluded from analysis in order to link protein array results (n = 8) to behavioural results (n = 9; n = 8 with exclusion). This meant that this animal was also excluded from the analysis of weight changes. As the NOCR experiment was run with uneven groups (n = 5 for control, n = 4 for HFD), the excluded mouse was a control diet subject that had the lowest NI in the control group, which fell outside the mean +/- SD for control animals (mean = 0.178, SD = 0.061, excluded value = 0.0758).

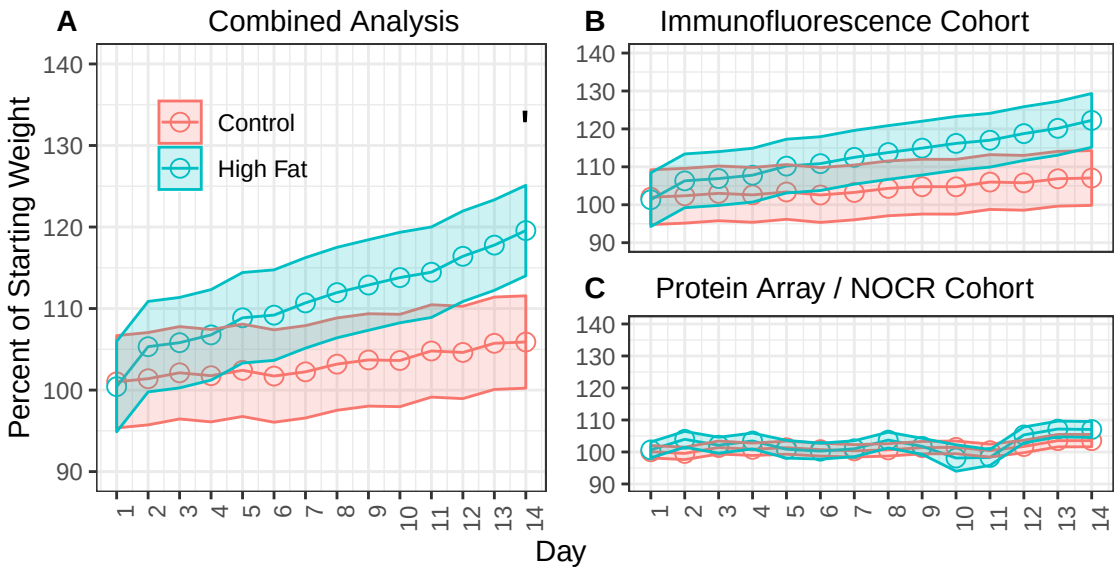

Figure 3.1: Two Weeks of HFD Increases Weight. (**A**) Weight normalised to starting values showed a trend level increase after two weeks of HFD feeding in the combined analysis, and the rate of weight gain was significantly increased by HFD. (**B**) Restricting analysis to the mice used in immunofluorescence experiments showed a persistent effect of HFD on rate of weight gain, though here the increased weight at day 14 no longer reached trend level. (**C**) The mice used in the protein array / NOCR behavioural test showed none of the effects of diet seen in the combined or immunofluorescence analyses (' indicates $p < 0.1$. Combined analysis n = 70 mice (n = 35 HFD), immunofluorescence cohort n = 62 mice (n = 31 HFD), protein array cohort n = 8 mice (n = 4 HFD)).

3.3 Results

3.3.1 Two Weeks of HFD Increases Weight Gain and the Rate of Weight Gain

HFD feeding promotes weight gain, though cognitive impairments associated with HFD feeding in rodents have been reported both with and without significant changes in weight. To assess the effect of diet on weight gain in my model, mice were weighed daily. To control for differences in starting weight, weight was normalised to its starting value and compared over the two week timecourse (**Fig 3.1**). Analysis of the timecourse revealed a significant positive correlation between time and weight gain ($F(13,788) = 6.74$, $p = < 0.001$). Additionally, there was a significant interaction between time and diet whereby HFD mice gained weight at a greater rate than control mice ($F(13,788) = 3.01$, $p = 0.004$). Corrected pairwise comparisons revealed a trend level increase in the weight of HFD animals at day 14 (**Fig 3.1 A**; $t(61) = 2.81$, $p = 0.094$).

Given the data in this chapter are split between mice used for immunofluorescence and those used in protein array / behavioural analyses, the effect of diet on weight gain in each group was analysed. In the immunofluorescence cohort (**Fig 3.1 B**) the significant effects of time ($F(13,696) = 6.14$, $p = < 0.001$) and diet by time ($F(13,696) = 2.72$, $p = < 0.001$) were present. However,

the trend level increase in weight seen in the HFD group at day 14 in the combined dataset was no longer present (though this was near trend level; *t(54) = 2.80, p = 0.101*).

The protein array / behavioural cohort (**Fig 3.1 C**) also showed a significant effect of time (*F(13,27) = 3.04, p = 0.007*). However, the interaction between time and diet was not significant. As in the immunofluorescence analysis, weight did not significantly differ between dietary groups at any timepoint in either dataset.

Results therefore suggest that weight increased over the timecourse of dietary manipulation, but whilst HFD feeding induced an increased rate of weight gain in the animals used in the immunofluorescence experiments, this was not the case in the protein array / behavioural cohort of mice. A chi-squared test was carried out comparing the distribution of sexes between the protein / behavioural and immunofluorescence cohorts to see if this could account for the lack of a diet by time interaction in the former. This was non-significant $X^2(1, N = 70) = 0.39, p = 0.534$. Similarly, age did not vary significantly between the two cohorts (*F(1,2) = 0.00, p = 0.963*).

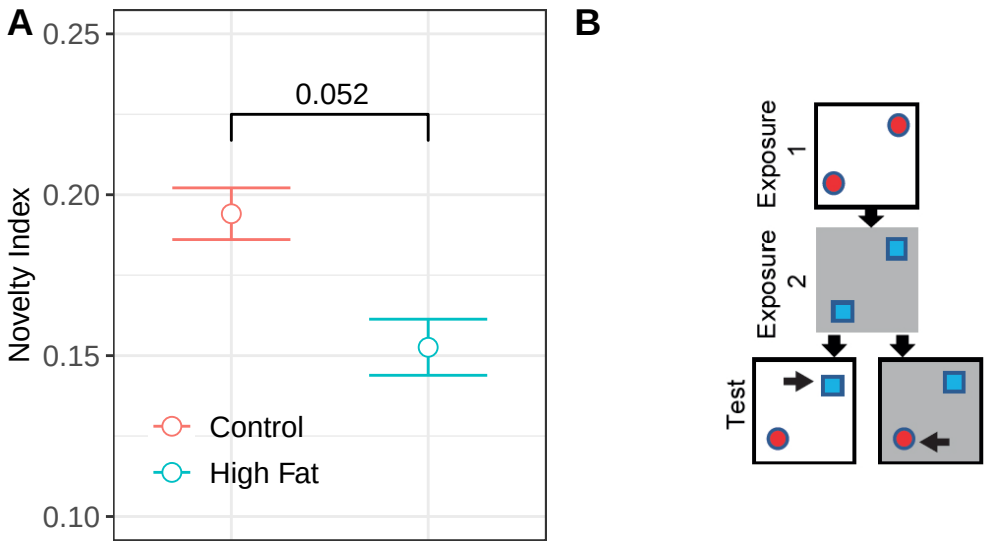

Figure 3.2: HFD Impairs NOCR Performance. (**A**) Mice fed a HFD for two weeks and tested on NOCR showed a trend level decrease in NI, indicating impaired hippocampal cognition. (**B**) The task involved mice learning to associate object pairs with contexts (**Exposure**) before one object from each pair was swapped and the time mice spent exploring objects that were novel in a given context (**Test**) was analysed (number on brackets indicates p value of the main effect of diet on NI, n = 8 mice (n = 4 HFD)).

3.3.2 HFD Mice Trended Towards Impaired Hippocampal Cognition

Short-term HFD feeding is associated with hippocampus-specific cognitive deficits (McLean et al., 2018; Kanoski and Davidson, 2010). In order to investigate this in my model and correlate it with changes detected in the immunofluorescence data, I tested mice on NOCR performance. The hippocampal-specific nature of the NOCR task is described briefly in the introduction to this chapter, and the assessment of performance using a novelty index (NI) is described in the main methods chapter. Results showed that HFD animals trended towards a lower NI (**Fig 3.2 A**, *F(1,1) = 147.01, p = 0.052*) than control animals.

3.3.3 Short-Term HFD Does Not Alter Hippocampal Protein Expression

Hippocampal inflammatory cytokine levels in HFD studies have been demonstrated to both correlate with (Liu et al., 2014), and show no correlation with (Kaczmarczyk et al., 2013), cognitive impairment. To investigate this I collected hippocampal lysates from mice that had undergone NOCR behavioural testing, and analysed them using a protein array to look at changes in expression across a broad range of proteins, inflammatory cytokines included. NOCR performance values (NI) were included as a factor in the analysis of protein changes to investigate any possible correlation. After correcting for multiple comparisons there were no significant effects of diet, NOCR performance, nor their interaction, on the levels of hippocampal protein expression (**Table 3.2**). This may reflect an underpowered experiment rather than an experimental effect however, given that there were only four mice per diet group, but the absence of any change in such a broad range of proteins, many of them inflammation-related, suggests a lack of diet-induced inflammation in the hippocampus.

3.3.4 Microglial Cell Density was Increased by HFD

Microglial proliferation is a key component of the damage response in the brain and is widely documented in HFD research (Thaler et al., 2012; André et al., 2017; Zhou et al., 2018). I calculated the density of microglial cells by dividing their number by the volume of tissue analysed. Two weeks of HFD induced a significant increase in microglial density (**Fig 3.3 C**; *F(1,33) = 4.40, p = 0.044*). Given the inclusion of data from NG2-DsRed/Cx3CR1-GFP mice in the analysis (in order to investigate the effect of heterozygous Cx3CR1-GFP expression given this mutation was to be used in future *in vivo* work), genotype was included as a factor. This showed a significant effect on microglial density (*F(1,33) = 7.05, p = 0.012*) where NG2-DsRed/Cx3CR1-GFP mice had greater

Protein	Novelty Index	Diet	Diet:Novelty Index	Protein	Novelty Index	Diet	Diet:Novelty Index
Axl	0.995	0.327	0.706	Il-6	0.262	0.104	0.142
BLC	0.976	0.564	0.987	IL-9	0.372	0.699	0.979
CD30	0.874	0.659	0.823	KC	0.384	0.360	0.533
CD30 Ligand	0.307	0.290	0.398	L Selectin	0.562	0.993	0.424
CD40	0.489	0.390	0.586	Leptin	0.640	0.451	0.275
CRG-2	0.882	0.660	0.474	Lepth R	0.835	0.554	0.333
CTACK	0.084	0.547	0.344	LIX	0.540	0.138	0.542
CXCL16	0.251	0.602	0.343	Ltn	0.863	0.521	0.937
Eotaxin-1	0.200	0.041	0.182	M-CSF	0.506	0.393	0.743
Exotaxin-2	0.792	0.900	0.220	MCP-1	0.493	0.579	0.848
Fas Ligand	0.455	0.735	0.185	MCP-5	0.280	0.401	0.996
Fractalkine	0.900	0.359	0.790	MIG	0.348	0.816	0.973
GCSF	0.336	0.570	0.213	MIP-1 Alpha	0.695	0.211	0.938
GM-CSF	0.832	0.904	0.455	MIP-1 Gamma	0.673	0.545	0.480
I-309	0.917	0.544	0.809	MIP-2	0.669	0.421	0.582
IFN-Gamma	0.343	0.490	0.496	MIP-3 Alpha	0.381	0.668	0.554
IGFBP-3	0.933	0.177	0.464	MIP-3 Beta	0.328	0.984	0.364
IGFBP-5	0.084	0.458	0.057	P-Selectin	0.945	0.922	0.471
IGFBP-6	0.820	0.378	0.669	PF-4	0.548	0.793	0.754
IL-1 Alpha	0.904	0.664	0.381	RANTES	0.256	0.741	0.202
IL-1 Beta	0.995	0.176	0.947	SCF	0.341	0.263	0.836
IL-10	0.962	0.291	0.456	SDF-1 Alpha	0.370	0.925	0.342
IL-12 p40/p70	0.834	0.750	0.984	TARC	0.726	0.156	0.197
IL-12 p70	0.668	0.294	0.660	TECK	0.308	0.579	0.555
IL-13	0.549	0.202	0.180	TMP-1	0.469	0.606	0.725
IL-17A	0.917	0.595	0.262	TNFAlpha	0.478	0.921	0.319
IL-2	0.600	0.201	0.209	TNF R1	0.530	0.921	0.319
IL-3	0.373	0.510	0.271	TNFR2	0.178	0.854	0.591
IL-3 R Beta	0.355	0.044	0.990	TPO	0.757	0.681	0.382
IL-4	0.381	0.587	0.899	VCAM-1	0.340	0.745	0.379
IL-5	0.639	0.740	0.425	VEGF-A	0.728	0.773	0.926

Table 3.2: Hippocampal Protein Levels are Unaffected by HFD. Unadjusted p values for each measured protein for NI, diet, and the interaction between diet and NI (Diet:Novelty Index) are listed. Once adjusted for multiple comparisons no effects reached significance (**Darker shading** indicates larger values. **Red text** indicates $p < .05$. **Green text** indicates $p < 0.1$. Analysis used n = 16 readings per protein (n = 8 HFD) where readings were taken in duplicate for each mouse; n = 8 mice (n = 4 HFD))

microglial densities than NG2-DsRed animals. This is likely the result of clearer microglial labelling by endogenous GFP expression in the NG2-DsRed/Cx3CR1-GFP mice compared to the use of the Iba1 antibody in NG2-DsRed animals. Results of the statistical analysis of diet, region, and their interaction, are presented in **Table 3.3**.

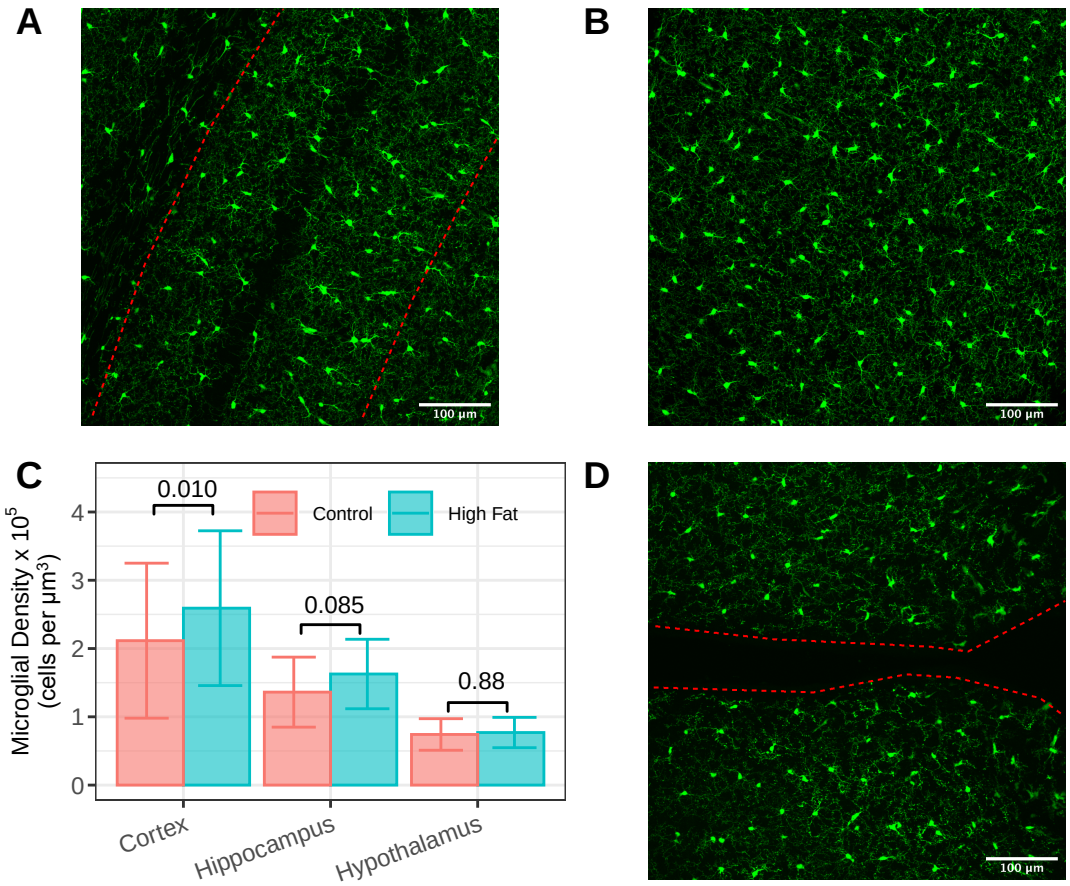

Figure 3.3: Short-Term HFD Increases Microglial Density. (**A, B, D**) Cx3CR1-GFP labelled microglial cells in the hippocampus, cortex, and hypothalamus respectively, with red lines denoting hippocampal CA1 and the third ventricle. (**C**) Microglial density was elevated globally by HFD feeding. Though the effect of diet appeared to differ in strength between regions, the interaction between diet and region was not significant in the overall model (numbers on brackets indicate pairwise corrected dietary comparisons, analysis used n = 571 images (n = 218 cortex, n = 243 hippocampus, n = 110 hypothalamus; n = 303 HFD) that were taken over n = 46 mice (n = 24 HFD)).

numDF	denDF	F-value	P-value	Factor	Sig
1	33	4.40	0.044	Diet	*
2	521	1.53	0.218	Region	
2	521	1.74	0.176	Diet:Region	

Table 3.3: Short-Term HFD Microglial Density Statistics. The effects of diet, region, and their interaction, on microglial density were analysed using an LMM (numDF and denDF refer to degrees of freedom. F and p values are rounded to 4 decimal places. **Red text** indicates significance. **Green text** indicates trend level. **Background shading** indicates size of p value where darker is larger. Sig shows significance indicator. Factor indicates factors in the model).

3.3.5 Using Dimensionality Reduction to Create a Compound Morphology Score

Microglial activation correlates not only with changes in proliferation and cell density, but also in morphological changes. Cell morphology was quantified by counting the number of branches at increasing distances from the centre of the cell soma. Not surprisingly these values showed a high degree of multicolinearity given their adjacency in space (**Fig 3.4 F**). As a result, the approach used by Heindl et al. (2018) was taken, where the dimensionality of microglial morphology measurements was reduced by using the first PC (PC1) of a PCA run on the data as a compound morphology score. The first two PCs explained 74.6% of the total variance in the data, and the PC1 essentially reflected the mean number of branches (**Fig 3.4 C**) with a significant Pearson's correlation between them $r(265) = 0.99,\ p = < 0.001$. As a result, the PC1 was used as a compound measure of morphology.

3.3.6 Short-Term HFD Does Not Alter Microglial Morphology

Microglia shift their phenotype from a ramified to an amoeboid shape in response to injury, which correlates with the extent of microglial activation (Hanisch and Kettenmann, 2007). An analysis of the compound morphology score (**Fig 3.4 B**), which correlated with the mean number of branches on a microglial cell (**Fig 3.4 C**), showed no effect of diet ($F(1,20) = 0.07,\ p = 0.799$) nor region ($F(2,234) = 1.89,\ p = 0.154$) on morphology.

3.3.7 HFD Did Not Effect BBB Integrity and GLUT1 Expression

GLUT1 is involved in glucose uptake into the brain as well as BBB integrity, and has been shown to be transiently downregulated by short-term HFD feeding (Jais et al., 2016). A change in GLUT1 expression could make neurons more susceptible to the other detrimental effects of a HFD, and indeed HFD feeding associated GLUT1 changes are implicated in the enhanced susceptibility of HFD animals to ischaemic damage (Haley et al., 2019). GLUT1 expression levels, as assessed by the intensity of GLUT1 staining, were unaffected by diet (**Fig 3.5 C**; $F(1,3) = < 0.01,\ p = 0.997$) and showed no diet by region interaction ($F(2,\ 67) = 0.46,\ p = 0.635$) though did vary significantly by region ($F(2,67) = 5.63,\ p = 0.006$) where corrected pairwise tests revealed greater GLUT1 staining in the hypothalamus relative to the hippocampus ($t(67) = 3.13,\ p = 0.008$) and the cortex (at trend level; $t(67) = 2.39,\ p = 0.059$). Results of the statistical analysis of diet, region, and their interaction, are presented in **Table 3.4**.

The detection of endogenous plasma proteins in the brain, including IgG, has been used to

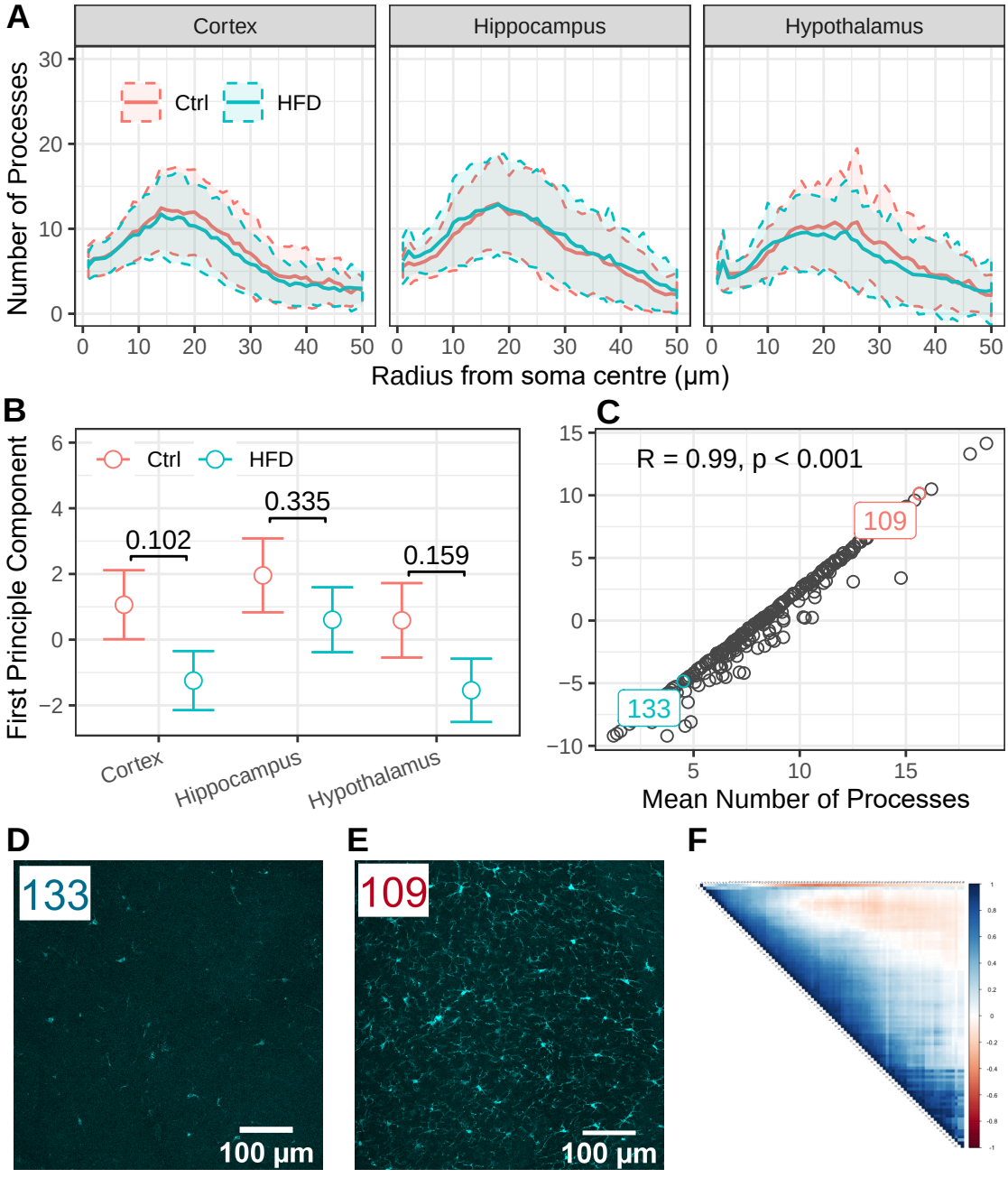

Figure 3.4 Legend on the following page. .

numDF	denDF	F-value	P-value	Factor	Sig
1	3	0.00	0.997	Diet	
2	67	5.63	0.006	Region	**
2	67	0.46	0.635	Diet:Region	

Table 3.4: Short-Term HFD GLUT1 Intensity Statistics. The effects of diet, region, and their interaction, on GLUT1 intensity were analysed using an LMM (numDF and denDF refer to degrees of freedom. F and p values are rounded to 4 decimal places. **Red text** indicates significance. **Green text** indicates trend level. **Background shading** indicates size of p value where darker is larger. Sig shows significance indicator. Factor indicates factors in the model).

evaluate changes in BBB integrity (Saunders et al., 2015), with HFD-induced BBB disruption being suggested to mediate its detrimental cognitive effects (cognitive effects of HFD reviewed in Cordner and Tamashiro 2015). IgG staining intensity (**Fig 3.6**) was greatest on vessels so analysis was conducted within vessel ROIs. This was interpreted as reflecting extravasated IgG molecules, given the vascular lumen had been cleared by perfusion. There was no effect of diet ($F(1,4) = 3.37$, $p = 0.140$), region ($F(2,90) = 2.22$, $p = 0.114$), nor any interaction between the two ($F(2,90) = 0.68$, $p = 0.511$) on the levels of IgG staining intensity. Results of the statistical analysis of diet, region, and their interaction, are presented in **Table 3.5**. IgG staining intensity in the brain parencyhma was also analysed (excluding vessels). This showed no effect of diet, region, or any interaction between the two (data not shown).

Figure 3.4 *(preceding page)*: Microglial Morphology is Resistant to Short-Term Dietary Effects. (**A**) Microglial morphology was quantified by counting the number of processes at increasing distances from the centre of the microglial soma. (**B**) These measurements showed a high degree of multicolinearity, so a PCA was used to reduce their dimensionality and the PC1 was used as a compound morphology score. This showed no effect of diet or region. (**C**) The compound morphology score showed an incredibly strong correlation with the mean number of branches on microglial cells. (**D, E**) Illustrative images of microglial morphology showing cells that had a low number of mean branches and a negative PC1 value, compared to cells with a high mean number of branches and a positive PC1 value. Numbers on the images refer to numbers in **C**. (**F**) The correlation matrix of raw morphology measurements (blue indicates a correlation of 1, red of -1, distance from soma centre increases from top left outwards (**A** solid line indicates mean, dashed line indicates SD. **B** numbers indicate p values of corrected pairwise dietary comparisons. **C** text shows correlation values. Analysis used n = 267 cells (n = 71 cortex, n = 121 hippocampus, n = 75 hypothalamus; n = 134 HFD) that were taken from n = 29 mice (n = 15 HFD))

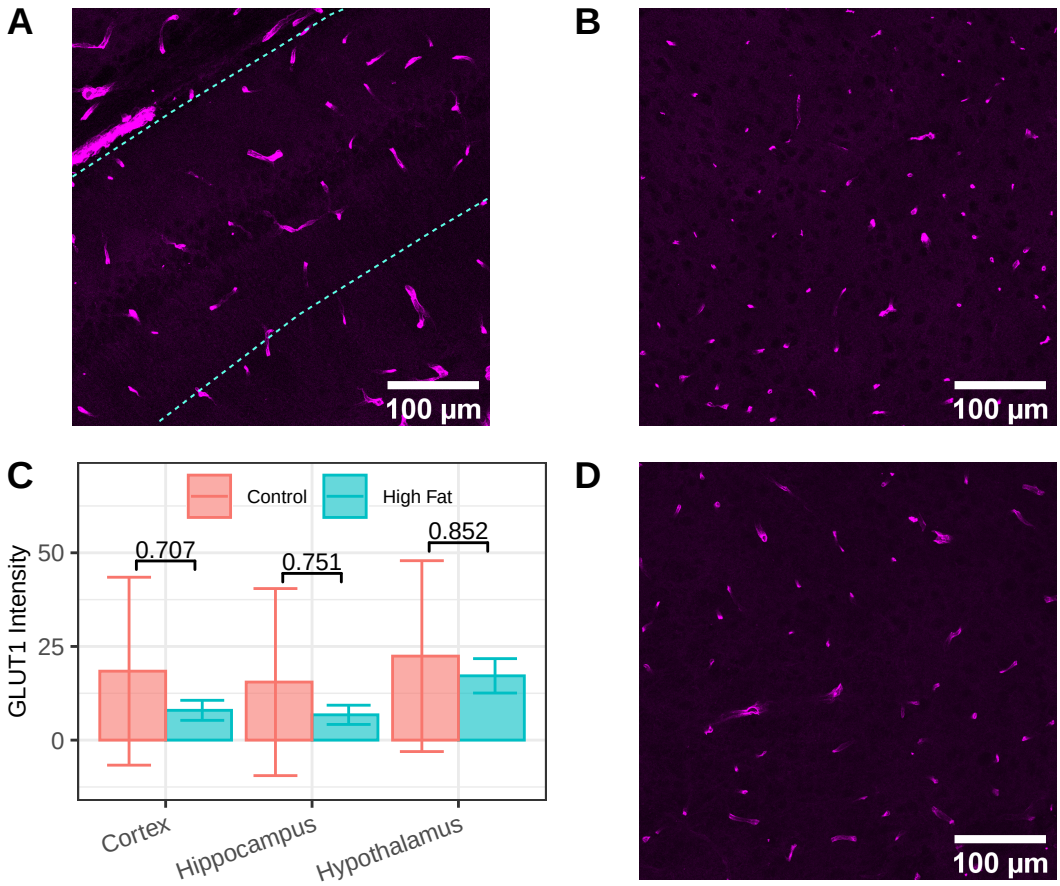

Figure 3.5: GLUT1 Expression is Unaffected Following Two Weeks of HFD. (**A, B, D**) GLUT1 labelling in the hippocampus, cortex, and hypothalamus respectively, with blue lines denoting hippocampal CA1. (**C**) GLUT1 intensity was unaffected by diet but varied between regions (numbers on brackets indicate pairwise corrected dietary comparisons, analysis used n = 82 images (n = 25 cortex, n = 27 hippocampus, n = 30 hypothalamus; n = 56 HFD) that were taken over n = 11 mice (n = 7 HFD)).

numDF	denDF	F-value	P-value	Factor	Sig
1	4	3.37	0.140	Diet	
2	90	2.22	0.114	Region	
2	90	0.68	0.511	Diet:Region	

Table 3.5: Short-Term HFD IgG Intensity Statistics. The effects of diet, region, and their interaction, on vessel-associated IgG intensity were analysed using an LMM (numDF and denDF refer to degrees of freedom. F and p values are rounded to 4 decimal places. **Red text** indicates significance. **Green text** indicates trend level. **Background shading** indicates size of p value where darker is larger. Sig shows significance indicator. Factor indicates factors in the model).

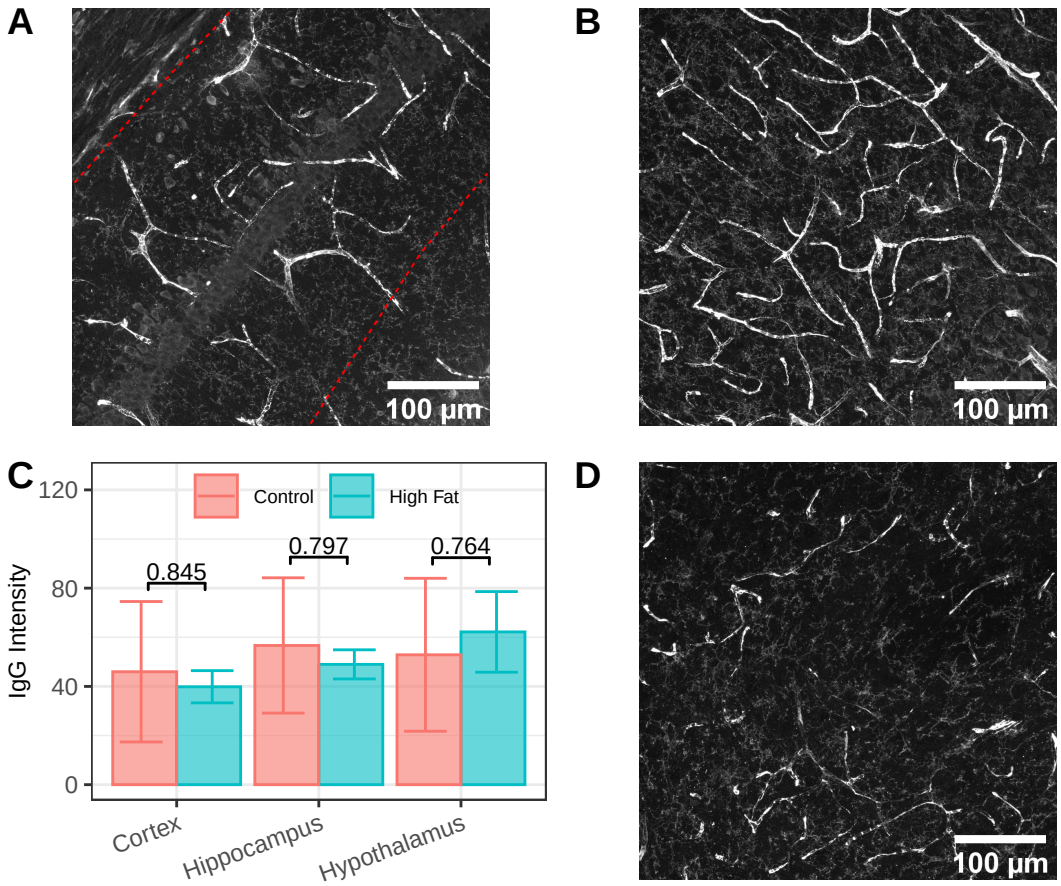

Figure 3.6: HFD Did Not Affect BBB Integrity. (**A, B, D**) IgG labelling in the hippocampus, cortex, and hypothalamus respectively, with red lines denoting hippocampal CA1. (**C**) Vessel-associated IgG intensity did not differ by brain region or dietary manipulation (numbers on brackets indicate pairwise corrected dietary comparisons, analysis used n = 107 images (n = 30 cortex, n = 41 hippocampus, n = 36 hypothalamus; n = 65 HFD) that were taken over n = 13 mice (n = 8 HFD)).

3.3.8 Pericyte Coverage is Smallest in the Hippocampus and Resistant to Short-Term HFD

Pericytes are vascular mural cells that are involved in regulating blood flow, maintaining BBB integrity, and stabilising newly formed capillaries. Hippocampal pericytes have been observed to occupy less volume and cover less of the vascular area during long-term HFD feeding (Yamamoto et al., 2019; Tucsek et al., 2014b), with this implicated in cognitive deficits. Pericyte coverage in my data was assessed by measuring the distance between adjacent NG2-DsRed labelled pericyte somas (**Fig 3.7 A Inset**). The advantage of using inter-soma distance (ISD) rather than pericyte cell density or number to investigate changes in pericytes is that it is independent of differences in vascular density. Pericytes were only measured on capillaries (vessels that were two or more branches away from penetrating arterioles) and identified by their distinct 'bump on a log' mor-

phology using NG2 labelling. Care was taken to avoid including ensheathing pericytes, smooth muscle cells, and oligodendrocyte precursor cells, all of which also express NG2 but are morphologically distinct from capillary pericytes. Pericyte subtypes are described in Grant et al. (2019).

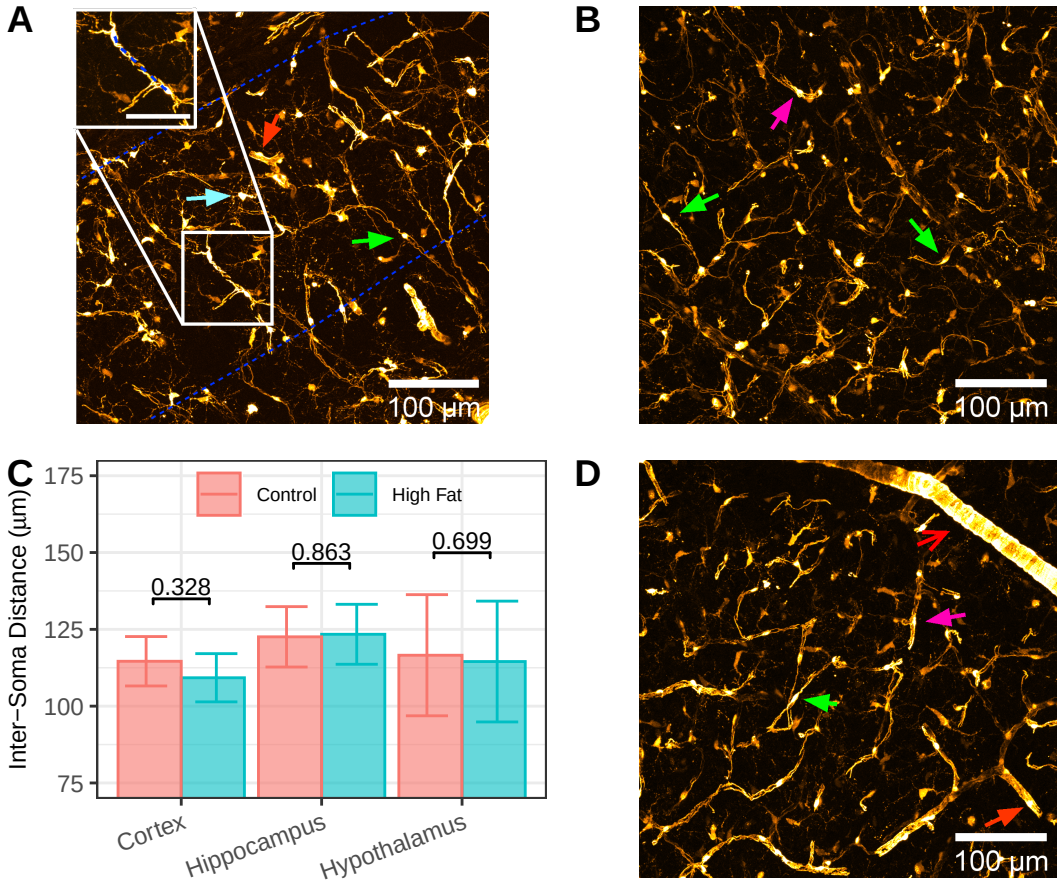

Figure 3.7: Pericyte Spacing is Greatest in the Hippocampus. (**A, B, D**) NG2-DsRed labelled pericytes in the hippocampus, cortex, and hypothalamus respectively, with blue lines denoting hippocampal CA1. (**A Inset**) Example of ISD measurement inset with 50 µm scale bar. (**C**) The ISD between capillary pericytes was unaffected by diet, but varied significantly by region with the hippocampus showing the greatest ISD value (analysis of coverage was restricted to capillary pericytes. Numbers on brackets indicate pairwise corrected dietary comparisons. Capillary pericytes are indicated by green (thin-strand pericytes) and magenta (mesh pericytes) arrows. Red arrows indicate ensheathing pericytes on pre-capillary arterioles. Open red arrow indicates a smooth muscle cell on a penetrating arteriole. Cyan arrow indicates an NG2 positive oligodendrocyte precursor cell, seen predominantly in hippocampal CA1. Pericyte subtypes defined as in Grant et al. (2019). Analysis used n = 569 images (n = 183 cortex, n = 205 hippocampus, n = 181 hypothalamus; n = 300 HFD) that were taken over n = 45 mice (n = 23 HFD)).

Pericyte ISD, which increases as coverage decreases, was unaffected by diet (**Fig 3.7 C**; *F(1,32) = 0.065, p = 0.801*) but varied significantly by region (*F(2,520) = 4.67, p = 0.010*) where the hippocampus had the greatest pericyte ISD (Hippocampus: 123 +/- 10 µm, Cortex: 112 +/- 7 µm, Hypothalamus: 116 +/- 20 µm). Pairwise comparisons between regions adjusted with the Bonferroni correction showed that the hippocampus had a significantly greater pericyte ISD than

the cortex (*t(520) = 2.86, p = 0.013*) with no other regional comparisons approaching significance. Results of the statistical analysis of diet, region, and their interaction, are presented in **Table 3.6**.

Given pericyte data was analysed across mice with different genotypes, this was included as a factor in the statistical model. Data from different genotypes were pooled in order to evaluate the effect of the Cx3CR1-GFP mutation on dietary changes, given that this mutation was to be used in future *in vivo* work. There was a trend level effect of genotype on ISD (*F(1,32) = 3.83, p = 0.059*) where NG2-DsRed animals had a greater ISD (126 +/- 12.1 µm) than NG2-DsRed/Cx3CR1-GFP animals (108 +/- 12.7 µm). This may be a reflection of age-related effects given that as age increased so did ISD (*F(1,43) = 30.59, p = < 0.001*) and the NG2-DsRed/Cx3CR1-GFP animals had a significantly greater age than the NG2-DsRed animals (*t(18.906) = 5.88, p = < 0.001*).

Pericyte data was also analysed across different diet combinations (the first immunofluorescence study I conducted was a pilot experiment, and used a slightly different combination of high fat and control diets). To account for this, diet combination was included as a factor in the analysis (diet combinations are described in the main methods chapter). A trend level effect of diet type was present (*F(1,1) = 90.68, p = 0.067*) where the ISD in animals fed the combination of diets supplemented with Fenbendazole (i.e. the diets used for all work except the pilot immunofluorescence study) was larger. As with genotype, age was significantly greater in the Fenbendazole group (*t(31.266) = 5.55, p = < 0.001*), suggesting the effect of diet type may be a reflection of differences in age.

3.3.9 Capillary Perfusion Showed a Trend Level Reduction by HFD

The length of capillaries was assessed by measuring the length of vessels labelled with a perfusion of a FITC-gelatin. However, this labelling was not complete (**Fig 3.8**), with non-perfused sections appearing in-between perfused segments (**Fig 3.8 A, B; Inset**). As such, the length of these non-perfused segments was added to the length of the perfused capillaries to calculate total capillary length. These non-perfused segments were not the result of methodological issues, as animals that showed reduced perfusion in one region of the brain had near complete perfusion in others (**Fig 3.8 A** and **D** illustrate the hippocampus and hypothalamus from the same mouse). The proportion of total capillary length that was perfused was analysed to investigate if this was affected by diet, with this proposed to reflect an increase in resistance to blood flow in capillaries. Here there was a trend level decrease in the HFD group (*F(1,16) = 3.39, p = 0.084*) but this did not vary significantly by region (*F(2,346) = 1.01, p = 0.367*), suggesting that capillaries in the HFD group may provide more resistance to flow.

HFD Increases the Odds of Poor Capillary Perfusion

The distribution of capillary length perfusion proportions showed more of a bimodal than normal distribution, and so a logistic regression was carried out to look at the probability of having a capillary perfusion percentage below 50%. This revealed that HFD was associated with a significantly greater chance of having poor capillary perfusion (**Fig 3.8 E**; $F(1,375) = 41.54$, $p = < 0.001$). The probability of having poor perfusion was 0.20% in the HFD group, and 0.012% in the control diet group. There was a trend level effect of region ($F(2,373) = 5.41$, $p = 0.067$), where the probability of poor perfusion in the hypothalamus was 0.05%, whilst it was 0.13% in the cortex and 0.14% in the hippocampus.

numDF	denDF	F-value	P-value	Factor	Sig
1	32	0.06	0.801	Diet	
2	520	4.67	0.010	Region	**
2	520	0.85	0.430	Diet:Region	

Table 3.6: Short-Term HFD ISD Statistics. The effects of diet, region, and their interaction, on the ISD between capillary pericytes were analysed using an LMM (numDF and denDF refer to degrees of freedom. F and p values are rounded to 4 decimal places. **Red text** indicates significance. **Green text** indicates trend level. **Background shading** indicates size of p value where darker is larger. Sig shows significance indicator. Factor indicates factors in the model).

numDF	denDF	F-value	P-value	Factor	Sig
1	16	3.39	0.084	Diet	'
2	346	1.01	0.367	Region	
2	346	0.84	0.432	Diet:Region	

Table 3.7: Short-Term HFD Perfusion Statistics. The effects of diet, region, and their interaction, on the proportion of total capillary length perfused by FITC were analysed using an LMM (numDF and denDF refer to degrees of freedom. F and p values are rounded to 4 decimal places. **Red text** indicates significance. **Green text** indicates trend level. **Background shading** indicates size of p value where darker is larger. Sig shows significance indicator. Factor indicates factors in the model).

3.3.10 The Hippocampus had the Smallest Capillary Radii, and Lowest Radius Variance and Capillary Density, with Radius and Radius Variance Decreased by Short-Term HFD

A reduction in CBF is reported in the cortex in obesity, which correlates with memory impairment (Birdsill et al., 2013), and obstructions of cerebral microvascular lumina have been observed following HFD feeding (He et al., 2016; Constantinescu et al., 2011). To evaluate changes in

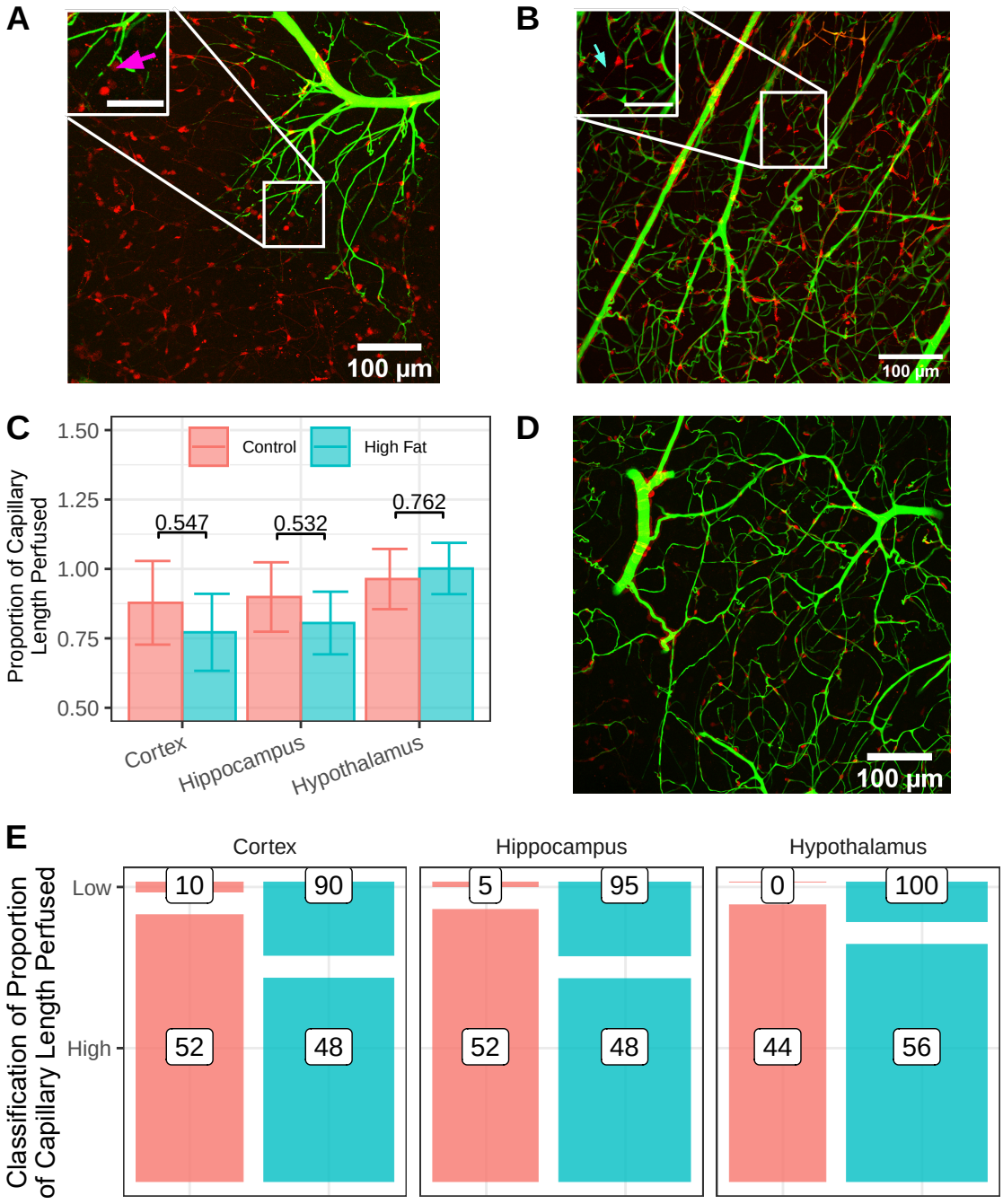

Figure 3.8: Short-Term HFD Reduces Capillary Perfusion. (**A, B, D**) FITC perfused vessels in the hippocampus, cortex, and hypothalamus respectively. (**A Inset**) Example of a non perfused segment situated between perfused segments indicated by magenta arrow. (**B Inset**) Example of non perfused segment associated with pericyte process indicated by cyan arrow. (**C**) Analysis of the proportion of the total capillary length perfused showed a a trend level reduction by HFD feeding. (**E**) Mosaic plot illustrating the proportion of images classified as low and high perfusion split by brain region and diet group. Numbers indicate the percentage of low and high perfusion images from control and HFD mice (numbers in **C** indicate pairwise corrected dietary comparisons. Scale bars in **A** and **B** insets indicate 50 µm. Analysis used n = 377 images (n = 124 cortex, n = 135 hippocampus, n = 118 hypothalamus; n = 213 HFD) that were taken over n = 27 mice (n = 15 HFD)).

capillary radii, which could be linked to a reduction in blood flow, I analysed measurements of luminal capillary radii. These showed a significant reduction in the HFD group (**Fig 3.9 F**; *F(1,18) = 7.70, p = 0.013*) and varied significantly by region (*F(2, 392) = 5.77, p = 0.003*) where radius was greatest in the hypothalamus (2.27 +/- 0.49 µm), followed by the cortex (2.24 +/- 0.84 µm) and then the hippocampus (2.11 +/- 0.68 µm).

The ability of the capillary bed to locally dilate is important in neurovascular coupling, the mechanism whereby blood flow is redirected to regions of greater neuronal activity. HFD-induced impairments in neurovascular coupling are suggested to lead to cognitive impairment (Sorop et al., 2017). Changes in this ability can be reflected in reductions in the variation of radius measurements. The effects here mimicked those on radius, where the radius SD was significantly reduced by HFD (**Fig 3.9 G**; *F(1,18) = 22.14, p = < 0.001*) and varied by region (*F(2,382) = 3.19, p = 0.042*) where pairwise Bonferroni corrected comparisons revealed a significantly smaller radius SD in the hippocampus compared to the hypothalamus. Overall, the hippocampus had the smallest radius standard deviation (0.893 +/- 0.042 µm) relative to the cortex (0.901 +/- 0.084 µm) and the hypothalamus (0.989 +/- 0.026 µm). An analysis of proportional variance, i.e. the SD as a proportion of the mean, revealed no effect of diet or region.

HFD feeding and obesity are associated with changes in cerebrovascular density. This has been seen as both a pathological increase (Coucha et al., 2019) and decrease (Tucsek et al., 2014b) that correlated with impaired cognitive performance. Analysis of the length of capillaries normalised to tissue volume (**Fig 3.9 E**) revealed no effect of diet, but there was significant variance by region (*F(2,339) = 2.35, p = < 0.001*) where pairwise Bonferroni corrected comparisons revealed that the cortex had significantly greater capillary length density than the hippocampus. The hippocampus had the smallest capillary length density (0.00299 +/- 0.00083 mm/mm^2) followed by the hypothalamus (0.00303 +/- 0.00051 mm/mm^2) and the cortex (0.00629 +/- 0.00170 mm/mm^2). There was no effect of diet.

3.4 Discussion

3.4.1 HFD Increased the Rate of Weight Gain, with Differences in Weight Emerging Shortly After Beginning HFD Feeding

Weight was analysed relative to starting values to control for differences in weight at baseline, with two weeks of HFD feeding leading to an increase in the rate of weight gain and a trend to increased weight in HFD animals at day 14 in the combined analysis. Given the split between

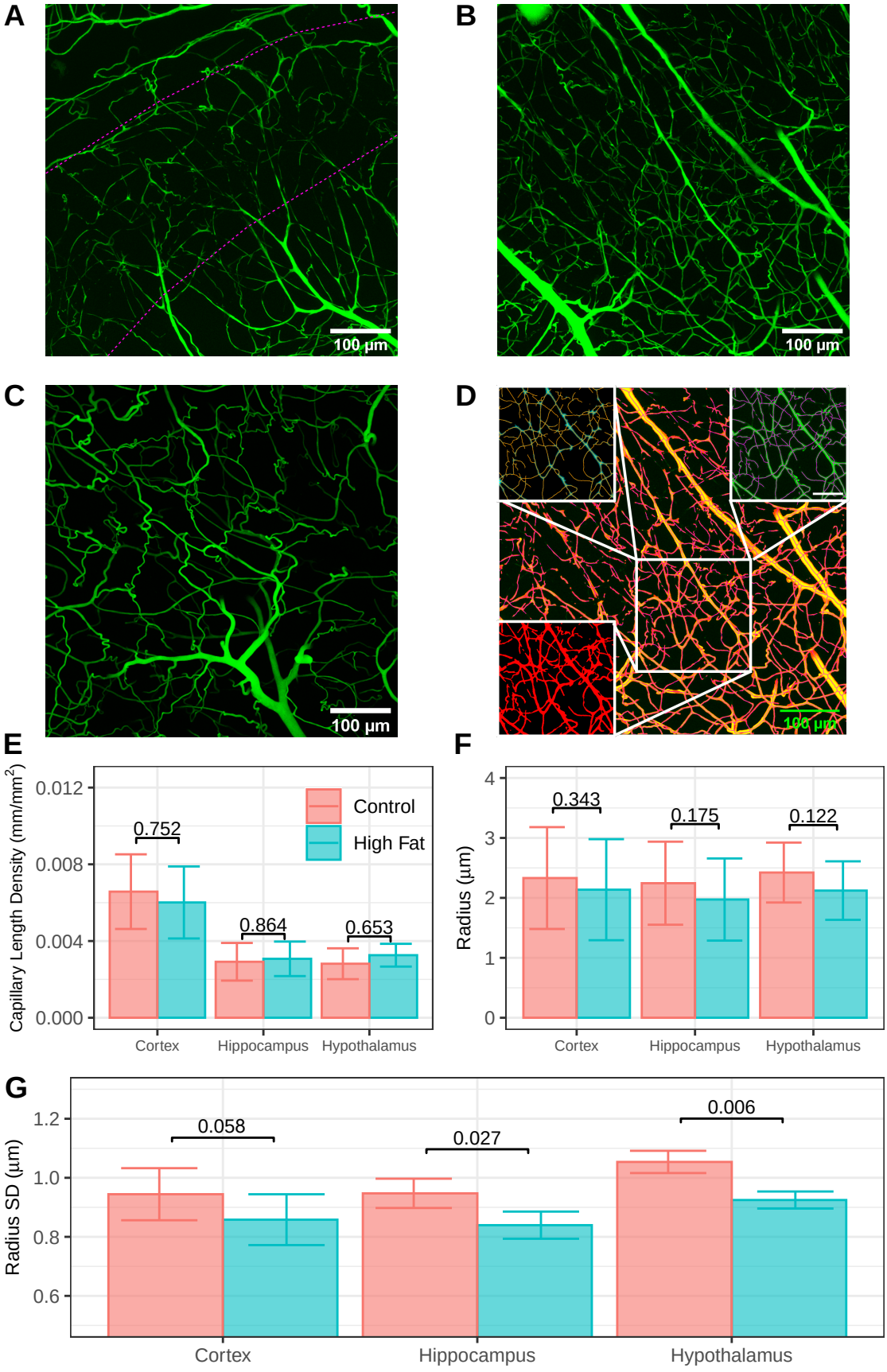

Figure 3.9 Legend on the following page.

numDF	denDF	F-value	P-value	Factor	Sig	Measure
1	16	2.35	0.145	Diet		Density
2	339	9.02	0.000	Region	***	
2	339	0.38	0.681	Diet:Region		
1	18	7.70	0.013	Diet	*	Radius
2	392	5.77	0.003	Region	**	
2	392	0.71	0.492	Diet:Region		
1	18	22.05	0.000	Diet	***	Radius Variation
2	382	3.19	0.042	Region	*	
2	382	0.48	0.622	Diet:Region		

Table 3.8: Short-Term HFD Vessel Statistics. The effects of diet, region, and their interaction, on capillary density, radius, and radius variance, were analysed using an LMM (numDF and denDF refer to degrees of freedom. F and p values are rounded to 4 decimal places. **Red text** indicates significance. **Green text** indicates trend level. **Background shading** indicates size of p value where darker is larger. Sig shows significance indicator. Factor indicates factors in the model. Measure indicates the measurement analysed).

immunofluorescent and protein array / behavioural experiments in this chapter, weight analyses split by cohort were conducted, where mice in the immunofluorescence cohort demonstrated the same effects as were present the grouped analysis, though the effect of diet at day 14 was no longer present (albeit near trend level). The protein array / behavioural cohort only demonstrated an increase in weight over time with no effects of diet. These results contribute to the established body of literature demonstrating that a switch to a HFD promotes rapid increases in weight gain, but also highlight that the immunofluorescence results presented in this chapter must be interpreted differently from the protein array and behavioural data, given the former is associated with HFD-induced weight gain (and its associated metabolic effects) whilst the latter is not.

In the combined analysis the trend level increase in weight at day 14 appears to reflect the imminent onset of diet-induced weight gain following two weeks of HFD feeding, though non-

---

Figure 3.9 *(preceding page)*: Capillary Density, Radius, and Radius Variance, are Lowest in the Hippocampus and Radius and Radius Variance are Reduced by HFD. (**A, B, C**) FITC perfused vessels in the hippocampus, cortex, and hypothalamus respectively. Hippocampal CA1 indicated by magenta lines. (**D Top Left**) Skeleton of **B** in yellow overlaid on Euclidean distance map in cyan. (**Bottom Left**) Thresholded image in red. (**Top Right**) Thresholded image in green, skeleton overlaid in magenta. (**Main Panel**) Raw signal in green merged with threshold in red. Yellow indicates overlapping signal. Skeleton in magenta. (**E**) Diet had no effect on capillary density though it was lowest in the hippocampus. (**F**) Capillary radii were diminished by HFD feeding, and were lowest overall in the hippocampus. (**G**) The variation in capillary radii was reduced by HFD, and was smallest in the hippocampus (p values of within region dietary comparisons are indicated on brackets. Analysis of length density / radius / radius variation used n = 370/425/415 images (n = 121/152/147 cortex, n = 132/150/145 hippocampus, n = 117/123/123 hypothalamus; n = 206/233/225 HFD) taken over n = 27/29/29 mice (n = 15/16/16 HFD)).

significant differences in mean weight (relative to starting weight) were apparent between diet groups from one day of feeding onwards. This timecourse fits with other studies, where male C57BL/6J mice fed a 45% HFD (the same percentage used in my experiments) showed a difference in weight after a week, and significant weight increases from four weeks onwards (Ouyang et al., 2014). Similarly, a 60% HFD used by Jais et al. (2016) was associated with significant weight increases after 3 days, and though only significant after 5 weeks, Kim et al. (2008) showed non-significant HFD-induced increases in weight after a week of feeding. In addition, McLean et al. (2018) used a 60% HFD with weight increasing from the second day onwards, and reaching significance by day 3. In rats, a 60% HFD has been associated with significant increases in weight after one week (Calvo-Ochoa et al., 2014; Posey et al., 2009; Thaler et al., 2012). Since a positive relationship exists in both rats and mice between dietary fat content and body weight or fat gain (reviewed in Hariri and Thibault 2010), an accelerated onset of diet-induced weight gain with a 60% diet is to be expected. Overall, my results agree with other published studies showing an effect of HFD feeding on weight gain beginning shortly after the start of dietary manipulation, with the fact that I used a large sample size (n = 70 mice) and saw no significant effect on weight within 2 weeks of HFD likely down to the use of a 45% rather than 60% HFD.

It also important to consider the fact that the mice I analysed varied both in sex and age. HFD-induced weight gain has previously been shown to be mediated by sex, with males more susceptible to diet-induced weight gain (Hwang et al., 2010), and old mice seen to be more susceptible to the metabolic effects of HFD feeding (Nunes-Souza et al., 2016), with a significant difference in weight only detected in aged (54-56 weeks old) mice from 8 weeks onwards during 60% HFD feeding, something that was not detected over 14 weeks in young (6-8 weeks old) mice, though young mice did show reduced glucose tolerance, hyperlipidaemia, and elevated abdominal fat levels (Nunes-Souza et al., 2016). However, in my statistical analysis neither sex nor age significantly affected weight gain, perhaps owing to the short duration of dietary manipulation used, given that Hwang et al. (2010) only showed significant differences in diet-induced weight gain between sexes from 4 weeks onwards, and the restricted range of ages incorporated in my experiments (relative to Nunes-Souza et al. 2016), given the mean and standard deviation of this was 15.76 +/- 8.87 weeks.

Cohort Differences

The difference in dietary effects between the immunofluorescence and behavioural cohorts in my results was not down to any sex or age-related effects, as a chi-squared test revealed no difference in the distribution of sexes, and mean age did not vary significantly between them. It may be

the case that genotype played a role, as the protein array / behavioural cohort were wild type C57BL/6J mice, whereas transgenic animals were used in the immunofluorescence experiments. Additionally, the behavioural cohort were handled to a greater extent, so it is possible that this was associated with levels of stress that interacted either with dietary effects or overall feeding behaviour.

The mice used in the immunofluorescence experiments had either one, or both, of two reporter mutations. These were the NG2-DsRed mutation that labels pericytes, oligodendrocyte precursor cells, and smooth muscle cells, and the Cx3CR1-GFP mutation, which labels microglial cells, as well as circulating monocytes and subsets of natural killer and T cells (Imai et al., 1997). Only mice heterozygous for this latter mutation were used, given it involves the knockout of the Cx3CR1 gene, with its complete knockdown associated with impairments in cognition and synaptic plasticity (Rogers et al., 2011). Cx3CR1 and its ligand are important in neuroinflammation and are involved in signalling between neurons and microglia, and impaired Cx3CR1 signalling is associated with age-related macular degeneration and neurodegeneration in mouse models of Parkinson's disease and amyotrophic lateral sclerosis (Lee et al. (2010) introduce the effects of Cx3CR1 dysfunction). Whilst it is possible that genotype effects are responsible for the different trajectory of HFD-induced weight gain in wild type versus transgenic animals, the results I present are in the opposite direction of what would be expected.

Polymorphisms in the Cx3CR1 gene are associated with obesity and metabolic traits (Sirois-Gagnon et al. 2011 cited by Shah et al. 2015), and results from work on diet-induced obesity show that complete Cx3CR1 deficiency protects against obesity and the inflammation of visceral adipose tissue (Polyák et al., 2014), with partial deficiency also associated with resistance to diet-induced weight gain and cognitive impairment (Cope et al., 2018). However, work by Shah et al. (2015) showed no effect of complete Cx3Cr1 deficiency on diet-induced weight gain, fat content, feeding, or energy expenditure at any point over 24 weeks, in HFD fed mice, though these mice did show attenuated glucose-intolerance at baseline and after 12 weeks, and improved insulin sensitivity after 24 weeks of HFD. Indeed, looking more closely at the work by Polyák et al. (2014), they showed that weight gain on a HFD is only significantly reduced by complete Cx3CR1 deficiency after 8 weeks, with the inflammatory changes they report only investigated after 10 weeks. These results support the possibility that Cx3CR1 deficiency is associated more with altered dietary effects after long-term rather than short-term HFD feeding. In contrast Cope et al. (2018) show a significant HFD-induced increase in weight after 2 weeks in wild type mice, with the same effect only seen after 5 weeks in partially Cx3CR1 deficient mice. In addition, partially Cx3CR1 deficient mice were also resistant to diet-induced cognitive deficits after 12 weeks of HFD feeding.

The reason for discrepancies between studies are unclear, given they all used male mice with ages ranging from 7-10 weeks at the start of a 45% HFD (though Polyák et al. (2014) used a 2:1 mixture of standard chow and lard). If anything it appears that partial (as in Cope et al. 2018) rather than complete Cx3CR1 deficiency is associated with the modulation of short-term dietary effects.

Ultimately then there is some evidence that Cx3CR1-GFP mutants may be resistant to short-term diet-induced weight gain on a HFD. However, the partially Cx3CR1 deficient mice I used were included in my immunofluorescence cohort, which showed elevated, rather than reduced, susceptibility to diet-induced weight gain relative to wild-type behavioural animals. These mice were in the minority of the immunofluorescence cohort, so their presence may have dampened the effect of HFD on the overall cohort, though genotype did not significantly affect weight gain, or the rate of weight gain, in my statistical analysis. An alternative explanation for differences between cohorts relates to the extra degree of handling, and perhaps stress, associated with behavioural testing. However, behavioural testing and training only began at day 11 of dietary manipulation, so an effect of HFD on weight would be expected prior to this if this was an influencing factor, with no such effect present. As such, the question of why the cohorts differ in terms of susceptibility to diet-induced weight gain remains unanswered. It is possible that the NG2-DsRed mutation present in the immunofluorescence cohort could play a role in this, but to my knowledge no studies have yet looked at the effect of this mutation on HFD-induced weight gain.

3.4.2 HFD Treatment Impairs Hippocampal Cognition

HFD feeding was associated with a trend level deficit in NOCR. Though not significant, in light of the small sample size used (n = 4 mice per diet group), this suggests the presence of a dietary impairment in hippocampus-specific cognition following short-term HFD feeding. The NOCR task relies not only on hippocampus-dependent (Mumby et al., 2002), but also hippocampus-specific (Balderas et al., 2008) cognitive processes, though the medial frontal cortex also appears to be involved given that when damaged, object-context recognition is impaired (Spanswick and Dyck, 2012). McLean et al. (2018) demonstrated an impairment in NOCR after only 48 hours of HFD feeding, as well as impairments in hippocampus-specific tests of object-place-context and object-place recognition after a single day of HFD feeding (using a sample size of 48 mice), with their results representing the earliest time at which HFD-induced cognitive impairments have been investigated.

My results support the work by both McLean et al. (2018) and Kanoski and Davidson (2010) that demonstrate hippocampus-specific deficits in cognition following short-term HFD feeding.

Whilst finding HFD-induced cognitive deficits at large appears inconsistent, tasks that measure hippocampus-dependent cognition show impairment more reliably than those that utilise non-hippocampal, or more distributed, processes (HFD and cognition reviewed in Cordner and Tamashiro 2015). The fact that the deficits I report are detected in mice that showed no effect of HFD on their weight or rate of weight gain fits with other studies cited in a review by Cordner and Tamashiro (2015) that demonstrate hippocampal deficits in the absence of weight gain, particularly given that the rapid deficits reported by McLean et al. (2018) and Kanoski and Davidson (2010) aren't associated with significant weight increases. The fact that Kanoski and Davidson (2010) report non-spatial cognitive deficits taking 30 days to appear (when animals show significant increases in weight) suggests that hippocampus-independent cognition deficits could be driven via obesity-related mechanisms, whilst hippocampus-dependent deficits may not rely on the presence of obesity. Whilst other studies that have used more hippocampus-specific variants of the novel object recognition task report a link between deficits and weight gain (Heyward et al., 2012; Valladolid-Acebes et al., 2013), this is likely a result of the length of dietary manipulation used (27 and 8 weeks respectively) rather than a causative factor, as hippocampus-specific deficits persist beyond the onset of significant weight gain (McLean et al., 2018; Kanoski and Davidson, 2010).

It is important to note that HFD associated cognitive deficits are likely not the result of altered locomotive activity, given that Heyward et al. (2012) report no difference in the distance travelled or time spent in the center of an open field task in diet-induced obese HFD fed mice, though these mice did show elevated signs of anxiety which it was suggested could confound anxiety-evoking tests of memory. Rats fed a HFD for 6 weeks showed no effect on locomotion in an elevated plus maze (Aslani et al., 2015), with spontaneous locomotor activity not affected after 9 weeks (Chia-Ying et al., 2017). With regards to motivation, 3 weeks of a HFD in rats did not affect responding to a sucrose reinforcer on a progressive ratio schedule (Tracy et al., 2015), demonstrating that at least in terms of food rewards, short-term HFD feeding doesn't influence motivation.

A final point to make concerns the age of mice tested, given Valladolid-Acebes et al. (2013) show cognitive deficits in mice aged 5 weeks at the start of dietary manipulation, but not those aged 8 weeks, though the reason for this is unclear given that hippocampus-specific deficits have been reported in 12 week old mice (Heyward et al., 2012; McLean et al., 2018). The detection of differences appears unrelated to sample size, with Heyward et al. (2012) using 5-8 mice per diet group, McLean et al. (2018) using 24 per group, and Valladolid-Acebes et al. (2013) using 15 and 12 mice per group in their 8 and 5-week experiments respectively. All three studies used male mice exclusively. With regards to my own results, no effect of age or sex was seen on behavioural performance, though the sample size used was likely too small to detect any effects of these factors,

with age only ranging from 8 to 14 weeks. In summary, evidence suggests that hippocampus-specific cognitive impairments induced by HFD feeding are independent of increases in weight or the presence of diet-induced obesity, fitting with my results, and that deficits aren't related to changes in locomotive or motivational behaviour.

Mechanisms of Early HFD Induced Hippocampal Deficits

Two mechanisms proposed to underlie HFD-induced hippocampal cognitive deficits include glucose intolerance, which develops after only three days (McLean et al., 2018), and resistance to leptin and insulin signalling. Both the leptin and insulin receptors are highly expressed in the hippocampus, with evidence suggesting that they play a role in hippocampal-dependent learning and memory via the regulation of receptor trafficking and synaptic plasticity (briefly reviewed in Cordner and Tamashiro 2015).

Diet induced obesity leads to impaired central responses to peripheral leptin throughout the brain (Morabito et al., 2017) though reductions in sensitivity to peripherally administered leptin appear to take a long time to develop, with no evidence of it after 16 days of HFD feeding (Van Heek et al., 1997) though it is reported after 8 weeks (Van Heek et al., 1997; Lin et al., 2000). Resistance to centrally administered leptin seems to take even longer to manifest, with it only beginning to appear after 15 (El-Haschimi et al., 2000) and 19 (Lin et al., 2000) weeks. Leptin resistance therefore seems an unlikely mechanism for mediating the early effect of HFD feeding on hippocampal cognition. This is supported by my protein array data that demonstrated no effect of two weeks of HFD feeding on the hippocampal levels of leptin or its receptor. In contrast to leptin, central insulin resistance appears after only three days of HFD feeding in rats independent of changes in weight or adiposity (Clegg et al., 2011), and changes in the hippocampal insulin signalling pathway have been reported after a week of HFD feeding (Calvo-Ochoa et al., 2014), making it a much more likely candidate mechanism, and one that is relevant to my model given the absence of dietary effects on weight I observed in the behavioural cohort of mice.

Besides a potential role for insulin resistance, evidence exists that supports roles for oxidative stress, BBB impairment, inflammation, and changes in BDNF levels, in diet induced hippocampal deficits (briefly reviewed in Cordner and Tamashiro 2015). HFD induced increases in the level of oxidative stress in the hippocampus (Xia et al., 2015; Kishi et al., 2015; Liu et al., 2014; Molteni et al., 2004; Cui et al., 2012) and cortex (Liu et al., 2014) are associated with cognitive deficits, although the earliest that this has been demonstrated is 8 weeks making the relevance of HFD-induced oxidative stress to early cognitive deficits unclear. HFD also induces BBB disrup-

tion (Davidson et al., 2012; Chang et al., 2014; Pallebage-Gamarallage et al., 2012; Elahy et al., 2015) that is associated with cognitive impairment (Kanoski et al., 2010; Davidson et al., 2012, 2013). However, as well as seeing no effect of HFD on BBB integrity in my model, the evidence that hippocampal BBB disruption only occurs in obese mice (Davidson et al., 2012, 2013) makes it likely unrelated to the behavioural changes I report. Elevated levels of inflammatory cytokines (Liu et al., 2014; Thirumangalakudi et al., 2008; Pistell et al., 2010) have also been linked to HFD-related cognitive impairment, although there is evidence for this in the absence of cytokine changes as well (Kaczmarczyk et al., 2013). Given that HFD feeding had no effect on the expression of hippocampal inflammatory cytokines in my model, the latter study seems most relevant, especially given that Kaczmarczyk et al. (2013) demonstrated behavioural changes after only a week of HFD feeding. Kaczmarczyk et al. (2013) link their results to decreased levels of BDNF, which modulates synaptic plasticity and is decreased in models of HFD feeding in both the hippocampus (Molteni et al., 2002; Stranahan et al., 2008; Kishi et al., 2015; Molteni et al., 2004; Camer et al., 2015) and cortex (Xia et al., 2015; Kaczmarczyk et al., 2013; Pistell et al., 2010; Camer et al., 2015). It may therefore be the case that HFD induced alterations in BDNF-related synaptic plasticity are what underlie the cognitive deficits in my model, although Kaczmarczyk et al. (2013) reported no change in hippocampal BDNF levels. This doesn't rule BDNF out entirely however, given that transient and biphasic dietary effects have been documented (Thaler et al., 2012; Jais et al., 2016) so it is possible that BDNF levels in the hippocampus could be downregulated prior to one week before returning to basal levels, and that this is partly responsible for the hippocampal cognitive deficits..

3.4.3 Hippocampal Protein Levels were Unaffected by HFD and Did Not Correlate with Behavioural Performance

Analysis of protein array data revealed that two weeks of HFD feeding had no effect on the hippocampal expression of a selection of proteins. Additionally, neither NOCR performance nor its interaction with diet showed significant effects on protein expression. The array included measurements of proinflammatory cytokines (for a full list see **Table 3.2**), with results indicating the absence of an inflammatory response. It should be noted that the protein array experiment was exploratory and severely underpowered. Using the levels of IL-1β as an example, the experiment achieved a 12.1% power level, where 80% power would have required 21 animals per group (compared to the 4 per group used). In addition, given 62 proteins were measured, changes would have needed to be highly significant to pass a correction for multiple comparisons. As such, the absence of significant changes I report is not surprising, and likely more related to the study design

than real dietary effects. However, the unadjusted p values show a lack of change in the vast majority inflammation-related proteins in response to dietary manipulation, which could indicate a lack of hippocampal inflammation. With the study limitations in mind, an appropriately powered follow-up experiment is needed to confirm this.

Detecting a HFD-induced deficit in cognitive performance without a concurrent elevation in hippocampal cytokine levels fits with work by Kaczmarczyk et al. (2013), and this relationship seems to be associated with short-term HFD feeding (Kaczmarczyk et al. (2013) used a week of HFD) given that studies where cytokine elevations and cognitive deficits correlated used longer manipulations (e.g. Liu et al. (2014) used 16 weeks of HFD). Since the early effects of HFD include hypothalamic inflammation (after 24 hours; Thaler et al. 2012) and reactive gliosis in the hippocampus (after a week; Calvo-Ochoa et al. 2014) an absence of early changes in the levels of hippocampal cytokines is surprising. This could be related to time-specific dietary effects, given that HFD induces a biphasic inflammatory response in the hypothalamus where proinflammatory cytokine mRNA levels are elevated before returning to baseline after a week of HFD feeding only to show increases again after four weeks (Thaler et al., 2012). Whilst it may appear strange that I opted to investigate hippocampal inflammation following two weeks of dietary manipulation in light of this, it seemed likely that any phasic hippocampal inflammatory changes would follow a different timecourse to that in the hypothalamus given the lack of any close association of the hippocampus to a CVO. The mechanisms underlying the biphasic response in the hypothalamus are unclear, but Mendes et al. (2018) make the point that a biphasic pattern is seen in inflammatory responses in other tissues, and suggest that the initial peak is driven by microglia, but their gradual replacement by bone-marrow derived myeloid cells (Valdearcos et al., 2017) alters proinflammatory cytokine expression levels. In general, investigation of whether inflammation follows a phasic pattern in the hippocampus is lacking, with existing evidence being inconsistent and drawn from multiple studies looking at individual timepoints. At later timepoints there have been reports of both increases and an absence of changes in cytokine levels (no changes; Boitard et al. 2014; Sobesky et al. 2014, increases; Thirumangalakudi et al. 2008; Liu et al. 2014), whilst no changes were detected after 1 or 3 weeks (Kaczmarczyk et al., 2013). Evidence seems to suggest that rather than showing phasic cytokine changes in response to HFD feeding, the hippocampus is resistant to HFD-induced changes in proinflammatory cytokine levels.

Sobesky et al. (2016) suggest that HFD induced increases in the expression of proinflammatory cytokines in the brain relies on the presence of a substantial sugar component in the HFD regimen, and that HFDs without this component require a secondary insult to induce an elevation of proinflammatory cytokines or memory impairments. Though there is evidence against the ne-

cessity of cytokine production for the development of cognitive impairment, their suggestion that HFD primes rather than activates microglial cells, and thereby does not promote cytokine production, could explain my results. Primed microglia show signs of activation such as proliferation (priming reviewed in Li et al. 2018), though they show less distinct morphological changes (they remain highly ramified despite showing larger and less-round somata than resting cells; Torres-Platas et al. 2014) and do not produce inflammatory cytokines (Perry and Holmes (2014) cited by Hoogland et al. 2018). They also show an elevated degree of cytokine production in response to a secondary inflammatory stimulus (microglial priming reviewed in Perry and Holmes 2014). Given my data showed an increase in microglial cell density, no change in microglial ramification, nor any increase in proinflammatory cytokine levels, the priming rather than activation of microglia in my model seems a possible explanation. The fact that HFD induced priming is detected in the hippocampus (Sobesky et al., 2016) and hypothalamus (Souza et al., 2019) after only 3 days of feeding suggests that early HFD may prime microglia.

With regards to models that lack a substantial sugar component and still demonstrate elevated cytokine levels or cognitive impairment (such as my own), Sobesky et al. (2016) suggest that this is the result of a secondary insult. In my model this secondary insult may have been the stress of behavioural testing, which involved $\sim$90 minutes in total of handling, context exposure, and testing. This duration is most relevant to measures of acute stress, which are associated with upregulated hippocampal IL-1β and signs of microglial reactivity (Piskunov et al., 2016; Chen et al., 2016). The fact that acute stress increases cytokine expression however doesn't fit with my detection of cognitive impairment in the absence of cytokine changes.

Ultimately, it seems that whilst HFD-induced hippocampal priming of microglia can explain my results, there is no evidence that a secondary insult occurred (a necessary factor for the detection of cognitive impairment according to the suggestions of Sobesky et al. 2016) given that the effects of acute stress on cytokine expression don't match my data. In addition, other work provides evidence that the activation of primed microglia is not necessary to induce early cognitive impairment (Kaczmarczyk et al., 2013). This leads to a number of suggestions, either that primed microglia could affect hippocampal processing in a cytokine-independent manner, that hippocampal inflammatory changes are irrelevant to early HFD-induced cognitive deficits, or that microglial activation occurs in a transient manner, with an early increase in proinflammatory cytokine levels mediating the behavioural effects of inflammation. No studies so far have looked at hippocampal changes earlier than 1 week, so future work should investigate inflammatory changes in the hippocampus prior to this in order to evaluate this latter hypothesis. In addition, it would interesting to use a specific marker of circulating monocytes such as chemokine receptor type 2 (CCR2;

Saederup et al. 2010) to evaluate the presence of hippocampal myeloid cell infiltration following short-term HFD feeding, given this is the mechanism proposed to mediate phasic hypothalamic inflammation and has been seen to occur after only a week (Valdearcos et al., 2017). It is possible that the increased microglial cell density I report could be down to immune cell infiltration rather than resident microglial proliferation given the immune cell markers used in my experiments (Iba1 and Cx3CR1) are unable to distinguish between resident and infiltrating inflammatory cells (Greter et al., 2015). Lastly, it is important to note that my microglial analysis was conducted in different mice to those that were used in the protein array, with both cohorts showing differential effects of diet on weight gain. As such, the simultaneous presence of microglial proliferation in the absence of cytokine or morphology changes cannot be confirmed in my model, so future work should attempt to address this.

3.4.4 Microglial Cell Density was Increased by HFD, Though Morphology was Unchanged

Whilst no changes in hippocampal protein levels were detected, HFD was associated with an increased microglial cell density across the cortex, hypothalamus, and hippocampus. This indicates microglial activation and is usually accompanied by morphological shifts from a ramified to an amoeboid shape, an additional indicator of activation (microglia reviewed in Kettenmann et al. (2011) and Hanisch and Kettenmann 2007). Though morphological changes were absent in my model, Sobesky et al. (2016) suggest that HFD studies that demonstrate elevated markers of microglial activation without simultaneous increases in the levels of proinflammatory cytokines are the result of HFD-induced microglial priming (as previously discussed). As an alternative to the priming theory, it may be the case that transient microglial activation in the hippocampus prior to the two week timepoint leads to proliferation of microglial cells and morphological changes, though the latter are reversed when this transient elevation subsides, leading to the results I observe at the two week point. Transient early dietary effects have been reported previously (Thaler et al., 2012; Jais et al., 2016), though evidence from Kaczmarczyk et al. (2013) shows no change in hippocampal inflammation after 1 or 3 weeks. However, no studies have yet looked prior to 1 week, so this theory cannot be disregarded. Such a mechanism could follow a similar pattern to the phasic hypothalamic inflammation reported by Thaler et al. (2012), where inflammatory cytokine levels return to baseline following a peak at one and three days, only to peak again at four weeks. This coincided with an elevated microglial cell density at one, three, seven, and 14 days, providing evidence that increases in microglial cell density persist beyond transient decreases in proinflammatory cytokine expression.

Mendes et al. (2018) have proposed that the infiltration of the hypothalamus by circulating monocytes (Valdearcos et al., 2017) mediates the phasic hypothalamic inflammatory changes reported by Thaler et al. (2012), given this infiltration has been reported after only a week (Valdearcos et al., 2017), though whether these infiltrating cells potentiate or inhibit existing inflammatory processes in the hypothalamus has not yet been studied. Circulating monocytes can cross the BBB during inflammation (reviewed in Ashhurst et al. 2014) and though Valdearcos et al. (2017) make the point that previous evidence regarding HFD induced monocyte infiltration appears inconsistent (for Buckman et al. 2014; Morari et al. 2014, against Baufeld et al. 2016), these studies were confounded by the effect of irradiation on BBB integrity, a confound Valdearcos et al. (2017) overcame by using head/neck lead shielding - though they also observed infiltration in mice that never underwent irradiation (Valdearcos et al., 2017).

No studies have looked at hippocampal monocyte infiltration following short-term HFD feeding, so whether this plays a role is still uncertain. The potential for the presence of activated, proinflammatory resident microglia, coupled with resting ramified infiltrating cells, or vice versa, could explain the increased microglial cell density I observe, given that neither Iba1 nor Cx3CR1 (the microglial markers used in my studies) are able to distinguish between resident and infiltrating inflammatory cells (microglial and myeloid markers reviewed in Greter et al. 2015). Future work should track hippocampal inflammatory changes over the first two weeks of dietary manipulation, and investigate the presence of infiltrating monocytes (using a marker such as CCR2) as well as any differential inflammatory phenotype between resident and infiltrating immune cells.

It is important to note that some of the mice used in the microglial analyses carried the Cx3CR1-GFP mutation, which evidence suggests could impart resistance to the effects of HFD feeding on microglial activation (Cope et al., 2018). Of the 46 mice used in microglial cell density analysis, 12 carried the Cx3CR1-GFP mutation, and of those analysed for morphology, none were Cx3CR1-GFP mutants. Genotype did not significantly affect microglial cell density in my analysis, suggesting that my microglial results are unaffected by the the inclusion of Cx3CR1-GFP mice.

3.4.5 Short-Term HFD Did Not Affect BBB Integrity

The BBB isolates the CNS from the rest of the body is formed of specialised endothelial cells, pericytes, and astrocytic endfeet. Disruptions in its integrity are associated with cognitive decline and can be both a cause and consequence of CNS pathologies (reviewed in Hawkins and Davis 2005). My results showed no effect of diet or region-specific dietary effects on IgG leakage (either

looking at vessel-associated extravasated IgG, or IgG signal in the parenchyma), though both dietary and regional differences have been reported (Yamamoto et al., 2019; Pallebage-Gamarallage et al., 2012; Elahy et al., 2015). However, this is likely down to the short timecourse I used relative to other studies. The earliest time at which HFD-induced impairments in BBB integrity have been investigated is 1 week, where Rijnsburger et al. (2019) showed no effect of HFD on hypothalamic BBB integrity, though by 8 weeks, evidence of decreased integrity in the cortex exists (Chang et al., 2014), with the earliest documented HFD-induced leakage of IgG seen after 12 weeks in the cortex, brainstem, and hippocampus (Elahy et al., 2015; Pallebage-Gamarallage et al., 2012). Though no early hippocampal studies exist, evidence suggests that HFD-induced BBB impairment is the result of long-term dietary manipulations, rather than an early effect. In conjunction with my behavioural results, this suggests that BBB breakdown, and any associated neurotoxic and proinflammatory effects it may have, does not play a role in early HFD hippocampus-specific deficits. However, it should be noted that Rijnsburger et al. (2019) used Evans blue to interrogate BBB integrity, a tracer with documented issues regarding the evaluation of BBB integrity (reviewed in Saunders et al. 2015), and my own work used IgG, a relatively large molecule compared to other plasma constituents such as albumin ($\sim$155kDa vs 69kDa) so early reductions in BBB integrity may be detectable through the use of alternative markers. Finally, work by Salameh et al. (2019) illustrates that HFD could have time and region-specific effects on BBB integrity, and also may exert differential effects on the mode of transport across the BBB. Future studies should therefore look at a timecourse of early HFD-related changes in the integrity of hippocampal BBB para- and transcellular transport with regards to physiologically relevant molecules smaller than IgG, such as albumin, in order to fully establish whether it plays a role in the development of early HFD-induced cognitive impairment. However, current evidence suggests this is not the case.

In addition to the absence of early HFD studies on BBB integrity, the mechanisms proposed to mediate dietary changes have generally not been investigated at early timepoints. Oxidative stress has been suggested to link HFD feeding to BBB breakdown, given that anti-oxidant treatment has been reported to attenuate HFD-induced impairments in BBB integrity (Elahy et al., 2015; Takechi et al., 2013; Chang et al., 2014), though the earliest this has been investigated is 8 weeks (Chang et al., 2014). In addition, antagonism of Adora2a, a receptor expressed on both endothelial cells and pericytes, prevents HFD induced BBB breakdown (Yamamoto et al., 2019), an effect proposed to result from Adora2a-mediated upregulation of NFκB activity leading to the downregulation of tight junction proteins (Yamamoto et al., 2019). However, this was only investigated after 16 weeks of HFD feeding. In contrast to these delayed studies, evidence of early peripheral inflammation (3 days of HFD elevated inflammatory markers in the spleen and liver

Souza et al. 2019) suggests that peripheral cytokine mediated BBB breakdown (Fung et al. (2012) review mechanisms of peripheral inflammation leading to central inflammation) could occur at an early timepoint in HFD feeding. However it may also be the case that more chronic peripheral inflammation is necessary to induce BBB changes. In summary, BBB integrity can be compromised through a number of mechanisms, and short-term HFD studies looking at changes in BBB integrity to small molecules, oxidative stress, and NFκB activity, will go a long way to improving our understanding of the early effects of HFD.

3.4.6 The Distance Between Capillary Pericytes is Greatest in the Hippocampus and Unaffected By HFD

Pericytes are vascular mural cells that play a role in the regulation of capillary blood flow (Hall et al., 2014), maintain BBB integrity (Haddad-Tóvolli et al., 2017), and provide support to capillaries (where their loss leads to a loss of capillary density; reviewed in Hirunpattarasilp et al. 2019). My results demonstrate that short-term HFD feeding does not influence their spacing on the vasculature. Although this is not a direct measure of pericyte function, the absence of a dietary effect on spacing suggests a lack of pericyte loss which may indicate their physiological roles are similarly unaffected. Though confirming this requires more work, this suggests that the HFD-induced reduction in capillary radius seen in my vascular results may be more likely mediated by dietary effects on endothelial cells, or the physical obstruction of the capillary lumen, than through pericyte dysfunction (aberrant pericyte constriction is observed in a model of Alzheimer's disease; Nortley et al. (2019), and pericyte constriction and death occurs in ischaemia; Hall et al. 2014). Similarly, my results showed a reduction in radius variation, a measure suggested to reflect the ability of the capillary bed to vary its radii in order to support neurovascular coupling, which therefore also appears to be independent of pericyte dysfunction. Future work should investigate HFD-induced functional pericyte changes, and determine whether short-term HFD leads to pericyte constriction to confirm these suggestions.

Other studies have shown that hippocampal pericytes occupy less volume and cover less of the vessel area following HFD feeding (Yamamoto et al., 2019; Tucsek et al., 2014b), though this was with much longer dietary durations (16 and 20 weeks respectively). Pericytes are sensitive to oxidative stress, so the promotion of this by HFD feeding could be responsible for the loss of their coverage seen in long-term dietary studies. Pericyte loss could lead not only to microvascular rarefaction as seen in Tucsek et al. (2014b), but also BBB disruption and neurovascular uncoupling.

An important consideration is that I quantified the effect of diet on pericytes by measuring their

ISD, whilst Yamamoto et al. (2019) and Tucsek et al. (2014b) quantified the proportion of labelled vasculature they covered. This likely enabled the detection of more subtle changes, so it remains possible that short-term HFD feeding affects pericytes but my methodology lacked the sensitivity to detect this. In addition, a slight difference in the timecourse of dietary effects on pericytes seen by Yamamoto et al. (2019) and Tucsek et al. (2014b) suggests that HFD-induced pericyte effects may be time-specific. Though Yamamoto et al. (2019) saw deficits after 16 weeks of HFD in 8 week old mice, 20 weeks was insufficient to induce a reduction in pericyte coverage in mice of the same age in Tucsek et al. (2014b) (who instead report coverage deficits in 19 month old mice). This could not be attributed to differences in genotype, sex, HFD composition, or pericyte subtype analysed (using the definitions outlines by Grant et al. 2019), so may relate to potential variation in control diet sucrose content, microscopic technique used, or phasic effects of dietary manipulation on pericyte coverage. An interesting direction for future work would be to quantify the timecourse of early HFD induced changes in pericyte coverage, perhaps using electron microscopy as in Yamamoto et al. (2019) to detect any time-specific dietary effects with a high degree of precision. It is important to note that in my own results neither age nor sex modulated the effect of diet on pericyte spacing, though overall pericyte spacing did increase with age.

The effect of age on pericytes has previously been reported as a decrease in numbers, degeneration and loss, and a reduction in their cross-sectional area (reviewed in Erdö et al. (2017), cited by Berthiaume et al. 2018), with 21 month old female mice demonstrating cortical and CA1 pericyte loss and loss of coverage relative to 4 month old mice (Soto et al. (2015), cited by Berthiaume et al. 2018). However, another study found no difference in pericyte coverage or pericyte number in primary somatosensory cortex, hippocampus, or posterior thalamus, between mice aged either 4-6, 12-16, or 36-48 weeks old (Nikolakopoulou et al., 2017). Reasons for these discrepancies could come down to ages used (as the oldest animals in the Soto et al. (2015) study were more than twice the age of the oldest in Nikolakopoulou et al. 2017), the inclusion of males in Nikolakopoulou et al. (2017), differences in genetic background (C57BL/6J or 129S1/SvlmJ in Soto et al. (2015) and Nikolakopoulou et al. (2017) respectively), methodological differences (e.g. CD13 labelled pericytes on lectin labelled vessels, PDGFRB pericytes and laminin vessels, in Nikolakopoulou et al. (2017) and Soto et al. (2015) respectively), or subtypes of pericytes included in the analysis (Soto et al. (2015) looked at microvessels, though did not define what this meant, and Nikolakopoulou et al. (2017) looked at vessels with a diameter of 6 microns or less). My data included males, looked at a small age range, and attempted to restrict analysis to capillary pericytes, similar to Nikolakopoulou et al. (2017), though used mice on a C56BL/6J background and found an effect of age, as in Soto et al. (2015). Furthermore, I did not characterise pericyte number or

vessel coverage in the same way as either study, making it very difficult to pinpoint where the variation in results originates from.

Though my results showed no dietary effects on pericyte ISD they did show that the hippocampus had the largest ISD in comparison to the cortex and hypothalamus, a novel finding since no other work has investigated regional differences in capillary pericyte spacing to my knowledge. Given that ISD is independent of capillary density, this suggests that the hippocampal vasculature has a poorer level of support by pericytes, which could result in the hippocampal BBB being more vulnerable to disruption, vessels being more susceptible to rarefaction, and a relatively worse regulation of local blood flow changes. When considered in combination with my other data, which showed that capillary radii and density were lowest in the hippocampus, this could explain why the hippocampus is more susceptible to pathology associated with hypoxia (Ng et al., 1989), Alzheimer's Disease, and ageing (reviewed in Fjell et al. 2014). This may be how global HFD-induced deficits in vascular structure are translated into hippocampus-specific cognitive impairment.

3.4.7 GLUT1 Levels are Unaffected by Two Weeks of HFD

GLUT1 is involved in glucose transport into the brain and the maintenance of BBB integrity, with HFD induced reductions in GLUT1 implicated in the enhanced susceptibility of HFD animals to ischaemic damage (Haley et al., 2019). As such, changes in GLUT1 expression could play a role in cognitive impairment by enhancing neuronal susceptibility to damage by reducing glucose availability. My results showed no effect of diet on GLUT1 expression as assessed by the intensity of GLUT1 staining, something also observed at the two week timepoint in the cortex by Jais et al. (2016), who demonstrate that HFD feeding initially decreases the expression of GLUT1 following three, five, and seven days of HFD feeding, but that its expression recovers to control levels by two weeks. Other studies also corroborate this profile of GLUT1 changes, where three days of HFD feeding was associated with its downregulation in cortex (Haley et al., 2019), seven days of a diet supplemented with a sucrose solution and saturated fat showed no change in GLUT1 expression in the hypothalamus (Rijnsburger et al., 2019), and a high-fat high-cholesterol diet for six months showed no effect on GLUT1 levels in the hippocampus (Freeman and Granholm, 2012). My results add to this body of work, showing that hippocampal, hypothalamic, and cortical GLUT1 expression is unchanged by two weeks of HFD.

Whilst it is possible that early decreases in GLUT1 expression, and the associated reduction in glucose uptake (Jais et al., 2016), could drive the genesis of hippocampal cognitive deficits

by promoting greater tissue vulnerability to damage (Haley et al., 2019), Jais et al. (2016) did not observe early reductions in glucose uptake in the hippocampus, casting doubt on this theory. However, it must be considered that hippocampal effects could exist prior to the 72 hour timepoint investigated in Jais et al. (2016), given that McLean et al. (2018) reported hippocampus-dependent cognitive deficits after a day of HFD. In addition, though Jais et al. (2016) looked at glucose uptake in multiple brain areas, they only investigated cortical changes in GLUT1 levels, so the phasic nature of dietary effects on its expression in the hippocampus still remains to be investigated. Future work should track GLUT1 and glucose uptake changes after a day of HFD feeding, and investigate whether inducing transient decreases in GLUT1 expression can lead to rapid hippocampus-specific cognitive impairments.

Jais et al. (2016) noted that in their model the recovery of GLUT1 levels was associated with elevated serum vascular endothelial growth factor (VEGF), which they suggest is derived from CD206 positive macrophages that were present in greater numbers and showed increased VEGF expression in the perivascular space in HFD animals. In addition, they demonstrated that the ablation of macrophage derived VEGF attenuated serum VEGF increases and reduced GLUT1 expression following 6 months of HFD feeding. Though I did not measure serum VEGF levels in my model, my protein array data showed no effect of diet on VEGF levels in the hippocampus, although the underpowered nature of my protein array must be reiterated. This could relate to region-specific effects of HFD, given that the results reported by Jais et al. (2016) are based on cortical tissue, or perhaps the sparse distribution of perivascular macrophages apparent in Jais et al. (2016) meant their contribution to total hippocampal VEGF levels was below the sensitivity level of the protein array I used. As well as investigating the timecourse of hippocampal GLUT1 changes, it would be interesting to look at VEGF expression in the hippocampus using immunofluorescent labelling as done in Jais et al. (2016) to see if their findings are region-specific.

An additional point to consider regarding the effect of HFD feeding on GLUT1 expression is the HFD fat percentage used. Work by Lizarbe et al. (2019) suggests that the metabolic effects of long-term HFD feeding vary depending on the percentage of fat content used. Though it is unclear how relevant this is to short-term effects, that fact that both Jais et al. (2016) and Haley et al. (2019) used a 60% HFD and observed effects of HFD on GLUT1, whilst Freeman and Granholm (2012) and Rijnsburger et al. (2019) showed no changes and used a 45% HFD, and a lard and sucrose supplemented chow diet, respectively, suggests this could be important. Whilst the differences between these studies could also be accounted for in a number of other ways - either the timecourse of changes proposed by Jais et al. (2016), or regional differences in dietary effects - this is a point worth considering, especially since the HFDs I used were 45%, which may

also explain the lack of hippocampal VEGF changes I detect.

My results showed regional differences in GLUT1 expression driven by the greater GLUT1 staining intensity in the hypothalamus. Zeller et al. (1997) looked a regional differences in GLUT1 and demonstrated that the density of staining shows regional heterogeneity, whilst Takimoto and Hamada (2014) showed that exercise leads to region-specific changes in GLUT1 levels. Whilst these studies suggest that GLUT1 expression may be modulated in a region-specific manner, it appears no studies that have directly compared regional levels of baseline GLUT1 expression, and included the hypothalamus, exist. Though regional differences in GLUT1 expression appear to be well founded, the fact that the hypothalamus showed the greatest level of GLUT1 staining in my results is unusual. Areas with leaky BBBs, such as the hypothalamus, showed no GLUT1 staining in work by Rahner-Welsch et al. (1995), and though the absolute nature of this deficiency is not supported by other studies that demonstrate hypothalamic GLUT1 staining (e.g. Rijnsburger et al. 2019), the suggestion that its levels are reduced in areas with lower BBB integrity conflicts with my results. Revisiting these findings when more work has been done investigating basal differences in GLUT1 expression between brain regions will help with the interpretation of these inconsistencies.

3.4.8 HFD Increases Capillary Bed Resistance

The primary function of the microcirculation (arterioles, capillaries, and venules) in the brain is to supply oxygen and nutrients and remove carbon dioxide and waste products. Cerebral microvascular disease is associated with microbleeds, lacunas, and microlacunas (Kalaria, 2012), which are seen more commonly in obese individuals with insulin resistance and dyslipidaemia (microvasculature in obesity reviewed by Sorop et al. 2017). Additionally, cerebral small vessel disease is associated with visceral fat accumulation (Yamashiro et al., 2014). My results demonstrated that short-term HFD decreases the luminal radius, and variance of the luminal radius in the capillary bed. Additionally, HFD feeding led to a reduction in the proportion of capillary length that was perfused by FITC-conjugated albumin. Together, these results suggest that HFD feeding not only decreases capillary volume and therefore increases resistance to flow, but also impairs the ability of the capillary bed to regulate local changes in diameter. This latter implication suggests that HFD impairs neurovascular coupling, whilst the former may be related to an overall decrease in the ability of the capillary bed to perform vital functions like nutrient delivery and waste removal.

3.4.9 Short-Term HFD Does Not Affect Capillary Density

Though my results indicate that short-term HFD has no effect on capillary density, models of obesity are associated with a reduction in microvascular density (reviewed in Sorop et al. 2017), whilst long-term HFD feeding in rodents also leads to decreases in vascular density (Estato et al., 2017; Obadia et al., 2017), the extent of which in hippocampal CA1 has been correlated with the learning index of animals on an elevated plus maze (Tucsek et al., 2014b), a measure the authors claim correlates with hippocampal function (Tucsek et al. 2014a cited by Tucsek et al. 2014b). Microvasular rarefaction can induce non-uniform blood flow distributions, and affects spatial haemodynamics of flow (Chantler et al., 2015), changes which could underlie cognitive deficits associated with long-term dietary manipulations. Tucsek et al. (2014b) suggest the microvascular rarefaction they report is related to the loss of pericyte coverage they observe (pericyte loss or aberrant constriction in hypertension may mediate capillary loss; reviewed in Hirunpattarasilp et al. 2019). As well as capillary rarefaction, there is also evidence demonstrating that long-term HFD feeding leads to the opposite effect, i.e. a HFD associated increase in capillary length density. This has been seen in the hippocampus after 12 and 16 weeks (Yamamoto et al., 2019), and in the ARC after 18 weeks (Yi et al., 2012), of HFD feeding. Coucha et al. (2019) demonstrated a correlation between aberrant angiogenesis and cognitive impairment, where inhibiting pericyte Ephrin-B2 expression attenuated the angiogenesis and rescued behavioural performance. The absence of both pericyte dysfunction and changes in capillary density in my model supports a role for pericytes in mediating the effect of HFD on capillary stability.

3.4.10 HFD Decreases Capillary Luminal Radii

As previously described, HFD led to a decrease in the radii of capillaries in all brain regions analysed, which likely has detrimental effects on blood flow and therefore nutrient exchange. Determining the cause of the HFD induced capillary radius reduction I observe is difficult, given that studies investigating the effects of HFD feeding on cerebral capillary structure are limited, though a few exist that look at the microcirculation in general. Ten weeks of HFD decreased the size of the lumen of the cerebral microvasculature through the binding together of collagen fibres (which may be related to the HFD-induced elevation of collagen 1 expression; Deutsch et al. 2009) and microvessel lumina showed more microvilli, indentations, vacuoles, and wider gaps between endothelial cells (He et al., 2016). In addition, endothelial surfaces were rougher, which it was suggested could result in haemodynamic changes and increase the risk of microcirculatory blood clots (He et al., 2016). Six months of a HFD in hamsters led to enlarged endothelial cells, irregularly

shaped vessels with large perivascular spaces, and some lumina filled with lipoprotein particles (Constantinescu et al., 2011). This same duration of HFD in rats led to changes in myofibrils in smooth muscle cells, the thinning of endothelial cells, and the enlargement of subendothelial spaces (Mato et al., 1996). Endothelial pathology and the exposure of subendothelial connective tissue, as is documented in these cited studies, can increase the likelihood of blood flow retardation and platelet aggregation (blood flow control reviewed in Itoh and Suzuki 2012) and ultimately thrombosis (He et al., 2016), another potential mechanism for reducing the size of capillary lumina.

3.4.11 Capillary Radius Variation is Reduced by HFD

In the brain, regional changes in neuronal activity require changes in blood flow distribution to facilitate region-specific nutrient exchange and removal of waste products. My results demonstrated a reduction in the variation of radii in the capillary bed, suggesting an impaired ability of the vessels to regionally vary their diameter. This is typically stimulated through metabolic vasodilatory signalling, and given that deficits in the ability of the vasculature to respond to vasodilatory signals has been documented in a model of HFD feeding (Obadia et al., 2017), such an impairment could be behind the decreased radius variance I report. However, dietary effects on vasodilatory capacity have not been investigated following short-term HFD feeding. My results, suggesting a reduction in the dilatory capacity of the capillary bed, may be associated with deficits in neurovascular coupling *in vivo*, as is reported by Tucsek et al. (2014b) and Li et al. (2013) following longer periods of HFD feeding.

3.4.12 Two Weeks of HFD Decreases Capillary Perfusion

Capillary perfusion by FITC-conjugated albumin was associated with the presence of non-perfused gaps between perfused segments of the vasculature. A comparison of the proportion of total capillary length perfused revealed a trend level effect of diet, where HFD animals showed reduced vascular perfusion levels. In addition, given the data appeared to have more of a bimodal than normal distribution, a logistic regression was conducted. This showed that the probability of having a perfusion percentage below 50% of total capillary length was significantly increased in the HFD group.

As for what may cause this incomplete perfusion, it is possible that the endothelial pathology seen in longer term HFD feeding (He et al., 2016; Constantinescu et al., 2011) occurs early as well, and in doing so may promote platelet aggregation, and ultimately thrombosis (He et al.,

2016), where the presence of aggregates could underlie the appearance of non-perfused vascular segments. An alternate source of capillary lumen blockage or obstruction could relate to leukocytes, as leukocyte adhesion to endothelial cells could plug capillaries and disturb flow (del Zoppo et al., 1991). Indeed, Obadia et al. (2017) observed a significant increase in the number of rolling and adherent leukocytes in HFD fed animals, although this was in post-capillary venules, and again, has only been looked at after long-term HFD feeding.

The fact that these non-perfused segments occur in-between perfused regions of the vasculature make it unlikely that they are due to total blockages of the capillary bed, unless there was a degree of retrograde movement of perfusate from venous circulation back into the capillaries. Assuming this is not the case, it therefore seems that as the FITC-conjugated albumin / gelatin perfusate begins to set, parts of the capillary bed exert enough pressure to force out the semi-solidified gelatin once the positive pressure of the perfusion has ceased. These regions of increased pressure could be areas of platelet aggregation or leukocyte adhesion, or may be parts of the capillary bed where bound collagen fibres or lipoprotein particles partially obstruct the luminal radius. Another possibility is that these proposed high-resistance areas of the capillary bed are areas where pericytes have constricted, as they do in a model of Alzheimer's disease (Nortley et al., 2019), or where they have constricted and then died, as they do in ischaemia (Hall et al., 2014). Though my results suggest an absence of early dietary effects on pericytes, I only evaluated changes in ISD, so early HFD induced pericyte constriction remains a possible mechanism. This could also explain both the perfusion results, and the overall capillary radius reductions.

To investigate the mechanisms underpinning the perfusion reduction observed in my model, experiments should look at the prevalence of rolling and adherent leukocytes in the capillary bed, as well as the detection of platelet aggregates, thromboses, lipoprotein particles, and bound collagen fibres, following short-term HFD feeding. An analysis of pericyte death in the capillary bed, as well as the distribution of capillary radii at the points where pericytes are located, could help reveal if their constriction (and possible death) are involved.

3.4.13 The Hippocampus has a Poorer Ratio of Vascular Supply to Metabolic Demand than the Cortex

Capillary length density was lowest in the hippocampus, followed by the hypothalamus and then the cortex. These results fit with work by Todorov et al. (2019), who demonstrated (in a preprint) that vessel density was greater in visual cortex than the arcuate hypothalamic area in mice, and Klein et al. (1986), who reported a significantly lower vessel segment density between the

hippocampus and all of frontal, visual, and auditory cortices in rats. In Wu et al. (2004b) vessel density was estimated using MRI, and the value in the cerebral cortex was almost twice that in the hippocampus, whilst Bohn et al. (2016) demonstrated an elevated vessel density in frontal cortex relative to hippocampus in both rats and mice. Both Patt et al. (1997) and Zeller et al. (1997) showed greater vessel number density in the cortex compared to the hippocampus. Results also showed that capillary radius, and radius variance, were lowest in the hippocampus, followed by the cortex and then the hypothalamus. Studies looking at regional differences in vessel radius are rare, though Todorov et al. (2019) demonstrate heterogeneity in vascular radii between brain regions, and showed reduced vessel radii in the hypothalamus compared to the cortex - although this was not significant. Weiss et al. (1982) found no significant differences between rat brain regions in terms of vessel diameter, though they note this was not a measure of lumen exclusively as it also included endothelial walls. There appear to be no other studies that have reported their vessel radius data by region, or made it available to interrogate personally or by vessel type, so it is hard to say if my results fit with the literature. Overall however, the lack of vascular support in the hippocampus (assessed as capillary density, radius, and radius variance) relative to the cortex suggests it has reduced blood volume and blood flow, which could make it more sensitive to the effects of HFD, and in doing so, underlie the fact that HFD feeding leads to hippocampus-specific deficits. Indeed, in rats blood volume and blood flow in the hippocampus is reduced relative to the cortex (somatosensory, visual, auditory, and frontal; Cremer and Seville 1983).

Given the correlation between regional vessel density, local blood flow, and glucose utilisation (Klein et al., 1986), my results suggest that the hippocampus receives less vascular support in terms of energy/nutrient supply and metabolic waste removal than the cortex. Though this also suggests vascular support is proportional to energy demand, evidence indicates that the hippocampus has equal, if not greater, neuronal metabolic demands than the cortex. Neuronal density in the parietal and visual cortices (regions of the neocortex imaged in my data; 150,000 +/- 100,000 and 164,000 +/- 50,000 cells/mm^3) is reduced relative to that of hippocampal CA1 (the primary hippocampal subfield imaged; 307,000 +/- 200,000 in dorsal, 180,500 cell/mm^3 in ventral) in mice (numbers taken from Keller et al. 2018). In addition, the uptake of glucose, as indexed using mass spectrometry by the relative abundance of the distribution of hexose phosphate (Kleinridders et al., 2018) appears similar between the hypothalamus ($\sim$140), hippocampus ($\sim$145) and cortex ($\sim$110) in mice, with Zeller et al. (1997) reporting a similar degree of glucose utilisation in cortical V1 and hippocampal CA1. Together these findings suggest that the metabolic requirements are similar, if not greater, in the hippocampus relative to the cortex, which when considered with regional differences in vascular support, demonstrates the uncoupling of hippocampal vascular supply from

metabolic demand. This is likely what underlies the elevated susceptibility of the hippocampus to damage in a number of pathologies, and could translate global HFD-induced changes (such as microglial proliferation, reductions in capillary radius, radius variance, and perfusion extent) into hippocampus-specific cognitive deficits.

3.5 Conclusion

To conclude, two weeks of HFD feeding was associated with the imminent onset of diet induced weight gain, though in the cohort of mice that displayed hippocampus-specific cognitive deficits HFD feeding had no effect on weight, supporting the evidence that HFD can induce early hippocampus-specific cognitive impairment through weight-gain independent mechanisms. This may be through effects on insulin signalling or BDNF expression. Analysis of hippocampal proteins and proinflammatory cytokines revealed no diet induced changes, nor any correlation between protein levels and behavioural performance. When considered with the evidence of diet-induced microglial proliferation in the absence of morphological changes, these results suggested that short-term HFD feeding may prime, rather than activate, hippocampal microglia. A mechanism linking microglial priming to HFD-induced cognitive deficits is unclear, though the inflammatory results reported may also be driven by the infiltration of circulating monocytes. Short-term HFD did not affect BBB integrity, though more work needs to be done in order to evaluate hippocampal changes using smaller molecules, and neither the distance between capillary pericytes, nor levels of GLUT1 expression, were affected by diet. HFD feeding was associated with numerous detrimental effects on the capillaries themselves, including a reduction in the radius of capillary lumina and a reduction in the length of the capillaries that were perfused by a gelatin solution. These changes likely reflect diet induced capillary obstruction or blockage by platelet aggregates, adherent leukocytes, collagen fibres, lipoprotein particles, or constricted (and potentially dead) pericytes. Finally, regional differences support the suggestion that the hippocampus suffers from a relative uncoupling of blood supply from metabolic demand due to its reduced capillary density and smaller average capillary radius relative to regions such as the cortex. My results therefore support the evidence that short-term HFD feeding is associated with hippocampus-specific cognitive deficits, and suggest this could result from global dietary effects having a greater detrimental effect on hippocampal processing relative to other brain regions due to the enhanced vulnerability of its neurons to damage given their paucity of vascular support.

Chapter 4

In Vivo Microglial Changes

4.1 Introduction

Short-term exposure to a HFD is associated with hippocampus-specific cognitive deficits (McLean et al., 2018; Kanoski and Davidson, 2010), though the mechanisms behind this remain poorly investigated. In the previous chapter I demonstrated that this is likely the result of global HFD-induced detrimental changes, such as microglial proliferation and capillary bed structural impairments, that are translated into hippocampus-specific deficits as a result of its poor vascular support system leading to enhanced neuronal susceptibility to damage. However, I only investigated this after two weeks of HFD feeding, given this was the time at which my group previously demonstrated HFD-induced impairments in the hippocampus-specific NOCR task in unpublished work. I was therefore unable to determine whether microglial changes contribute to the genesis of early cognitive deficits given they appear within 24 hours (McLean et al., 2018). In addition, I hypothesised that microglia may be primed, rather than activated, by short-term HFD feeding, given I observed evidence of their proliferation in the absence of morphological or cytokine level changes. As an alternative theory, a transient peak in microglial activation that subsides within the first two weeks of HFD could promote initial proliferation and morphological and cytokine changes, with the only persistent evidence of this being an increased microglial density once it has subsided. Whilst phasic inflammatory changes have been documented in the hypothalamus (Thaler et al., 2012) their existence has not been investigated in the hippocampus and cortex. To answer these questions I used *in vivo* timecourse imaging of mice implanted with cranial windows over cortical V1 and hippocampal CA1 to investigate microglial changes starting at the very beginning of dietary treatment and lasting for 8 weeks. At the end of this timecourse mice were injected with LPS to induce an inflammatory response. This served as a positive control in order to confirm my

analyses were able to detect inflammatory microglial changes, but also allowed me to evaluate the microglial priming theory.

4.1.1 Microglial Priming

Results from the previous chapter demonstrated cognitive impairment without any concurrent elevation of hippocampal proinflammatory cytokines, something that has been shown previously after short-term HFD (Kaczmarczyk et al., 2013). Though this suggests an absence of inflammatory changes, microglia were present in greater numbers, a sign of microglial activation. However, this was not coupled with any change in microglial morphology, an additional marker of activation (microglia reviewed in Kettenmann et al. 2011). An explanation for microglial proliferation in the absence of either cytokine or morphological changes is that these cells were primed rather than activated.

Microglial priming is widely observed with age and in neurodegenerative diseases (reviewed in Tay et al. 2017; Norden and Godbout 2013; Perry and Holmes 2014). Like activated microglia, primed cells proliferate (priming reviewed in Li et al. 2018) and their somas increase in size (Torres-Platas et al., 2014). However, they are highly ramified like resting microglia (Torres-Platas et al., 2014) and do not produce inflammatory mediators (Perry and Holmes 2014 in Hoogland et al. 2018). They also produce an exaggerated inflammatory response following a proinflammatory stimulus, and aged (and therefore likely primed) microglia demonstrate reduced process motility (reported in the outer plexiform layer of the retina; Damani et al. 2011). There is evidence that obesity is associated with altered responses to immune challenge that might be associated with inflammatory priming, where obese individuals have impaired wound healing, and alongside obese rodents, are more susceptible to infections (Wilson and Clark, 2004; Falagas and Kompoti, 2006; Smith et al., 2007). With regards to HFD feeding, Sobesky et al. (2016) and (Souza et al., 2019) both demonstrated evidence of microglial priming after only 3 days of HFD, and after 8 weeks diet-induced obese rats showed greater LPS induced elevations in levels of hypothalamic IL-1β, IL-6, and SOCS3 mRNA (Pohl et al., 2009). However, after 16 weeks of HFD isolated hypothalamic microglia demonstrated no evidence of priming (Baufeld et al., 2016), illustrating that HFD-induced priming may be an inconsistent dietary effect.

4.1.2 Phasic Inflammatory Changes

The uncoupling of microglial proliferation from morphological and cytokine changes could relate to phasic patterns of HFD-induced inflammation. Thaler et al. (2012) showed that proinflammat-

ory cytokine mRNA levels in the hypothalamus are elevated after 1 and 3 days of HFD, but return to basal levels by 7 days. They are then elevated again after four weeks. If a similar pattern of inflammation occurs throughout the brain, it is possible that its initial peak drives microglial proliferation and morphological changes, before the latter returns to baseline as cytokine production falls at the end of the first week of HFD feeding. This would result in an environment at the two week point where microglial cells that proliferated at an earlier timepoint are still present, but have returned to a resting morphology. In addition, basal levels of cytokines would be detected. With regards to the associated cognitive deficits, inflammation could drive the genesis of behavioural impairment during the initial cytokine peak, with the results of this persisting beyond the transient activation.

Though demonstrated in the hypothalamus (Thaler et al., 2012), evidence for similar phasic changes in the hippocampus is mixed, though admittedly not well studied. Within 1 and 3 weeks of HFD feeding there are no signs of hippocampal inflammation (Kaczmarczyk et al., 2013), though this would fit with the timecourse established by Thaler et al. (2012), whilst long-term studies show both increases (Thirumangalakudi et al., 2008; Liu et al., 2014) and no change (Boitard et al., 2014; Sobesky et al., 2014) in hippocampal cytokine levels. What underlies the biphasic cytokine response to HFD reported by Thaler et al. (2012) remains unclear, though Mendes et al. (2018) suggest that it could be due to the HFD induced infiltration of circulating monocytes (Valdearcos et al., 2017). However, this has thus far only been reported in the hypothalamus, where it took place after a week (Valdearcos et al., 2017).

4.1.3 Aims, Hypotheses, and Experimental Approach

Thus far no work has looked at inflammatory changes in the hippocampus or cortex at any timepoint prior to one week of HFD feeding. In addition, no studies have tracked inflammatory changes over time in the hippocampus or cortex, so it remains unclear if phasic inflammatory responses to HFD occur in these regions as they do in the hypothalamus (Thaler et al., 2012). Finally, no studies have looked at the effect of HFD on microglia *in vivo*, and have also therefore not been able to correlate cognitive performance with cellular measures within the same animal. I hypothesised that hippocampal inflammation would show a phasic pattern, with it being detected initially but returning to baseline by the two week timepoint, before becoming elevated again at a later time. The initial peak would be responsible for driving mechanisms involved in hippocampal cognitive impairment, and therefore mice undergoing cognitive testing at any point during the inflammatory return to baseline would show no correlation between behaviour and microglial activation. Al-

ternatively, I hypothesised that no changes in microglial activation would be detected until later in the dietary manipulation, and that microglia would show evidence of priming instead of phasic patterns of activation.

My aims with the work presented in this chapter were to to investigate whether microglial changes contribute to the genesis of early cognitive deficits resulting from HFD feeding by investigating them at multiple timepoints within the first week of manipulation, to look at microglial changes at multiple points over a timecourse to evaluate the presence of phasic inflammatory changes in the cortex and hippocampus, to combine *in vivo* microglial imaging with hippocampus-specific NOCR behavioural testing in order to correlate changes in microglia with cognitive performance, to evaluate whether hippocampal window surgery affected behavioural performance relative to naive mice (mice that had not undergone any surgery), and to determine whether HFD feeding primed microglia.

To address these aims I used two photon microscopy to conduct *in vivo* timecourse imaging of awake, behaving, mice with fluorescently labelled microglia (using the Cx3CR1-GFP mutation that labels microglia and circulating monocytes; Imai et al. 1997) implanted with cranial windows over cortical V1 and hippocampal CA1 to image microglia starting at the very beginning of dietary treatment and lasting for 8 weeks. At the end of this timecourse mice were injected with LPS to induce an inflammatory response. By imaging both cortex and the hippocampus I was able to determine whether HFD-induced inflammatory changes showed any region-specific effects at multiple timepoints, since the global effects I detected in my previous chapter were only related to dietary changes following two weeks of feeding, and taking an *in vivo* approach allowed me to not only quantify changes in microglial activation (by analysing changes in their morphology, with this being a widely accepted metric of inflammatory microglial changes; Kettenmann et al. 2011), but also to look at microglial process motility. Microglia extend and retract their processes in order to survey their environment and continuously interact with surrounding elements (Nimmerjahn et al. 2005 cited in Hierro-Bujalance et al. 2018). This process is ATP dependent (Davalos et al., 2005) and the extent of their motility varies with neuronal activity (in a preprint; Nebeling et al. 2019). Inflammation induced by systemic administration of LPS decreased process motility (Paris et al., 2018), which would suggest that proinflammatory HFD exposure should do the same. The effect of HFD treatment on process motility however has thus far not been published, with the most relevant work conducted by Madore et al. (2014) (cited in Paolicelli and Ferretti 2017) who looked at the effects of n-3 polyunsaturated fatty acid (PUFA) deficiency, and noted a change in motility at postnatal day 21 in mice raised by mothers that were fed PUFA deficient diets throughout gestation and lactation.

By looking at timepoints that span from within the first week of dietary manipulation to up to 2 months, I was able to both evaluate microglial activation at the very beginning of dietary treatment, thereby shedding light on the contribution of inflammatory changes to the genesis of early HFD-induced cognitive impairment, as well as investigate the presence of a phasic inflammatory response to HFD feeding over an 8 week period. In addition, the systemic administration of LPS, which induces central inflammation through stimulation of microglia TLR4 at CVOs (Laflamme and Rivest, 2001), allowed me to evaluate whether hippocampal and cortical microglia are primed by 8 weeks of HFD feeding given that primed microglia produce a greater inflammatory response after a secondary immune challenge (microglial priming reviewed in Perry and Holmes 2014). This also served as a positive control, allowing me to confirm that my analyses were able to detect signs of microglial activation. Finally, hippocampal window mice were tested on hippocampus-specific NOCR at the two week timepoint in parallel with the wild type mice described in the previous chapter. Besides correlating cognition with microglial changes, this allowed me to evaluate the effect of surgery on baseline hippocampal cognition and diet induced cognitive deficits. I elected to perform behavioural testing after two weeks of HFD feeding as this was the duration used in the HFD induced deficits reported previously in unpublished work in my lab. The fact that my imaging was conducted in awake mice is important, as arousal state can influence microglial morphology and process motility, with microglia in awake mice demonstrating reduced ramification and increased levels of process motility relative to anaesthetised animals (in a preprint; Stowell et al. 2019). Additionally, during development, the contact of microglial processes with dendrites induced the formation of new spines, but only in awake mice (Miyamoto et al., 2016).

4.2 Methods

4.2.1 Animals, Dietary Manipulation, and Experimental Approach

Details of animal genotypes, diets used, behavioural testing, window implantation surgeries, and imaging setup, are presented in the main methods (**Chapter 2**). All *in vivo* imaging data were collected from Cx3CR1-GFP heterozygotes that had undergone either cortical, or hippocampal, window implantation. These mice were housed in a reverse light-dark cycle to minimise the impact of imaging sessions on circadian rhythms, and fed either a HFD or control diet for 57 days. In some cases, window implanted mice had to be culled prior to 57 days for welfare purposes. After imaging on day 56, window implanted mice were injected with LPS to induce microglial activation and then imaged again 24 hours later. Following this, mice were either culled using

cervical dislocation or given a terminal dose of i.p. sodium pentobarbital (Dolethal; Vétoquinol Ltd) at 120mg/kg (diluted to 10% in saline). Behavioural testing was run on hippocampal window mice alongside a cohort of wild type C57BL/6J naive mice in order to evaluate the effect of surgery, and dietary manipulation, on hippocampal functioning. As with the *in vivo* mice, these wild type animals were fed either a HFD or control diet. The behavioural protocol began on day 11 of dietary manipulation, and ran until day 14, the day on which testing took place. After testing wild type mice were culled using cervical dislocation. Mice were weighed daily, though not always at the same time of day. A summary of mice used is presented in **Table 4.1**. The mice used in this chapter and the chapter following (**Chapter 5**) were the same.

	Naïve	Cortical Window	Hippocampal Window
Genotype	Wild type	Cx3CR1-GFP	Cx3CR1-GFP
Count (HFD)	9 (4)	17 (8)	12 (6)
Male:Female	6:3	15:2	7:5
Mean Age +/- SD (Weeks)	12.43 +/- 1.92	15.75 +/- 3.92	16.13 +/-4.31

Table 4.1: Summary Statistics of Mice Used in Chapters 4 and 5. Mouse information split by surgery status. **Genotype** indicates the genotype of mice used. **Count** indicates the total number of mice with those fed a HFD denoted in parentheses. **Male : Female** displays the ratio of male to female mice. **Age** represents age at the start of dietary manipulation, and is presented as the mean +/- 1 SD in units of weeks.

4.2.2 Two-Photon Microscopy

High-resolution imaging of vessels and microglia was performed with a commercial two-photon microscope (SP5, Leica), a high numerical aperture water-dipping objective (Olympus 20X XLUMPLFLN20XW; Nikon 16X N16XLWD-PF), and a mode-locked Ti-sapphire multiphoton laser (Chameleon, Coherent). Tissue was excited at a 940nm wavelength, and the emitted light was filtered to collect red and green light from Texas Red Dextran (vessel lumina) and Cx3CR1-GFP (microglia). Imaging sessions were recorded in the SciScan software (Scientifica). Laser power at the objective was kept below 25mW to minimize photodamage. Laser power and photodetector gain was kept relatively constant between imaging sessions to prevent drastic variations in the signal to noise ratio of images. Stacks sampling 100 µm of tissue were collected for microglial morphology analysis from a depth below the window of 50 µm down to 150 µm. These were acquired at a resolution of 512 x 512 pixels with a voxel size of 580 x 580 x 1000nm (XYZ). Six

frames were taken at each imaging plane. These parameters were based on work by Kozlowski and Weimer (2012). Likewise, the stacks used for microglial process motility quantification sampled 50 µm of tissue from a depth of 75 µm down to 125 µm below the window. These were captured at 512 x 512 pixels with a voxel resolution of 270 x 270 x 2000nm (XYZ). Fourteen frames were taken per plane, and six motility stacks, 386 seconds apart, were recorded per animal per timepoint to create a timelapse of z-stacks. These parameters were chosen given they provided a good balance between quick stack acquisition and a high enough frame count, as frames that were contaminated by motion had to be removed. Capturing 14 frames per plane provided a good likelihood that at least one frame would be unaffected by motion, allowing me to recompile the stack after motion correction. Given the clear difference in appearance between control and high fat pellets, imaging was not blinded to dietary manipulation. Additionally, imaging was not blind to timepoint or window placement, as cortical and hippocampal windows required the use of different objectives.

4.2.3 Image Processing

Images were processed and analysed using the Fiji distribution of ImageJ (Schindelin et al., 2012). Custom scripts were written to detect and remove motion-contaminated frames. First, contrast levels within a stack were normalised using the Stack Contrast Adjustment plug-in (Čapek et al., 2006) before a Laplacian of Gaussian filter was applied to the images and the maximum pixel grey value was used as a measure of distortion, where higher values represent more distorted images. The frame from each plane that had the lowest maximum grey value was selected, and the selected frames were recompiled into a z-stack. Stacks were then registered with the MuliStackReg plug-in (Thévenaz et al., 1998). In the case of stacks acquired for process motility analysis, these were registered across time by registering them to the previously acquired z-stack. Following frame selection and registration, stacks were inspected for the quality of preprocessing. Where this wasn't satisfactory, manually selected frames were recompiled and registered. If this was still not adequate, images were excluded from further analysis. Image processing was done blind to diet group, window placement, timepoint, and mouse identity.

4.2.4 Image Quantification

All image quantification was done blind to diet group, window placement, timepoint, and mouse identity.

Microglial Morphology

The methodology used to semi-automatically generate microglial cell masks from two-photon image stacks is based on the work of Kozlowski and Weimer (2012). 100 µm deep z-stacks were split into three 10 µm stacks separated by 20 µm, where this separation would prevent the same cells being sampled in multiple 10 µm sub-stacks. A mean intensity projection was taken of each sub-stack and these were used for quantification. Cell locations were marked manually on these projections and a 120 x 120 µm ROI was drawn around each cell. Otsu's method (Otsu, 1979), which minimizes the interclass pixel intensity variance between the two pixel classes ('on' or 'off') within the image (Kozlowski and Weimer, 2012), was used to compute an initial grey value for thresholding. This was applied in the Find Connected Regions plug-in, where all pixels that fell above this threshold and were in contact with the marked cell location were used to form a cell mask. The area of this mask was calculated and then compared to a user defined target area. If the area of the mask fell within these values (+/- a user defined range), the mask was considered complete and mask generation moved onto the next cell location. Otherwise, iterative thresholding was used whereby the applied threshold value was adjusted until either the cell area fell within the desired range, or the cell area stabilised for three consecutive iterations. The formula used to determine the threshold for the next iteration

$$T_{IT+1} = T_{IT} + T_{IT}\frac{A_{IT} - TCA}{n(TCA)}$$

relates the threshold for the next iteration (T_{IT+1}) to the current threshold (T_{IT}), the area of the current threshold (A_{IT}), the target cell area (TCA), and the number of iterations thus far (n). Cell masks were excluded from further analysis if an accepted mask contacted the edge of the 120 x 120 µm ROI. For accepted masks, masks of the cell soma were generated using automated thresholding and particle detection, where particles that were smaller than 20 µm^2 and had a circularity value of less than 0.6 were excluded.

An analysis of different target cell area (TCA) values (200 - 800 µm^2) was conducted to select the value that provided the best discrimination between resting and LPS-induced activated microglia in control diet fed animals. This was done based on the size of the effect of LPS treatment on a composite morphology index I dubbed an 'inflammation index' (**Fig 4.6**). The calculation of this index is outlined in the statistical analysis section. A TCA of 500 µm^2 with a range of 100 µm^2 not only provided good discrimination between resting and activated cells, but was also used by Kozlowski and Weimer (2012), so was selected as the value to use for all future analyses.

Automatically generated cell and soma masks were inspected manually. Cell masks were

excluded if they contained more than one cell, clearly misrepresented the cell at the indicated location, or represented cells that were not positioned within the imaged volume. Soma masks were redrawn manually if the automated generation was inadequate, and were excluded from analysis if their associated cell mask has been excluded.

Finally, cell and soma masks that passed inspection were quantified. Multiple parameters were calculated. This involved the use of a sholl analysis (Ferreira et al. 2014; **Fig 4.1 B, C, D**), quantification of simple shape descriptors (**Fig 4.1 A**), skeletonisation of the mask, and the use of a fractal and hull and circularity morphometrics analysis using FracLac for ImageJ (Karperien 2013; **Fig 4.1 A**). A full list of measures is presented in **Table 4.2**.

Microglial Motility

The analysis of microglial process motility was based on work by Sipe et al. (2016). After image stack preprocessing, ROIs were drawn around cells in z-stacks before these were manually thresholded. Within each ROI, overlays were created for each pair of adjacent timepoints and pixels were classified as either retraction (present in the first time point, but absent in the second), extension (absent in the first but present in the second) or stable (present at both timepoints).

These classifications were used to calculate a motility index (MI; sum of extension and retraction pixels / the number of stable pixels), a retraction index (RI; the number of retraction pixels / the number of stable pixels), an extension index (EI; the number of extension pixels / the number of stable pixels), a stability index (SI; the proportion of pixels that were classified as extension that became stable pixels at the subsequent timepoint), and an instability index (II; the proportion of stable pixels that were classified as retraction at the subsequent timepoint). These classifications and indices were calculated separately for each z plane. **Figure 4.2** illustrates how two-photon images were thresholded and used to create timepoint overlays that were used to classify pixels for the calculation of various motility indices.

4.2.5 Statistical Analysis

As stated in the main methods chapter, all analyses were run using LMMs and all plotted values represent the estimated marginal mean +/- 1 SEM derived from the appropriate LMM, unless otherwise indicated. The use of cells or mice as subjects in an analysis is indicated in the appropriate figure legends. Where cells were used as subjects this was accounted for by including a random effect structure in the appropriate statistical model that grouped measurements by animal.

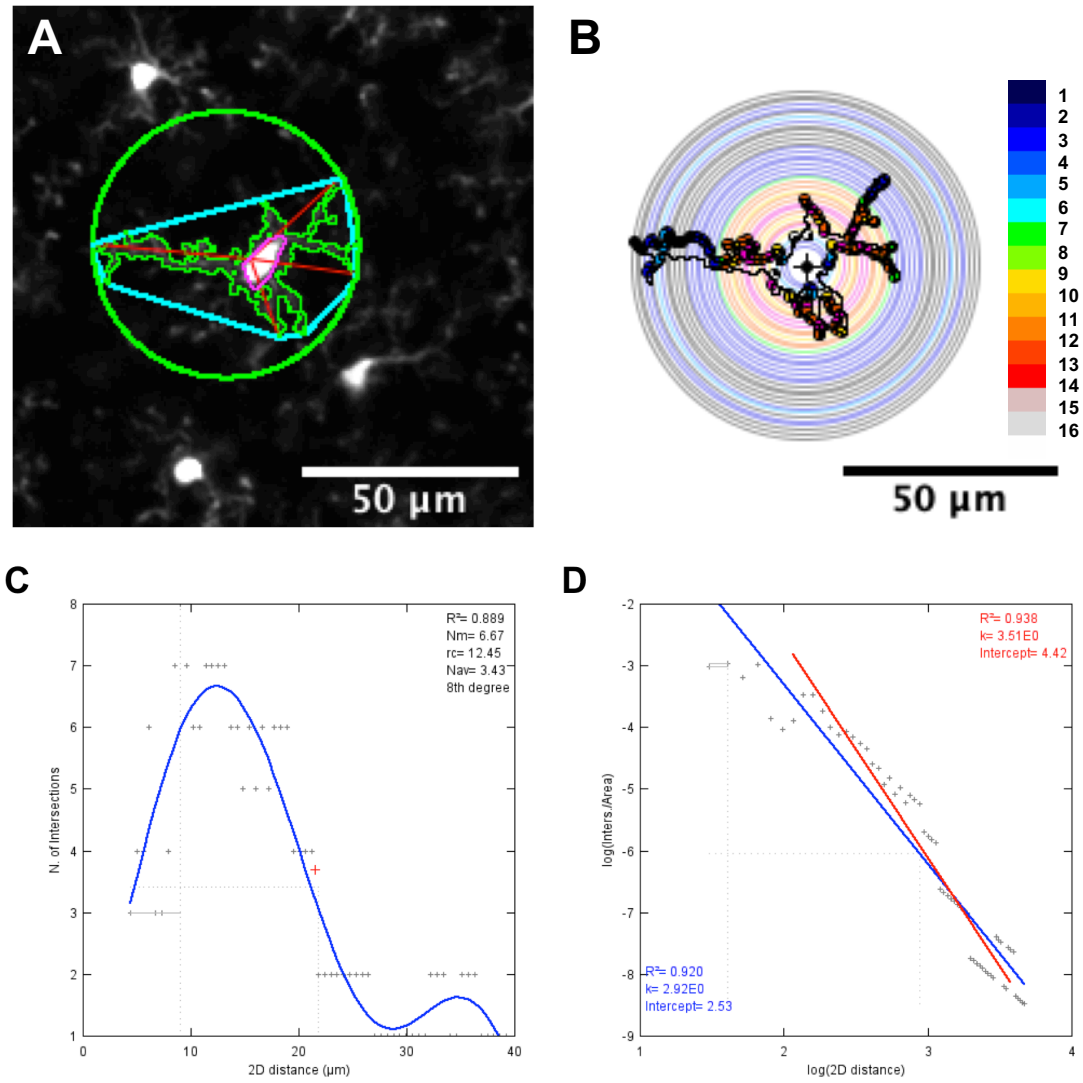

Figure 4.1: Example of Automated Morphology Measure Generation. **(A)** Semi-automated generation of microglial cell masks was involved in quantifying parameters such as cell perimeter (**green outline**), soma area (**magenta outline**), and cell spread (**red lines**). Hull and circle morphometrics were based on analysis of the convex hull (**cyan outline**) and bounding circle (**green circle**). **(B)** A sholl analysis performed on the cell mask counted the number of branches at varying distances from the cell soma. The analysis began from a distance equal to the circular radius of the soma (**white circle in the mask centre**) from the centre of the cell soma (**black dot**). **Coloured rings** indicate the number of branches at increasing distances. **Coloured spots** on branches are colour coded by number of branches at that distance. **Colour scale** indicates colour coding. **(C)** A linear sholl analysis was used to compute values such as the mean, median, and sum of branches (here called intersections), as well as the centroid (**red dot**, the mean position of all plotted points). Values were derived for both the sample data, and data based on the best fit polynomial (**blue line**). **(D)** A log-log sholl analysis. For both semi-log and log-log analyses, the numbers of intersections are normalised to the area of the mask, then plotted either against distance or the log of the distance respectively. Plotting a linear regression (**blue line**) can be used to derive a regression coefficient (**k**) and intercept. This can also be calculated for data within the 10th to 90th percentiles (**red line**). Plots **C, D** were output by the sholl analysis plug-in in ImageJ.

Perimeter	Cell Spread	Eccentricity	Roundness	Soma Area	Mask Area	Branches
Junctions	End-point Voxels	Junction Voxels	Slab Voxels	Average Branch Length	Triple Points	Quadruple Points
Maximum Branch Length	Longest Shortest Path	Skeleton Area	Primary Branches	Intersecting Radii	Sum Intersections	Mean Intersections
Median Intersections	Skewness (sampled)	Kurtosis (sampled)	Max Intersections	Max Intersection Radius	Ramification Index (sampled)	Centroid Radius
Centroid Value	Enclosing Radius	Critical Value	Critical Radius	Mean Value	Ramification Index (fit)	Skewness (fit)
Kurtosis (fit)	Polyn. Degree	Regression Coefficient (Semi-log)	Regression Intercept (Semi-log)	Regression Coefficient (Semi-log) [P10-P90]	Regression Intercept (Semi-log) [P10-P90]	Regression Coefficient (Log-log)
Regression Intercept (Log-log)	Regression Coefficient (Log-log) [P10-P90]	Regression Intercept (Log-log) [P10-P90]	Density	Span Ratio	Maximum Span Across Hull	Convex Hull Area
Convex Hull Perimeter	Convex Hull Circularity	Maximum Radius from Hull's Centre of Mass	Max/Min Radii	CV For All Radii	Mean Radius	Diameter of Bounding Circle
Maximum Radius from Circle's Centre	Max/Min Radii From Circle's Centre	CV for all Radii from Circle's Centre	Mean Radius from Circle's Centre	Fractal Dimension	Lacunarity	Branching Density

Table 4.2: Automatically Generated Microglia Morphology Measures. A wide range of parameters were used to quantify microglial morphology. These were from five different analyses. **Yellow;** simple shape descriptors. **Green;** measures based on the cell mask skeleton. **Purple;** parameters derived from sholl analyses. Intersections refer to processes. Fit and sampled refer to measures derived from the polynomial fit or raw data of linear sholl analyses respectively. Semi-log and log-log refer to values derived from the semi-log and log-log sholl analyses. [P10-P90] refers to values derived from data within the 10th to 90th percentiles, rather than all the data. **Red;** indicates hull and circularity morphometrics. **Blue;** fractal analysis. **Orange;** branching density is calculated by dividing the skeleton area by the convex hull area.

The impact of diet and time on weight gain was analysed by normalising weights for each animal to their weight at the beginning of dietary manipulation. This was done to control for differences in starting weight, given the use of mice of both sexes and varied age. On occasion mice were not weighed everyday throughout the 8 week dietary manipulation. To account for this. missing weight readings were filled in for each animal using linear regression predictions. The number of missing weights by day (and percent by diet group) are presented in **Table 4.3**. Separate analyses were done for *in vivo* imaging mice and behaviourally tested mice (these mice

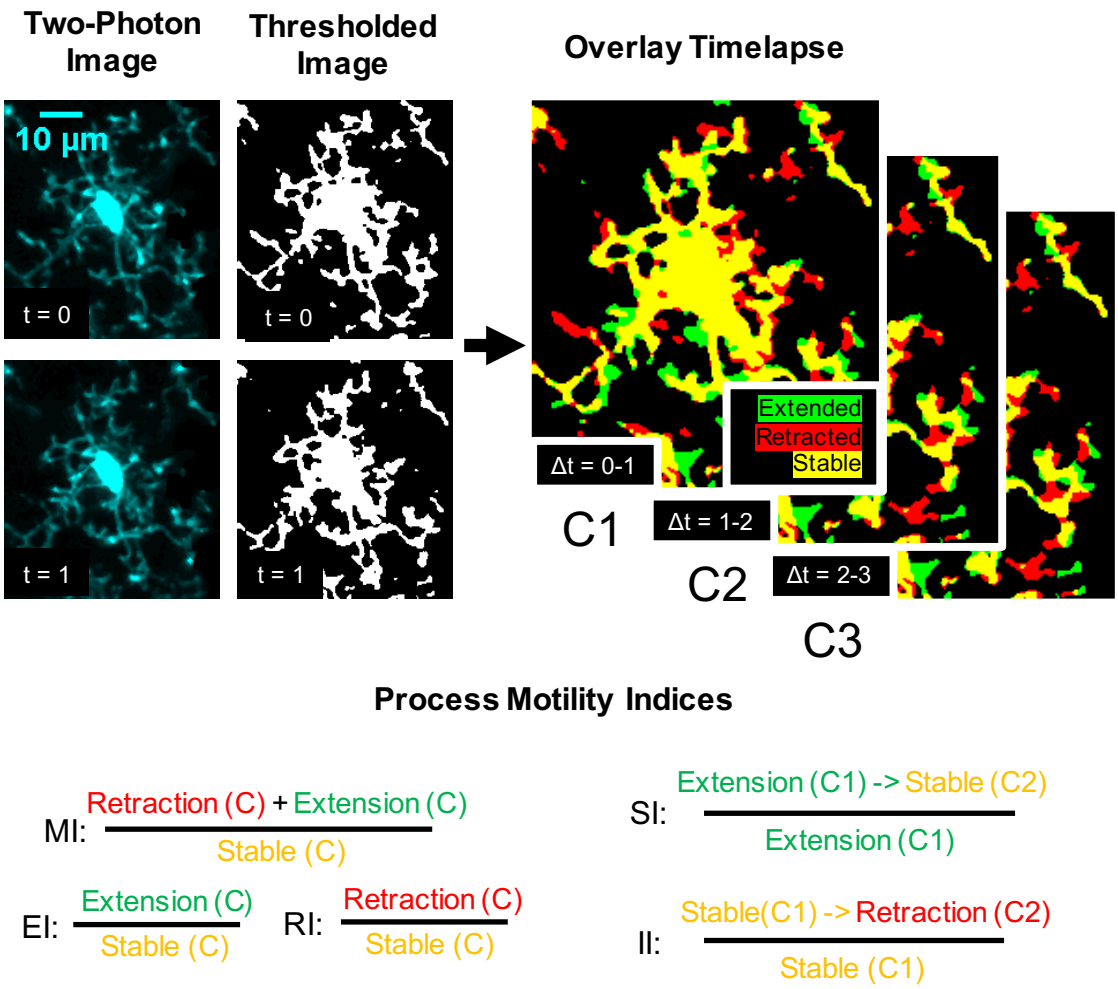

Figure 4.2: Calculation of Indices of Process Motility. Two-Photon Image; Process motility indices were calculated by thresholding stacks of microglial cells obtained with two-photon microscopy. **Thresholded Image;** Adjacent timepoints were compared between manually thresholded stacks. **Overlay Timelapse;** Pixels were classified either as extension (**green**), retraction (**red**) or stable (**yellow**), depending on whether they appeared, disappeared, or remained, from one timepoint to the next. **Process Motility Indices;** The MI, EI, and RI were calculated within each timepoint comparison i.e. within C1, C2, or C3. The SI and II were calculated across timepoint comparisons i.e. using both C1 and C2, or C2 and C3. SI was calculated using the number of extension pixels in a previous comparison that became stable pixels in the next. This was divided by the number of extension pixels in the previous comparison. II was calculated using the number stable pixels in a previous comparison that became retraction pixels in the next. This was divided by the number of stable pixels in the previous comparison.

also included the hippocampal window *in vivo* mice). Fixed effects were specified as diet, day and surgery status (cortical window, hippocampal window, or naive), as well as their interactions. The main effects of sex and age were also included as factors. Random intercepts were included for each animal with random slopes for the relationship between days. An autoregressive order 1 model for the correlation between days was included.

NOCR performance was analysed with NI as the dependent variable, and fixed effects were

Day	High Fat	Control	Day	High Fat	Control	Day	High Fat	Control
1	0 (0.0)	0 (0.0)	**20**	7 (50.0)	6 (40.0)	**39**	5 (35.7)	7 (46.7)
2	1 (7.2)	2 (13.3)	**21**	8 (57.1)	4 (26.7)	**40**	5 (35.7)	7 (46.7)
3	2 (14.3)	5 (33.3)	**22**	6 (42.9)	5 (33.3)	**41**	7 (50.0)	7 (46.7)
4	2 (14.3)	2 (13.3)	**23**	9 (64.3)	9 (60.0)	**42**	6 (42.9)	8 (53.3)
5	2 (14.3)	5 (33.3)	**24**	10 (71.4)	9 (60.0)	**43**	6 (42.9)	3 (20.0)
6	2 (14.3)	3 (20.0)	**25**	8 (57.1)	10 (66.7)	**44**	5 (35.7)	5 (33.3)
7	3 (21.4)	4 (26.7)	**26**	6 (42.9)	10 (66.7)	**45**	5 (35.7)	7 (46.7)
8	2 (14.3)	4 (26.7)	**27**	7 (50.0)	6 (40.0)	**46**	3 (21.4)	9 (60.0)
9	5 (35.7)	7 (46.7)	**28**	6 (42.9)	7 (46.7)	**47**	6 (42.9)	5 (33.3)
10	5 (35.7)	10 (66.7)	**29**	7 (50.0)	6 (40.0)	**48**	8 (57.1)	4 (26.7)
11	5 (35.7)	8 (53.3)	**30**	7 (50.0)	8 (53.3)	**49**	4 (28.6)	2 (13.3)
12	7 (50.0)	6 (40.0)	**31**	1 (7.1)	5 (33.3)	**50**	3 (21.4)	5 (33.3)
13	5 (35.7)	6 (40.0)	**32**	4 (28.6)	7 (46.7)	**51**	2 (14.3)	7 (46.7)
14	5 (35.7)	5 (33.3)	**33**	6 (42.9)	5 (33.3)	**52**	5 (35.7)	8 (53.3)
15	6 (42.9)	5 (33.3)	**34**	6 (42.9)	5 (33.3)	**53**	5 (35.7)	6 (40.0)
16	5 (35.7)	8 (53.3)	**35**	6 (42.9)	3 (20.0)	**54**	5 (35.7)	7 (46.7)
17	5 (35.7)	8 (53.3)	**36**	5 (35.7)	4 (26.7)	**55**	4 (28.6)	5 (33.3)
18	9 (64.3)	9 (60.0)	**37**	5 (35.7)	6 (40.0)	**56**	4 (28.6)	2 (13.3)
19	10 (71.4)	7 (46.7)	**38**	7 (50.0)	7 (46.7)	**57**	7 (50.0)	8 (53.3)

Table 4.3: Record of Missing In Vivo Weights. The number of missing weight recordings by day and diet group for *in vivo* imaging mice, with the percentage of weights missing by day and diet group indicated in brackets.

specified as diet, surgery status, and their interaction. The main effects of sex, age, and weight change (relative to baseline) were included. A random intercept for animal was included.

Microglial Statistical Analysis

Microglial morphology changes were analysed using a similar technique to that of Heindl et al. (2018). This involved first identifying the morphological measures that were best able to distinguish LPS-activated from resting microglial cells (i.e. cells imaged at day 57 of dietary manipulation, 24 hours after LPS injection, compared to cells imaged at day 56) in control diet fed, cortical window mice. This was done to avoid the influence of dietary manipulation and tissue aspiration on the ability of morphological measures to distinguish between the conditions. The discriminatory ability of the measures was quantified using receiver operating characteristic (ROC) analysis. ROC curves plot the false positive and true positive rates of binary classification against one another at differing thresholds, with the area under the curve (AUC) of the plot used to quantify the accuracy of the binary classifier (examples are demonstrated in **Fig 4.5**). A PCA with feature centering and scaling was run on the measures that had the best AUC values to further reduce the dimensionality of the dataset, and the PC1 was used as an index of inflammation-related morphology changes. This is what is referred to in this chapter as an 'inflammation index'. When selecting measures based on ROC performance, measures that were present in variant forms were compared with one another and the poorest performing variant was dropped. Variants existed for sholl parameters derived from all, or a percentile of the data, as well as from sampled or fitted data, and from hull and circle morphometrics based on the bounding circle centre or centre of mass.

Microglia motility indices were averaged across all z-depths. Each index was analysed separately, as was a combined motility index constructed using a PCA with feature centering and scaling run on all calculated motility indices. This compound index is referred to in this chapter as the compound motility score.

The main effects of sex, age, and weight change were included for all the following described models, except for those used for TCA selection. Cells were used as subjects in all analyses. For all analyses, except those looking exclusively at changes at the two week timepoint, an autoregressive order 1 model for the correlation between days was included. Data at the 49 day timepoint was excluded from morphology analysis as no hippocampal HFD cells passed manual checking.

Analysis of timecourse data for morphology and motility measurements was done specifying timepoint, diet, region (cortex or hippocampus), and their interactions, as fixed effects. A random intercept for each animal was specified, with a random slope for the relationship between days.

A separate analysis was run to look at the effects of LPS, where LPS treatment, diet, region, and their interactions, were specified as fixed effects. A random intercept for animal was specified with a random slope for LPS condition.

In addition, an analysis of behaviourally tested hippocampal window mice was run to look at changes at the two week timepoint and correlate them with performance. Here diet and NI and their interaction were specified as fixed effects. A random intercept for animal was included. As well as this, analysis of changes at two weeks across all *in vivo* mice was conducted. This analysis included diet and region and their interaction as fixed effects, with a random intercept for animal.

For TCA selection, the analysis was restricted to animals fed a control diet with cortical windows. The effect of LPS treatment, with no covariates specified, on the inflammation index at different TCA values was analysed. A random slope for LPS condition, and a random intercept for animal, were included.

4.3 Results

4.3.1 HFD Did Not Significantly Affect Weight Gain of *In Vivo* Mice

In order to evaluate the effect of HFD feeding on weight gain, weights were compared. These were normalised to their value at the beginning of dietary manipulation to control for differences in starting weight, and the effect of diet on this value in *in vivo* imaging mice (that were heterozygous Cx3CR1-GFP mutants) was analysed using an LMM (**Fig 4.3**). From here on, this value will be referred to as weight. The following results are relevant to **Chapter 5** as well given the results presented there are based on the same mice. As time passed weight increased ($F(56,983) = 5.49$, $p = < 0.001$), and though HFD appeared associated with greater weights and a greater rate of weight gain, it did not reach significance. There was a significant interaction between surgery type (cortical or hippocampal) and time ($F(56,983) = 1.70$, $p = < 0.001$). This effect was driven by seemingly greater weights in the hippocampal window mice from days 40 to 42, although these differences were not significant.

In order to directly correlate the results of behavioural testing with dietary effects on weight, a separate analysis was limited to behaviourally tested mice **(Fig 4.3 Inset)**. This included both naive wild type, and hippocampal window Cx3CR1-GFP mice. As in the previous analysis, there was a significant increase in weight with time ($F(14, 175) = 4.08$, $p = < 0.001$), however no other factors significantly affected weight.

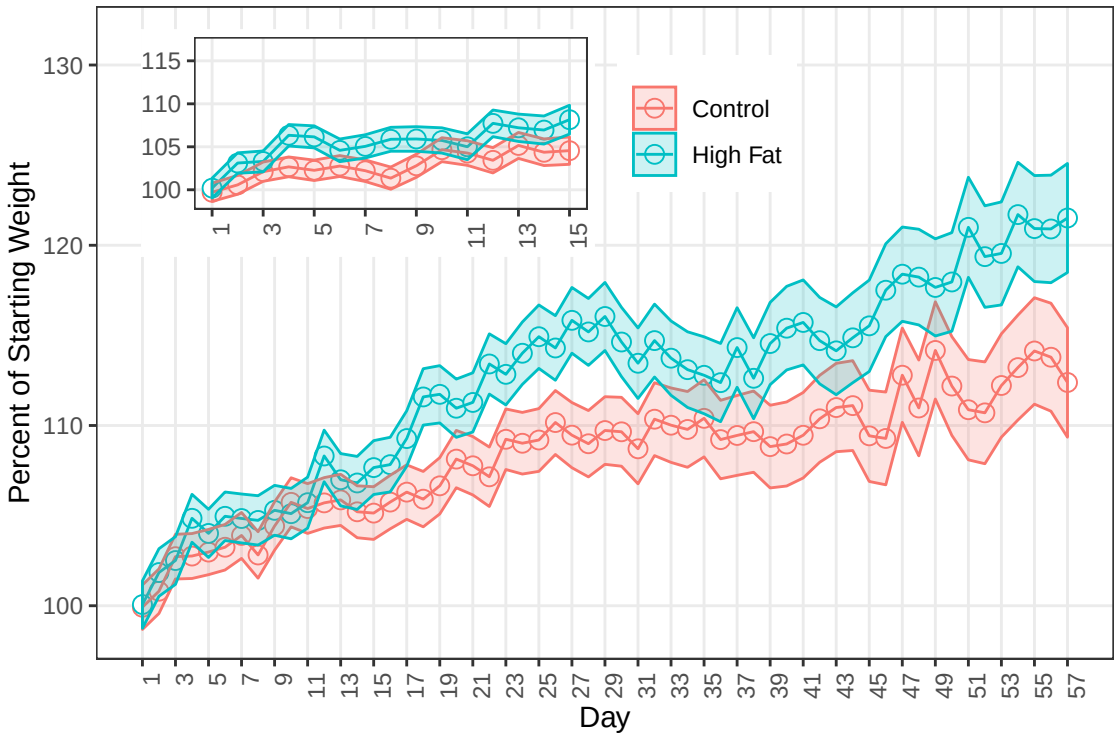

Figure 4.3: HFD Did Not Affect *In Vivo* Weight Gain. Weight relative to its value at the start of dietary manipulation (day 1) increased with time, but was resistant to the effect of HFD both in mice used for *in vivo* imaging, and those involved in behavioural testing (**Inset**). Day 57 indicates the 56th day of dietary manipulation. *In vivo* Cx3CR1-GFP heterozygotes n = 29 mice (n = 14 HFD), behavioural (combination of wild type C57BL/6J and Cx3CR1-GFP heterozygotes) n = 21 mice (n = 9 wild type C57BL/6J where n = 4 HFD; n = 12 Cx3CR1-GFP where n = 6 HFD).

4.3.2 NOCR Performance was Unaffected by Diet or Surgery

Short-term HFD feeding is associated with hippocampal deficits. To investigate the effect of hippocampal window surgery, and diet, on hippocampus-specific cognition, and to correlate cognitive performance with *in vivo* microglial data, the performance of wild type mice that had not undergone surgery, and Cx3CR1-GFP heterozygote hippocampus window implanted mice, on a hippocampus-specific NOCR task following two weeks of dietary manipulation was assessed (**Fig 4.4**). Performance was quantified using the calculation of a NI. Though the NI was reduced in HFD mice (**Fig 4.4 A**; mean +/- SEM = 0.102 +/- 0.042, control = 0.187 +/- 0.039), this difference was not significant (*F(1,13) = 0.96, p = 0.346*). There was also no difference in NI between hippocampal window Cx3CR1-GFP mice (**Fig 4.4 A Left**) and naive wild type animals (**Fig 4.4 A Right;** *F(1,13) = 0.06, p = 0.807*), nor did this interact with the effect of diet (*F(1,13) = 0.29, p = 0.60*).

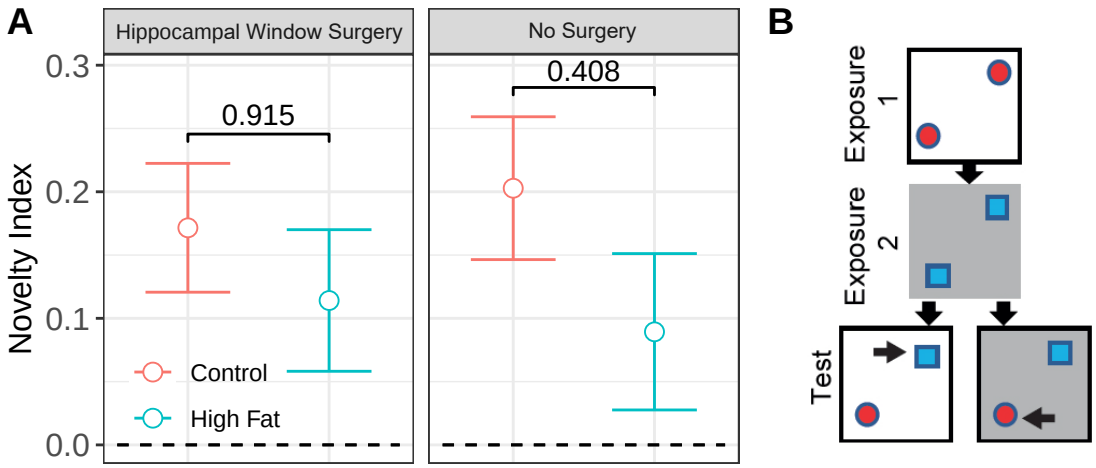

Figure 4.4: NOCR Performance Was Resistant to the Effects of HFD and Hippocampal Window Surgery. (A) NOCR performance was assessed by calculating a novelty index (NI), which represents the difference in the proportion of time mice spent exploring novel versus familiar objects. This was unaffected by diet or surgery status (**Left;** hippocampal surgery, **Right;** no surgery). There was also no surgery and diet interaction (p value of corrected within-surgery status diet comparisons indicated on brackets; dotted line at 0 represents no discrimination between novel and familiar objects). (**B**) The NOCR behavioural protocol took place over three days. On the first day mice were habituated to two different contexts with no associated objects, before being exposed to the two contexts with their associated object pairs for the next two days (**Exposure**). On the third day, mice were tested by placing them in each context with a single object swapped between object pairs such that the swapped object was novel in the given context (**Test**; n = 20 mice (n = 10 HFD; n = 11 hippocampal surgery)).

4.3.3 Semi-Automated Quantification of Activation-Induced Microglial Morphological Changes

In order to process the large number of microglial cells imaged, I took a semi-automated approach to quantifying microglial morphology. In order to ensure that this approach was sensitive to changes in morphology, mice that had reached the end of their dietary manipulation (at day 56) were injected with a 4mg/kg dose of LPS in order to induce microglial activation. Microglial activation is associated with a morphological shift from a ramified to an amoeboid phenotype and systemic LPS application induces microglia activation via TLR4. Two-photon imaging stacks were collected 24 hours after LPS administration and quantified. This was done to refine my analysis approach so that it could detect morphological changes associated with microglial activation, allowing me to have confidence in its sensitivity when applied to analysing the effects of HFD feeding.

Microglial morphology can be quantified in a number of ways. In order to avoid my results being influenced by which of these I elected to measure, I instead opted to measure a wide array of 63 different facets of morphology **(Table 4.2; Figure 4.1)** before using dimensionality reduction

techniques to create a compound measure of morphology. These 63 measures were derived from five different analyses. Basic shape descriptors (**Table 4.2;** yellow; **Fig 4.1 A;**), skeleton analysis (**Table 4.2;** green), sholl analyses (**Table 4.2;** purple; **Fig 4.1 B, C, D**), hull and circularity morphometrics (**Table 4.2;** red; **Fig 4.1 A**), and fractal analysis (**Table 4.2;** blue). These different domains have previously been used to quantify microglial morphology (Kozlowski and Weimer, 2012; Heindl et al., 2018; Fernández-Arjona et al., 2017).

Given the large number of measures in the morphology dataset, the approach used by Heindl et al. (2018) to create a compound measure of morphological changes was taken. Briefly, a subset of measures were selected based on their ability to discriminate between activated and resting microglia using an ROC analysis, before a PCA was run on these to create a compound morphology score. Given that the automated segmentation and measurement of microglia was based on user selected TCA values, this was done across a range of TCA values in order to select the TCA value that provided the best identification of activation-induced morphological changes.

ROC Analysis and Dimensionality Reduction

In order to identify which of the 63 measures provided the best ability to discriminate between activated and resting microglia, an ROC analysis was run on each measure. The curves generated by ROC analyses quantify the discrimination performance of a binary classifier system by plotting the true positive rate against the false positive rate at various thresholds, i.e. different values of the variable (**Fig 4.5; Rightmost Column**). In this way, the ability of each measure to identify the effects of LPS administration on morphology can be quantified. This was done by measuring the AUC of the ROC plot, where a higher value signifies better discrimination.

All 63 measures were analysed in this way for a range of TCA values (I chose a range of 200 to 800 μm^2 given the TCA value used in Kozlowski and Weimer (2012) was 500 μm^2) with the best five performing measures for each TCA value retained. The best five were chosen as a starting point, with the exact number to be retained for final analysis optimised at a later phase. If any measures were present in the form of multiple variants, the worst performing variant was dropped given this was the approach taken by Heindl et al. (2018), the paper on which this part of my analysis was based. In order to create a single measure of activation associated morphological changes, the dimensionality of the dataset was further reduced by running a PCA on the measures selected by the ROC analysis to create a single 'inflammation index' i.e. a composite value based on the measures most sensitive to the effects of LPS on microglial morphology.

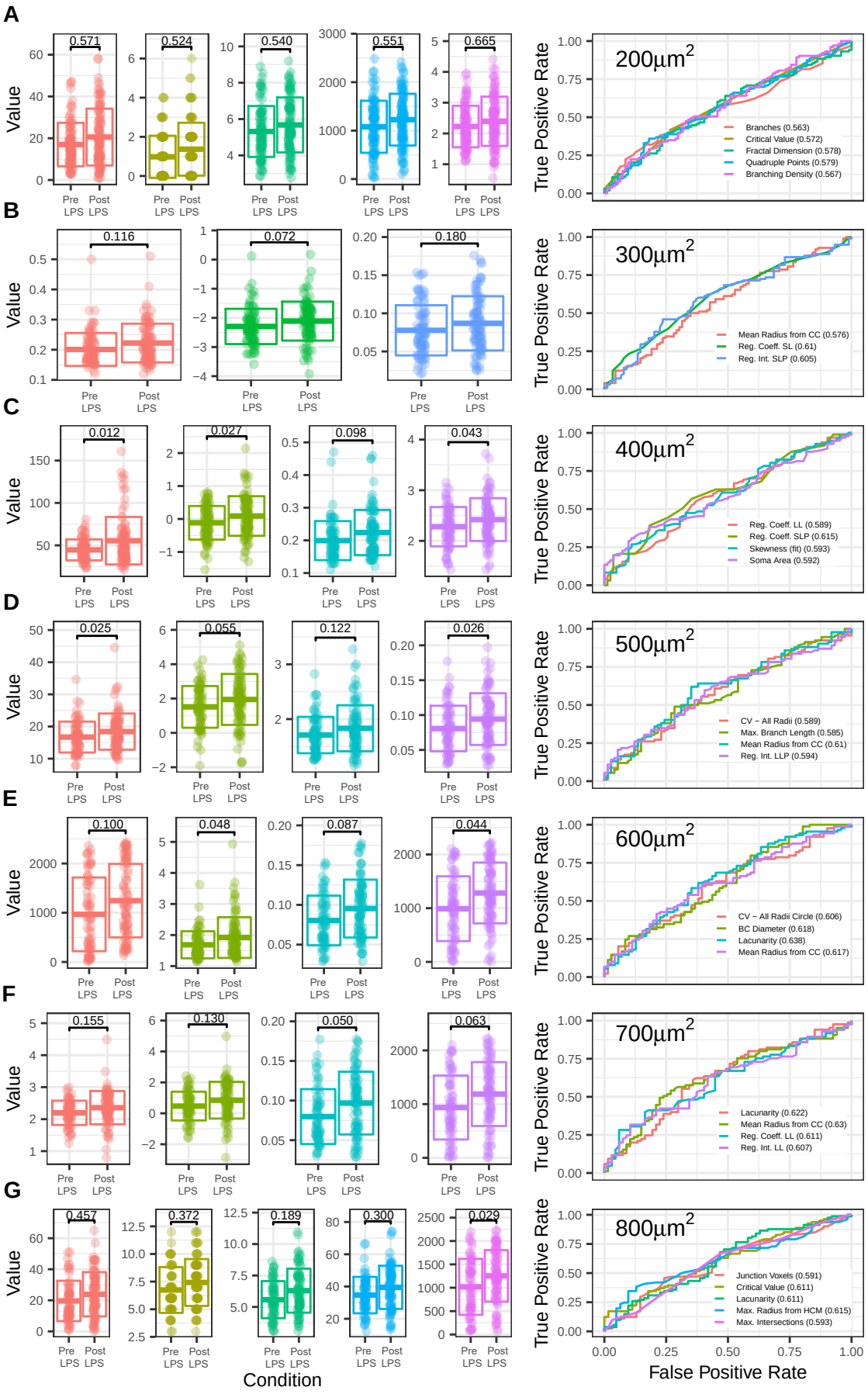

Fig 4.5. Legend on the following page

TCA Selection

This 'inflammation index' was calculated for each TCA value in the range I analysed, before the effect of LPS on its value was analysed with a LMM (**Fig 4.6**). In this way the TCA value that provided the inflammation index with the best ability to identify microglial morphological changes associated with activation could be identified, and used for analysis of dietary effects. Results showed a significant effect of LPS on the inflammation index built from TCA values of 300-500 μm^2 inclusive, with the strongest effect at 400 μm^2 (*F(1,174) = 14.21, p = 0.002* followed by 500 μm^2 (*F(1,161) = 4.87, p = 0.029*). Given the strong performance of 500 μm^2, and the fact that it was the value used by Kozlowski and Weimer (2012), this was chosen for use in further analyses.

Inflammation Index Refinement

To further hone the ability of the inflammation index (built using the 5 best performing measures based on ROC results with a TCA value of 500 μm^2) to detect LPS induced morphological changes, the effect of LPS on its value was compared between indices constructed with between 3 and 15 of the best performing measures from the ROC analysis (**Fig 4.7**). The most significant effect of LPS was seen when the 10 or 11 best performing measures were included (*F(1,161) = 9.16, p = 0.003*). The 11 measures selected are described in **Table 4.4**. The reason the effect size was identical between them is that once variant measures were dropped (as described in the subsection regarding ROC analysis and dimensionality reduction), both the 10 and 11 best measures were refined down to the same 7. This is why the effect sizes for 5 and 6, 7 and 8, and 12 and 13 measures are identical as well. After dropping variants from the best 11 measures, the remaining seven were used to construct the inflammation index used for all following analyses. The weighting of the measures in this index was consistent across analyses. Two example cells, their inflammation

---

Figure 4.5 *(preceding page)*: LPS Discrimination by Morphological Measures per TCA Value Trialled. Rightmost Column; An ROC analysis was run on 63 morphology measures to identify those that performed best at discriminating between cells imaged on day 56 (pre LPS) of dietary manipulation, and those imaged following LPS administration 24 hours later (post LPS), in control diet mice with cortical windows. This was done for each TCA value ranging from 200 to 800 μm^2. (**A-G; Left Columns**) The top five performing measures, as assessed by the AUC (indicated for each measure in the legend key of the associated ROC curve) are plotted. Where present, worst performing variants were dropped (points represent raw values, crossbars indicate mean +/- 1 standard deviation, p values indicate the effect of LPS treatment, colours correspond to colours in the associated ROC curves. Analyses used n = 1184 cells (n = 197/187/179/166/160/152/143 cells for TCA 200/300/400/500/600/700/800, n = 539 cells pre LPS treatment) measured over n = 4 mice, with all mice imaged both before and after LPS administration)).

index values, and the values of the constituent individual measures, are illustrated in **Figure 4.8**.

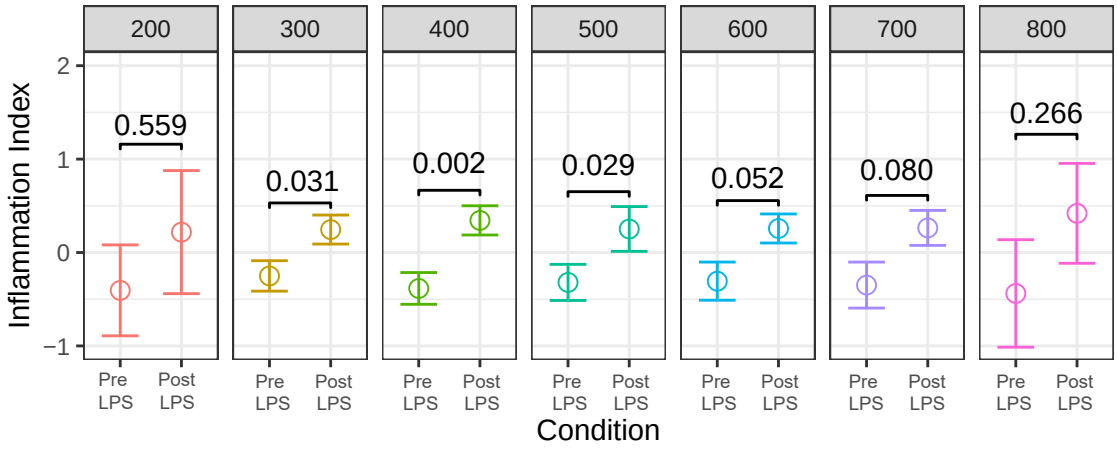

Figure 4.6: Inflammation Index Sensitivity by TCA Value. The construction of a compound 'inflammation index' was done by running a PCA on the five measures selected from the ROC analysis for each TCA value (200 to 800 μm^2; labelled at the top of each panel). The effect of LPS treatment on these indices was significant for TCAs of 400,500, and 300 μm^2 in order of effect size. Values on brackets indicate p values for the effect of LPS. Analysis used n = 1988 cells (n = 949 pre LPS, n = 804 HFD, n = 329/315/297/280/269/255/243 for TCA values of 200/300/400/500/600/700/800) measured over n = 7 mice (n = 3 HFD).

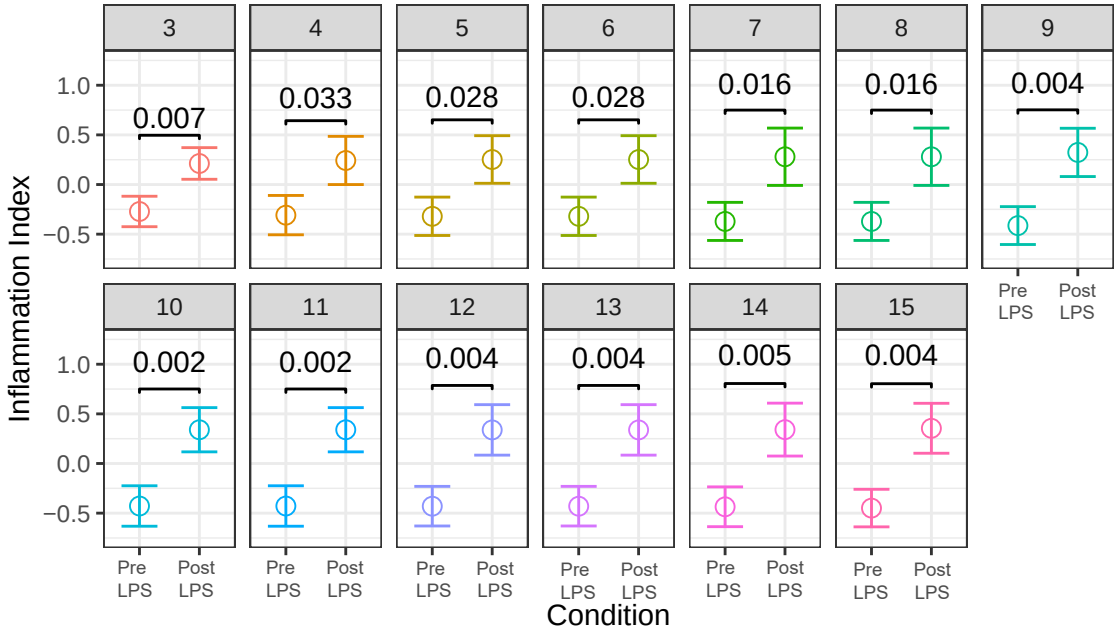

Figure 4.7: Inflammation Index Sensitivity by Number of Measures Included. The significance of the effect of LPS on the inflammation index constructed with a TCA of 500 μm^2 was compared between the numbers of best performing measures included. This ranged from 3 to 15 (labelled at the top of each panel). This was greatest when the 10 or 11 best performing were included. Analysis used n = 280 cells (n = 131 pre LPS, n = 114 HFD) measured over n = 7 mice (n = 3 HFD).

Label	AUC	Type	Definition
Soma Area	0.576	Simple	Area occupied by the microglial soma mask
Maximum Branch Length	0.585	Skeleton	The maximum length of the branches of the skeletonised cell
Regression Coefficient (Log-log) [P10-P90] #	0.574	Sholl	The regression coefficient of the linear regression run on the log-log Sholl plot based on the data within the 10^{th}-90^{th} percentiles
Regression Intercept (Log-log) [P10-P90] #	0.594	Sholl	The intercept of the linear regression run on the log-log Sholl plot based on the data within the 10^{th}-90^{th} percentiles
CV For All Radii #	0.589	HC Morph.	The coefficient of variation in the length of the radii from the centre of mass of the convex hull to an exterior point
Mean Radius from Circle's Centre #	0.610	HC Morph.	Mean length from the centre of the circle to points on the convex hull
Lacunarity	0.575	Fractal	A quantification of the inhomogeneity in the cell mask, also understood as a measure of 'gappiness' , visual texture, and translation and rotational invariance
Regression Intercept (Log-log) #	0.585	Sholl	The intercept of the linear regression run on the log-log Sholl plot
Regression Coefficient (Log-log) #	0.573	Sholl	The regression coefficient of the linear regression run on the log-log Sholl plot
CV For All Radii from Circle's Centre #	0.582	HC Morph.	The coefficient of variation in the length of the radii from the centre of the circle to points on the convex hull
Mean Radius #	0.594	HC Morph.	The mean length from the centre of mass of the convex hull to to an exterior point

Table 4.4: Morphological Measures Included in Finalised Inflammation Index. AUC values and definitions of the 11 best performing morphological measures with a TCA of 500 μm^2. **Orange** indicates variant measures with the lowest AUC values that were dropped (e.g. the regression intercept (log-log) for all data had a lower AUC than that based on data in the 10th-90th percentiles). The # symbol indicates variants. **Simple;** simple shape descriptors. **Skeleton;** measures derived from skeleton analysis. **Sholl;** values from sholl analyses. **HC Morph.;** measures based on covex hull and bounding circle morphometrics. **Fractal;** values from fractal analysis.

4.3.4 Inflammation Index, Diet, Region, and LPS

In order to investigate diet and LPS induced changes in microglial activation, the inflammation index (a composite measure of morphological changes) was compared between diets, brain regions, and timepoints. I injected mice with LPS to investigate if HFD feeding primed microglia, given that this would lead to their differential response to an inflammatory stimulus. LPS administration elevated the inflammation index significantly (**Table 4.5 A; Fig 4.9 A;** *F(1,313) = 7.89, p = 0.005*), indicating LPS induces microglial activation. However, this activation was not modulated

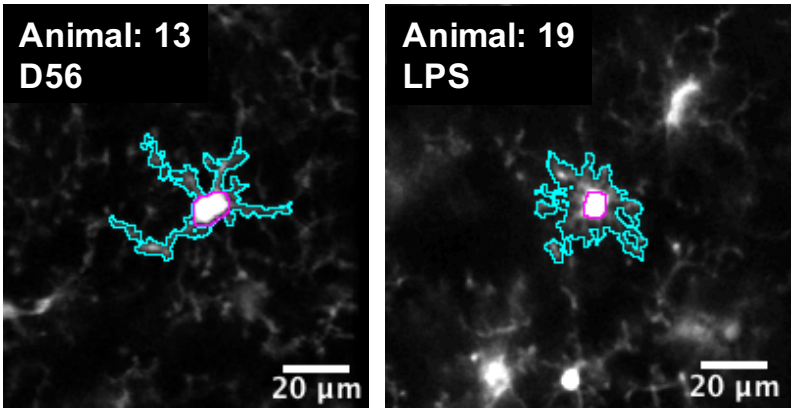

Animal	13	19
Region	Hippocampus	Cortex
LPS Condition	**Pre LPS**	**Post LPS**
Inflammation Index	**-1.93**	**1.34**
Soma Area	62.57	54.16
Maximum Branch Length	24.103	27.421
Regression Coefficient (Log-log) [P10-P90]	3.91	2.34
Regression Intercept (Log-log) [P10-P90]	4.90	1.08
CV For All Radii	1.3909	1.4234
Mean Radius from Circle's Centre	0.0586	0.0298
Lacunarity	0.750	0.639

Figure 4.8: Inflammation Index Example Cells. Example cells with their inflammation index value indicated. In addition, the values of all the measures that are used to compose the inflammation index are listed. **Cyan;** cell perimeter, **Magenta;** soma area

by dietary or regional effects (**Table 4.5 A**) or any diet, region, and LPS interactions.

In order to evaluate microglial morphological changes occurring at the same timepoint that I report evidence of hippocampus-specific NOCR deficits in HFD fed mice in my previous chapter, I restricted analysis of the inflammation index to the two week timepoint (**Fig 4.9 B**). Here there were no effects of diet or region (**Table 4.5 B**). In addition, I restricted this analysis further to mice implanted with hippocampal windows that had undergone NOCR behavioural testing in order to correlate cognitive performance with microglial activation. There was no significant correlation between behavioural performance and the inflammation index (data not shown).

To investigate the possibility of HFD feeding having phasic effects on microglial activation in the hippocampus and cortex, I looked at changes in the inflammation index in both brain regions at multiple timepoints through the 8 week dietary timecourse. Analysis of the timecourse (**Fig 4.9 C**) revealed no significant effects of time, diet, region, or their interactions, on the in-

LPS Treatment

numDF	denDF	F-value	P-Value	Factor	Sig	Measure
1	9	0.3301	0.5797	Diet		LPS
1	9	0.0030	0.9573	Diet:Region		
1	9	0.8415	0.3829	Region		
1	313	7.8850	0.0053	LPS Condition	**	
1	313	0.0035	0.953	LPS Condition:Diet		
1	313	1.1230	0.2901	LPS Condition:Diet:Region		
1	313	0.0093	0.9234	LPS Condition:Region		

Changes at Day 14

1	15	0.0660	0.8007	Diet		D14
1	15	0.0868	0.7723	Diet:Region		
1	15	1.4893	0.2412	Region		

Dietary Timecourse

1	22	1.6805	0.2083	Diet		Timecourse
1	22	0.3841	0.5418	Diet:Region		
1	22	0.3760	0.5461	Region		
13	3911	1.2139	0.2617	Timepoint		
13	3911	1.5011	0.1086	Timepoint:Diet		
13	3911	0.7369	0.7277	Timepoint:Diet:Region		
13	3911	1.1788	0.288	Timepoint:Region		

Table 4.5: Inflammation Index Analysis Statistics. Analyses were run using LMMs to investigate the change in the inflammation index in response to LPS treatment, two weeks of HFD feeding, and the 8 week dietary timecourse (numDF and denDF refer to degrees of freedom. F and p values are rounded to 4 decimal places. **Red text** indicates significance. **Green text** indicates trend level. **Background shading** indicates size of p value where darker is larger. Sig shows significance indicator. Factor indicates factors in the model. Measure indicates the model run. Colons indicate interaction effects).

flammation index (**Table 4.5 C**), suggesting that microglial morphology was unchanged over the 8 week manipulation period.

Analysis of the Inflammation Index Component Measures

The same analyses were also run on the measures that the inflammation index was composed of (unshaded rows in **Table 4.4**). These results are presented in the **Appendix A**.

4.3.5 Microglial Process Motility

Microglial process motility is involved in immune surveillance of the brain environment (Nimmerjahn et al., 2005) and is reduced following systemic LPS administration (Paris et al., 2018).

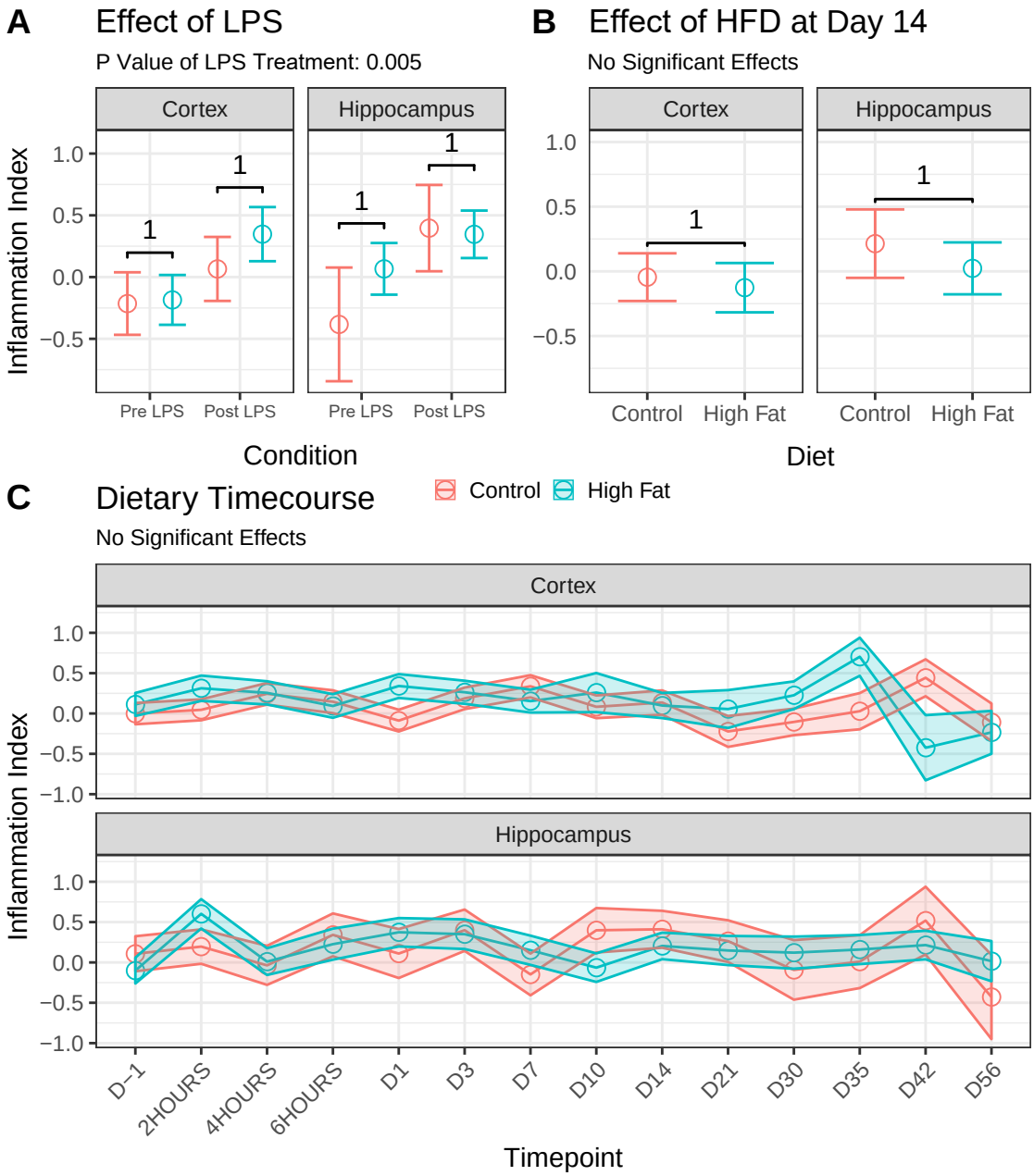

Figure 4.9: LPS Increased the Inflammation Index, which was Resistant to Dietary Effects at all Timepoints. **(A)** LPS significantly elevated the inflammation index, though there were no regional or dietary effects or interactions. **(B)** Analysing data collected at day 14 showed no effects of diet, region, behavioural performance, or their interactions. **(C)** Over the 8 weeks of dietary manipulation there were no significant effects or interactions between diet, region, or time, nor did any corrected pairwise dietary comparisons approach significance (brackets and numbers in **A, B** indicate p values of corrected pairwise dietary comparisons. In **C** D-1 refers to measurements taken a day before the beginning of dietary manipulation, and hours are relative to the the start of dietary manipulation. For LPS/Day 14/Timecourse analyses subjects used were n = 333/300/3992 cells (n = 198/167/2138 HFD, n = 135/114/1365 hippocampus) measured over n = 16/22/28 mice (n = 10/12/14 HFD, n = 6/10/11 hippocampus).

It was quantified using indices that capture the magnitude of process movement (MI), extension (EI), retraction (RI), extended processes stabilising (SI), and retracted processes remaining retracted (II). The calculation of these indices is illustrated in **Fig 4.2**. In addition, a PCA was used to create the compound motility score (CMS) that was also analysed.

LPS Decreases Microglia Process Motility

To confirm results that suggest LPS alters process motility (Paris et al., 2018) and see if changes in process motility provided evidence of HFD-induced priming of microglia, I looked at changes in process motility following LPS administration. The motility index was significantly reduced by LPS treatment (**Fig 4.10**; *F(1,75) = 13.89, p = < 0.001*) as was the retraction index (*F(1,75) = 13.52, p = < 0.001*) and extension index (*F(1,75) = 14.14, p = < 0.001*). The stability index was unaffected whilst the instability index showed a trend level decrease (*F(1,75) = 3.65, p = 0.060*). The compound motility score was significantly lowered by LPS administration (**Table 4.6**; *F(1,75) = 14.43, p = < 0.001*), confirming its ability to reflect process motility changes detected in other indices. No significant of region, diet, or their interaction, on any of the motility indices calculated, were detected. Values of the statistical analyses for all measures are presented in the **Appendix A**.

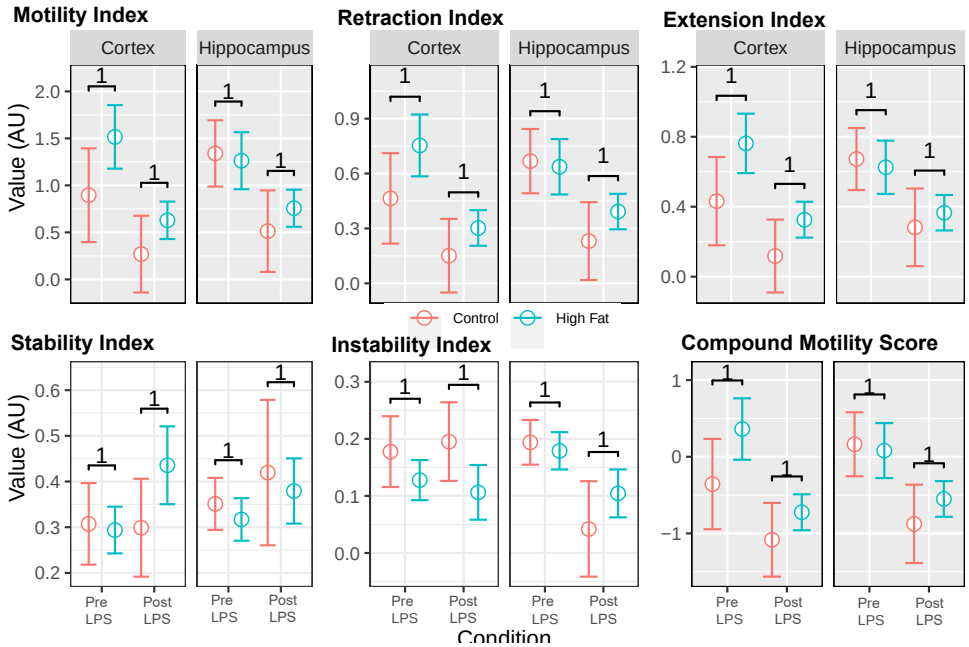

Figure 4.10: LPS Decreases Process Motility. LPS treatment reduced the motility, retraction, and extension indices, and the compound motility score. The instability index showed a trend level decrease, whilst the stability index was unaffected. There were no significant effects of region, diet, or any interactions, on any of the indices (corrected p values of dietary comparisons are indicated on brackets. **Grey background** indicates a significant main effect of LPS. AU indicates arbitrary units. Analysis used n = 97 cells (n = 58 HFD, n = 49 hippocampus) measured over n = 18 mice (n = 10 HFD, n = 9 hippocampus)).

The Effects of Two Weeks of HFD Feeding on Microglial Process Motility

As with the inflammation index I restricted analysis of process motility to the two week timepoint to investigate changes occuring at the same time as the NOCR deficits I reported in the previous chapter. Analysis of the two week timepoint showed a trend level interaction between diet and region on the motility index (**Fig 4.11**; *F(1,18) = 3.54, p = 0.076*). Here HFD feeding increased the motility index in the cortex, whilst decreasing it in the hippocampus. This trend level effect, and the direction of the interaction, were the same for the retraction index, extension index, and compound motility score (**Table 4.6**). Neither the stability nor instability index showed any effects in the two week analysis. To correlate cognitive performance with process motility changes I further limited analysis to behaviourally tested animals. This did not show any significant correlation between behavioural performance and any of the indices (data not shown). Values of the statistical analyses for all measures are presented in the **Appendix A**.

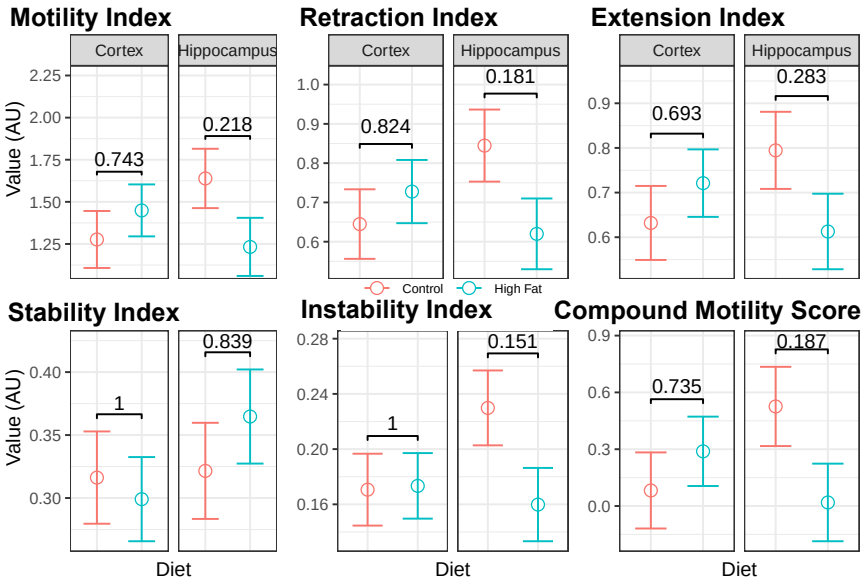

Figure 4.11: Trend Level Region-Specific Dietary Effects on Process Motility. The compound motility score, as well as the motility, retraction, and extension indices, all showed a trend level diet by region interaction, where their values were decreased by HFD in the hippocampus, and unaffected - if not marginally increased - in the cortex. Neither the stability nor the instability index showed any significant effects in the two week analysis (p values of corrected pairwise dietary comparisons are indicated on brackets. AU indicates arbitrary units. Analysis used n = 84 cells (n = 43 HFD; n = 31 hippocampus) measured over n = 25 mice(n = 13 HFD; n = 19 hippocampus)).

Dietary Timecourse Analysis of Microglial Process Motility

As with the inflammation index I looked at changes in motility indices over 8 weeks of HFD feeding in both the hippocampus and cortex to investigate the possibility of phasic HFD inflammatory effects. This revealed a significant effect of region on the motility index (**Figure 4.12**, *F(1,23) = 8.25, p= 0.009*), extension index (*F(1,23) = 8.47, p = 0.008*), retraction index (*F(1,23) = 7.99, p = 0.010*), and compound motility score (**Table 4.6 C**; *F(1, 23) = 8.26, p = 0.009*) where these were all greater in the hippocampus than the cortex. The stability index showed a significant timepoint and diet interaction (*F(13,991) = 2.28, p = 0.006*) that was driven by an elevated stability index in HFD cells at day 49 (*t(23) = 3.29, p = 0.048*). The instability index was significantly greater in control cells overall (*F(1,23) = 5.17, p = 0.033*) and was also significantly greater in the hippocampus (*F(1,23) = 20.36, p = < 0.001*). Values of the statistical analyses for all measures are presents in the **Appendix A**.

LPS Treatment

numDF	denDF	F-value	P-Value	Factor	Sig	Measure
1	11	0.8230	0.3837	Diet		LPS
1	11	0.3904	0.5448	Diet:Region		
1	11	0.7953	0.3916	Region		
1	75	14.4335	0.0003	LPS Condition	***	
1	75	0.0449	0.8328	LPS Condition:Diet		
1	75	0.5516	0.4600	LPS Condition:Diet:Region		
1	75	0.0131	0.9091	LPS Condition:Region		

Changes at Day 14

1	18	0.0723	0.7910	Diet		D14
1	18	3.8156	0.0665	Diet:Region	'	
1	18	0.8563	0.3670	Region		

Dietary Timecourse

1	23	1.4671	0.2381	Diet		Timecourse
1	23	0.2590	0.6156	Diet:Region		
1	23	8.9328	0.0066	Region	**	
14	1035	1.0928	0.3596	Timepoint		
14	1035	1.0433	0.4069	Timepoint:Diet		
14	1035	0.8993	0.5592	Timepoint:Diet:Region		
14	1035	0.8129	0.6557	Timepoint:Region		

Table 4.6: Compound Motility Score Analysis Statistics. Analyses were run using LMMs to investigate the change in the compound motility score in response to LPS treatment, two weeks of HFD feeding, and the 8 week dietary timecourse (numDF and denDF refer to degrees of freedom. F and p values are rounded to 4 decimal places. **Red text** indicates significance. **Green text** indicates trend level. **Background shading** indicates size of p value where darker is larger. Sig shows significance indicator. Factor indicates factors in the model. Measure indicates the model run. Colons indicate interaction effects).

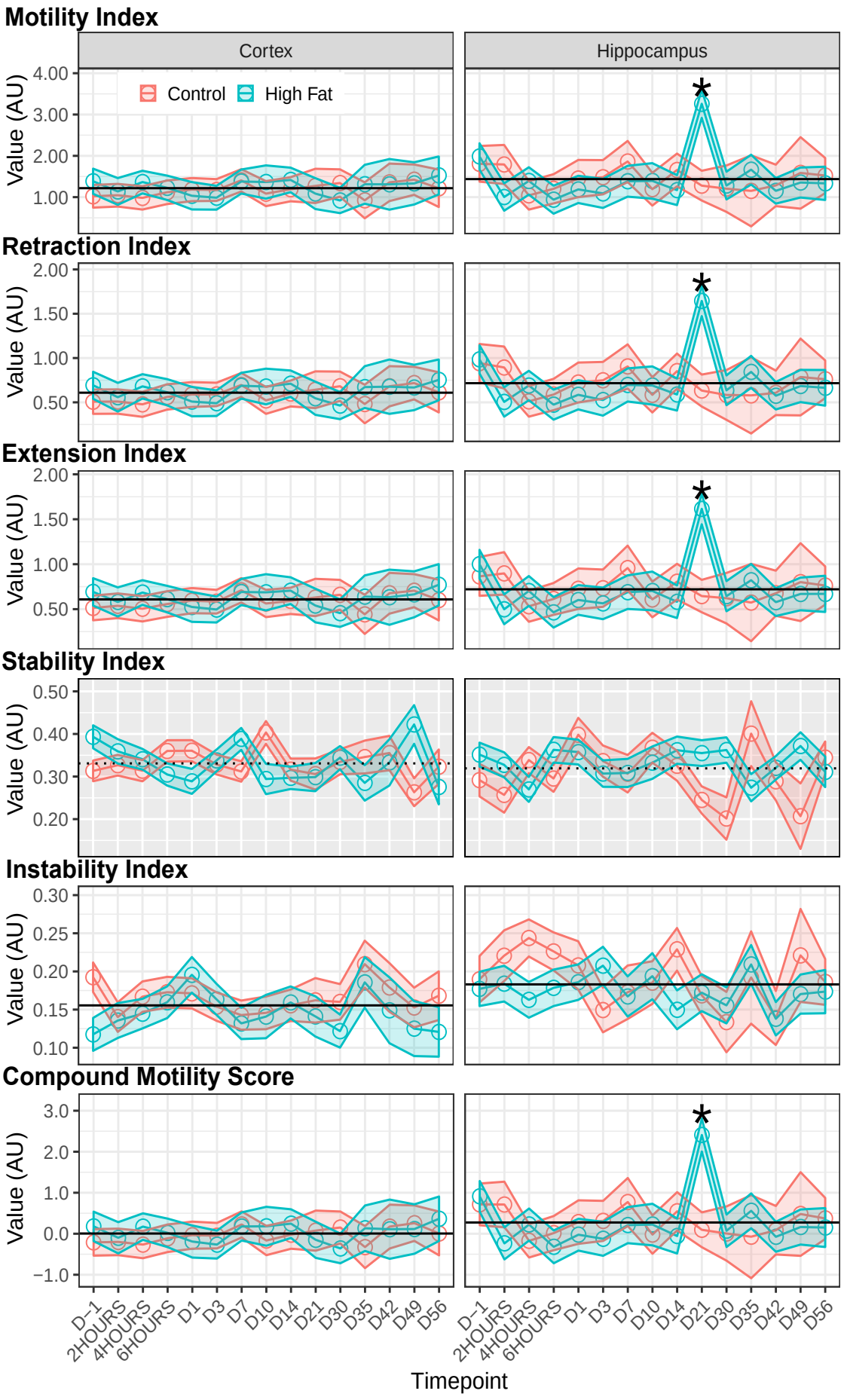

Figure 4.12. Legend on the following page

4.4 Discussion

Morphological changes are a key feature of microglial activation (Kettenmann et al., 2011) that generally involve the retraction of processes and the shift from a ramified to an amoeboid phenotype. Morphological changes occur immediately upon acute damage, as demonstrated by two-photon lesion studies (Nimmerjahn et al., 2005). Similarly, microglial process motility, an important part of the surveillance by microglia of the parenchyma (Nimmerjahn et al., 2005), is decreased by LPS (Paris et al., 2018). Given that HFD feeding has been widely reported to induce microglial activation (Thaler et al., 2012; André et al., 2017; Zhou et al., 2018) that has been documented after as little as 72 hours in the hypothalamus (Thaler et al., 2012; Valdearcos et al., 2014) and one week in the hippocampus (Calvo-Ochoa et al., 2014), shifts in microglial morphology and decreases in process motility during the 8 week dietary timecourse were anticipated. In addition, I hoped my *in vivo* analysis of microglial changes could shed light on the mechanism behind the results reported in the previous chapter (**Chapter 3**), where two weeks of HFD increased microglial density without any associated morphological changes or increases in cytokine levels. Two explanations for this were proposed, either the priming of microglia by HFD feeding, or the existence of transient and phasic inflammation in regions outside of the hypothalamus. I sought to address these two hypotheses by tracking microglial morphology and process motility over the dietary timecourse, and investigating their response to proinflammatory LPS administration. In addition, given the absence of studies investigating hippocampal inflammatory changes within the first week of HFD feeding, I hoped to provide evidence regarding the timecourse of early inflammatory changes and therefore evaluate the likely contribution of microglial activation to the early HFD-induced hippocampus-specific cognitive deficits reported by McLean et al. (2018) and Kanoski and Davidson (2010).

Figure 4.12 ***(preceding page)*****: Process Motility is Unaffected by Diet and Lower in the Hippocampus.** 8 weeks of dietary manipulation revealed that compound motility score, and motility, retraction, and extension indices were lower in the hippocampus on average. The stability index showed a diet by time interaction driven by its elevation in HFD cells at day 49 in both regions (* indicates $p < .05$ in corrected pairwise comparisons. **Horizontal lines** indicate regional means, where solid lines indicate regional differences were significant. **Grey background** indicates a significant interaction between diet and time. Analysis used n = 1121 cells (n = 590 HFD; n = 458 hippocampus) measured over n = 29 mice (n = 14 HFD; n = 12 hippocampus)).

4.4.1 Semi-Automated Quantification of Morphological Changes

In order to process the large number of cells needed to detect small changes in morphology across a wide span of timepoints, I developed a semi-automated approach. The initial phase of the morphology analysis was based on the methodology used by Kozlowski and Weimer (2012), where an iterative thresholding technique, tuned using results from LPS induced microglial activation studies, was used to automatically generate masks of microglial cells from two photon image stacks. I combined this with the work by Heindl et al. (2018), who took a multitude of automatically generated microglial shape measurements and refined them into a compound index of morphology. The measures my analysis automatically generated fell into five categories of descriptor; simple shape, cell skeleton, sholl analysis, fractal analysis, and hull and circle morphometrics. These different approaches have been used to quantify microglial morphology in the literature (Kozlowski and Weimer, 2012; Heindl et al., 2018; Fernández-Arjona et al., 2017). Heindl et al. (2018) used an ROC analysis to select the measures that best distinguished between resting and activated cells, before running these through a PCA and using the first component as a compound index. For my approach, I used an ROC analysis to identify measures that best distinguished microglia activated by systemic LPS administration. I then analysed the effect size of LPS treatment on the value of the compound index built using these measures. This was done initially on a subset of data to tune the parameters used in the automated cell mask generation so that these best captured the morphological changes seen in activated microglia. After tuning, this approach was used to analyse the rest of the dataset.

4.4.2 LPS Induced Microglial Activation is Consistent Across Diet Groups and Brain Regions

Microglial priming occurs both in ageing and neurodegenerative diseases (reviewed in Tay et al. 2017; Norden and Godbout 2013; Perry and Holmes 2014). Given that primed microglia show an exaggerated inflammatory response to proinflammatory stimuli (microglial priming reviewed in Perry and Holmes 2014) I used LPS administration to test whether microglia were primed by HFD feeding. An analysis of the compound morphology index, which I have referred to in this chapter as an 'inflammation index', revealed that it was significantly elevated by LPS treatment, confirming its ability to capture inflammation related morphological changes. However, there was no effect of region or diet, nor any interaction between them, on the index value. Similarly, microglial process motility showed a decrease following LPS treatment, with no main effects or interactions between diet and brain region. These results demonstrated that LPS induced microglial

activation as expected, but also provided evidence that microglial cells are not primed following 8 weeks of HFD feeding.

Evidence for Diet and Obesity Induced Microglial Priming

Evidence in the literature for HFD induced inflammatory priming is mixed, where Baufeld et al. (2016) demonstrated no evidence of it in isolated hypothalamic microglia following 16 weeks of diet, and Maric et al. (2014) reported no differences in the fever response of rats fed a HFD for 8 weeks following LPS administration. Though these studies support my own results, Pohl et al. (2009) reported that not only did diet-induced obese rats demonstrate a greater fever response to LPS, they showed greater LPS induced elevations in levels of circulating IL-6 and TNF-α, and hypothalamic mRNA levels of IL-1β, IL-6, and SOCS3. In addition, 3 days of HFD led to an exaggerated inflammatory response in the hippocampus (Sobesky et al., 2016) and the hypothalamus (Souza et al., 2019) following LPS administration.

Evaluation of the differences between the studies initially suggested that the difference in results might relate the degree of weight gain induced. The HFD fed rats (with butter derived fat) in Maric et al. (2014) that showed no evidence of priming were only 3.6% heavier than control counterparts, versus the 15% increase in body weight reported in Pohl et al. (2009) where HFD induced priming seemed apparent. However, the microglia that demonstrated no priming in Baufeld et al. (2016) were taken from HFD mice that were approximately 35% heavier than controls, and in Sobesky et al. (2016), HFD fed mice were only $\sim$5% heavier than control counterparts. An alternative explanation relates to cell-specific priming. Baufeld et al. (2016) looked specifically at the response of microglial cells by isolating them, whilst the responses measured by Maric et al. (2014) and Pohl et al. (2009) were not cell-type specific. It therefore seems possible that whilst obesity doesn't induce microglial priming, it may be associated with non-microglial cell priming to inflammatory stimuli. Indeed, Valdearcos et al. (2014) observed only a small decrease in the hypothalamic inflammatory response to LPS following microglial depletion, demonstrating either that non-microglial cells play a significant part in LPS induced inflammation, or that they are readily able to compensate for the ablation of the microglial response. It is of course also possible that HFD induced microglial priming requires not only an elevated degree of weight gain, but also the presence of other cell types, such that looking at them in isolation would mask any priming effects. Evidence demonstrating the importance of microglia and astrocyte communication in the enhancement of inflammatory responses (Saijo et al., 2009) suggests this could play a role.

However, neither of these theories can explain the results reported by Sobesky et al. (2016),

where rats showed a low degree of weight gain and still demonstrated evidence of HFD-induced priming. Differences in LPS dosage may be responsible, where Sobesky et al. (2016) used a 10 µg/kg dose to avoid the possibility of a large inflammatory response masking signs of priming (Sobesky et al. (2016) suggest that work by Johnson et al. (2002) using this dosage indicates it induces a sub-threshold inflammatory response). Whilst initially this appears to explain the null results reported by Maric et al. (2014), who used a 100 µg/kg dose, this was the same dosage used by Pohl et al. (2009) where evidence of priming was reported. It may be the case that a high degree of weight gain is required to observe evidence of priming in the face of large-scale inflammation. A final consideration is that the differences may simply be the result of regional effects. Sobesky et al. (2016) investigated hippocampal priming, whilst both Pohl et al. (2009) and Maric et al. (2014) looked in the hypothalamus. Here it would appear that a high degree of weight gain is necessary for hypothalamic, but not hippocampal, inflammatory priming.

In the context of these studies, the absence of diet-related priming I detected may be the result of insufficient weight gain, given my HFD fed animals were only 8.1% heavier than controls at the time of LPS administration. However, hippocampal HFD priming appears independent of large changes in weight (Sobesky et al., 2016), so my results may be best explained by the high dose of LPS used (4mg/kg compared to the 10 µg/kg in Sobesky et al. 2016). This likely produced an inflammatory response large enough to mask signs of diet-induced microglial priming. I opted to use this high dose of LPS initially as I wanted to ensure it would induce microglial activation strong enough for my analysis techniques to detect. Part of my semi-automated cell analysis technique was based on work by Kozlowski and Weimer (2012), who demonstrated that a dose of 4mg/kg induced morphological changes that were highly significant using an automated analysis approach. Though these results do not shed more light on the role of HFD-induced priming in my post-mortem tissue results (described in the previous chapter), the fact that HFD mice in those experiments were ∼14% heavier than controls (close to the 15% reported by Pohl et al. 2009), coupled with consideration of the evidence of rapid HFD-induced microglial priming (Sobesky et al., 2016; Souza et al., 2019), means this still seems an appealing explanation. Future work should repeat my *in vivo* experiments with a lower dose of LPS. In addition, correlating results against the degree of weight gain would help evaluate the theories I have proposed to explain the differences between studies.

LPS Induced Inflammation is Consistent Between Regions

No regional differences in the effect of LPS on microglial morphology or process motility were detected, suggesting that microglia in both regions are activated to a similar extent and in a similar

manner. Studies investigating regional differences in microglial activation are few. Furube et al. (2018) looked at the effect of LPS on microglial proliferation by analysing bromodeoxyuridine (BrdU) uptake and reported no effect of a 1mg/kg dose of LPS on the density or percentage of BrdU labelled microglial cells in the cortex, whilst both the density and percentage of labelled microglia in the dentate gyrus was increased. However, an important factor to consider is that their measurements were taken 3 days after LPS administration, compared to the 24 hours in my experiments. Hoogland et al. (2018) demonstrated that 48 hours post-LPS administration, microglial densities were seen to be increased in both the hippocampus and cortex, suggesting that microglia in both regions proliferate in response to LPS, though it seems by the 3 day point only hippocampal microglia continue to do so. This agrees with my results demonstrating no regional differences in the microglial response to LPS treatment within the first 24 hours.

With regards to process motility, LPS administration in the hippocampus (Madore et al., 2013) and cortex (Paris et al., 2018) both significantly reduce process motility, though it appears no studies but my own have directly compared the response in a single model. As a result, the evidence I present that no quantitative differences exist in the extent of LPS-mediated effects on process motility provides a novel insight into regional differences in microglial activation.

In summary, my results demonstrate a lack of region-specific effects of LPS on microglial activation that seems consistent with published research. My work also represents some of the first to investigate this. It should be noted that whilst my conclusions are based on morphological and process motility changes, the work by Furube et al. (2018) and Hoogland et al. (2018) centers on proliferation. As evidenced by my own work, these facets of microglial activation can be uncoupled and so do not necessarily reflect similar inflammatory responses. Investigating LPS-induced changes in microglial density in my data will help relate my findings more closely to those already published.

4.4.3 Microglial Activation is Resistant to 8 Weeks of HFD Feeding

Neither HFD-feeding, nor time, had any effect on microglial morphology or process motility over the 8 weeks of dietary manipulation. This suggests an absence of diet-induced inflammation, and therefore agrees with my post-mortem data that demonstrated no microglial morphological changes following two weeks of HFD. Though I did not measure cytokine levels, these results provide evidence that the biphasic pattern of hypothalamic inflammation reported by Thaler et al. (2012) does not occur in either the cortex or the hippocampus, where it seems instead that microglia show no signs of activation. This would indicate that phasic inflammatory changes are not

responsible for the uncoupling of microglial proliferation and morphology detected in my post-mortem results, nor is early HFD induced activation related to the early hippocampus-specific cognitive impairment reported (McLean et al., 2018; Kanoski and Davidson, 2010). It is important to note however that the HFD used in Thaler et al. (2012) was composed of 60% calories from fat, with their study also focusing on rats, in comparison to my 45% diet in mice. It is quite possible that species or dietary fat percentage are responsible for mediating the phasic inflammatory effects of diet they report. Alternatively, the partial deficiency of Cx3CR1 expression associated with Cx3CR1-GFP heterozygosity in my *in vivo* mice could have led to resistance to the proinflammatory effects of HFD feeding in my experiments, masking the existence of phasic inflammatory changes. The influence of Cx3CR1 deficiency on my results is discussed in greater detail in the discussion for **Chapter 3**, and later in this chapter's discussion.

A diet by region interaction was detected in microglial motility measures at the two week timepoint when all other timepoints were excluded. Here HFD feeding in the cortex increased, and in the hippocampus decreased, the motility, retraction, and extension indices, and the compound motility score. Whilst this might suggest the presence of region-specific dietary inflammatory effects at a timepoint relevant to the detection of hippocampus-specific cognitive deficits (as detected in the previous chapter), when considered in combination with the variation over multiple timepoints in the full dietary timecourse, the differences seen at day 14 are well within the normal time-related variation in readings and therefore are likely unrelated to dietary effects. In addition, to address the significant pairwise comparison within the hippocampal motility data at day 21, where motility, retraction, and extension indices, and the compound motility score, are elevated by HFD, this effect is driven by a single cell with aberrantly high values.

The Timeline of HFD-Induced Microglial Activation Varies Between Studies

Though my results may seem unusual initially, given the rapid inflammatory response detected by Thaler et al. (2012) and Calvo-Ochoa et al. (2014), early HFD-induced microglial changes are not always reported. No change in the number of activated hippocampal microglia (cells with enlarged/irregular cell bodies, and thickened, partial, or complete loss of processes) was reported following 1 to 2 months of HFD (Knight et al. 2014; with no increase seen until 13-14 months), whilst after 3 weeks there was no change in hippocampal microglial density or morphology (André et al., 2017). No change in hippocampal microglial morphology (Spencer et al., 2019), or hypothalamic (Baufeld et al., 2016) morphology and density, was seen after 3 days of HFD feeding. The latter study also showed no increase in hypothalamic density after 4 weeks, though by 8 weeks this was apparent (Baufeld et al., 2016). Finally, 8 weeks of HFD was associated with

increased microglial process length in the prefrontal cortex, though there were no effects in CA1 or perirhinal cortex (Bocarsly et al., 2015).

In contrast, Thaler et al. (2012) reported increased microglial density and size in the hypothalamus after 3 days of HFD, whilst Calvo-Ochoa et al. (2014) observed activated microglia in the hippocampi of rats fed a HFD supplemented with fructose syrup for a week. Valdearcos et al. (2017) saw an elevation in Iba1 stained microglial cells in the ARC and median eminence of the hypothalamus after 4 weeks of HFD feeding, whilst André et al. (2017) saw an increase in hypothalamic microglial density after 3 weeks. This was coupled with an increase in the number of microglia with enlarged somata (in contrast to the lack of microglial activation they observed in the hippocampus). Zhou et al. (2018) saw an elevated density and size of microglia in the ARC after 4 weeks of HFD.

Ultimately, the timecourse of reported HFD-induced microglial activation is inconsistent. What seems clear is that microglial activation tends to occur earlier in the hypothalamus, and that it is not uncommon to detect an absence, or low levels of, microglial activation in the cortex and hippocampus within the first 8 weeks of dietary manipulation. Where discrepancies exist, these may relate to differences in diet composition, species and age of subjects used, and subdivisions of the regions imaged. A role for the sugar content in mediating the inflammatory effects of HFD feeding has also been proposed (Sobesky et al., 2016). The lack of morphological changes I detect fits with my post-mortem results, that together suggest there is no role for early HFD-induced microglial activation in the genesis of hippocampus-specific cognitive deficits. Additionally, this indicates that HFD-induced priming of microglia in my model, rather than activation, may be what drives the uncoupling of proliferation and morphological changes. Future analysis of microglial density in my *in vivo* data will help to confirm the agreement with post-mortem data.

Baseline Process Motility is Reduced in the Hippocampus

Microglial process motility showed an effect of region, driven by an overall lower value in the hippocampus of the motility, extension, and retraction indices. There do not appear to be any published studies that have explicitly looked at baseline differences in microglial process motility between regions, however plenty of work has been described using alternative approaches to demonstrate regional heterogeneity in microglial populations (reviewed in Stratoulias et al. 2019; Hanisch 2013). In one such study, Grabert et al. (2016) looked at the transcriptome of isolated microglia and demonstrated region-dependent clustering and separation of cortical and hippocampal microglia, with regional variation also seen using single cell RNA sequencing (Hammond et al.,

2019; Masuda et al., 2019). There are also morphological differences between microglia from different brain regions (Lawson et al., 1990). As such, finding differences in baseline process motility between regions is not surprising. Process motility also correlates with neuronal activity (in a preprint; Nebeling et al. 2019), so perhaps regional differences in the patterns of neuronal activity could underlie the differences in microglial process motility demonstrated in my results.

In spite of these process motility differences, no regional differences in overall morphology were detected, nor did the microglial response to LPS differ by region. Indeed, if regional differences in microglial transcriptomes exist, one would predict variation in regional morphologies and inflammatory responses. The lack of evidence for this in my results could be the result of methodological choices. The inflammation index I used to investigate changes in morphology was designed to detect LPS-specific indicators of microglial activation, and it is possible that these measures are unsuited to identifying regional differences. Work by Young et al. (2018) (in a preprint) supports this. They demonstrated differences between the cortex and hippocampus in microglial process length, number of process endpoints, fractal dimension, lacunarity, and density, but not span ratio. Though the measurements I took included all of these (except for process length), only lacunarity was included in the inflammation index I constructed, supporting the suggestion it is insensitive to regional differences. However, analysis of lacunarity (see **Appendix Fig A.7, Table A.7**) revealed no regional differences. It may then be the case that the reduced image quality in my dataset relative to that in Young et al. (2018) (my data was collected in awake, behaving mice, whilst they used confocal microscopy on post-mortem tissue) blunts the ability of my analyses to detect regional differences. However, my own post-mortem analyses in **Chapter 3** showed no evidence of regional variation in microglial morphology, though this did not use the same measures as Young et al. (2018). Future work should look at other measurements that overlap between our studies, both *in vivo* and in post-mortem tissue, to better understand these differing results.

4.4.4 Hippocampal Cognitive Deficits Were Not Detected Following Two Weeks of HFD

Mice were tested on hippocampus-dependent object-context recognition (Balderas et al., 2008; Mumby et al., 2002) following 14 days of HFD feeding. This involved testing all mice implanted with hippocampal windows alongside a cohort of naive C57BL/6J wild type mice to assess the impact of surgery on performance. Results demonstrated that hippocampal window implantation did not influence cognitive performance, although neither did HFD feeding. This contradicts the detrimental effect of HFD on NOCR reported at the same timepoint in the previous results chapter,

though it is worth noting that despite not reaching significance, HFD feeding still decreased performance. Indeed, considering the NOCR experiment reported in this chapter was designed to evaluate effects of both diet and surgery, the sample size of 20 meant the study was underpowered. The NOCR results reported both here and in the post-mortem chapter are derived from the same data, though in the post-mortem analysis hippocampal window mice were excluded, as was a single wild type mouse, in order to correlate behavioural performance with hippocampal protein array measurements.

Despite the low statistical power, finding no effect of HFD on NOCR is surprising given the demonstration of a deficit in NOCR in previous unpublished work by my group, and the fact that this deficit is present when analysis is limited to a subset of mice (as in the previous chapter). Additionally, other studies have shown detrimental effects of HFD on hippocampus-dependent cognition, where it seems to appear very early after the beginning of HFD-feeding (McLean et al., 2018; Kanoski and Davidson, 2010). One possibility is that the lack of dietary effects on cognitive performance seen in my data could result from genotype differences, as the hippocampal window mice included in the analysis in this chapter were Cx3CR1-GFP heterozygous mutants. The Cx3CR1-GFP mutation is associated with knockdown of the Cx3CR1 gene, and partial Cx3CR1 deficiency appears to impart resistant to diet induced weight gain and cognitive deficits (Cope et al., 2018), as discussed in the previous chapter. Briefly, Cx3CR1 and its ligand play a role in neuroinflammation and signalling between neurons and microglia (Lee et al. (2010) introduce the effects of Cx3CR1 dysfunction), with complete Cx3CR1 deficiency being protective against obesity and the inflammation of visceral adipose tissue (Polyák et al., 2014). In contrast, work by Shah et al. (2015) showed no effect of Cx3Cr1 deficiency on diet-induced weight gain, fat content, feeding, or energy expenditure at any point over 24 weeks in HFD fed mice. It therefore seems possible that excluding the hippocampal window Cx3CR1-GFP mice from the NOCR analysis, as was done in the previous chapter, may have revealed dietary effects that their genotype masks in the overall analysis described here. Indeed, the immunofluorescence cohort of mice (of which Cx3CR1-GFP mutants were a minority) analysed in the previous chapter appear more susceptible to HFD induced weight gain than the Cx3CR1-GFP mice described in this chapter (with HFD immunofluorescence animals showing a 20% increase relative to their starting weight after two weeks, in comparison to the roughly 7% increase seen after two weeks in the Cx3CR1-GFP *in vivo* mice). This fits with the resistance to diet-induced obesity associated with Cx3CR1-GFP heterozygotes on a 45% HFD reported in Cope et al. (2018).

However, my analysis showed no interaction of surgery status (and given all hippocampal window mice were Cx3CR1-GFP heterozygotes, genotype) with diet, and when I included genotype

as a factor in my analyses in the previous chapter, partial Cx3CR1 deficiency appeared to have no real effect on any of the metrics analysed (its effect on microglial density likely being related to clearer microglial labelling, and its association with greater pericyte spacing probably due to the greater mean age in the Cx3CR1-GFP cohort given greater spacing correlated significantly with increased age). It must be considered though that the underpowered nature of my NOCR study was insufficient to detect genotype differences. Indeed, though not significant, hippocampal window mice did appear to show a smaller decrease in NOCR performance in response to HFD feeding. An effect of Cx3CR1-GFP deficiency on my *in vivo* results could also explain the lack of activation related microglial morphological changes I detect over 8 weeks of dietary manipulation, given that in Cope et al. (2018) this genotype showed no signs of microglial activation after 12 weeks of HFD feeding in the hippocampus.

Genotype and power issues aside, the potential role of hippocampal window surgery (and the associated cortical aspiration) on NOCR performance must also be addressed. In this regard, NOCR is a hippocampus-specific task (Mumby et al., 2002; Balderas et al., 2008) so should be unaffected by cortical changes, and overall performance levels were not different between naive and hippocampal window mice in my results. Gu et al. (2014) report that the hippocampal window surgery did not influence performance on an open-field and contextual fear-conditioning paradigm, and the surgical procedure utilised (as described in Dombeck et al. 2010) is not associated with any direct contact with the hippocampus as the overlying structures are "peeled away" without applying direct pressure, with the external capsule (which is left intact) providing a barrier to hippocampal CA1. In addition, neuronal properties measured with electrophysiological and optical techniques following hippocampal window surgery were reported to be highly similar to electrophysiological recordings from mice that had not undergone surgery, and the aspirated cortical areas do not provide strong direct projections to the hippocampus (Dombeck et al., 2010). It may instead be possible that hippocampal window implantation influences the mechanisms responsible for mediating the detrimental effect of HFD on hippocampal processing, with results from my previous chapter suggesting this relates to HFD-induced vascular structural changes. Whilst future work in post-mortem tissue could evaluate whether hippocampal window surgery modulates the effects of HFD on the vasculature reported in my post-mortem work, and in doing so could help shed light on these behavioural results, it is important that an adequately powered repeat of the NOCR task described in this chapter is done.

4.5 Conclusion

In conclusion, the data presented in this chapter demonstrate that a semi-automated method of quantifying microglial morphological changes is capable of detecting LPS-induced microglial activation, and supports findings demonstrating a reduction in microglial process motility in response to LPS treatment. Additionally, some of the first results investigating differences in process motility between brain regions suggests that the magnitude of this is reduced overall in the hippocampus relative to the cortex. The use of a high dose of LPS in my experiments may have masked the presence of microglial priming reported to be induced by HFD feeding in other studies. It therefore remains a likely explanation for the profile of microglial and cytokine changes observed in my post-mortem data, a suggestion supported by the fact that I observed no changes in microglial morphology over 8 weeks of HFD feeding *in vivo*. Future work is needed to validate this. In addition, my results provided no evidence that the phasic inflammatory response to HFD seen in the hypothalamus (Thaler et al., 2012) exists in either the hippocampus or the cortex, though this is not conclusive as I did not measure inflammatory cytokine levels. This would suggest that early HFD-induced microglial activation is not necessary for the genesis of hippocampus-specific deficits. Finally, the attenuation of the detrimental effect of HFD on NOCR through the inclusion of hippocampal window mice was suggested to be mediated either by an effect of hippocampal window surgery, where this may influence the detrimental vascular changes induced by HFD feeding, or the influence of partial Cx3CR1 deficiency. In order to further investigate this, an appropriately powered NOCR study should be conducted.

Chapter 5

In Vivo Neurovascular and Blood Supply Changes

5.1 Introduction

Recent years have seen a growth in the interest surrounding the vascular changes underlying the pathology of diseases such as Alzheimer's disease (reviewed in de la Torre 2002). Dysfunction in the brain's vascular network disrupts its ability to support neuronal activity through the delivery of oxygen and nutrients and the removal of metabolic waste products. This can result from changes such as a loss of vessel density, or disruption in the mechanisms supporting neurovascular coupling. The cognitive deficits seen in obesity have been proposed to stem from impairments in the vascular support system (Sorop et al., 2017).

Vascular changes have been widely reported in models of HFD feeding and obesity. Cerebral microvascular disease is associated with microbleeds, lacunas, and microlacunas (Kalaria, 2012), and these are seen more commonly in obese individuals with insulin resistance and dyslipidaemia (Park et al., 2007a). Additionally, cerebral small vessel disease is associated with visceral fat accumulation (Yamashiro et al., 2014). HFD feeding and obesity in rodents has been associated with both a loss of cerebral microvascular density, otherwise known as rarefaction, and aberrant angiogenesis. Both of these processes correlated negatively with cognitive performance (Tucsek et al., 2014b; Coucha et al., 2019). HFD associated reductions in vascular diameter have also been reported (He et al., 2016; Constantinescu et al., 2011), as have reductions in blood flow and perfusion in obesity (Birdsill et al., 2013) and HFD fed rats (Glaser et al., 2012; Obadia et al., 2017), with cortical blood flow reductions correlating with memory impairment (Birdsill et al., 2013).

Besides passive support of neuronal metabolism, the cerebrovasculature also has the ability to vary regional blood flow levels to support regional differences in neuronal activity. This is referred to as neurovascular coupling, and generally relies on metabolic signalling to vascular cells. Models of obesity show deficits in the ability of the vasculature to respond to dilatory signals (Chantler et al., 2015; Phillips et al., 2005; Schwaninger et al., 2003) whilst HFD fed animals showed a reduction in endothelial dependent dilation of pial arterioles following 20 weeks of diet (Obadia et al., 2017). This was associated with elevated levels of NADPH oxidase, a major source of ROS (Zhang et al., 2016), in the cerebrovasculature. Increases in NADPH oxidase expression and activity are associated with impairments in neurovascular coupling (Toth et al., 2014; Park et al., 2007b), and HFD-associated decreases in neuronally stimulated CBF responses in the whisker barrel cortex were partially attenuated by NADPH oxidase inhibition (Tucsek et al., 2014b). In addition, a marker of oxidative and nitrosative stress, 3-nitrotyrosine, is elevated by HFD in aged mice (Tucsek et al., 2014b).

5.1.1 Aims, Hypotheses, and Experimental Approach

Currently, no studies have investigated the effects of short-term (i.e. within the first 8 weeks) HFD feeding on blood flow. My aim with the work presented in this chapter was to address this by measuring changes in flow across a variety of parameters (e.g. blood volume, oxygen saturation) over an 8 week dietary timecourse in both the hippocampus and cortex. This would allow me to not only evaluate whether flow changes occurred rapidly enough following the start of HFD feeding to contribute to the development of hippocampus-specific cognitive deficits (reported after 24 hours in McLean et al. 2018), but also to see if diet-induced changes followed a phasic pattern over time, and if they occurred in a global or region-specific manner. In this way I hoped to relate hippocampus-specific deficits either to hippocampus-specific flow changes, or global changes having a greater effect on the hippocampus than other brain areas.

Beyond this, I also wanted to evaluate hypotheses based on results from the post-mortem tissue work I described in **Chapter 3**. These showed that following two weeks of dietary manipulation, HFD feeding reduced capillary radii, the variation in capillary radii, and the extent of capillary perfusion. As a result, I hypothesised that the reduction in capillary radii and perfusion levels would be reflected *in vivo* by a reduction in blood volume, and if not also a reduction in CBF, then a compensatory increase in flow speed. In addition I interpreted the decrease in radius variability as an indicator of an impoverished ability to regulate vascular diameter, which therefore may indicate an impairment in neurovascular coupling. Whilst I detected vascular structural changes across the

brain, HFD feeding induces hippocampus-specific cognitive impairment that occurs after only 24 hours (McLean et al., 2018) and remains region-specific for up to 30 days (Kanoski and Davidson, 2010). This suggests the presence of hippocampus-specific vascular deficits that may be picked up by an analysis of *in vivo* functional blood flow changes, in contrast to the post-mortem structural vascular analysis that showed no region-specific differences.

Results from **Chapter 3** also suggested that basal differences in hippocampal vascular support could translate global diet induced deficits into region-specific cognitive effects. Data showed that the hippocampus not only had the lowest capillary density compared to the hypothalamus and cortex, but that this was also the case for capillary radii measurements, capillary radii variation, and pericyte coverage. I therefore hypothesised that *in vivo* the hippocampus would display a lower level of oxygen availability, and if not, then a greater flow speed that could compensate for the reduced vascular density and volume. Literature suggests that the hippocampus might have at least equal, if not greater, neuronal demand for energy supply (discussed in **Chapter 3**), indicating the hippocampus likely suffers from worse vascular support relative to its metabolic requirement than other brain regions. This was hypothesised to underlie its sensitivity to damage in a number of pathologies including Alzheimer's Disease, ageing (reviewed in Fjell et al. 2014), and hypoxia (Ng et al., 1989; Michaelis, 2012). I aimed to evaluate this by comparing blood flow and neuronal metabolism between the cortex and hippocampus. In addition, though non-significant and underpowered, the NOCR behavioural data I presented in the previous two chapters suggested the presence of hippocampus-specific cognitive deficits following HFD feeding for two weeks. As such, this suggests that behavioural performance and vascular changes could be correlated.

Finally, it has been suggested that locomotion leads to the uncoupling of blood flow and neuronal activity (Pisauro et al., 2013), though this was only assessed using intrinsic optical imaging (Huo et al., 2014; Pisauro et al., 2013). Locomotion increases neuronal activity in visual (Niell and Stryker, 2010), somatosensory, and frontal cortices, though this does not always correlate with increases in haemodynamic activity (Huo et al., 2014). However, to date this has not been investigated using a comprehensive readout of blood flow changes, something I aimed to address. Optical imaging is largely restricted to estimates of blood volume, where the absorbance of light with a wavelength at the isosbestic point of the oxy- and deoxyhaemoglobin absorption spectra (530nm) represents changes in blood volume (Sirotin et al. (2009) cited by Pisauro et al. 2013).

To investigate the hypotheses and aims proposed I took measurements using a combined laser doppler flowmetry/haemoglobin spectroscopy probe (Oxy-CBF probe) that measures an assortment of blood flow-related parameters (oxygen saturation, blood volume, flow speed etc., from which the rate of neuronal oxygen metabolism can also be calculated) in mice implanted with

cranial windows over hippocampal CA1 and cortical V1 over 8 weeks of dietary manipulation. This was done in awake, behaving animals, that could run freely during data acquisition. This allowed me to avoid any confounding effects of anaesthesia, which decreases the amplitude, and changes the timecourse of, haemodynamic responses in mice (Pisauro et al., 2013). I analysed data acquired whilst the mice were at rest to evaluate differences in blood flow and neuronal metabolism between the hippocampus and cortex, whilst I used the presentation of visual stimuli to induce neurovascular coupling events in V1 to investigate the effect of diet and locomotion. The sparse hippocampal coding of stimuli makes eliciting strong peaks of hippocampal activity challenging, so investigating hippocampal neurovascular coupling required an alternative approach. To achieve this I detected peaks in a calculated $CMRO_2$ value, which represents summed neural activity, and averaged the haemodynamic responses occurring during these peaks. This allowed me to evaluate changes in haemodynamic parameters associated with peaks in neuronal activity. Finally, by testing hippocampal window mice on their NOCR performance, I was able to correlate hippocampus-specific cognition with changes in blood flow *in vivo*.

The data presented here represents some of the first to investigate the effects of HFD on blood flow and neurovascular coupling changes *in vivo* in hippocampus. In addition, it provides a novel insight into the relationship between hippocampus-specific cognition and blood flow, and evaluated the effect of HFD feeding across more numerous haemodynamic parameters than just CBF as has typically been done in other studies.

5.2 Methods

5.2.1 Animals, Dietary Manipulation, and Experimental Approach

Details of animal genotypes, diets used, behavioural testing, window implantation surgeries, and imaging setup, are presented in the main methods (**Chapter 2**). All *in vivo* results were collected from Cx3CR1-GFP heterozygotes that had undergone either cortical, or hippocampal, window implantation. These mice were housed in a reverse light-dark cycle to minimise the impact of imaging sessions on circadian rhythms, and fed either a HFD or control diet for 57 days. In some cases, window implanted mice had to be culled prior to 57 days for welfare purposes. After imaging on day 56, window implanted mice were injected with LPS to induce microglial activation and then imaged again 24 hours later. Following this, mice were either culled using cervical dislocation or given a terminal dose of i.p. sodium pentobarbital (Dolethal; Vétoquinol Ltd) at 120mg/kg (diluted to 10% in saline). Behavioural testing was run on hippocampal window mice

alongside a cohort of wild type naive mice in order to evaluate the effect of surgery, and dietary manipulation, on hippocampal functioning. As with the *in vivo* mice, these wild type animals were fed either a HFD or control diet. The behavioural protocol began on day 11 of dietary manipulation, and ran until day 14, the day on which testing took place. After testing wild type mice were culled using cervical dislocation. Mice were weighed daily, though not always at the same time of day. As the mice used in this chapter were the same as those used in the microglia *in vivo* results (**Chapter 4**), a table of summary statistics, of count, age, sex split, and diet group allocation by surgery status, is available there (**Table 4.1**).

5.2.2 Combined Laser Doppler Flowmetry/Haemoglobin Spectroscopy

A combined laser doppler flowmetry/haemoglobin spectroscopy probe (Oxy-CBF probe, VMS Oxy, Moor Instruments) allowed for monitoring of the following net haemodynamic measures: blood flow (CBF), flow speed, oxygen saturation (SO_2), oxygenated haemoglobin (HbO), deoxygenated haemoglobin (HbR), and total haemoglobin (HbT). The cerebral metabolic rate of oxygen consumption ($CMRO_2$) was calculated from these variables, where (t) indicates time.

$$CMRO_2(t) = CBF(t)\frac{HbR(t)}{HbT(t)}$$

All measures taken using the Oxy-CBF probe except SO_2 are measured in arbitrary units, with SO_2 being measured in percent. Recordings were taken by positioning the probe vertically above the cranial window, as close as was possible without making direct contact. Data were available as a 2D matrix to visualise continuous haemodynamic activity. The matrix also included recordings of locomotion and indicators of periods of visual stimulation. Data points were collected at a rate of 40Hz. Recordings typically lasted $\sim$10 minutes. These were obtained at the end of imaging sessions that began with the acquisition of two photon image stacks for the microglial analysis described in **Chapter 4**. Acquiring these images typically took around 1.5 hours.

5.2.3 Stimulation of Visual Cortex Neuronal Activity

To investigate stimulus-induced neurovascular coupling in mice with cortical windows implanted over V1, drifting gratings of black bars on a white background (PsychoPy; spatial frequency of 0.04 cycles per degree, temporal frequency of 2Hz, gratings angled at 315°, bars sized at 220 degrees of visual space at a 17cm distance from the mouse) were presented on screens (Asus VC239H, 50.92cm x 28.64cm, mean luminance of 15 cd/m^2, screen refresh rate of 60 frames per

second) and paired with simultaneous Oxy-CBF probe recordings (**Fig 5.1**).

A single visual-stimulus recording session consisted of 10 presentations of the visual stimulus, each lasting five seconds, with each stimulus period preceded by a five-second-long pre-stimulus period and followed by a 20 second post-stimulus period (**Fig 5.1 D**). During the pre- and post-stimulus periods, mice were presented with grey screens that were equi-luminescent with the visual stimulus. Visual stimulus onset and offset was recorded using a LabJack, and locomotion was recorded using a rotary encoder (Kubler). Raw locomotion data for each Oxy-CBF probe recording session was normalised first by setting any values less than 2 standard deviations below the mean value to 0, and then normalising the values from 0 to 1 (between their minimum and maximum; **Fig 5.1 C**).

Trials were assigned to locomotion categories. Analysis was limited to those where locomotion occurred both in the pre-stimulus period, and during stimulus presentation (locomotion trials), and those where there was no locomotion in either of these windows (non-locomotion trials).

5.2.4 Resting Data Detection

Data were categorised as occurring during periods of rest when there was no locomotion or visual stimulus presentation. Additionally, any resting data that were within 5 seconds of a previous visual stimulus presentation, or 1 second of any previous locomotion, was excluded. Resting data were averaged within epochs i.e. periods of continuous rest within a recording session, and periods of rest were excluded if their duration was less than 2 seconds (**Fig 5.1 C**).

5.2.5 $CMRO_2$ Peak Aligned Data Extraction

To detect $CMRO_2$ peaks, the data were first smoothed using a locally weighted smoother (LOESS) with a span of 0.01. Following this the baseline was made local to 0 (by subtracting the minimum of the trace, dividing by the maximum of the trace, and then subtracting a further smoothed trace. This further smoothed trace consisted of data smoothed using a moving average window over 2.5 seconds). Any discrete signal spikes which were >10% of the total maximum value (across the entire trace) were provisionally identified as peaks (**Fig 5.2 B**). Peaks that occurred within 3 seconds of one another were compared, and the peak with the greatest value was retained. Events were excluded if the $CMRO_2$ peak was smaller than 2 standard deviations above the baseline. Events were classified as occurring during locomotion if there was locomotion in the second preceding the detected peak. Events were classified as occurring during stimulus presentation if there was a

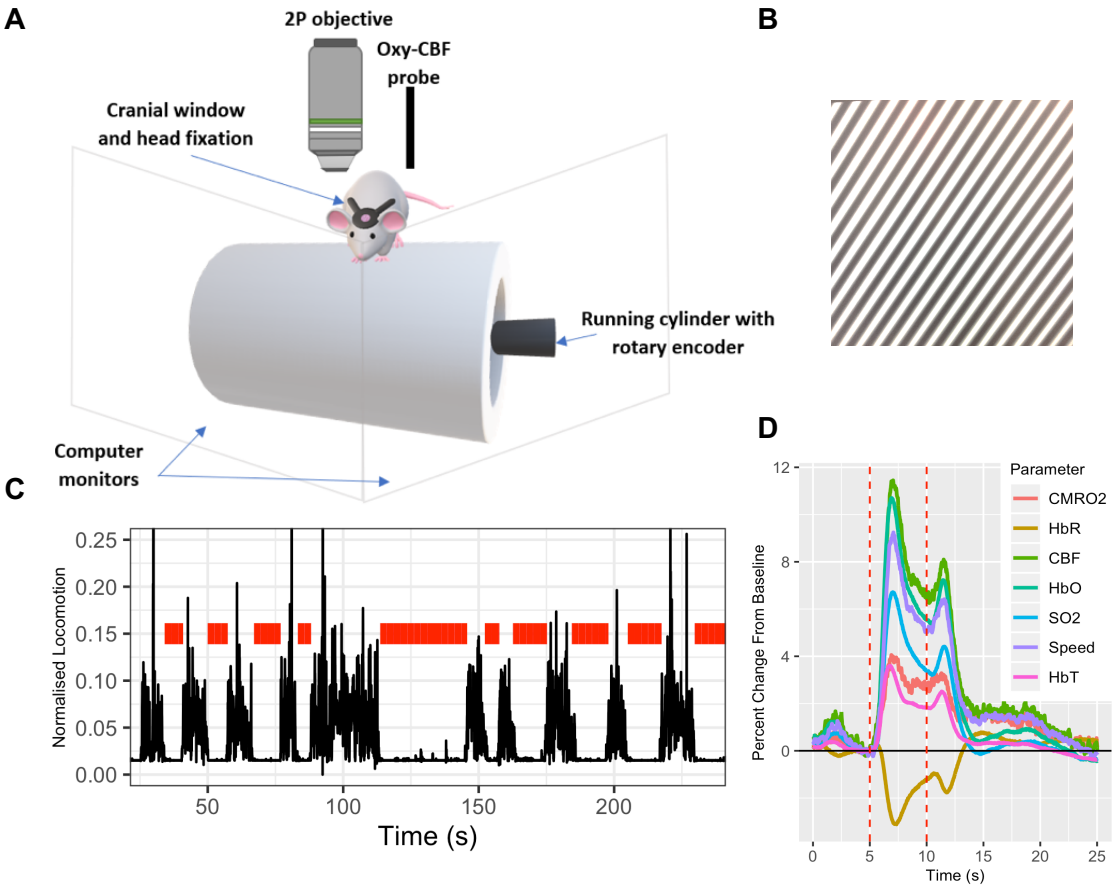

Figure 5.1: Experimental Setup and Example Data. (**A**) Imaging setup schematic. (**B**) Drifting gratings were presented on the screens in **A** to stimulate neuronal activity in V1 during visual stimulus data collection. (**C**) Example locomotion trace from a recording session. Raw locomotion values were normalised between their min and max values for plotting. Red bars indicate resting epochs. Periods of rest were defined as occurring at least 1 second after previous locomotion, and at least 5 seconds after any previous visual stimulation event. (**D**) Example haemodynamic recordings from V1 using the Oxy-CBF probe during visual stimulus presentation (red dotted lines indicate stimulus presentation, mean of data normalised to baseline (4-5s) plotted. Plotted data averaged over n = 2947 trials, captured over 155 sessions from 17 mice).

stimulus presentation at any time in a 12 second window beginning 8 seconds before the detected peak and ending 4 seconds after.

5.2.6 Statistical Analysis

As stated in the main methods chapter, all analyses were run using LMMs and all plotted values represent the estimated marginal mean +/- 1 SEM derived from the appropriate LMM, unless otherwise indicated. The use of trials (i.e. data averaged around visual stimulus presentations, resting periods, or peaks in neuronal metabolism) or mice as subjects in an analysis is indicated in the appropriate figure legends. Where trials were used as subjects this was accounted for by

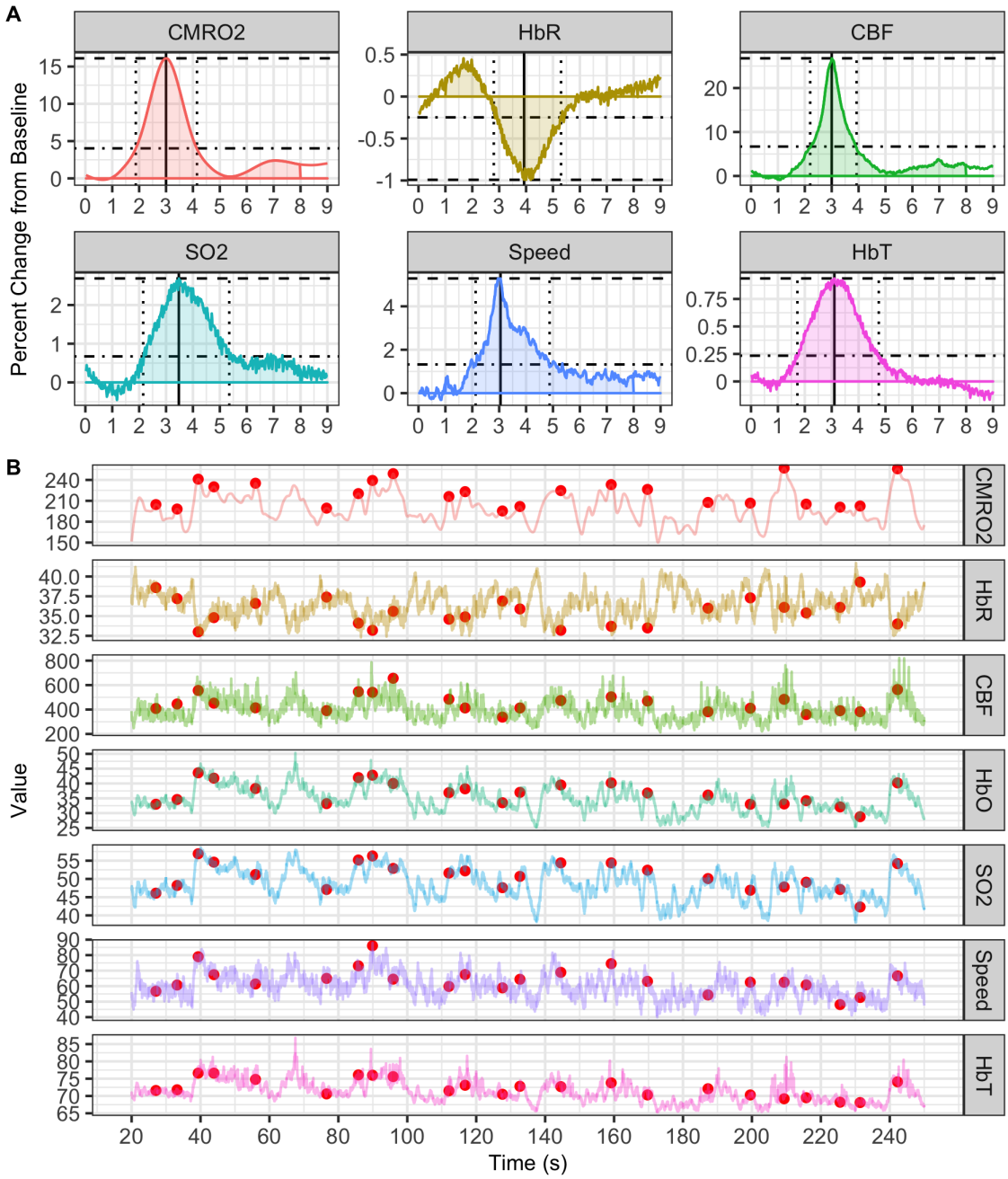

Figure 5.2: $CMRO_2$ Peak Aligned Data Extraction. (**A**) Mean traces from baseline (D-1) for $CMRO_2$, HbR, CBF, SO_2, speed, and HbT data that were cut 3 seconds before, and 6 seconds after, detected peaks in $CMRO_2$ signal. Plotted values are normalised to the first second and represent percent change (averaged over n = 1385 events, captured over 29 sessions from 29 mice; **vertical solid and dotted lines** indicate t2o, t2p, and t2r respectively. **Horizontal dashed** and **dot-dash lines** indicate peak and 25% of peak respectively. **Shaded areas** indicate the AUC). (**B**) Peaks in $CMRO_2$ signal were detected (**red circles**) and parameters were cut into segments starting 3 seconds before and ending 6 seconds after these peaks.

including a random effect structure in the appropriate statistical model that grouped measurements by animal.

Visual Stimulus and $CMRO_2$ Peak Aligned Analyses

Visual Stimulus and CPA data were averaged around stimulus presentations and $CMRO_2$ peaks respectively. The former was averaged over a window starting 5 seconds before stimulus onset, and ending 20 seconds after stimulus offset, whilst for the latter this window began 3 seconds before and ended 6 seconds after the detected $CMRO_2$ peak. Averaged data were normalised as a percent change using the δ F/F method compared to baseline, where the baseline was the second before stimulus onset in visual stimulus data, and the first second of events in CPA data.

Visual stimulus and CPA data were characterised by finding the peak value (p), timing of the peak value (t2p), the minimum value (m), timing of the minimum value (t2m), time taken to reach 25% of the peak value (t2o), time taken to fall to 25% of the peak value (t2r), and AUC (**Fig 5.2 A**). Given that CPA data were aligned to $CMRO_2$ peaks, the t2p was not analysed for $CMRO_2$. This was done for each haemodynamic parameter recorded (CBF, speed, SO_2, HbO, HbR, HbT, and $CMRO_2$). In visual stimulus data these values were characterised over the 10 seconds following stimulus presentation, whilst for CPA data these were characterised from 1 second from the start of the cut event (the end of the baseline period) through to 8 seconds post event start.

Principle Component Analysis

For visual stimulus timecourse data, a PCA with feature centering and scaling was run on the raw data for each haemodynamic parameter. The first principle component was taken as a composite measure of the haemodynamic response and analysed alongside the other metrics (e.g. p, AUC, t2p). To illustrate how they varied by timepoint, the loadings for each parameters were standardised to their standard deviation using the formula $(L-\mu_L)/\sigma_L$, where L indicates the loading value, μ_L indicates the mean loading, and σ_L indicates the standard deviation of loading values. These are plotted by timepoint and haemodynamic parameter in **Fig 5.3**.

Ratio of SO_2 and HbT to $CMRO_2$

For all analyses, the ratio of SO_2 and HbT to $CMRO_2$ was calculated. This was done using the AUC values in the visual stimulus and CPA data.

Statistical Models

The main effects of sex, age, and weight change, were included for all the following described models. Additionally, neurovascular coupling data were analysed with locomotion group, rather

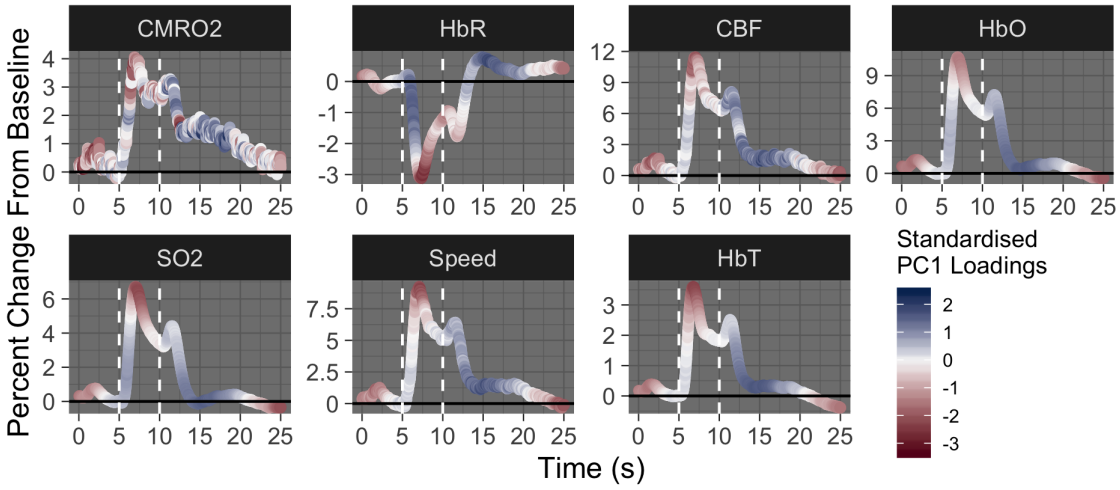

Figure 5.3: Visual Stimulus Composite Measure PC1 Loadings by Time. A PCA was run on visual stimulus responses, and the first principal component was chosen as a composite measure. **Colour coding** indicates the standardised loadings of the composite measure, which are indicated by time across all measured parameters. Traces represent the average data normalised to baseline (4-5 seconds) regardless of diet, timepoint, or locomotion status. **Dashed white lines** indicates the period of visual stimulus presentation. **Horizontal black lines** indicate the mean value at baseline (plotted average of n = 2135 stimulus presentations (n = 1146 locomotion trials) captured over 148 sessions from 17 mice (n = 8 HFD)).

than brain region, as a fixed factor. Data were classified as a locomotion trial if there was locomotion during both the stimulus presentation and the pre-stimulus baseline period, and as non-locomotion if there was no locomotion in either period. Individual visual stimulus and CPA trials, as well as resting epochs, were used as subjects. For all analyses, except those looking exclusively at day 14, an autoregressive order 1 model for the correlation between days was included. Data were analysed using LMMs.

Analyses of timecourse data were done specifying timepoint, diet, brain region, and their interactions, as fixed effects. A random intercept for each animal and each trial nested within animal was specified, with a random slope included for the relationship between days.

In both resting and CPA data, hippocampal values showed a consistent trend towards cortical values over time, where this corresponded to increases in the resting data, and decreases in the CPA data. This appeared to stabilise at days 42, 49, and 56. As such, a separate analysis of these three timepoints was conducted. Timepoint, diet, brain region, and their interactions, were specified as fixed effects. A random intercept for each animal and each trial nested within animal was specified, with a random slope included for the relationship between days.

Data from hippocampal window mice that underwent behavioural testing at day 14 were analysed separately to investigate any effect of behavioural performance on haemodynamic data. Here

diet, behavioural performance, and their interaction, were specified as fixed effects. A random intercept was specified for animal, with a random slope for the relationship between trials.

In order to look at cortical changes at this same timepoint, analyses were run on all mice limited to day 14. Diet, region, and their interaction, were specified as fixed effects. A random intercept was specified for animal, with a random slope for the relationship between trials.

5.3 Results

5.3.1 HFD Did Not Significantly Affect *In Vivo* Weight Gain or NOCR Performance

In order to evaluate the effect of HFD feeding on weight gain, weights were compared between groups following normalisation to their value at the beginning of the dietary manipulation in order to control for differences in starting weight. This value was analysed using an LMM. As the mice used for both this chapter, and the *in vivo* microglial work (**Chapter 4**) were the same, see **Fig 4.3** and the associated results section there for a detailed description. In brief, there was no effect of diet, nor any modulatory effect of diet, on the significant increase in normalised weight seen as time progressed in either the window implanted mice, or when looking within the first two weeks of dietary manipulation in mice that underwent behavioural testing.

Short-term HFD feeding is associated with hippocampal deficits. To investigate the effect of hippocampal window surgery, and diet, on hippocampus-specific cognition, and to correlate cognitive performance with *in vivo* blood flow changes, the performance of mice that had not undergone surgery, and hippocampus window implanted mice, on a hippocampus-specific NOCR task following two weeks of dietary manipulation was assessed. As with the analysis of weight, the mice used in the previous chapter were the same as those described here. Therefore for a full presentation of the results and discussion see **Chapter 4**. Briefly, though HFD impaired NOCR performance in the subset of mice analysed in the post-mortem chapter (**Chapter 3**), the HFD-associated decrease in NI value was attenuated and did not approach significance when hippocampal window mice were included in the analysis.

5.3.2 Neurovascular Coupling in Visual Cortex

HFD induced cognitive impairment has been proposed to be mediated by deficits in neurovascular coupling (Sorop et al., 2017). In addition, results from **Chapter 3** demonstrating a HFD induced

reduction in capillary radius variation suggested that neurovascular coupling may be impaired in my model. To investigate the effect of diet on neurovascular coupling, I presented mice with visual stimuli (drifting gratings) to stimulate neuronal activity in V1 whilst simultaneously taking Oxy-CBF probe recordings. These recordings were averaged around the 5 seconds of stimulus presentation, including the 5 seconds before and 15 seconds after. Data were normalised using δ F/F to the mean value 1 second before stimulus presentation began.

This approach also allowed me to investigate the suggestion that during locomotion, neuronal activity is uncoupled from blood supply (Pisauro et al., 2013). To do this, I assigned trials (data averaged around stimulation events) from the visually stimulated V1 recordings a locomotion category. Trials where the mouse was running both before and during the stimulus presentation were classified as locomotion trials. Trials with no locomotion either before or during stimulus presentation were classified as non-locomotion trials. In this way I could investigate whether locomotion leads to neurovascular uncoupling using a more comprehensive readout of blood flow changes than had been used previously in Huo et al. (2014) and Pisauro et al. (2013). I was also able to explore whether this was associated with any dietary effects. As such, locomotion and non-locomotion trials were compared over time and between diet groups.

Effects of Locomotion on V1 Neurovascular Coupling

Analysing the effect of locomotion on neurovascular coupling in V1 showed that locomotion reduced peak and AUC values for HbO and SO_2, and increased them for CBF and HbT (**Fig 5.4**). HbR showed simultaneously more positive, and therefore weaker, peak responses in locomotion trials, as well as an elevated AUC value. The timing of peaks, peak onsets, and peak offsets, were accelerated by locomotion for all parameters except $CMRO_2$. The PCA-based composite measures also showed locomotion effects for all parameters except $CMRO_2$ (**Appendix A.8**). The ratio of oxygen availability (SO_2) to oxygen metabolism ($CMRO_2$) was reduced by locomotion, whilst the ratio of blood volume (HbT) to $CMRO_2$ was elevated. Values from statistical analyses are presented in **Table 5.1**. These results reflect that locomotion, whilst not influencing neuronal activity or overall CBF, leads to a decrease in oxygen saturation despite an elevation in blood volume and an acceleration of the haemodynamic response to neuronal activity. The decrease in SO_2 suggests that despite the increase in blood volume (HbT), the balance between oxy- and deoxy- haemoglobin levels is tilted towards deoxyhaemoglobin during locomotion. This is supported in the data by the presence of locomotion-associated increases in the AUC of HbR responses.

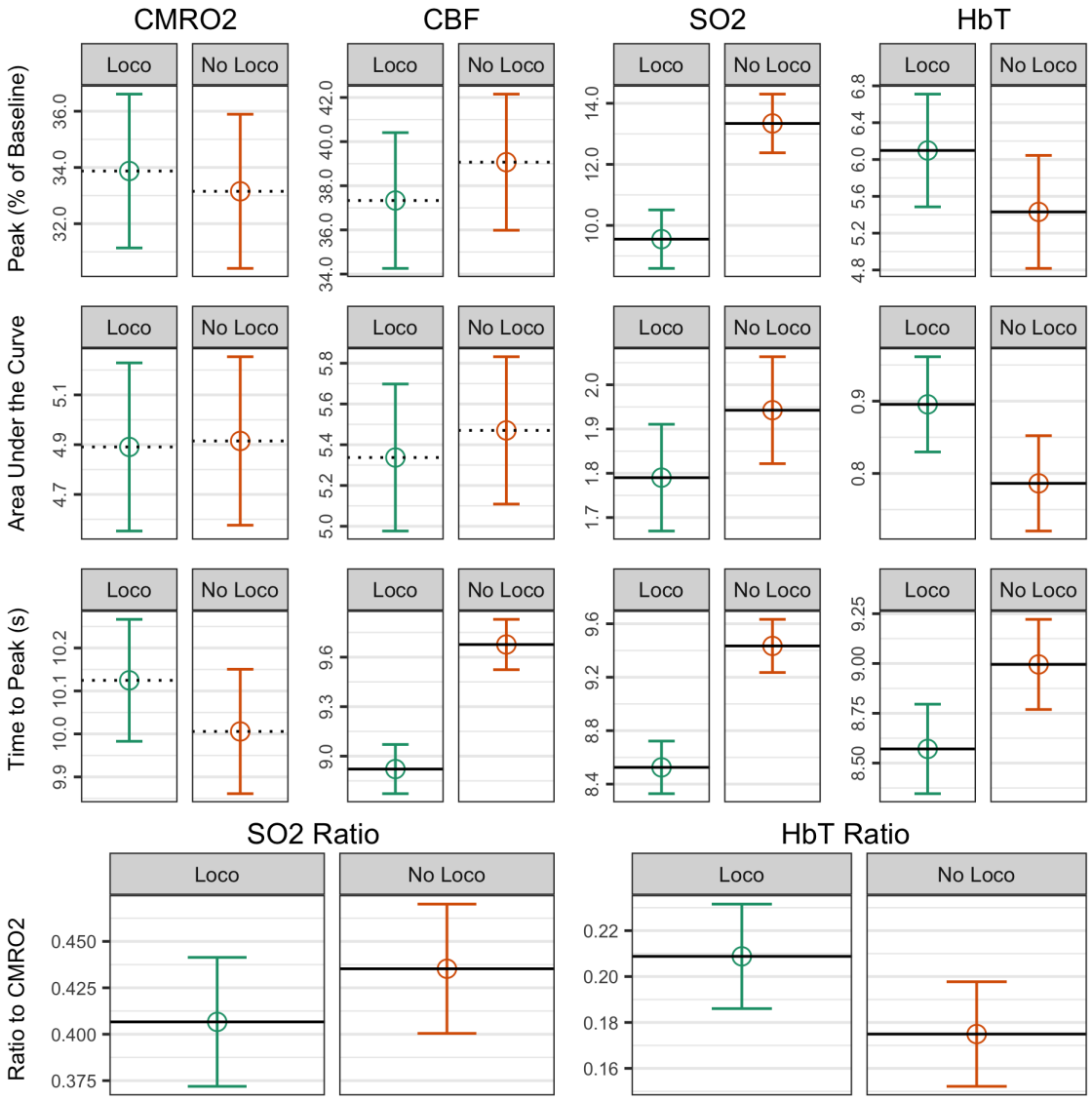

Figure 5.4: Locomotion Increases Blood Volume, Decreases Oxygen Availability, and Accelerates Haemodynamic Responses. Locomotion increased both the peak and AUC values for HbT, whilst decreasing them for SO_2, something that is reflected in both a reduced ratio of SO_2, and an elevated ratio of HbT, to $CMRO_2$. Locomotion also accelerated the peak timing for CBF, SO_2, and HbT responses to visual stimulation (**'Loco'** refers to trials with locomotion both during and preceding stimulus presentation. **'No Loco'** refers to trials where no locomotion was present in either window. The baseline period was the second preceding stimulus presentation. Ratios to $CMRO_2$ are calculated using AUC values. Time to peak times are relative to the beginning of stimulus trials, where stimulus presentation occurs from 5 to 10 seconds. **Horizontal lines** indicate locomotion group means. **Solid lines** indicate significant ($p < .05$) differences. Analysis used n = 2135 trials (n = 1146 locomotion) recorded over 148 sessions taken from n = 17 mice (n = 8 HFD)).

Dietary Effects on V1 Neurovascular Coupling

Investigating the effects of diet revealed time-specific effects on the AUC values of all haemodynamic measures. In addition, $CMRO_2$, CBF, SO_2, speed, and HbR showed diet by time by

numDF	denDF	F-value	p.value	Sig	Measure	Factors	Parameter	Analysis
1	1759	0.3384	1.0000		AUC	LocoGroup	CMRO2	VisStim
1	1759	3.4872	1.0000		AUC	LocoGroup	CBF	VisStim
1	1759	18.0572	0.0011	**	AUC	LocoGroup	SO2	VisStim
1	1760	63.6758	0.0000	***	AUC	LocoGroup	HbT	VisStim
1	1759	12.1623	0.0070	**	Ratio	LocoGroup	SO2	VisStim
1	1759	67.4690	0.0000	***	Ratio	LocoGroup	HbT	VisStim
1	1759	0.2632	1.0000		p	LocoGroup	CMRO2	VisStim
1	1759	4.0204	1.0000		p	LocoGroup	CBF	VisStim
1	1759	111.8309	0.0000	***	p	LocoGroup	SO2	VisStim
1	1759	14.7842	0.0061	**	p	LocoGroup	HbT	VisStim
1	1759	0.0300	1.0000		t2p	LocoGroup	CMRO2	VisStim
1	1759	41.0211	0.0000	***	t2p	LocoGroup	CBF	VisStim
1	1759	59.3591	0.0000	***	t2p	LocoGroup	SO2	VisStim
1	1759	16.7577	0.0022	**	t2p	LocoGroup	HbT	VisStim

Table 5.1: Statistics for the Effect of Locomotion on Visually Stimulated Neurovascular Coupling. The effect of locomotion on haemodynamic responses to visually stimulated neuronal activity in V1 was analysed using LMMs (numDF and denDF refer to degrees of freedom. F and p values are rounded to 4 decimal places. **Red text** indicates significance. **Green text** indicates trend level. **Background shading** indicates size of p value where darker is larger. Sig indicates significance indicators. Measure indicates the measure analysed. Factors indicate factors in the model. Parameter indicates the haemodynamic parameters analysed. Analysis indicates the type of data analysed. P values are corrected for multiple comparisons across parameters using the Bonferroni adjustment).

locomotion interactions, where timepoint-specific dietary differences also varied by locomotion status (**Appendix A.10**). These effects were more sparse in peak analyses (**Appendix A.9**), and of the timings analysed, only the t2p and t2o for CBF showed a three-way diet, locomotion, timepoint interaction (data not shown). Corrected pairwise dietary comparisons however, revealed no significant differences between diet groups at any timepoint for either locomotion category in any measure, suggesting these detected effects were driven by time-related noise.

Besides characterising haemodynamic responses by measuring values such as the AUC and peak levels, I also constructed a composite measure of the neurovascular response in V1 to visual stimulus using a PCA. This measure was significantly affected by diet by time and diet by time by locomotion interactions, as well as being associated with a significant dietary effect on speed and CBF at day 3 in locomotion trials (**Fig 5.5**). In order to interpret what exactly a significant effect on the PCA based measure meant, I investigated the raw data traces at day 3 (**Fig 5.6**) in locomotion trials. This revealed that whilst peak values and the timing of responses appeared similar between diet groups, the response in HFD animals seemed to remain elevated for a longer duration in CBF and flow speed measures. Though potentially a result of noisy data, in the absence of similar dietary effects on $CMRO_2$, this could suggest that short-term HFD feeding is associated

with an impaired ability to regulate the dynamics of flow speed (which leads to alterations in CBF) during neurovascular coupling in V1 during locomotion. Values from statistical analyses of the composite response measures are presented in **Table 5.2**.

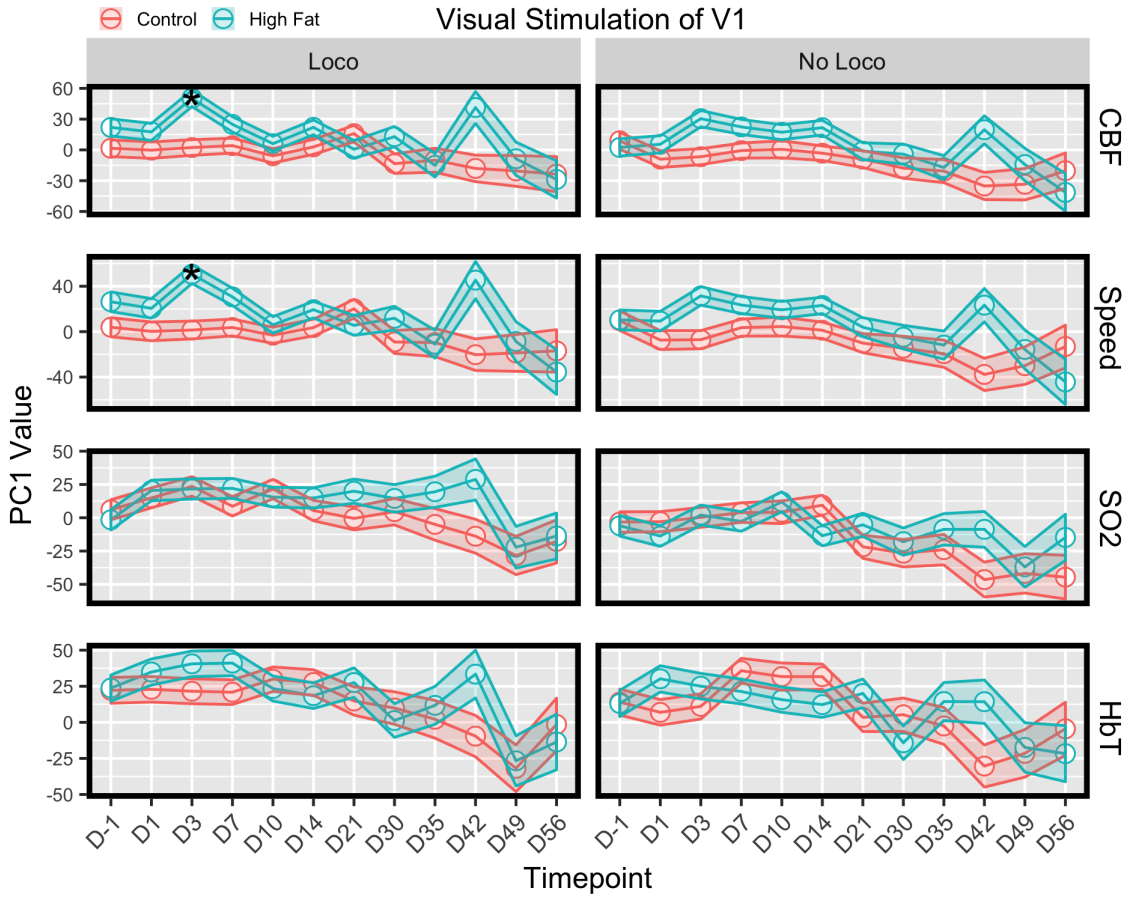

Figure 5.5: HFD Feeding Induces Early Dysfunction in V1 Neurovascular Coupling During Locomotion. Visual stimulation of neuronal activity in V1 appeared unaffected by HFD in analysis of peak, AUC, and timing values. However, a composite PCA-based measure of the haemodynamic response showed dietary effects at day 3 of manipulation in locomotion trials in both speed and CBF readings. (The composite response measure is the first principal component (PC1) of a PCA run on the data. **'Loco'** refers to trials with locomotion both during and preceding stimulus presentation, **'No Loco'** refers to trials where no locomotion was present in either window. The baseline period was the second preceding stimulus presentation. **Thick borders** indicate diet by time interactions. **Grey backgrounds** indicate diet by time by locomotion interactions. * indicates $p < .05$. Analysed using n = 2135 trials (n = 1146 locomotion) recorded over 148 sessions from n = 17 mice (n = 8 HFD)).

The Effects of Two Weeks of HFD on V1 Neurovascular Coupling

Whilst underpowered, the NOCR results presented in **Chapter 4** provided some evidence (though results weren't significant) that supports the presence of hippocampus-specific cognitive impairment following two weeks of HFD feeding. In order to correlate this with dietary effects on V1

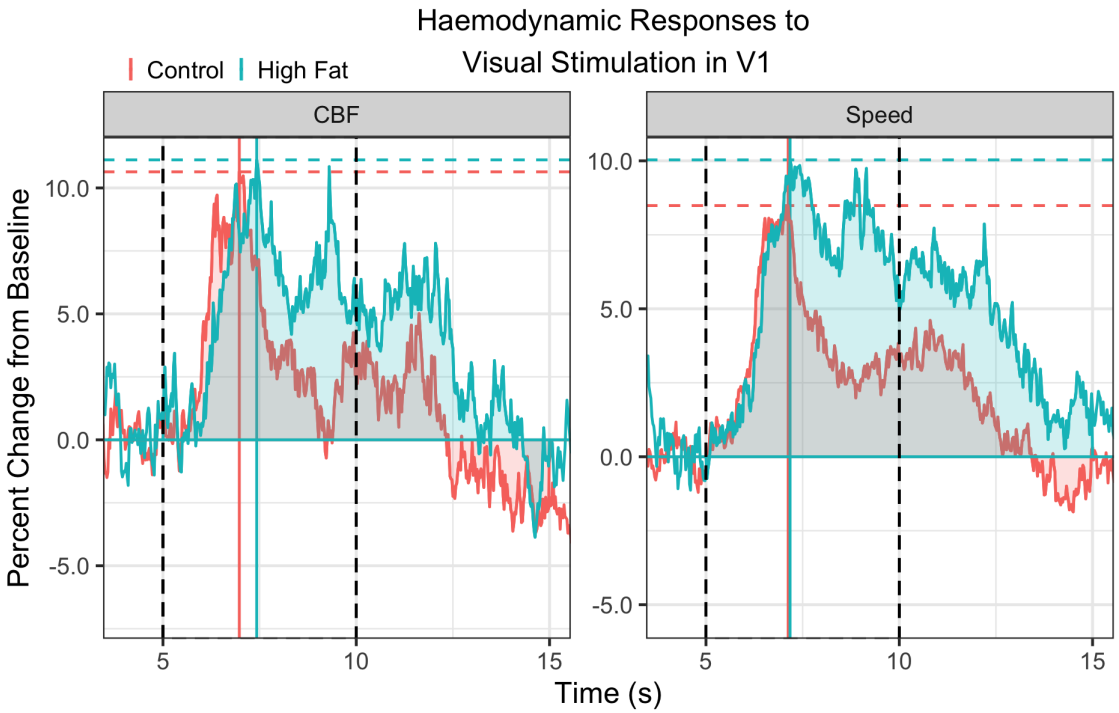

Figure 5.6: Three Days of HFD Prolongs Visually Stimulated Haemodynamic Responses in V1. Analysis of the composite response measure indicated dietary effects in locomotion trials after three days of HFD feeding. Normalised traces indicate that this represents a prolonging of the CBF and flow speed responses to visual stimulation in V1 (Plotted data represents the mean. **Vertical dashed lines** indicate stimulus presentation. **Vertical solid lines** indicate the timing of peak responses. **Horizontal dashed lines** indicate the peak values. **Shading** indicates the AUC. Data were normalised to the second before stimulus presentation and averaged over n = 248 trials captured over 16 sessions from n = 16 mice (n = 8 HFD)).

neurovascular coupling, I limited analysis of V1 neurovascular coupling trials to the two week timepoint. Here only the PCA based composite response measure showed dietary effects, where there was a significant diet by locomotion group interaction for speed, and trend level effects on HbO and HbT. However, pairwise dietary comparisons revealed no differential dietary effects by locomotion status (**Fig 5.7**), suggesting the absence of a correlation between V1 neurovascular deficits and hippocampus-specific cognitive impairment.

5.3.3 Resting Data

Regional Differences in Resting Haemodynamic Values

The results presented in **Chapter 3**, where the hippocampus showed the lowest levels of capillary density and smallest capillary radius, suggested that the hippocampus may show an uncoupling of oxygen availability, and general vascular support, from neuronal demand. To investigate this, I analysed haemodynamic parameters during periods of rest, when neither locomotion nor visual

numDF	denDF	F-value	p.value	Sig	Measure	Factors	Parameter	Analysis
1	13	4.5722	1.0000		PC1	Diet	CBF	VisStim
1	13	0.1736	1.0000		PC1	Diet	SO2	VisStim
1	13	5.3489	1.0000		PC1	Diet	Speed	VisStim
1	13	0.0516	1.0000		PC1	Diet	HbT	VisStim
11	1759	15.4370	0.0000	***	PC1	Timepoint	CBF	VisStim
11	1759	24.4326	0.0000	***	PC1	Timepoint	SO2	VisStim
11	1759	12.5213	0.0000	***	PC1	Timepoint	Speed	VisStim
11	1759	31.3358	0.0000	***	PC1	Timepoint	HbT	VisStim
11	1759	5.0898	0.0000	***	PC1	Timepoint:LocoGroup	CBF	VisStim
11	1759	7.9623	0.0000	***	PC1	Timepoint:LocoGroup	SO2	VisStim
11	1759	7.0332	0.0000	***	PC1	Timepoint:LocoGroup	Speed	VisStim
11	1759	6.3370	0.0000	***	PC1	Timepoint:LocoGroup	HbT	VisStim
1	1759	4.2844	1.0000		PC1	Diet:LocoGroup	CBF	VisStim
1	1759	10.0728	0.0750	'	PC1	Diet:LocoGroup	SO2	VisStim
1	1759	4.0239	1.0000		PC1	Diet:LocoGroup	Speed	VisStim
1	1759	16.3256	0.0027	**	PC1	Diet:LocoGroup	HbT	VisStim
11	1759	26.1028	0.0000	***	PC1	Timepoint:Diet	CBF	VisStim
11	1759	5.7139	0.0000	***	PC1	Timepoint:Diet	SO2	VisStim
11	1759	30.1324	0.0000	***	PC1	Timepoint:Diet	Speed	VisStim
11	1759	28.3709	0.0000	***	PC1	Timepoint:Diet	HbT	VisStim
11	1759	5.0321	0.0000	***	PC1	Timepoint:Diet:LocoGroup	CBF	VisStim
11	1759	6.9545	0.0000	***	PC1	Timepoint:Diet:LocoGroup	SO2	VisStim
11	1759	4.7040	0.0000	***	PC1	Timepoint:Diet:LocoGroup	Speed	VisStim
11	1759	5.6431	0.0000	***	PC1	Timepoint:Diet:LocoGroup	HbT	VisStim

Table 5.2: Statistics for the Effect of Diet on Visually Stimulated Neurovascular Coupling. The effect of time, diet, and locomotion, on the haemodynamic responses to visually stimulated neuronal activity in V1 was analysed using LMMs (numDF and denDF refer to degrees of freedom. F and p values are rounded to 4 decimal places. **Red text** indicates significance. **Green text** indicates trend level. **Background shading** indicates size of p value where darker is larger. Sig indicates significance indicators. Measure indicates the measure analysed. Factors indicate factors in the model. Parameter indicates the haemodynamic parameters analysed. Analysis indicates the type of data analysed. P values are corrected for multiple comparisons across parameters using the Bonferroni adjustment).

stimulation was taking place (including in the second, or five seconds prior, respectively) and compared them between V1 and hippocampal CA1. A trend over time in CBF, speed, and $CMRO_2$ values in the hippocampus to increase towards the levels seen in the cortex from an initially lower point was apparent in the timecourse data. These appeared to plateau for the final three imaging timepoints (D42, D49, D56) so in order to compare values between regions, comparisons were restricted to days 42, 49, and 56, of dietary manipulation. Here neither $CMRO_2$ nor CBF differed by region, though SO_2 and HbT, and their ratios to $CMRO_2$, were reduced in the hippocampus (**Fig 5.8**). These results indicate that despite similar neuronal energy demands ($CMRO_2$), the hippocampus has a poorer level of both absolute and relative oxygen availability and blood volume.

The results of statistical analyses are presented in **Table 5.3**.

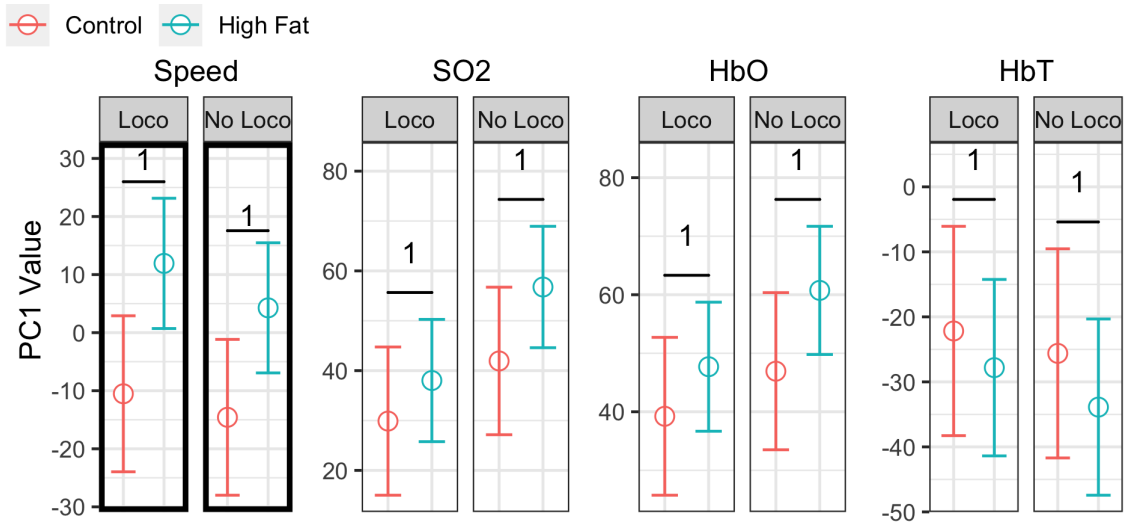

Figure 5.7: Changes in V1 Neurovascular Coupling Did Not Coincide with Hippocampus-Specific Behavioural Deficits. To link any potential dietary effects on neurovascular in V1 to the deficits seen in the NOCR task in a subset of mice after two weeks of dietary manipulation, analyses restricted to the 14 day recording timepoint were conducted. Only the composite measure showed dietary effects, with the only significant result being a diet by locomotion interaction for flow speed. However, pairwise dietary comparisons revealed no differential dietary effect between locomotion and non-locomotion trials (The composite response measure is the first principal component (PC1) of a PCA run on the data. **'Loco'** refers to trials with locomotion both during and preceding stimulus presentation. **'No Loco'** refers to trials where no locomotion was present in either window. **Thick borders** indicate diet by locomotion group interactions. Numbers on brackets indicate corrected pairwise dietary p values. Analysed over n = 249 trials (n = 108 locomotion) captured over 16 sessions from n = 16 mice (n = 8 HFD)).

numDF	denDF	F-value	p.value	Sig	Measure	Factors	Parameter	Analysis
1	12	11.9109	0.0096	**	Ratio	Region	SO2	Resting
1	13	48.4661	0.0000	***	Ratio	Region	HbT	Resting
1	12	0.0845	1.0000		Rest	Region	CMRO2	Resting
1	12	3.0108	0.7581		Rest	Region	CBF	Resting
1	12	115.6155	0.0000	***	Rest	Region	SO2	Resting
1	12	0.0050	1.0000		Rest	Region	Speed	Resting
1	12	361.4234	0.0000	***	Rest	Region	HbT	Resting

Table 5.3: Statistics for the Differences between Regions in Resting Haemodynamic Values The difference in resting haemodynamic values between regions was analysed using LMMs (numDF and denDF refer to degrees of freedom. F and p values are rounded to 4 decimal places. **Red text** indicates significance. **Green text** indicates trend level. **Background shading** indicates size of p value where darker is larger. Sig indicates significance indicators. Measure indicates the measure analysed. Factors indicate factors in the model. Parameter indicates the haemodynamic parameters analysed. Analysis indicates the type of data analysed. P values are corrected for multiple comparisons across parameters using the Bonferroni adjustment).

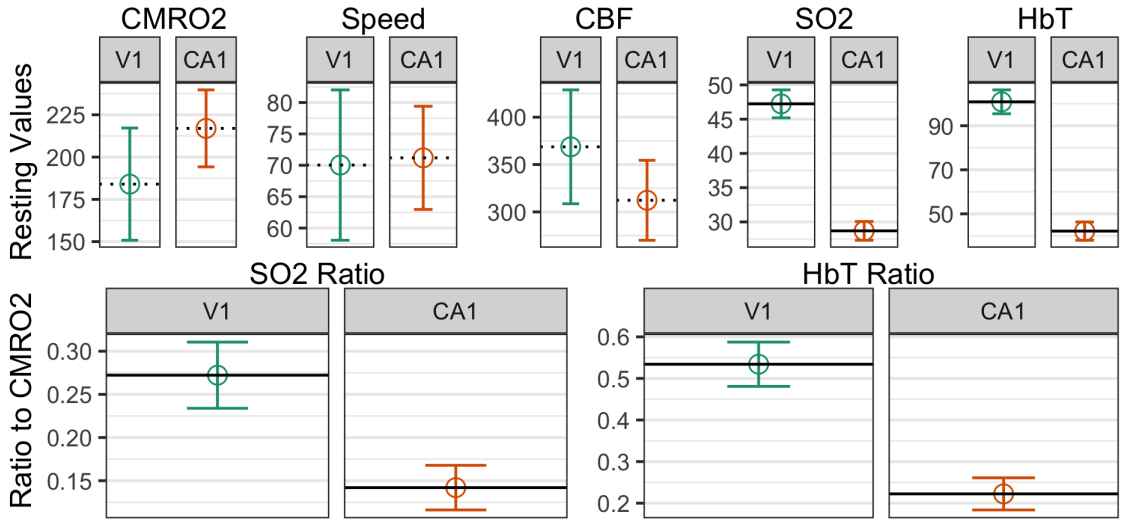

Figure 5.8: Neuronal Metabolism is Uncoupled From Oxygen Supply in the Hippocampus. Restricting analysis to periods of rest and timepoints where hippocampal values plateaued revealed that despite similar levels of neuronal oxygen metabolism between V1 and CA1 ($CMRO_2$), the hippocampus had reduced levels of oxygen availability (SO_2) and blood volume (HbT; **'V1'** refers to primary visual cortex, **'CA1'** refers to hippocampal CA1. Periods of rest were epochs where no locomotion or visual stimulation occurred, or had occurred in the preceding one or five seconds respectively. **Horizontal lines** indicate regional group means. **Solid lines** indicate significant ($p < .05$) differences. n = 18 (HFD: 10, CA1: 11) animals; 50 sessions; 845 resting epochs).

Dietary Effects on Resting Haemodynamic Values

Results described in **Chapter 3** demonstrated a reduction in capillary radii and perfusion in both the hippocampus and cortex after 14 days of HFD feeding. I hypothesised that this could be associated with *in vivo* decreases in blood volume, and potentially in CBF as well, if compensatory increases in flow speed were absent. In the resting timecourse analyses (**Fig 5.9**) all haemodynamic parameters showed significant diet by region by time interactions that were associated with a significant and trend level increase in CBF and speed values respectively in HFD animals at day 3 in the cortex. This elevation persisted to day 7, though non-significantly, and correlates with elevated $CMRO_2$ values at the same timepoints. Additionally, the ratio of HbT to $CMRO_2$ was reduced by HFD feeding at the 14 day timepoint in the cortex. Analysis statistics are presented in **Table 5.4**. These results indicate that despite reduced capillary radii, no overall decrease in regional blood volume is observed after two weeks of HFD feeding, and the reduction in the HbT to $CMRO_2$ ratio at D14 appears driven by an elevation in $CMRO_2$ rather than a reduction in HbT. In addition, as suggested by the V1 neurovascular coupling analysis, HFD feeding is associated with transient dysfunction in haemodynamic responses in the cortex at an early timepoint. This seems most likely related to an elevation in neuronal oxygen metabolism that, though not significant, appears to drive an increased cortical perfusion by increasing the speed of blood flow within

the first week of HFD feeding. Presentation of the full dietary timecourse for all parameters is presented in the **Appendix A.12**.

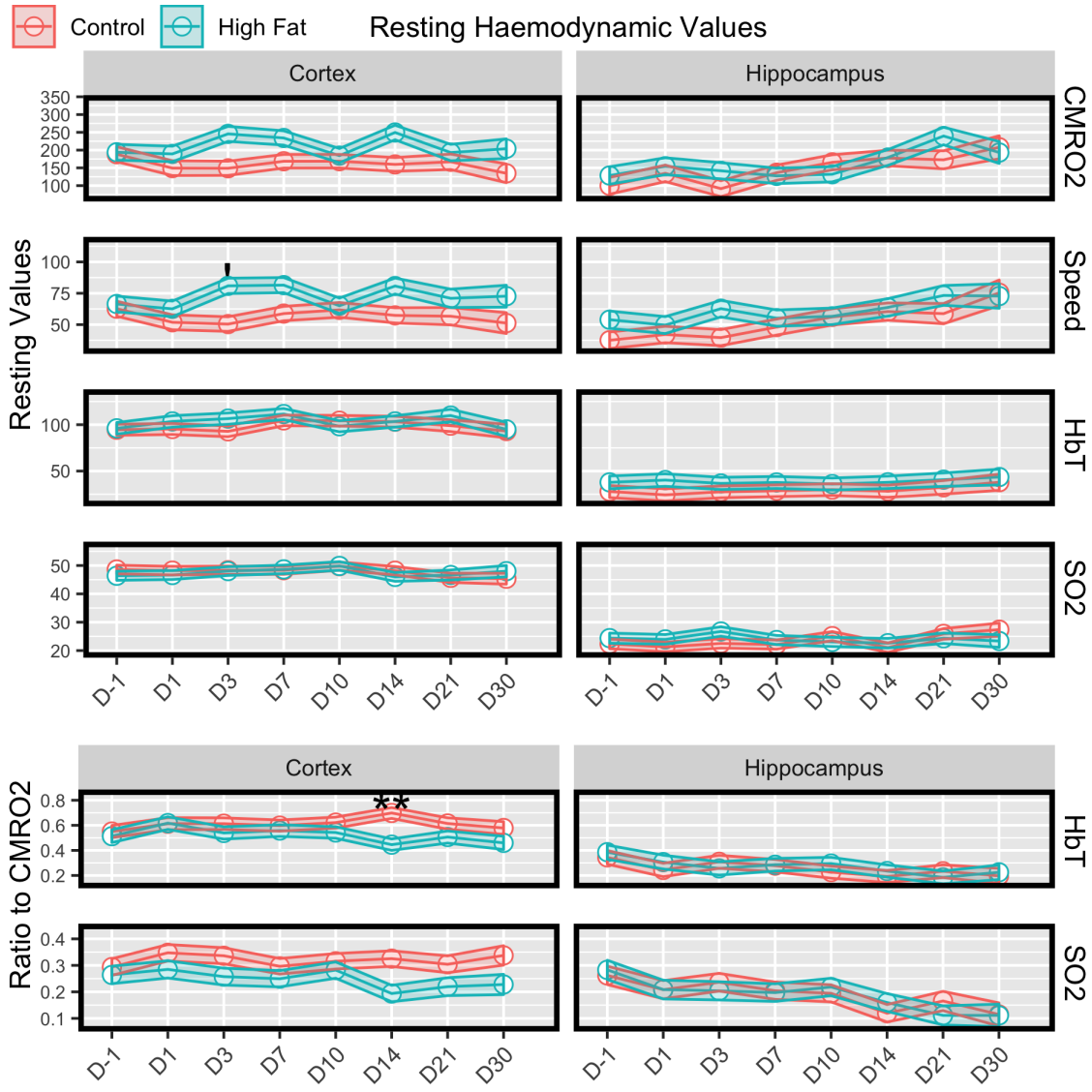

Figure 5.9: Early HFD Induced Dysfunction in Resting Cortical Haemodynamic Regulation. Resting epoch analysis revealed a trend level HFD induced increase in flow speed in V1 at day 3, an elevation that persisted, though non-significantly, to day 7. This correlated with a non-significant elevation in $CMRO_2$. In addition, the ratio of blood volume to $CMRO_2$ was decreased in V1 at day 14 (epochs of rest were periods where no locomotion or visual stimulation occurred, or had occurred in the preceding one or five seconds respectively. **Thick borders** indicate diet by time interactions. **Grey backgrounds** indicate diet by time by region interactions. ** and ' indicates $p < .01$ and $< .10$ respectively. Analysis used n = 4460 resting epochs recorded over 259 sessions from n = 29 mice (n = 14 HFD). Plotted data excludes the final four imaging timepoints and therefore represents n = 3380 resting epochs captured over 193 sessions from n = 29 mice (n = 14 HFD)).

numDF	denDF	F-value	p.value	Sig	Measure	Factors	Parameter	Analysis
1	23	0.7398	1.0000		Ratio	Diet	SO2	Resting
1	23	0.9526	1.0000		Ratio	Diet	HbT	Resting
1	23	1.3233	1.0000		Rest	Diet	CBF	Resting
1	23	0.6152	1.0000		Rest	Diet	SO2	Resting
1	23	2.5743	1.0000		Rest	Diet	Speed	Resting
1	23	0.0087	1.0000		Rest	Diet	HbT	Resting
11	3344	18.9986	0.0000	***	Ratio	Timepoint	SO2	Resting
11	3344	8.2345	0.0000	***	Ratio	Timepoint	HbT	Resting
11	3344	13.6727	0.0000	***	Rest	Timepoint	CBF	Resting
11	3344	11.1222	0.0000	***	Rest	Timepoint	SO2	Resting
11	3344	24.9357	0.0000	***	Rest	Timepoint	Speed	Resting
11	3344	30.7669	0.0000	***	Rest	Timepoint	HbT	Resting
11	3344	14.9296	0.0000	***	Ratio	Timepoint:Region	SO2	Resting
11	3344	25.1290	0.0000	***	Ratio	Timepoint:Region	HbT	Resting
11	3344	25.4634	0.0000	***	Rest	Timepoint:Region	CBF	Resting
11	3344	20.2675	0.0000	***	Rest	Timepoint:Region	SO2	Resting
11	3344	29.6868	0.0000	***	Rest	Timepoint:Region	Speed	Resting
11	3344	31.6675	0.0000	***	Rest	Timepoint:Region	HbT	Resting
1	23	1.3898	1.0000		Ratio	Diet:Region	SO2	Resting
1	23	1.2802	1.0000		Ratio	Diet:Region	HbT	Resting
1	23	0.9894	1.0000		Rest	Diet:Region	CBF	Resting
1	23	0.2678	1.0000		Rest	Diet:Region	SO2	Resting
1	23	0.3658	1.0000		Rest	Diet:Region	Speed	Resting
1	23	0.1052	1.0000		Rest	Diet:Region	HbT	Resting
11	3344	21.2827	0.0000	***	Ratio	Timepoint:Diet	SO2	Resting
11	3344	20.0300	0.0000	***	Ratio	Timepoint:Diet	HbT	Resting
11	3344	56.7824	0.0000	***	Rest	Timepoint:Diet	CBF	Resting
11	3344	13.1480	0.0000	***	Rest	Timepoint:Diet	SO2	Resting
11	3344	71.7085	0.0000	***	Rest	Timepoint:Diet	Speed	Resting
11	3344	26.3544	0.0000	***	Rest	Timepoint:Diet	HbT	Resting
11	3344	14.2273	0.0000	***	Ratio	Timepoint:Diet:Region	SO2	Resting
11	3344	23.7303	0.0000	***	Ratio	Timepoint:Diet:Region	HbT	Resting
11	3344	33.6556	0.0000	***	Rest	Timepoint:Diet:Region	CBF	Resting
11	3344	26.7106	0.0000	***	Rest	Timepoint:Diet:Region	SO2	Resting
11	3344	41.0710	0.0000	***	Rest	Timepoint:Diet:Region	Speed	Resting
11	3344	25.7698	0.0000	***	Rest	Timepoint:Diet:Region	HbT	Resting

Table 5.4: Statistics for the Effect of Diet on Resting Haemodynamic Values The difference in resting haemodynamic values between regions and diet groups was analysed using LMMs (numDF and denDF refer to degrees of freedom. F and p values are rounded to 4 decimal places. **Red text** indicates significance. **Green text** indicates trend level. **Background shading** indicates size of p value where darker is larger. Sig indicates significance indicators. Measure indicates the measure analysed. Factors indicate factors in the model. Parameter indicates the haemodynamic parameters analysed. Analysis indicates the type of data analysed. P values are corrected for multiple comparisons across parameters using the Bonferroni adjustment).

Behavioural Correlations

As described in **Chapter 4**, two weeks of HFD feeding did not significantly impair hippocampus-specific NOCR performance, though results suggested this may be the case in an adequately

powered study. In order to correlate hippocampal cognition with changes in resting haemodynamics, analyses that were restricted to day 14 in hippocampal window mice that had undergone NOCR testing were run with NOCR performance included as a factor. No effects in the model had a significant or trend level association with resting haemodynamic parameters (data not shown).

5.3.4 Data Aligned to Peaks of Oxygen Metabolism

Results from **Chapter 3** suggested that HFD feeding might be related to deficits in neurovascular coupling (due to the detection of a HFD induced reduction in capillary radius variation). This result was not region-specific, suggesting it occurs in the hippocampus as well as the cortex. Whilst stimulating synchronised neuronal activity in cortical V1 can be done using the presentation of visual stimuli, doing so in the hippocampus is difficult given its sparse coding of stimuli. To do so I averaged haemodynamic data over peaks detected in a calculated cerebral metabolic rate of oxygen consumption ($CMRO_2$) value, which reflects energy used by summed neuronal activity. By averaging data around peaks in this value, I was able to investigate changes in the relationship between neuronal oxygen consumption and vascular supply (**Fig 5.2**). Differences in these events were compared between timepoints, diet groups, and regions.

Regional Differences

As in the analysis of resting data, a trend for hippocampal values to become more similar to those in cortex over time was apparent for a number of haemodynamic parameters. In contrast to resting values however, this was associated with values decreasing over time. This pattern was seen in both the magnitude of the peaks and AUC values of CPA data. Therefore, to compare regional differences, analyses restricted to the final three imaging timepoints (D42, D49, D56) where hippocampal values seemed to plateau was conducted. Here hippocampal peak and AUC values were not different for $CMRO_2$, but reduced for HbT and elevated for SO_2. The ratio of SO_2 to $CMRO_2$ showed no difference however, whilst the ratio of HbT to $CMRO_2$ was reduced in the hippocampus (**Fig 5.10**). These results demonstrate that peaks of neuronal metabolism occur with a similar magnitude in both the cortex and hippocampus, and the similar ratio of SO_2 to $CMRO_2$ between them indicates that during peaks of neuronal activity, the neurovascular coupling of oxygen supply is consistent. However, the ratio of HbT to $CMRO_2$ is reduced in the hippocampus, indicating that increasing oxygen availability in the hippocampus in response to $CMRO_2$ peaks likely relies to a greater extent on changes in flow speed rather than blood volume relative to V1. This is partially supported by finding a trend level elevation in magnitude of flow speed responses in the

hippocampus.

The timings of CPA responses varied between regions. The t2p value for CBF was earlier in the hippocampus, with the same being true for the t2o for SO_2, HbR, HbO, and HbT. Similarly, the t2r for HbR, HbT, and $CMRO_2$, was earlier. However, $CMRO_2$ t2o times were delayed, as were speed t2r times (**Appendix A.14**). These results indicate that hippocampal $CMRO_2$ peaks are sharper, and CBF peaks occur earlier. The HbR and HbT responses seem to onset and offset sooner, despite no changes in the timing of their peaks, indicating more gradual onsets and sharper offsets. Altogether, it appears that the dynamics of neurovascular coupling in hippocampal CA1 follow a different timecourse to that in V1. Values for the statistical analysis of regional differences are presented in **Table 5.10**.

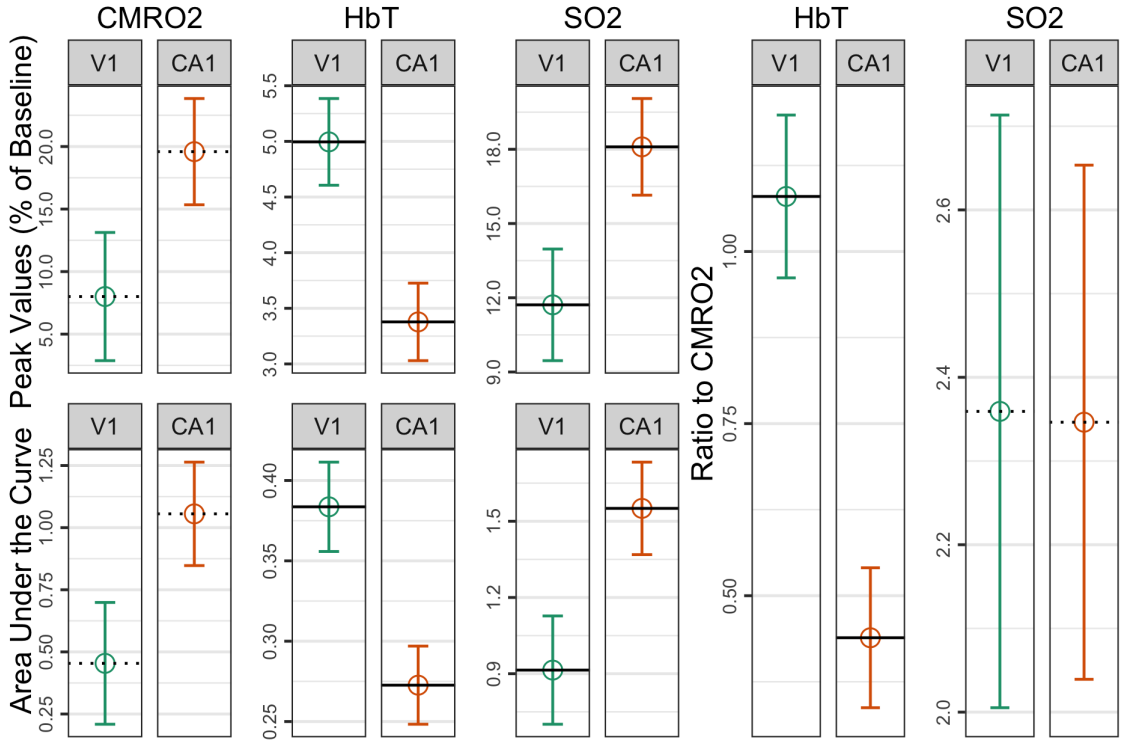

Figure 5.10: Cortical Neurovascular Coupling, Relative to the Hippocampus, Relies to a Greater Extent on Blood Volume Increases. To investigate neurovascular coupling in both CA1 and V1, data that were cut around peaks in $CMRO_2$ was analysed. At timepoints where the effect of time on hippocampal values was attenuated, the magnitude of $CMRO_2$ peaks did not differ between regions, though HbT did. The ratio of HbT to $CMRO_2$ was reduced in the hippocampus, despite no difference in the SO_2 ratio (**'V1'** refers to primary visual cortex, **'CA1'** refers to hippocampal CA1. Data were cut around detected peaks in $CMRO_2$ signal. **Horizontal lines** indicate regional group means. **Solid lines** indicate significant ($p < .05$) differences. Analysed using n = 2720 CPA events captured over 57 sessions from n = 21 mice (n = 11 HFD, n = 11 CA1)).

numDF	denDF	F-value	p.value	Sig	Measure	Factors	Parameter	Analysis
1	15	5.5881	0.2240		AUC	Region	CMRO2	CPA
1	15	1.5253	1.0000		AUC	Region	CBF	CPA
1	15	10.3099	0.0408	*	AUC	Region	SO2	CPA
1	15	21.3870	0.0023	**	AUC	Region	HbT	CPA
1	15	0.0971	1.0000		Ratio	Region	SO2	CPA
1	15	24.6153	0.0003	***	Ratio	Region	HbT	CPA
1	15	4.9030	0.2990		p	Region	CMRO2	CPA
1	15	3.5762	0.5466		p	Region	CBF	CPA
1	15	13.3537	0.0164	*	p	Region	SO2	CPA
1	15	25.9702	0.0009	***	p	Region	HbT	CPA
1	15	14.5964	0.0117	*	t2o	Region	CMRO2	CPA
1	15	4.9118	0.2979		t2o	Region	CBF	CPA
1	15	25.5221	0.0010	**	t2o	Region	SO2	CPA
1	15	89.3999	0.0000	***	t2o	Region	HbT	CPA
1	15	16.2009	0.0077	**	t2p	Region	CBF	CPA
1	15	0.6181	1.0000		t2p	Region	SO2	CPA
1	15	1.7648	1.0000		t2p	Region	HbT	CPA
1	15	25.9812	0.0009	***	t2r	Region	CMRO2	CPA
1	15	8.5721	0.0727	'	t2r	Region	CBF	CPA
1	15	0.2706	1.0000		t2r	Region	SO2	CPA
1	15	49.3705	0.0000	***	t2r	Region	HbT	CPA

Table 5.5: Statistics for the Differences between Regions in Neurovascular Coupling. Neurovascular coupling was compared between regions using LMMs (numDF and denDF refer to degrees of freedom. F and p values are rounded to 4 decimal places. **Red text** indicates significance. **Green text** indicates trend level. **Background shading** indicates size of p value where darker is larger. Sig indicates significance indicators. Measure indicates the measure analysed. Factors indicate factors in the model. Parameter indicates the haemodynamic parameters analysed. Analysis indicates the type of data analysed. P values are corrected for multiple comparisons across parameters using the Bonferroni adjustment).

Dietary Effects

Investigating dietary effects on neurovascular coupling, the AUC values for all haemodynamic responses showed significant diet by time, as well as three-way diet by time by region, interactions. This indicates not only the presence of time-specific, but also time and region-specific dietary effects. This was associated with a spike in hippocampal control AUC and peak values at day 1 for HbO and SO_2, whilst HFD induced an elevation in hippocampal HbR and flow speed AUC values at days 14 and 35 respectively. Whilst the dietary effect at day 1 is likely due to time-related noise, due to it being a spike in values in control diet fed animals, the HFD related elevation at day 14 in HbR AUC values was associated with a similar non-significant elevation at day 10, suggesting that during the second week of HFD feeding the HbR response to neuronal activity is elevated. This coincides with non-significant elevations in HbT, implying that though a greater volume of blood is present in the hippocampus, this is disproportionately associated with deoxyhaemoglobin.

Interestingly, this didn't correlate with any HFD related increases in $CMRO_2$ or CBF. The increase in HFD speed AUC values at day 35 is associated with a non-significant increase in CBF, though, as with the HbR AUC changes, $CMRO_2$ levels show no sign of elevation. No diet related effects were observed on the timings of responses, nor their ratio to $CMRO_2$. Full graphs for the analysis of peak and AUC values are presented in the **Appendix** (**Figs A.15, A.16**). Statistical analyses are presented in **Table 5.6**.

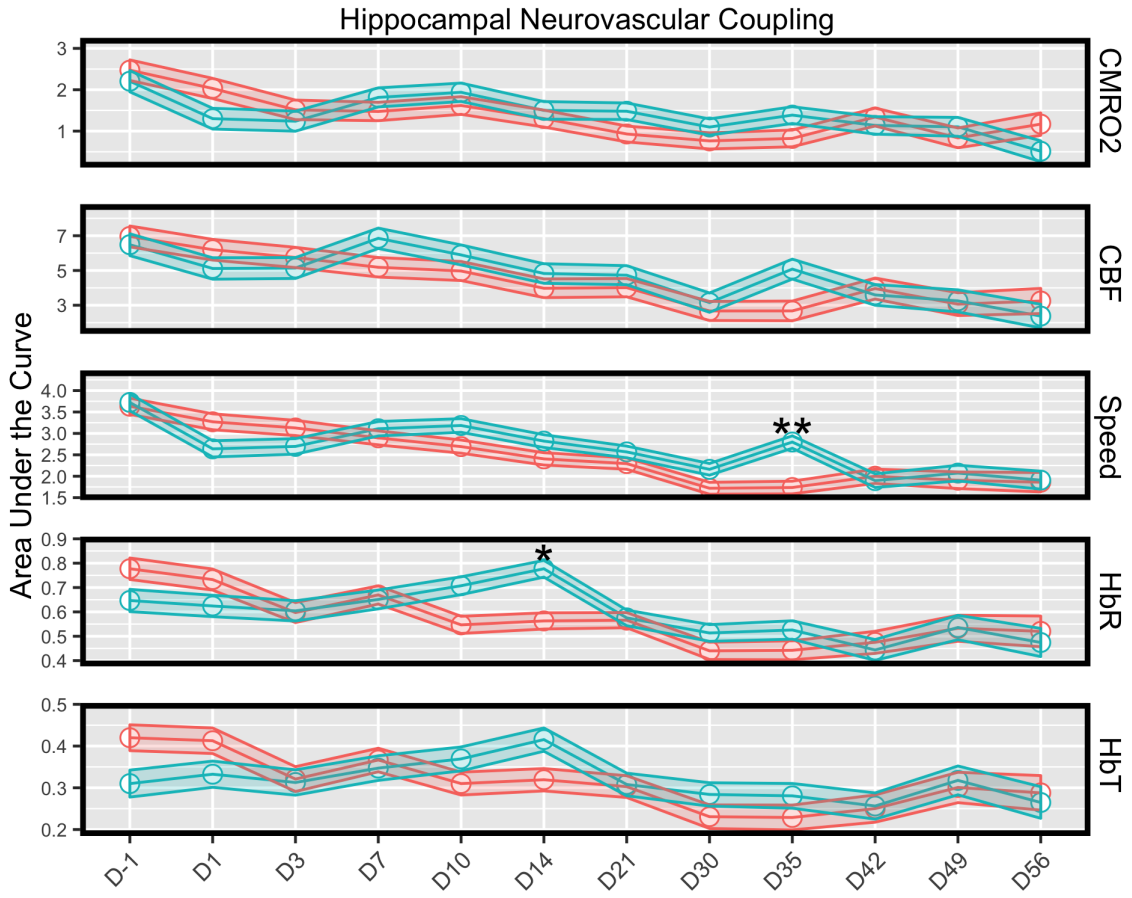

Figure 5.11: HFD Induces Dysfunctional Haemodynamic Regulation during Hippocampal Neurovascular Coupling. AUC values of neurovascular coupling responses show hippocampus-specific dietary effects, where HFD significantly elevated the AUC of HbR and speed at days 14 and 35 respectively. (Data were cut around detected peaks in $CMRO_2$ signal. **Thick borders** indicate diet by time interactions. **Grey backgrounds** indicate diet by time by region interactions. * and ** indicates $p < .05$ and $< .01$ respectively. Statistics were calculated using n = 13506 CPA events captured over 281 sessions from n = 29 mice (n = 14 HFD). Plotted data excludes cortical data and therefore represents n = 4708 CPA events captured over 133 sessions from n = 12 mice (n = 6 HFD)).

Behavioural Correlations

To investigate the relationship between hippocampus-dependent behaviour and neurovascular coupling, analysis of CPA data at day 14 in behaviourally tested hippocampal window mice was con-

numDF	denDF	F-value	p.value	Sig	Measure	Factors	Parameter	Analysis
1	23	0.1687	1.0000		AUC	Diet	CMRO2	CPA
1	23	0.0490	1.0000		AUC	Diet	HbR	CPA
1	23	0.1977	1.0000		AUC	Diet	CBF	CPA
1	23	1.4321	1.0000		AUC	Diet	Speed	CPA
1	23	0.3846	1.0000		AUC	Diet	HbT	CPA
11	11322	14.5709	0.0000	***	AUC	Timepoint	CMRO2	CPA
11	11322	17.1464	0.0000	***	AUC	Timepoint	HbR	CPA
11	11322	13.9686	0.0000	***	AUC	Timepoint	CBF	CPA
11	11322	32.4981	0.0000	***	AUC	Timepoint	Speed	CPA
11	11323	14.7001	0.0000	***	AUC	Timepoint	HbT	CPA
11	11322	25.2733	0.0000	***	AUC	Timepoint:Region	CMRO2	CPA
11	11322	17.5147	0.0000	***	AUC	Timepoint:Region	HbR	CPA
11	11322	18.4032	0.0000	***	AUC	Timepoint:Region	CBF	CPA
11	11322	33.2392	0.0000	***	AUC	Timepoint:Region	Speed	CPA
11	11323	8.7298	0.0000	***	AUC	Timepoint:Region	HbT	CPA
1	23	0.6086	1.0000		AUC	Diet:Region	CMRO2	CPA
1	23	1.2561	1.0000		AUC	Diet:Region	HbR	CPA
1	23	0.8132	1.0000		AUC	Diet:Region	CBF	CPA
1	23	2.7114	1.0000		AUC	Diet:Region	Speed	CPA
1	23	0.8822	1.0000		AUC	Diet:Region	HbT	CPA
11	11322	13.6295	0.0000	***	AUC	Timepoint:Diet	CMRO2	CPA
11	11322	8.2413	0.0000	***	AUC	Timepoint:Diet	HbR	CPA
11	11322	12.6829	0.0000	***	AUC	Timepoint:Diet	CBF	CPA
11	11322	26.2397	0.0000	***	AUC	Timepoint:Diet	Speed	CPA
11	11323	5.1775	0.0000	***	AUC	Timepoint:Diet	HbT	CPA
11	11322	15.7139	0.0000	***	AUC	Timepoint:Diet:Region	CMRO2	CPA
11	11322	30.3403	0.0000	***	AUC	Timepoint:Diet:Region	HbR	CPA
11	11322	13.9924	0.0000	***	AUC	Timepoint:Diet:Region	CBF	CPA
11	11322	27.9610	0.0000	***	AUC	Timepoint:Diet:Region	Speed	CPA
11	11323	16.9715	0.0000	***	AUC	Timepoint:Diet:Region	HbT	CPA

Table 5.6: Statistics for the Effects of Diet on Neurovascular Coupling. The effects on CPA data of time and diet, and differences between regions, were analysed using LMMs (numDF and denDF refer to degrees of freedom. F and p values are rounded to 4 decimal places. **Red text** indicates significance. **Green text** indicates trend level. **Background shading** indicates size of p value where darker is larger. Sig indicates significance indicators. Measure indicates the measure analysed. Factors indicate factors in the model. Parameter indicates the haemodynamic parameters analysed. Analysis indicates the type of data analysed. P values are corrected for multiple comparisons across parameters using the Bonferroni adjustment).

ducted with their behavioural performance as a factor. This analysis revealed a trend level interaction between diet and performance on the AUC and peak values of $CMRO_2$ and CBF. Here performance correlated negatively with both peak and AUC values in the control diet group, whilst there was no correlation in HFD animals (**Fig 5.12**). Graphs showing changes in peak and AUC values for all parameters are presented in the **Appendix** (**Figs A.17, A.18**).

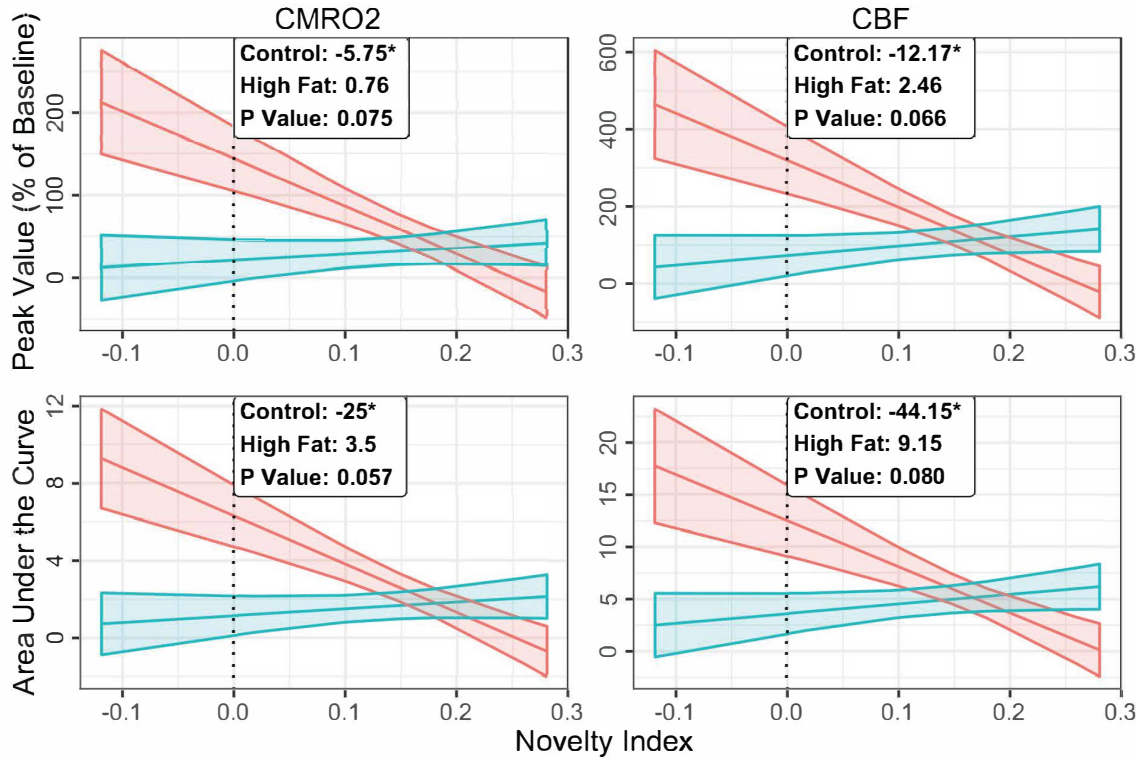

Figure 5.12: The Magnitude of Neuronal Activity During Peak Events Correlates Negatively With Hippocampal Performance Only In Control Animals. Analysis of CPA data at day 14, with NOCR performance included as a factor, showed that the peak and AUC values of $CMRO_2$ and CBF correlated negatively with NOCR performance but only in control animals (CPA data were cut around detected peaks in $CMRO_2$ signal. Novelty index reflects the difference between the proportion of exploration time spent exploring novel versus familiar objects. **Dotted line** indicates zero point where no difference exists in proportion of exploration time spent with novel versus familiar objects. Plotted lines represent the estimated marginal mean +/- 95% confidence intervals. These are predictions of the trend extracted from the relevant LMM. **Text boxes** indicate the slope of the trends by diet groups, and the p value of diet by performance interaction. * next to slope values indicates it is significantly different from zero. n = 11 (HFD: 6); 11 sessions; 374 CPA events).

5.4 Discussion

Results presented in this chapter explored dietary, regional, and time associated changes in resting and neurovascular coupling related haemodynamic responses. In addition, the effect of locomotion on visually stimulated responses in V1 was investigated. Analyses were split into four different models, where data were analysed either over the 8 weeks of the dietary manipulation, exclusively at day 14 (when NOCR behavioural testing was conducted), exclusively at day 14 in the hippocampal window mice that underwent behavioural testing, and over the final three recording timepoints (days 42, 49, and 56) given this was when time-related changes in hippocampal resting and CPA values appeared to plateau.

5.4.1 Locomotion During Visual Stimulation Accelerated the Vascular Response and Increased Blood Volume

By stimulating neuronal activity in cortical V1 and measuring associated blood flow responses and locomotion, I was able to investigate the effects of diet, time, and locomotion on visually-stimulated neurovascular coupling responses in the cortex (**Fig 5.4**). This paradigm is well established (Niell and Stryker, 2008; Pisauro et al., 2013). It has been suggested that during locomotion the strength of neurovascular coupling is diminished given that no effect of locomotion was seen on haemodynamic responses (Pisauro et al., 2013) despite the fact that locomotion increases V1 neuronal activity (Niell and Stryker, 2010). To investigate this I categorised visual stimulus trials in my data as locomotion trials if locomotion was present both during the pre-stimulus baseline and stimulus presentation period, and as non-locomotion trials if locomotion was absent in both periods, and compared them. $CMRO_2$ represents summed neuronal activity, and was unaffected by locomotion in my data, seemingly contradicting studies by Niell and Stryker (2010) and Ayaz et al. (2013), where locomotion is associated with increased neuronal activity during visual stimulus presentation. A reason for this is most likely that my readout of neuronal activity is calculated from haemodynamic parameters, and if locomotion is indeed associated with neurovascular uncoupling (a change in the relationship between neuronal activity and blood flow responses) as suggested by Pisauro et al. (2013), and documented in frontal cortex by Huo et al. (2014), it is reasonable to expect a haemodynamic based measure of neuronal activity to show no effect of locomotion. To address this future work should utilise the more comprehensive approach to measuring haemodynamic changes that I have used (i.e. measures of blood flow, oxygenation, blood volume, etc.) coupled with more direct readouts of neural activity. Conversely, if the absence of any change in my $CMRO_2$ value is unrelated to the fact it is based on haemodynamic responses, its possible that it simply lacks the sensitivity required to detect the increases reported in local field potential and single unit recordings by Niell and Stryker (2010) and Ayaz et al. (2013), given I used similar stimulus properties (with regards to spatial and temporal frequencies) to these studies.

My results showed that locomotion accelerated the haemodynamic responses to visually stimulated neuronal activity, and was associated with a reduced level of oxygen availability despite an elevation in blood volume. These differences persisted when calculating the ratio of SO_2 and HbT to $CMRO_2$, though as previously stated, the $CMRO_2$ value is based on haemodynamic parameters that may be uncoupled from neuronal activity during locomotion (Pisauro et al., 2013). These results indicate that despite locomotion elevating blood volume in the region, this does not occur to a great enough degree to significantly increase overall perfusion (CBF) levels, and also fails to

sustain the levels of oxygen availability seen in non-locomotion trials. This may be a result of enhanced neuronal activity (Niell and Stryker 2008; Ayaz et al. 2013; though not detected in my data for reasons outlined previously) leading to a reduction in tissue oxygen levels to a greater degree than an increase in blood volume is able to buffer. These results demonstrate that though locomotion is associated with neurovascular uncoupling to some degree (in that oxygen availability is decreased, and CBF levels are unchanged despite documented elevations in neuronal activity), this is not the case with regards to changes in blood volume (HbT). In addition, locomotion accelerates the haemodynamic response to neuronal activity. This is in contrast to work by Pisauro et al. (2013) that showed no effect of locomotion on neurovascular coupling related blood volume increases or time dynamics in V1. The difference in our results could be related to the classification of locomotion. Whilst Pisauro et al. (2013) distinguished between locomotion and stationary trials using a threshold for the average running speed, trials were only classified as stationary in my data if they were accompanied by the complete absence of locomotion during and prior to stimulus presentation. Consequently the comparison in my results more truly reflect the effect of locomotion on haemodynamic responses to visually stimulated neuronal activity in V1.

5.4.2 HFD Feeding May Induce Transient, Astrocyte-Mediated, Deficits in Cortical Neurovascular Coupling

Whilst HFD-induced deficits in neurovascular coupling have been reported previously with long-term dietary manipulations (20 weeks; Tucsek et al. 2014b), I found that the variation of capillary radii was reduced after 14 days of HFD feeding in post-mortem tissue, as described in **Chapter 3**. This suggested that *in vivo* neurovascular coupling deficits might be detectable at much earlier timepoints. However, Oxy-CBF probe data showed no significant pairwise dietary comparisons when looking across peak and AUC values, or the timing of peaks and their onset and offset. In contrast, analysis of a PCA-based composite measure of the haemodynamic response in V1 showed significant dietary effects at day 3 on flow speed and CBF in locomotion trials (**Fig 5.5**). Given the composite measure is based on differential weighting of data points, the direction of its dietary effects needs to be interpreted with this in mind. The measure showed strong negative weightings from 6 to 8 seconds, the period over which values tended to rise to a peak, and strong positive weightings from 12-18 seconds, a period over which responses tailed off following their peaks. As a result, more positive composite values suggest smaller peak and pre-peak values, along with higher values following the offset of responses.

Looking at raw data traces at day 3 in locomotion trials (**Fig 5.6**), HFD was clearly associated

with a prolonged CBF and speed response to visual stimulation. Whilst a clear double-bump neurovascular response is present in control animals, this seems dysregulated by HFD feeding, with HFD values elevating at the same point that they decline in control animals between the two phasic elevations. The bimodal response present in control animals appears to be related to two separate mechanisms of neurovascular coupling. The first rapid response has been suggested to be mediated by the uptake of synaptic glutamate and potassium by astrocytes, whilst the later response, which acts on the order of 10's of seconds, may be regulated by metabotropic astrocytic signalling triggered by the neurotransmitter N-acetylaspartate (reviewed in Baslow and Guilfoyle 2017). Though not a point made by the authors, work by Rosenegger et al. (2015) appears to show that antagonism of cyclooxygenase-1 (COX-1) located in astrocytic endfeet disrupts the secondary peak seen in the dilatory response of cortical arterioles to whisker stimulation. COX-1 mediated production of prostaglandins may link neuronal activity to pericyte regulation of blood flow (Hall et al., 2014), so this suggests that HFD feeding may alter communication between astrocytes and pericytes, which would alter their functionality without disrupting their coverage of the vasculature. Indeed, my post-mortem data demonstrated no effect of two weeks of HFD feeding on pericyte ISD. It seems possible then that HFD leads to an early and transient selective disruption of astrocytic mechanisms involved in neurovascular coupling. Why this appears to only be the case during locomotion is unclear, though it should be considered that this effect may be a result of the high degree of time-related noise seen in the value of the composite measure.

5.4.3 The Mechanisms Driving Hippocampus-Specific Trends Over Time in Haemodynamic Measures Are Unclear

In both the resting data, and CPA analyses, hippocampal values trended towards those in the cortex as time passed, showing consistent increases and decreases respectively. One possibility is that this could reflect a summation of detrimental effects over time, or alternatively, this may be a return of haemodynamic regulation to baseline levels. The former may be the result of repeated restraint-induced stress associated with chronic *in vivo* imaging, whilst the latter could reflect long-term surgical recovery. The effect of time on the hippocampus seemed to be attenuated by day 42, suggesting that 7 weeks of stress, or $\sim$10 weeks of surgical recovery (imaging typically began 3 weeks post-surgery), was sufficient either for stress effects to plateau, or surgical recovery to be complete.

Investigating the literature suggests that a role for chronic restraint-induced stress seems unlikely. Twelve weeks of stress, where rats were placed in 4°C water for 15 minutes a day, followed

by a 12 week recovery period, was associated with decreased resting hippocampal CBF in the dark cycle (Endo et al., 1999), and five weeks of daily social defeat stress in rats was led to a reduction in the number of hippocampal microvessels (Czéh et al., 2010). In addition, chronic stress seems largely associated with a blunted dilatory, and accentuated contractile, vascular response (reviewed in Burrage et al. 2018), which would likely reduce resting blood flow parameters. This contrasts to my results, where resting hippocampal CBF increases with time in synchrony with flow speed, whilst total blood volume (a proxy for vascular density) shows no time-related effects.

Surgical recovery therefore seems the more likely. However, no other studies have looked at changes in resting hippocampal blood flow using the hippocampal window technique over a timecourse, so it is hard to evaluate this theory. Whilst the effect of time is unlikely to be related to surgical inflammation, given that 20 days of recovery from hippocampal window implantation is sufficient for astrocytic and microglial inflammation to subside (Gu et al., 2014), it could be related to surgery associated BBB breakdown. This could permit the entry of circulating plasma factors, such as IgG, thrombin, fibrinogen, or albumin, with the latter shown to alter neuronal activity in the hippocampus (though this was only investigated within a 24 hour period; Frigerio et al. 2012). However, during acquisition of two-photon image stacks, mice were injected with a 3kDa fluorescently-tagged dextran to image vascular morphology. Though not analysed in detail, no clear leakage into the brain was observed. Given this dextran is far smaller than albumin, IgG, fibrinogen, or thrombin (69kDa, ∼155kDa, 340kDa; Saunders et al. 2015, 35.5kDa Davie and Kulman 2006) this suggests that the hippocampus-specific effects of time are not associated with long-term surgery-induced BBB disruption.

Ultimately it is unclear what is responsible for the consistent effect of time on hippocampal values. At rest, this seems to be linked to low rates of neuronal oxygen metabolism that increase, whilst in neurovascular coupling events, the magnitude of $CMRO_2$ responses is elevated to begin with before decreasing. This suggests that the underlying mechanism is associated with an initial down-regulation of hippocampal neuronal activity at rest, though during peaks in neuronal activity, it promotes greater synchronisation in neuronal responses.

5.4.4 Uncoupling of Oxygen Availability and Neuronal Metabolism in the Hippocampus at Rest

As discussed in the post-mortem tissue **Chapter 3**, the hippocampus has a lower capillary density and mean capillary radius than the cortex, though appears to posses equal, if not greater, neuronal energy demands (neuronal density in Keller et al. 2018; glucose uptake and utilisation in Klein-

ridders et al. 2018 and Zeller et al. 1997). As a result, one would predict the hippocampus to have a lower blood volume and level of oxygen availability, despite similar, if not greater, levels of $CMRO_2$. This could be responsible for its enhanced susceptibility to pathology (hypoxia Ng et al. 1989; Alzheimer's Disease Michaelis 2012) relative to other brain areas.

Resting data analysis limited to timepoints where the hippocampus-specific effects of time appeared to plateau (**Fig 5.8**) revealed that, as predicted, the hippocampus possesses significantly lower levels of oxygen saturation and blood volume, despite a similar, if not greater, rate of neuronal oxygen metabolism relative to the cortex. This was reflected by a decreased ratio of SO_2 and HbT to $CMRO_2$. These results indicate that the hippocampus at rest shows a relative degree of neurovascular uncoupling with regards to oxygen availability. Interestingly, a decrease in blood volume was not associated with differences in overall levels of perfusion (CBF). Whilst this could result from compensatory increases in hippocampal flow speed, this did not differ between regions. However, it should be noted that though non-significant, hippocampal CBF was reduced relative to the cortex.

5.4.5 Neurovascular Coupling is Consistent Between Brain Regions, but Mechanisms Differ

My post-mortem results showed a reduction in the variation of capillary radii in the hippocampus relative to the cortex, which suggested a relatively poorer ability to regulate vascular diameter changes. This was proposed to be associated with a degree of hippocampal neurovascular uncoupling during peaks in neuronal activity, unless this was compensated for by increases in flow speed. To investigate this, data was cut around peaks in the $CMRO_2$ signal (**Fig 5.2**), which represents summed neuronal activity. This revealed that during peaks in neuronal activity, the magnitude of the hippocampal HbT and SO_2 responses are reduced and elevated respectively. However, when compared to the magnitude of the $CMRO_2$ response, only HbT showed a significant reduction, owing to the non-significant increase in $CMRO_2$ seen in the hippocampus (**Fig 5.10**). These results indicate that the coupling of oxygen supply to neuronal activity during peaks in activity is conserved between regions, though this is mediated to a greater extent in the cortex by increases in blood volume. This was associated with a a trend towards increased flow speed in the hippocampus. Overall, it appears that as predicted, the hippocampus demonstrates a reduction in its ability to regulate vascular diameter during peaks in neuronal activity, but is able to maintain consistent levels of neurovascular coupling of oxygen supply by increasing flow speed. This is contrasted against the relatively worse ratio of oxygen supply to neuronal metabolism in the hippocampus at

rest, implying that the functional ability of the hippocampal vasculature to support synchronised neuronal activity can overcome anatomy-related deficits in neuronal support.

Whilst regional differences in neurovascular coupling have been reported (Devonshire et al., 2012; Sloan et al., 2010), investigations into whether the underlying mechanisms vary are lacking. This has been suggested by others (Hosford and Gourine, 2019) and is supported by modelling work (in a preprint by Jafarian et al. 2019) though work on this area is in its infancy. It is possible that the reduced ability of the hippocampus to regulate blood volume is related to the relatively lower coverage of its capillary bed by pericytes seen in my post-mortem tissue results. Pericytes can regulate capillary blood flow, which may be coupled to neuronal activity via neurotransmitter stimulated astrocytic calcium signalling (reviewed by Fellin and Carmignoto 2004) that drives astrocytic COX-1 activity and results in the generation of prostaglandins that can mediate the relaxation of capillary pericytes (Hall et al., 2014). How the hippocampus regulates flow speed increases however, is less obvious. Whilst initially it may seem this could be modulated by changes in blood pressure, there is evidence that the velocity of red blood cells is maintained despite alterations in blood pressure (Hudetz et al. 1995, cited in a review of capillary blood flow by Itoh and Suzuki 2012). Red blood cells can sense oxygen levels and regulate their own deformability and therefore flow speed accordingly (Wei et al., 2016), and signalling to endothelial cells from vascular components, such as red blood cells and leukocytes, has been suggested to also regulate blood flow (Itoh and Suzuki, 2012). It may therefore be the case that neurovascular coupling in the hippocampus relies more on red blood cell, and plasma constituent signalling mechanisms to increase flow speed, whilst in the cortex, greater coverage by pericytes helps to mediate neuronally stimulated increases in blood volume.

5.4.6 HFD Affects Cortical Neuronal Activity and Haemodynamic Regulation at Rest

In **Chapter 3** I showed that two weeks of HFD feeding, as assessed in post-mortem tissue, reduced both capillary radii and the extent of capillary perfusion in the cortex and hippocampus. This suggested that *in vivo*, HFD feeding could induce an overall reduction in blood volume and CBF in both brain areas. Unexpectedly, dietary effects at rest were specific to the cortex, where within the first week of HFD feeding speed and CBF values were increased, correlating with non-significant increases in $CMRO_2$ (**Fig 5.9**). This was not associated with any degree of neurovascular uncoupling, as neither the ratio of HbT nor SO_2 to $CMRO_2$ was affected by diet in the first week. These results suggest that HFD feeding leads to early increases in cortical neuronal activity, which is

associated with an elevated flow speed that maintains neurovascular coupling. This could relate to an imbalance in excitatory vs inhibitory neurotransmission, which HFD feeding seems capable of inducing. Models of HFD and obesity have been associated with a reduction in GABA levels in the hippocampus (Sandoval-Salazar et al., 2016) and prefrontal (Hassan et al., 2018) and frontal (Sandoval-Salazar et al., 2016) cortices. In addition, gephyrin, a protein associated with inhibitory neurotransmission, is reduced in the hippocampus and cortex following HFD feeding (Lizarbe et al., 2019), and the intensity of perineuronal nets, the degradation of which reduces GABAergic firing rates (Balmer, 2016), was reduced by HFD in the prefrontal cortex (Dingess et al., 2018). Finally, rodents fed a HFD show reductions in parvalbumin neurons, a major class of GABAergic interneurons, in the prefrontal cortex and hippocampus (Lowe et al., 2019). Though no studies as of yet have investigated the dietary effects on overall inhibitory vs excitatory cortical tone at as an early a time as one week of HFD feeding, my results suggest that early effects on cortical neurotransmission exist.

Additionally, the ratio of HbT to $CMRO_2$ was reduced by HFD feeding at the 14 day timepoint in the cortex. As with changes in the first week, this seems driven by a non-significant increase in $CMRO_2$, but unlike those changes, this was associated with an impairment in the coupling of blood volume to neuronal activity. The elevated $CMRO_2$ level could, again, be related to changes in neuronal transmission, whilst the reduction in the HbT to $CMRO_2$ ratio may derive from the HFD induced reduction in capillary radii detected after 14 days in my post-mortem results. This reduction was seem in both cortex and hippocampus, but appears insufficient to change overall *in vivo* HbT levels in either region. If the HFD induced reduction in capillary radii is responsible for the impaired HbT to $CMRO_2$ ratio, it may be the case that this change is transient, given the ratio was maintained at other timepoints. Otherwise it is possible that a compensatory dilation of non-capillary vessels, intended to maintain homeostatic levels of blood volume due to reductions in capillary radii, may be affected at the two week point.

Whilst these results suggest that HFD feeding induces a biphasic elevation in neuronal oxygen metabolism at days 3 and 14 in the cortex, pairwise comparisons at these timepoints were non-significant. In addition, the possibility that the dietary effects on speed, CBF, and the HbT to $CMRO_2$ ratio, are the result of time-related noise must also be considered. Whilst I am confident in the presence of cortical dietary effects within the first week of HFD feeding, given that speed, CBF, and $CMRO_2$ values are elevated by HFD feeding at both 3 and 7 days, the fact that these values, and the HbT to $CMRO_2$ ratio, only appear to be affected at day 14, but not days 10 or 21, makes this effect the more likely of the two to be related to noise. In future, imaging more timepoints around day 14 (e.g. days 10, 12, 14, 16, and 18) could help to establish whether the

effect detected here is spurious or legitimate. Otherwise, evidence from both resting, and visually stimulated neurovascular coupling experiments, appears to indicate the presence of early (within the first week) HFD induced dysfunctions in the cortex.

The Absence of Hippocampal Dietary Effects

The absence of any dietary effects on resting hippocampal values was unexpected, given that the my post-mortem tissue experiments showed HFD induced reductions in capillary radii and perfusion levels in both regions, and that the literature supports HFD induced neuronal effects (i.e. inhibition of GABAergic tone) in both regions as well (Lizarbe et al., 2019; Lowe et al., 2019). This may come down to timepoint specific regional effects of dietary manipulation, where longer dietary manipulation might be necessary to observe similar changes in the hippocampus as those that appear to be present early on in the cortex.

The existence of timepoint specific dietary effects on the hippocampus seems apparent in the literature, where neither 6, nor 6.5 months, of HFD feeding changed hippocampal microvascular blood flow or volume (Fu et al., 2017) or CBF (Zuloaga et al., 2016). In comparison, Gomez-Smith et al. (2018) demonstrated an increased resting CBF in the hippocampus of rats fed a cafeteria diet for 3 months, that they suggest could be related to an elevated cerebral metabolic rate, as seems to be the case in the early cortical dietary effects I detect. These studies show that whilst 3 months of dietary manipulation may be sufficient to induce $CMRO_2$ and CBF changes in the hippocampus, these are no longer present at the six month timepoint, highlighting not only that dietary effects on the hippocampus may be timepoint-specific, but that they also may take longer than 2 months to appear.

5.4.7 Hippocampus-Specific HFD-Induced Vascular Dysfunction during Neurovascular Coupling

In **Chapter 3** I reported that HFD feeding reduced the variation in the radii of capillaries in both the hippocampus and cortex after two weeks. This was proposed to reflect a reduction in the ability of both regions to modulate the resistance in their capillary bed, which could be linked to deficits in neurovascular coupling. To investigate this in both regions, data were cut around peaks detected in the $CMRO_2$ signal that reflects peaks in neuronal activity. Unexpectedly, this analysis revealed exclusive dietary effects in the hippocampus (**Fig 5.11**). Here it appeared that HFD elevated deoxyhaemoglobin levels during the second week, which correlated with non-significant HbT increases, indicating that two weeks of HFD feeding leads to an increase in the magnitude of

the blood volume response during peaks in neuronal activity, but this is predominantly associated with greater levels of deoxyhaemoglobin. This may indicate the presence of dysfunctional oxygen exchange, and seems unrelated to issues in linking blood supply to oxygen metabolism as the ratio of both HbT and SO_2 to $CMRO_2$ was unaffected by diet. There was an additional dietary effect detected at day 35, where hippocampal flow speed was elevated by HFD, which correlated with a non-significant increase in CBF. This appears to be an exaggerated response to a non-significant elevation in $CMRO_2$ levels at the same timepoint, and again, may reflect some degree of dysfunction in the regulation of haemodynamic responses. As stated previously however, to confirm that this is not a spurious effect relating to noise, future work should look at additional timepoints closer to 35 days to see if this effect is consistent.

Unlike the resting data analysis, where HFD associated effects on $CMRO_2$ and vascular parameters occurred exclusively in the cortex, these results indicate that during peaks in neuronal activity the hippocampus shows dysfunctional HFD-induced changes in haemodynamic responses. The hippocampus-specific nature of these effects could link to the hippocampus-specific cognitive deficits induced by 24 hours of HFD feeding (McLean et al., 2018) that persist for 30 days (Kanoski and Davidson, 2010) given that synchronised peaks in neuronal activity are likely more similar to the neuronal processing involved in task performance than those occurring at rest. The absence of any dietary effects on CPA data in the cortex suggests that it is only at rest that HFD induces elevations in cortical $CMRO_2$ levels. This may indicate that HFD promotes a blanket increase in cortical activity, but that this has no relation to the size of individual neuronal events. Investigating dietary differences in the rate of detected $CMRO_2$ peak events in the cortex could shed further light on this, where the elevation of cortical GABAergic tone proposed to occur may be associated with a reduction in the rate of synchronised neuronal events.

A final point to make concerns the detection of dietary effects on cortical neurovascular coupling associated with visual stimulation, but not when analysing CPA data. On one hand, this may strengthen the argument that former are a consequence of time-related noise, but on the other this difference could relate to the degree of associated neuronal activity in each analysis. Visually stimulated neurovascular coupling in V1 is associated with a much greater degree of synchronised neuronal activation than that seen in individual detected $CMRO_2$ peaks, something supported by the fact that V1 $CMRO_2$ peak values were $\sim$30% above baseline in the visually stimulated data, compared to $\sim$9% in the CPA analysis. It may therefore be the case that a greater degree of synchronised neuronal activity is necessary to reveal HFD induced effects in V1 neurovascular coupling.

5.4.8 Hippocampal Vascular Responses Correlate with NOCR Behavioural Performance but not Following HFD Feeding

The detection of HFD induced impairment in hippocampus-specific NOCR performance in a subset of mice described in the post-mortem chapter, in conjunction with the detrimental HFD associated reductions in capillary radii, radii variation, and perfusion, suggested that vascular changes and behavioural performance could be correlated. Though this was not the case at rest, CPA data analysis of hippocampal window mice that had undergone behavioural testing showed a negative correlation between the magnitude of the $CMRO_2$ and CBF responses during $CMRO_2$ peak events with behavioural performance, but only in control diet animals. These results suggest that improved hippocampal cognitive function is associated with a reduction in the magnitude of neuronal activity, and therefore also in the associated CBF response, during periods of synchronised neuronal firing. This could reflect that better cognition is associated with more efficient hippocampal neuronal activity. This may be explained by the neural efficiency hypothesis, which posits that intelligence correlates negatively with brain activation and metabolic rates. A review of studies that have looked into the validity of this suggests that it generally holds true, though it is modulated by effects of task complexity, existing task expertise, and brain region (reviewed in Neubauer and Fink 2009). Similar evidence comes from the finding that working memory training is associated with a reduction in activity in the frontoparietal network (Aguirre et al., 2019). However, work in this area is largely based in the cortex, and studies investigating the efficiency hypothesis in the hippocampus appear to be few in number. One study demonstrated that female subjects showed a negative correlation between measures of intelligence and reasoning and hippocampal volume (Colom et al., 2013), providing evidence at least for a structural, if not functional, basis for the efficiency hypothesis in the hippocampus. However, behavioural performance in HFD animals showed no correlations with haemodynamic parameters in any of the analyses. This indicates that the mechanisms that relate the magnitude of neuronal activity to cognitive performance are altered in HFD animals, who as a result may have to engage alternate strategies to cope with task-related demands. One such strategy could be over-recruitment, something observed in ageing studies during low-load memory tasks that could be associated with processes that are beneficial to performance (discussed in Suzuki et al. 2018), though my data shows an absence, rather than a positive, correlation between neuronal activity and performance in the HFD group, suggesting this particular strategy may not be at play.

5.5 Conclusion

Analysis of haemodynamic parameters in both cortex and hippocampus over 8 weeks of dietary manipulation supported the suggestions made based on post-mortem data analyses that the hippocampus has a poorer ratio between vascular support and oxygen supply and neuronal metabolism, which may underlie its increased susceptibility to pathology and diet induced cognitive deficits. Interestingly, CPA data analysis indicated a consistent level of neurovascular coupling between cortex and hippocampus during peaks of neuronal activity, though the coupling of oxygen delivery to neuronal metabolism appears to rely more on changes in flow speed rather than blood volume in the hippocampus. Future work should investigate the mechanisms involved in hippocampal flow speed regulation, which likely relate to signalling between plasma constituents and endothelial cells, and the action of oxygen-sensing red blood cells.

The absence of HFD-induced changes in resting blood volume or compensatory increases in flow speed, hypothesised to exist based on my post-mortem results, suggests that both the cortex and hippocampus engage the dilation of non-capillary vessels to maintain blood volume homeostasis. Resting data analysis revealed a cortex-specific HFD induced elevation of $CMRO_2$ within the first week, which could be linked to dietary effects on cortical GABAergic tone. Additionally, at day 14, there was evidence of HFD induced uncoupling between $CMRO_2$ and blood volume in the cortex. These results suggested that dietary effects on cortical neurotransmission occur much earlier than has been previously investigated, and that perhaps the engagement of compensatory dilatory mechanisms impairs the ability of the cortical vasculature to respond to HFD-induced increases in the basal levels of neuronal activity. This doesn't seem to influence the haemodynamic response to periods of synchronised neuronal activity however, given that no evidence of cortical neurovascular uncoupling at day 14 was detected in either the visual stimulus or CPA data, implying the effect seen at day 14 in the resting data could be due to noise. The presence of dietary changes at day 3 in the cortex were however replicated in the visual stimulus analysis, where HFD was associated with an dysfunctional haemodynamic response in flow speed and CBF regulation, suggested to relate to dietary effects on astrocyte to vessel signalling.

Whilst resting data analysis showed cortex-specific dietary effects, CPA analysis was associated with dietary effects exclusively in the hippocampus. The regional differences between the two analyses may be down to the magnitude of neuronal responses, and region-specific dietary effects on vascular mechanisms engaged at rest or during neurovascular coupling events. The hippocampus-specific CPA dietary effects were interpreted as reflecting HFD-induced dysfunction in haemodynamic regulation taking place during the second week of dietary manipulation.

These results suggest that during the first two months of dietary manipulation, diet does not influence neurovascular coupling during peaks of neuronal activity in V1, though following two weeks of HFD feeding it appears to disrupt this process in the hippocampus. At rest however, the hippocampus is resistant to dietary effects, whilst one week of manipulation appears to induce a large scale elevation of neuronal activity in the cortex.

The magnitude of the peaks in neuronal activity detected in the CPA analysis correlated negatively with hippocampal cognition exclusively in control animals. This may be the result of animals with more efficient neural processing performing better, a theory that fits with the neural efficiency hypothesis. In HFD animals this relationship was absent and the animals that performed well on the NOCR task may have instead used alternative task-related strategies.

Finally, it was suggested that hippocampal window implantation surgery may be associated with long-term changes in neuronal activity, and results demonstrated that during visually stimulated neuronal activity in V1, locomotion accelerates haemodynamic responses and increases blood volume.

Chapter 6

General Discussion

6.1 Main Findings

The primary aim of the work described in this thesis was to investigate the mechanisms underlying the rapid, hippocampus-specific, cognitive deficits induced by HFD feeding (McLean et al., 2018; Kanoski and Davidson, 2010). I hypothesised that this would be related to either immune or vascular changes, or both, and that in order for these changes to have hippocampus-specific cognitive effects, they would either be present in a hippocampus-specific manner, or that by being present across multiple brain regions, would have an elevated detrimental effect on hippocampal processing given its enhanced susceptibility to pathology. To investigate this I used immunofluorescence imaging approaches in both post-mortem tissue and awake behaving animals that were fed a HFD.

textbfChapter 3 looked at changes in post-mortem tissue following two weeks of HFD feeding in the hypothalamus, hippocampus and cortex. This allowed me to evaluate the nature of short-term dietary vascular and immune changes. I tested mice on a hippocampus-specific cognitive task to confirm the presence of cognitive deficits in my model. I found that short-term HFD feeding was associated with a trend towards impaired hippocampal cognition, as well as global microglial proliferation (without morphological changes) and global impairments in vascular structure, specifically a decreased capillary luminal radius, an increased resistance to perfusion, and a reduction in the variation of capillary radii measurements. In addition, compared to other brain regions, the hippocampus had a lower vessel density, capillary radius, variation in capillary radius, and a greater spacing between pericytes. These results suggested that short-term HFD feeding is associated with global priming (but not activation) of microglia, and deficits in the ability of the capillary bed to support neuronal activity, which likely had a greater effect on hippocampus-specific cogni-

tion given its impoverished level of vascular support at baseline.

Chapter 4 expanded upon this work by investigating changes in microglial morphology over an 8 week dietary manipulation *in vivo* to look into how the results after two weeks described in **Chapter 3** related to the overall timecourse of dietary effects. In addition, analysis of hippocampus-specific behaviour was expanded to include these *in vivo* imaging mice. These results revealed that including the *in vivo* mice abolished the trend towards decreased hippocampal cognition in the HFD group, that HFD feeding did not affect hippocampal or cortical microglial morphology at any point over the 8 week manipulation, and that hippocampus-specific cognitive performance did not correlate with microglial morphology in the hippocampus. These findings indicated that the genotype of *in vivo* mice may have had an influence on the cognitive effects of dietary manipulation, but also that vascular rather than inflammatory changes were likely more responsible for the rapid appearance of hippocampus-specific cognitive deficits.

Chapter 5 looked at *in vivo* measures of blood flow over an 8 week dietary timecourse to further investigate the suggestions from **Chapter 3** that vascular changes could underlie cognitive impairment. Results showed that the hippocampus has a worse ratio of oxygen availability to neuronal metabolism than the cortex at rest, but that during peaks in neuronal activity both regions show similar ratios between the two. Neurovascular coupling in the cortex appeared to be more dependent on changes in blood volume, whilst in the hippocampus it seemed to rely more on changes in blood flow speed. Finally, performance on a hippocampus-specific cognitive task correlated negatively with the magnitude of the haemodynamic and neural response during peaks in neuronal activity in the hippocampus in control animals, but in HFD fed animals this relationship was absent. These results provided *in vivo* evidence that the elevated susceptibility of the hippocampus to pathology likely results from its poor ratio of vascular support to neuronal activity (compared to the cortex), and that the mechanisms driving hippocampal neurovascular coupling differed from those in cortex. Lastly, it appears that short-term HFD feeding may lead to hippocampus-specific cognitive impairment by disrupting the relationship between haemodynamic responses and cognitive performance.

Overall, data presented in this thesis provides a new insight into the causes of HFD induced hippocampus-specific cognitive impairment, and a greater understanding of the mechanisms underlying the elevated susceptibility of the hippocampus to damage.

6.2 Diet-Induced Weight Gain

In order to evaluate the effect of my HFD manipulation on weight gain, I analysed changes in weight (normalised to weight at baseline) over the duration of HFD feeding. The results of this have raised a number of interesting points regarding the effects of behavioural testing, age, sex, and genotype, on the impact of HFD feeding on weight. Whilst the mice I used for post-mortem immunofluorescence experiments showed an elevated rate of weight gain in response to a HFD, with a non-significant difference in weight apparent after the very first day (reaching trend level by day 14), those used for behavioural testing (who were not also used for *in vivo* imaging) showed a very clear absence of dietary effect on weight gain. In addition, the *in vivo* imaging mice I used were resistant to the effects of HFD on weight gain (whilst it did appear to increase their weight and rate of weight gain, this was to a far lesser extent than the immunofluorescence mice).

Other studies have generally shown that HFD feeding in mice leads to differences in weight very rapidly. Though the rate of this also depends on dietary fat content (typically either 45% or 60%) given a positive relationship exists in both rats and mice between dietary fat content and body weight or fat gain (reviewed in Hariri and Thibault 2010), Ouyang et al. (2014) show a 45% diet leads to a difference in weight after a week, and significant weight increases from four weeks onwards. Diets composed of 60% fat are associated with significant weight increases after as little as 3 days (Jais et al., 2016; McLean et al., 2018), with non-significant increases reported in work by Kim et al. (2008) after a week and in McLean et al. (2018) after 2 days. The timecourse of these changes fits with the results described for my immunofluorescence mice, who it must also be remembered varied in age and sex. Male mice are more susceptible to HFD-induced weight gain (Hwang et al., 2010), with old mice seen to be more susceptible to the metabolic effects of HFD feeding (Nunes-Souza et al., 2016). A significant difference in weight was only detected in aged (54-56 week old) mice from 8 weeks onwards during 60% HFD feeding, something that was not detected over 14 weeks in young (6-8 week old) mice though they did show reduced glucose tolerance, hyperlipidaemia, and elevated abdominal fat levels. Neither sex nor age significantly affected weight in any of my statistical analyses however, with this perhaps related to the fact that significant differences in diet-induced weight gain between sexes only emerges from 4 weeks onwards (Hwang et al., 2010), and the age of the oldest mouse I used (36 weeks) was still some way away from the aged category in Nunes-Souza et al. (2016).

With regards to the absence of dietary effects on weight gain in the mice used for behavioural testing (who were not also used for *in vivo* imaging), this appeared unrelated to sex or age effects given neither of these differed significantly from the immunofluorescence mice. Here it is possible

that the extra handling involved in behavioural testing played a role in disrupting eating behaviours or elevating stress levels, thereby influencing dietary effects on weight. This could also be at play in the *in vivo* mouse results, who showed resistance to HFD effects on weight gain, and were also handled more often and exposed to more stressors due to the *in vivo* imaging sessions. Another factor to consider is the role that genotype could play in modulating susceptibility to diet-induced weight gain.

None of the immunofluorescence mice were wild type C57BL/6J mice, unlike the cohort of non *in vivo* behavioural mice. Immunofluorescence mice had either one, or both, of two reporter mutations. These were the NG2-DsRed mutation and the Cx3CR1-GFP mutation. Whilst no work has been published looking at the influence of the former on diet-induced obesity, the latter has been investigated. The Cx3CR1-GFP mutation involves the knockout of the Cx3CR1 gene, which is involved in monocyte function (Lee et al. (2010) introduce the effects of Cx3CR1 dysfunction). As a result, all mice used were only heterozygous for this mutation. Complete Cx3CR1 deficiency protects against obesity and the inflammation of visceral adipose tissue (Polyák et al., 2014), with partial deficiency also associated with resistance to diet-induced weight gain and cognitive impairment (Cope et al., 2018). With regards to interpreting my own results, this would suggest that if anything, the immunofluorescence mice should show greater resistance to diet induced weight gain than the behavioural cohort, the opposite of what I observed. This suggests the disruption and stress associated with behavioural testing is the main factor driving the absence of dietary effects on weight seen in the behavioural cohort. However, the implications of Cx3CR1 deficiency on diet-induced weight gain are relevant for my *in vivo* mice, given these were all heterozygous for the Cx3CR1-GFP mutation. Here it is quite possible that their resistance to diet-induced weight gain relative to the immunofluorescence mice (of whom Cx3CR1-GFP mutants were a minority) is the result of their genotype, with HFD immunofluorescence animals showing a 20% increase relative to their starting weight after two weeks, in comparison to the roughly 7% increase seen after two weeks in the Cx3CR1-GFP *in vivo* mice. However, the influence of *in vivo* associated stress must also not be discounted.

6.3 Hippocampus-Specific Cognitive Deficits

Besides its influence on HFD-induced weight gain, the Cx3CR1-GFP mutation has also been reported to impart resistance to dietary effects on cognition (Cope et al., 2018). This could explain the discrepancy in my NOCR results, given that when analysis was restricted to the wild type, non *in vivo* mice, there was a trend towards impaired cognition in HFD mice, with this trend being

abolished by the inclusion of Cx3CR1-GFP *in vivo* mice in the analysis. This is in stark contrast to other HFD studies that have reported rapid hippocampus-specific cognitive impairments following HFD feeding (McLean et al., 2018; Kanoski and Davidson, 2010). Complete Cx3CR1 knockdown is associated with impairments in cognition and synaptic plasticity (Rogers et al., 2011), with its partial deficiency in Cx3CR1-GFP mice protecting against HFD-induced impairments in the hippocampus-dependent object location task (Cope et al., 2018). It is therefore quite possible that this is responsible for the difference in dietary effects on NOCR reported in **Chapters 3** and **4**, although it should be noted that genotype did not significantly affect performance in my statistical analysis. This could well be related to the lack of power in my NOCR results, as these are only based on 20 mice and therefore lack sufficient power to evaluate the differential effects of both diet and genotype, particularly given the fact that behavioural data can be highly variable. It should be mentioned that whilst testing mice of mixed sex and age also may have influenced results (given that sex and age influence HFD-induced weight gain, they likely also mediate its cognitive effects), neither factor had a significant effect on performance in my analysis (though my study was underpowered) and the NOCR task has previously been shown to be unaffected by differences in sex in rats (Ramsaran et al., 2016). An additional factor that may have influenced NOCR performance is the impact of hippocampal window implantation.

Hippocampal window surgery is associated with aspiration of the cortex overlying dorsal CA1, however, the cognitive task I used (NOCR) is hippocampus-specific (Mumby et al., 2002; Balderas et al., 2008) so should be unaffected by cortical changes. In addition, Dombeck et al. (2010) report that the cortical areas aspirated do not provide strong direct projections to the hippocampus. In another study that used the same surgery, Gu et al. (2014) report that the hippocampal window surgery did not influence performance on an open-field and contextual fear-conditioning paradigm. It is however possible that hippocampal window implantation influences the mechanisms responsible for mediating the detrimental effect of HFD on hippocampal cognition, and that this could also be contributing to the abolishment of the diet induced NOCR deficits reported in **Chapter 3**. Future work should look at post-mortem tissue from hippocampal window mice fed a HFD for 2 weeks to see how the immune and vascular changes in their tissue compare to that I report in **Chapter 3** to see if this theory hold true.

6.4 Phasic Microglial Activation and Microglial Priming

HFD feeding has previously been associated with the early appearance of neuroinflammation, seen in the hypothalamus after only 24 hours in terms of elevations in the mRNA levels of proinflam-

matory cytokines (Thaler et al., 2012), although there are also numerous studies that report a lack of such early inflammatory responses. No change in hippocampal microglial morphology (Spencer et al., 2019), or hypothalamic (Baufeld et al., 2016) morphology and density, was seen after 3 days of HFD feeding. The latter study also showed no increase in hypothalamic density after 4 weeks, though by 8 weeks this was apparent (Baufeld et al., 2016). My own results after two weeks of HFD in post mortem tissue showed an increase in the cell density of microglia globally, although this was not accompanied by any changes in microglial ramification, with increases in microglial density and changes in morphology and ramification correlating with microglial activation and inflammation (microglia reviewed in Kettenmann et al. (2011) and Hanisch and Kettenmann 2007). The uncoupling of proliferation from morphological changes could indicate the presence microglial priming rather than overt activation, given that primed microglia show signs of activation such as proliferation (priming reviewed in Li et al. 2018) though they show less distinct morphological changes (they remain highly ramified despite showing larger and less-round somata than resting cells; Torres-Platas et al. 2014) and do not produce inflammatory cytokines (Perry and Holmes (2014) cited by Hoogland et al. 2018). To evaluate this theory I analysed the effect of LPS on microglial morphology *in vivo* given that primed microglia show an elevated response to secondary inflammatory stimuli (microglial priming reviewed in Perry and Holmes 2014).

My results revealed no effect of HFD feeding on the morphological response of microglia to LPS, suggesting that HFD does not prime microglia in my model, despite the fact that HFD induced priming in the hippocampus (Sobesky et al., 2016) and hypothalamus (Souza et al., 2019) after only 3 days has been reported. However, I used a far stronger dosage of LPS than in other priming studies. I used 4mg/kg, a much higher dose than the 10 µg/kg used in Sobesky et al. (2016), whose dosage was chosen in order to avoid the possibility of a large inflammatory response masking signs of priming. Indeed, my strong dosage likely did just that, and means that my results cannot be used to rule out the presence of microglial priming in my model. The reason I used such a high dosage was to induce robust microglial activation that could be used as a positive control when designing my analysis methods to detect morphological changes associated with microglial activation.

An alternative explanation for the uncoupling of microglial proliferation from ramification changes is that a transient phase of microglial activation occurred prior to the two week timepoint, resulting in an elevated density of microglial cells that were no longer activated by two weeks. This theory is supported by Thaler et al. (2012), who show that proinflammatory cytokine production in the hypothalamus peaks initially before subsiding after one week, and then returns to

elevated levels by 28 days. In their results this is coupled with significantly elevated microglial densities at 3, 7, and 14 days (no data was provided for 28 days), suggesting the initial cytokine peak leads to microglial cell density increases that persist beyond the transient cytokine production dip. I evaluated this theory by tracking changes in microglial morphology (as an indicator of inflammatory activation) at timepoints prior to the two week timepoint *in vivo*. Here my results showed no effect of HFD on microglial morphology, suggesting that unlike in the hypothalamus, neither the hippocampus or cortex show a phasic inflammatory response prior to the two week timepoint. However, it is quite possible that once again, the effect of Cx3CR1-GFP heterozygosity in the *in vivo* mice played a role. Cope et al. (2018) provide evidence that in contrast to wild type C57BL/6J mice, Cx3CR1-GFP hippocampal microglia showed no activation associated morphological changes in response to 12 weeks of HFD feeding. As such, it may indeed be the case that HFD feeding leads to phasic inflammatory activation in the hippocampus and cortex prior to the 2 week timepoint, but not in Cx3CR1-GFP heterozygotes. Ultimately, to properly evaluate the phasic microglial activation and microglial priming theories, more work must be done to look at transient microglial activation using a genotype that is not potentially resistant to dietary effects, and with a more appropriate dosage of LPS.

6.5 Dietary Vascular Changes

Whilst HFD induced vascular changes have been reported both in terms of blood flow and structural changes, with HFD feeding associated with reduced vascular diameters (He et al., 2016; Constantinescu et al., 2011) and levels of blood flow (Glaser et al., 2012; Obadia et al., 2017), these have so far not been investigated following short-term HFD feeding. My post mortem tissue work in **Chapter 3** addressed this, and showed that following two weeks of HFD feeding capillary luminal radii are reduced, the resistance to flow in capillaries is increased, and the variation in capillary luminal radii is reduced. These changes occurred across the hippocampus, hypothalamus, and cortex, and suggested that early impairments in blood flow and neurovascular coupling could underlie HFD-induced cognitive deficits. I investigated this further *in vivo*, where my results showed that after 14 days of HFD there was no decrease in blood volume as might be expected given the reduction in capillary radii and perfusion seen in my post-mortem experiments. In fact, no effect of HFD on blood volume was detected at any point over the 56 days of dietary manipulation, suggesting that non-capillary vessels dilate in order to compensate for the decreased capillary radii observed in the post-mortem data (given the *in vivo* measures didn't look exclusively at the capillary bed, as my post mortem tissue analysis did). In addition, neither flow speed nor CBF

showed any overall affects of diet. These results seem to fit with other longer-term studies, where dietary effects on blood flow are inconsistent. Twenty weeks of HFD in rats was associated with a reduced CBF (Obadia et al., 2017), whilst Fu et al. (2017) reported no effect of HFD on microvascular flow or blood volume in the hippocampus of rats after 6 months, and Zuloaga et al. (2016) saw no effect of 6.5 months of HFD feeding on either cortical or hippocampal blood flow in mice. Ultimately, whilst *in vivo* haemodynamic regulation seems resistant to dietary structural changes in the capillary bed, it may be the case that the engagement of the compensatory mechanisms that they encourage could be related to the development of HFD-induced cognitive deficits.

With regards to neurovascular coupling, HFD feeding appeared to have no effect, although there was the suggestion of some form of haemodynamic dysfunction in both the hippocampus and cortex. The lack of a correlation between a reduction in capillary radii variation in my post-mortem tissue (which reflects an impoverished ability of the vasculature to locally regulate dilations) with *in vivo* measures of neurovascular coupling is surprising. This suggests that HFD-induced deficits in neurovascular coupling do not play a role in early HFD-induced cognitive deficits. It may be the case that despite a reduction in dilatory capacity at basal levels (as would be detected in post-mortem tissue), short-term HFD does not impair the ability of the vasculature to respond to peaks in neuronal activity to a large enough degree to lead to neurovascular uncoupling. In addition, my *in vivo* data suggests that neurovascular coupling in the hippocampus relies more on flow speed regulation then vascular dilations, another reason why changes in dilatory capacity would not influence hippocampal neurovascular coupling.

However, whilst neurovascular coupling was largely resistant to HFD, the relationship between the magnitude of CBF responses during peaks in neuronal activity and cognitive performance was affected by HFD. Here there was a negative correlation between the magnitude of CBF responses during peaks of neuronal activity in the hippocampus and performance on the NOCR task in control animals, but not in HFD animals. The negative correlation in control animals could relate to the neural efficiency hypothesis that proposes intelligence correlates negatively with brain activation and metabolic rates (evidence reviewed in Neubauer and Fink 2009). What this means for HFD feeding however is less clear. Short-term HFD feeding could lead to hippocampus-specific cognitive deficits by disrupting the mechanisms underlying the relationship between neural efficiency and cognition, leading to HFD fed animals having to use less effective non-hippocampal strategies to cope with task demands. There is some evidence of this in Kesby et al. (2015), where HFD fed animals showed a difference in strategies used on the Barnes maze, whilst rats fed a HFD after weaning used a different strategy on the Morris water maze (Boukouvalas et al., 2008). My results shed light on what appears to be a relatively new avenue regarding cognition and HFD

research, and suggests more work should be done to investigate not only the differential use of cognitive strategies in HFD studies, but also the mechanisms proposed to underlie the neural efficiency hypothesis.

6.6 Hippocampal Susceptibility

With regards to the region-specific nature of dietary effects, across my results there is an absence of strong evidence for hippocampus-specific dietary changes taking place, suggesting the global detrimental effects of HFD feeding are translated into hippocampus-specific cognitive impairment by the enhanced susceptibility of the hippocampus to pathology. My results provide evidence that the increased susceptibility of the hippocampus to damage or pathology such as hypoxia (Ng et al., 1989), Alzheimer's disease, and ageing (reviewed in Fjell et al. 2014), is likely related to its paucity of vascular support relative to its neuronal demand. In **Chapter 3** I show that the hippocampus has a lower capillary density, capillary radius, and capillary radius variation, than the cortex, whilst my results in **Chapter 5** extend this, demonstrating that at rest the ratio of oxygen availability and blood volume to the rate of neuronal oxygen metabolism is reduced in hippocampal CA1 relative to cortical V1. Whilst my post mortem tissue results reflect the work of other studies that have looked at regional differences in vascular density (Klein et al., 1986; Wu et al., 2004b; Bohn et al., 2016), my *in vivo* work represents what appears to be the first to compare the hippocampus and cortex with regards to neuronal metabolism, blood volume, and oxygen availability. The fact that hippocampus-specific cognition is more susceptible to the early effects of HFD than hippocampus-independent behaviour (Cordner and Tamashiro, 2015), coupled with the global dietary effects I report, suggests that it is this uncoupling of oxygen supply from neuronal metabolism that underlies elevated hippocampal-susceptibility in HFD models.

6.7 Limitations

As pointed out in relevant sections, there are a number of limitations to the work presented in this thesis. The most generously discussed of these is the role of partial Cx3CR1 deficiency, and the role this may have in mediating dietary effects not only on weight gain, but also cognition and microglial activation. This may have had an impact on my behavioural results, as well as my analysis of microglial morphology changes in my *in vivo* timecourse experiments. Therefore, future *in vivo* worked aimed at investigating dietary effects on microglia, and correlating this with behaviour, should utilise alternative mouse lines that do not involve the knockdown or knockout of

genes. Such lines include the CD11b-CreERT2; R26-tdTomato mice used by Füger et al. (2017), or the newly generated Tmem119-EGFP reported in Kaiser and Feng (2019). In addition, the Cx3CR1-GFP mutation labels not only resident microglia, but also circulating monocytes (Imai et al., 1997), an additional limitation of my work given the high dosage of LPS I used in **Chapter 4** likely led to the entry of peripheral immune cells (as documented in Rummel et al. 2010), meaning my characterisation of the microglial morphological response to LPS was likely not limited to microglia. This may also have been the case in my post mortem tissue experiments, given that Iba1 also doesn't label microglia exclusively (Greter et al., 2015), and the infiltration of circulating immune cells has been documented in models of short-term HFD feeding before (Valdearcos et al., 2017). Use of the Tmem119-EGFP mutation *in vivo*, or an anti Tmem119 antibody in immunofluorescence experiments, would address this, as it only labels resident microglia (Kaiser and Feng, 2019).

Other limitations to consider involve the use of mice of varied age and both sexes. Whilst not limiting myself to a particular age range or sex allowed me to increase the sample size of my studies, it also likely introduced extra variability into my results given the elevated susceptibility of males to HFD induced weight gain (Hwang et al., 2010) and the modulation of dietary effects on weight with age (Nunes-Souza et al., 2016). The fact that these factors mediate dietary effects on weight suggests they likely also do so in other aspects of physiology. In future, limiting work to male mice from 8 to 12 weeks of age (as is predominantly done in the field) would likely help eliminate variability in results. An additional limitation, specific to my NOCR behavioural testing and protein array results described in **Chapter 3**, is to do with sample size, where both were underpowered. As a result, it is difficult to truly evaluate the effect of diet (and the other factors analysed, such as surgery status, and cognitive performance) on hippocampus-specific cognition and hippocampal protein expression. In future these studies need to be conducted with a larger sample size. Additionally, a limitation specific to my investigation of HFD induced microglial priming in **Chapter 4** is the dose of LPS used, which likely induced a severe enough inflammatory response that any evidence of a primed response to an inflammatory stimulus would be masked. To address this, future work should utilise a much smaller dose, as in Sobesky et al. (2016), when investigating the presence of dietary priming.

Additional limitations relate to the fact that in **Chapter 3** the immunofluorescence results were derived from mice that were not behaviourally tested and so therefore could not be directly correlated with cognitive deficits, and that in **Chapter 4** the cell density of microglia was not quantified, making it unclear how similar the *in vivo* microglial results are to those in post-mortem tissue, and therefore how helpful they are in explaining them. Addressing these limitations would

require behaviourally testing mice used for immunofluorescence studies, and further analysing the *in vivo* data I previously collected.

6.8 Future Directions

With regards to future directions, one of the most interesting avenues of future work centres on the potential for phasic inflammatory responses to HFD outside of the hypothalamus. Besides tackling this by addressing the limitations of my own work regarding my *in vivo* microglial studies, this also requires an investigation of changes in the production of inflammatory cytokines in the hippocampus and cortex over a similar timecourse to that used in Thaler et al. (2012), i.e. 1, 3, 7, 14, and 28 days, given this would provide a more sensitive measure of inflammation (as the microglial density and morphology measures in Thaler et al. (2012) showed no such phasic patterns). In addition, by using a marker of circulating monocytes such as CCR2 (Saederup et al., 2010), the question of whether circulating immune cells infiltrate brain regions other than the hypothalamus during HFD feeding could be answered. In line with these suggestions, and given the role that hypothalamic microglia play in mediating the effect of HFD on weight gain (Valdearcos et al., 2017), it would be interesting to use a drug such as the CSF1R inhibitor PLX5622, which can be used to selectively deplete microglia (Elmore et al., 2014), to see if the presence of microglia mediates the detrimental effects of short-term HFD feeding on hippocampus-specific cognition.

In terms of vascular changes, investigating the possible existence of compensatory non-capillary dilations following HFD feeding could help to explain my *in vivo* haemodynamic results, whilst investigating whether the use of a vasodilator, such as hydralazine, is able to attenuate the detrimental effect of HFD on hippocampal cognition would be one of the first steps towards establishing a causative role for impaired capillary blood flow in HFD induced cognitive deficits. This could be done in conjunction with a repeat of my *in vivo* work where I demonstrated the absence of a negative correlation between the magnitude of the hippocampal CBF response to peaks in neuronal activity and cognitive performance in HFD animals, in order to see if the use of a vasodilator is able to prevent the annulment of this relationship. In addition, measuring the magnitude of neuronal responses during peaks in neuronal activity more directly (through calcium imaging perhaps) and correlating this with behavioural performance could help to further investigate the role of the neural efficiency hypothesis in diet-induced cognitive impairment. Lastly, though noisy, visually stimulated neurovascular coupling data in **Chapter 5** suggested there may be an effect of short-term HFD on astrocytic regulation of neurovascular coupling. As such, investigating HFD induced changes in COX-1 activity, and astrocyte to pericyte communication, could be a worth-

while avenue of exploration.

Exploring the suggestion from my results that the hippocampus uses a different primary mechanism for neurovascular coupling than the cortex could also be very interesting. There is a lack of research into region-specific neurovascular coupling mechanisms, with the suggestion from my data that the hippocampus relies more on flow speed than blood volume regulation one of the first region-specific mechanisms to be proposed as far as I am aware. This could be further investigated by reducing hippocampal blood volume with a vasoconstrictor, and then comparing the ability of the hippocampus to maintain oxygen availability during peaks in neuronal activity. Should this be maintained, it would provide further evidence that hippocampal neurovascular coupling is not critically dependent on blood flow regulation, though more investigation of how exactly the hippocampus could regulate flow speed is necessary in order to design future interventions to investigate this. With regards to the trend over time seen in **Chapter 5** for hippocampal haemodynamic values to approach those in the cortex, I suggest this could be related to a down-regulation of hippocampal neuronal activity at rest that elevates over time, whilst during peaks in neuronal activity, a greater synchronisation in hippocampal neuronal responses declines over time. Investigating this could help establish the mechanisms behind the results I report. In addition, taking Oxy-CBF probe recordings from hippocampal window mice 12 weeks after surgery (or after a similarly long recovery period), with no recording sessions prior, could help to establish if these changes are associated with a return to baseline in the hippocampus following surgery, or if they are the result of persistent detrimental effects of repeated recording sessions.

6.9 Conclusions

The work in this thesis aimed to uncover the mechanisms responsible for the rapid, hippocampus-specific, cognitive impairment associated with HFD feeding. For the first time I provide evidence that this is related to diet-induced dysfunction in the mechanisms that relate blood flow during peaks in neuronal activity to cognitive performance (likely related to neural efficiency). In addition, my results suggests that a significant part of the elevated susceptibility of the hippocampus to HFD is due to its poor ratio between vascular support and neuronal metabolism, which though preserved relative to the cortex during neurovascular coupling events, is significantly reduced at rest. This has implications for the elevated susceptibility of the hippocampus to a wide range of pathologies. Though more work is needed to establish a role for phasic inflammatory changes or microglial priming in the genesis of cognitive deficits, evidence suggests vascular rather than inflammatory changes are the primary drivers.

Chapter 7

References

Abbott, K. N., Arnott, C. K., Westbrook, R. F., and Tran, D. M. (2019). The effect of high fat, high sugar, and combined high fat-high sugar diets on spatial learning and memory in rodents: A meta-analysis.

Aday, S., Cecchelli, R., Hallier-Vanuxeem, D., Dehouck, M. P., and Ferreira, L. (2016). Stem Cell-Based Human Blood-Brain Barrier Models for Drug Discovery and Delivery. *Trends in Biotechnology*, 34(5):382–393.

Aguirre, N., Cruz-Gómez, Á. J., Miró-Padilla, A., Bueichekú, E., Broseta Torres, R., Ávila, C., Sanchis-Segura, C., and Forn, C. (2019). Repeated Working Memory Training Improves Task Performance and Neural Efficiency in Multiple Sclerosis Patients and Healthy Controls. *Multiple Sclerosis International*, 2019:1–13.

André, C., Quevedo, O. G., Rey, C., Rémus-Borel, J., Clark, S., Castellanos-Jankiewicz, A., Ladeveze, E., Leste-Lasserre, T., Nadjar, A., Abrous, D. N., Laye, S., and Cota, D. (2017). Inhibiting microglia expansion prevents diet-induced hypothalamic and peripheral inflammation. *Diabetes*, 66(4):908–919.

Armulik, A., Genové, G., and Betsholtz, C. (2011). Pericytes: Developmental, Physiological, and Pathological Perspectives, Problems, and Promises. *Developmental Cell*, 21(2):193–215.

Arnold, S. E., Lucki, I., Brookshire, B. R., Carlson, G. C., Browne, C. A., Kazi, H., Bang, S., Choi, B.-R., Chen, Y., McMullen, M. F., and Kim, S. F. (2014). High fat diet produces brain insulin resistance, synaptodendritic abnormalities and altered behavior in mice. *Neurobiology of Disease*, 67:79–87.

Ashhurst, T. M., van Vreden, C., Niewold, P., and King, N. J. C. (2014). The plasticity of in-

flammatory monocyte responses to the inflamed central nervous system. *Cellular Immunology*, 291(1-2):49–57.

Aslani, S., Vieira, N., Marques, F., Costa, P. S., Sousa, N., and Palha, J. A. (2015). The effect of high-fat diet on rat's mood, feeding behavior and response to stress. *Translational Psychiatry*.

Avena, N. M., Rada, P., and Hoebel, B. G. (2008). Evidence for sugar addiction: Behavioral and neurochemical effects of intermittent, excessive sugar intake. *Neuroscience and Biobehavioral Reviews*, 32(1):20–39.

Ayaz, A., Saleem, A. B., Schölvinck, M. L., and Carandini, M. (2013). Locomotion controls spatial integration in mouse visual cortex. *Current Biology*, 23(10):890–894.

Balderas, I., Rodriguez-Ortiz, C. J., Salgado-Tonda, P., Chavez-Hurtado, J., McGaugh, J. L., and Bermudez-Rattoni, F. (2008). The consolidation of object and context recognition memory involve different regions of the temporal lobe. *Learning and Memory*, 15(9):618–624.

Balmer, T. S. (2016). Perineuronal nets enhance the excitability of fast-spiking neurons. *eNeuro*, 3(4):745–751.

Banks, W. A., Coon, A. B., Robinson, S. M., Moinuddin, A., Shultz, J. M., Nakaoke, R., and Morley, J. E. (2004). Triglycerides Induce Leptin Resistance at the Blood-Brain Barrier. *Diabetes*, 53(5):1253–1260.

Banks, W. A. and Farrell, C. L. (2003). Impaired transport of leptin across the blood-brain barrier in obesity is acquired and reversible. *American Journal of Physiology - Endocrinology and Metabolism*, 285(1 48-1).

Barrientos, R. M., O'Reilly, R. C., and Rudy, J. W. (2002). Memory for context is impaired by a post context exposure injection of interleukin-1 beta into dorsal hippocampus. *Behavioural Brain Research*, 134(1-2):291–298.

Baslow, M. and Guilfoyle, D. (2017). The Bimodal Nature of Neurovascular Coupling: Slow Tonic and Rapid Phasic Responses are Separately Controlled by Specific Astrocyte Metabotropic and Ionotropic Glutamate Receptors. *Journal of Molecular and Genetic Medicine*, 11(2).

Baufeld, C., Osterloh, A., Prokop, S., Miller, K. R., and Heppner, F. L. (2016). High-fat diet-induced brain region-specific phenotypic spectrum of CNS resident microglia. *Acta Neuropathologica*, 132(3):361–375.

Bellinger, F., Madamba, S., Campbell, I., and Siggins, G. (1995). Reduced long-term potentiation in the dentate gyrus of transgenic mice with cerebral overexpression of interleukin-6. *Neuroscience Letters*, 198(2):95–98.

Bello, N. T., Lucas, L. R., and Hajnal, A. (2002). Repeated sucrose access influences dopamine D2 receptor density in the striatum. *Neuroreport*, 13(12):1575–1578.

Bello, N. T., Sweigart, K. L., Lakoski, J. M., Norgren, R., and Hajnal, A. (2003). Restricted feeding with scheduled sucrose access results in an upregulation of the rat dopamine transporter. *American Journal of Physiology-Regulatory, Integrative and Comparative Physiology*, 284(5):R1260–R1268.

Bennett, L., Yang, M., Enikolopov, G., and Iacovitti, L. (2009). Circumventricular organs: A novel site of neural stem cells in the adult brain. *Molecular and Cellular Neuroscience*, 41(3):337–347.

Berthiaume, A.-A., Hartmann, D. A., Majesky, M. W., Bhat, N. R., and Shih, A. Y. (2018). Pericyte Structural Remodeling in Cerebrovascular Health and Homeostasis. *Frontiers in aging neuroscience*, 10:210.

Berthoud, H.-R., Lenard, N. R., and Shin, A. C. (2011). Food reward, hyperphagia, and obesity. *American Journal of Physiology-Regulatory, Integrative and Comparative Physiology*, 300(6):R1266–R1277.

Betteridge, D. J. (2000). What is oxidative stress? *Metabolism: Clinical and Experimental*, 49(2 SUPPL. 1):3–8.

Bhaskaran, K., Douglas, I., Forbes, H., Dos-Santos-Silva, I., Leon, D. A., and Smeeth, L. (2014). Body-mass index and risk of 22 specific cancers: a population-based cohort study of 5·24 million UK adults. *The Lancet*, 384(9945):755–765.

Birdsill, A. C., Carlsson, C. M., Willette, A. A., Okonkwo, O. C., Johnson, S. C., Xu, G., Oh, J. M., Gallagher, C. L., Koscik, R. L., Jonaitis, E. M., Hermann, B. P., Larue, A., Rowley, H. A., Asthana, S., Sager, M. A., and Bendlin, B. B. (2013). Low cerebral blood flow is associated with lower memory function in metabolic syndrome. *Obesity*, 21(7):1313–1320.

Biswas, S. K. (2016). Does the Interdependence between Oxidative Stress and Inflammation Explain the Antioxidant Paradox? *Oxidative Medicine and Cellular Longevity*, 2016:1–9.

Bocarsly, M. E., Fasolino, M., Kane, G. A., LaMarca, E. A., Kirschen, G. W., Karatsoreos, I. N., McEwen, B. S., and Gould, E. (2015). Obesity diminishes synaptic markers, alters microglial

morphology, and impairs cognitive function. *Proceedings of the National Academy of Sciences of the United States of America*, 112(51):15731–6.

Boehme, M., Guenther, M., Stahr, A., Liebmann, M., Jaenisch, N., Witte, O. W., and Frahm, C. (2014). Impact of indomethacin on neuroinflammation and hippocampal neurogenesis in aged mice. *Neuroscience Letters*, 572:7–12.

Bohn, K. A., Adkins, C. E., Mittapalli, R. K., Terrell-Hall, T. B., Mohammad, A. S., Shah, N., Dolan, E. L., Nounou, M. I., and Lockman, P. R. (2016). Semi-automated rapid quantification of brain vessel density utilizing fluorescent microscopy. *Journal of Neuroscience Methods*, 270:124–131.

Boitard, C., Cavaroc, A., Sauvant, J., Aubert, A., Castanon, N., Layé, S., and Ferreira, G. (2014). Impairment of hippocampal-dependent memory induced by juvenile high-fat diet intake is associated with enhanced hippocampal inflammation in rats. *Brain, Behavior, and Immunity*, 40:9–17.

Borsini, A., Zunszain, P. A., Thuret, S., and Pariante, C. M. (2015). The role of inflammatory cytokines as key modulators of neurogenesis. *Trends in Neurosciences*, 38(3):145–157.

Boukouvalas, G., Antoniou, K., Papalexi, E., and Kitraki, E. (2008). Post weaning high fat feeding affects rats' behavior and hypothalamic pituitary adrenal axis at the onset of puberty in a sexually dimorphic manner. *Neuroscience*.

Bruning, J. C., Gautam, D., Burks, D. J., Gillette, J., Schubert, M., Orban, P. C., Klein, R., Krone, W., Muller-Wieland, D., and Kahn, C. R. (2000). Role of brain insulin receptor in control of body weight and reproduction. *Science*, 289(5487):2122–2125.

Buckman, L. B., Hasty, A. H., Flaherty, D. K., Buckman, C. T., Thompson, M. M., Matlock, B. K., Weller, K., and Ellacott, K. L. J. (2014). Obesity induced by a high-fat diet is associated with increased immune cell entry into the central nervous system. *Brain, Behavior, and Immunity*, 35:33–42.

Burrage, E., Marshall, K., Santanam, N., and Chantler, P. (2018). Cerebrovascular dysfunction with stress and depression. *Brain Circulation*, 4(2):43.

Butland, D. B., Jebb, D. S., Kopelman, P. P., McPherson, K., Thomas, P. S., Mardell, J., and Parry, V. (2007). Tackling Obesities: Future Choices.

Calvo-Ochoa, E., Hernández-Ortega, K., Ferrera, P., Morimoto, S., and Arias, C. (2014). Short-term high-fat-and-fructose feeding produces insulin signaling alterations accompanied by neurite and synaptic reduction and astroglial activation in the rat hippocampus. *Journal of Cerebral Blood Flow and Metabolism*, 34(6):1001–1008.

Camer, D., Yu, Y., Szabo, A., Fernandez, F., Dinh, C. H., and Huang, X. F. (2015). Bardoxolone methyl prevents high-fat diet-induced alterations in prefrontal cortex signalling molecules involved in recognition memory. *Progress in Neuro-Psychopharmacology and Biological Psychiatry*, 59:68–75.

Čapek, M., Janáček, J., and Kubínová, L. (2006). Methods for compensation of the light attenuation with depth of images captured by a confocal microscope. *Microscopy Research and Technique*, 69(8):624–635.

Carreño-Müller, E., Herrera, A. J., De Pablos, R. M., Tomás-Camardiel, M., Venero, J. L., Cano, J., and Machado, A. (2003). Thrombin induces in vivo degeneration of nigral dopaminergic neurones along with the activation of microglia. *Journal of Neurochemistry*, 84(5):1201–1214.

Carvalheira, J. B., Siloto, R. M., Ignacchitti, I., Brenelli, S. L., Carvalho, C. R., Leite, A., Velloso, L. A., Gontijo, J. A., and Saad, M. J. (2001). Insulin modulates leptin-induced STAT3 activation in rat hypothalamus. *FEBS Letters*, 500(3):119–124.

Chang, H. C., Tai, Y. T., Cherng, Y. G., Lin, J. W., Liu, S. H., Chen, T. L., and Chen, R. M. (2014). Resveratrol attenuates high-fat diet-induced disruption of the blood-brain barrier and protects brain neurons from apoptotic insults. *Journal of Agricultural and Food Chemistry*, 62(15):3466–3475.

Chantler, P. D., Shrader, C. D., Tabone, L. E., D'Audiffret, A. C., Huseynova, K., Brooks, S. D., Branyan, K. W., Grogg, K. A., and Frisbee, J. C. (2015). Cerebral Cortical Microvascular Rarefaction in Metabolic Syndrome is Dependent on Insulin Resistance and Loss of Nitric Oxide Bioavailability. *Microcirculation*, 22(6):435–445.

Chen, H. J. C., Spiers, J. G., Sernia, C., and Lavidis, N. A. (2016). Acute restraint stress induces specific changes in nitric oxide production and inflammatory markers in the rat hippocampus and striatum. *Free Radical Biology and Medicine*, 90:219–229.

Cheng, J., Korte, N., Nortley, R., Sethi, H., Tang, Y., and Attwell, D. (2018). Targeting pericytes for therapeutic approaches to neurological disorders. *Acta Neuropathologica*, 136(4):507–523.

Chia-Ying, W., Yang, Y.-T., Chen, C.-H., Chang, J.-C., Tsai, S.-C., Chen, C.-Y., Chen, C.-N., Bernard, J. R., and Liao, Y.-H. (2017). Effects of a high-fat diet on spontaneous locomotor activity and blood metabolic biomarkers in Sprague Dawley rats. *The FASEB Journal*.

Clegg, D. J., Gotoh, K., Kemp, C., Wortman, M. D., Benoit, S. C., Brown, L. M., D'Alessio, D., Tso, P., Seeley, R. J., and Woods, S. C. (2011). Consumption of a high-fat diet induces central insulin resistance independent of adiposity. *Physiology and Behavior*, 103(1):10–16.

Colom, R., Stein, J. L., Rajagopalan, P., Martínez, K., Hermel, D., Wang, Y., Álvarez-Linera, J., Burgaleta, M., Quiroga, M. Á., Shih, P. C., and Thompson, P. M. (2013). Hippocampal structure and human cognition: Key role of spatial processing and evidence supporting the efficiency hypothesis in females. *Intelligence*, 41(2):129–140.

Constantinescu, E., Safciuc, F., and V. Sima, A. (2011). A Hyperlipidemic Diet Induces Structural Changes in Cerebral Blood Vessels. *Current Neurovascular Research*, 8(2):131–144.

Cope, E. C., Lamarca, E. A., Monari, P. K., Olson, L. B., Martinez, S., Zych, A. D., Katchur, N. J., and Gould, E. (2018). Microglia play an active role in obesity-associated cognitive decline. *Journal of Neuroscience*, 38(41):8889–8904.

Cordner, Z. A. and Tamashiro, K. L. (2015). Effects of high-fat diet exposure on learning & memory. *Physiology and Behavior*, 152:363–371.

Cottone, P., Sabino, V., Steardo, L., and Zorrilla, E. P. (2008). Intermittent access to preferred food reduces the reinforcing efficacy of chow in rats. *American Journal of Physiology-Regulatory, Integrative and Comparative Physiology*, 295(4):R1066–R1076.

Coucha, M., Barrett, A. C., Elgebaly, M., Ergul, A., and Abdelsaid, M. (2019). Inhibition of Ephrin-B2 in brain pericytes decreases cerebral pathological neovascularization in diabetic rats. *PLoS ONE*, 14(1):e0210523.

Cray, C., Villar, D., Zaias, J., and Altman, N. H. (2008). Effects of fenbendazole on routine immune response parameters of BALB/c mice. *Journal of the American Association for Laboratory Animal Science*.

Cremer, J. E. and Seville, M. P. (1983). Regional brain blood flow, blood volume, and haematocrit values in the adult rat. *Journal of Cerebral Blood Flow and Metabolism*.

Cui, Y., Shu, Y., Zhu, Y., Shi, Y., and Le, G. (2012). High-fat diets impair spatial learning of mice in the Y-maze paradigm: Ameliorative potential of α-lipoic acid. *Journal of Medicinal Food*, 15(8):713–717.

Czéh, B., Abumaria, N., Rygula, R., and Fuchs, E. (2010). Quantitative changes in hippocampal microvasculature of chronically stressed rats: No effect of fluoxetine treatment. *Hippocampus*, 20(1):174–185.

Damani, M. R., Zhao, L., Fontainhas, A. M., Amaral, J., Fariss, R. N., and Wong, W. T. (2011). Age-related alterations in the dynamic behavior of microglia. *Aging Cell*, 10(2):263–276.

Dantzer, R., O'Connor, J. C., Freund, G. G., Johnson, R. W., and Kelley, K. W. (2008). From inflammation to sickness and depression: When the immune system subjugates the brain. *Nature Reviews Neuroscience*, 9(1):46–56.

Davalos, D., Grutzendler, J., Yang, G., Kim, J. V., Zuo, Y., Jung, S., Littman, D. R., Dustin, M. L., and Gan, W. B. (2005). ATP mediates rapid microglial response to local brain injury in vivo. *Nature Neuroscience*, 8(6):752–758.

Davalos, D., Kyu Ryu, J., Merlini, M., Baeten, K. M., Le Moan, N., Petersen, M. A., Deerinck, T. J., Smirnoff, D. S., Bedard, C., Hakozaki, H., Gonias Murray, S., Ling, J. B., Lassmann, H., Degen, J. L., Ellisman, M. H., and Akassoglou, K. (2012). Fibrinogen-induced perivascular microglial clustering is required for the development of axonal damage in neuroinflammation. *Nature Communications*, 3(1):1227.

Davidson, T., Hargrave, S., Swithers, S., Sample, C., Fu, X., Kinzig, K., and Zheng, W. (2013). Inter-relationships among diet, obesity and hippocampal-dependent cognitive function. *Neuroscience*, 253:110–122.

Davidson, T. L., Jones, S., Roy, M., and Stevenson, R. J. (2019). The Cognitive Control of Eating and Body Weight: It's More Than What You "Think". *Frontiers in Psychology*, 10(FEB).

Davidson, T. L., Monnot, A., Neal, A. U., Martin, A. A., Horton, J. J., and Zheng, W. (2012). The effects of a high-energy diet on hippocampal-dependent discrimination performance and blood-brain barrier integrity differ for diet-induced obese and diet-resistant rats. *Physiology and Behavior*, 107(1):26–33.

Davie, E. W. and Kulman, J. D. (2006). An overview of the structure and function of thrombin. *Seminars in Thrombosis and Hemostasis*, 32(SUPPL. 1):3–15.

de la Torre, J. C. (2002). Vascular basis of Alzheimer's pathogenesis. *Annals of the New York Academy of Sciences*, 977(1):196–215.

del Zoppo, G. J., Schmid-Schönbein, G. W., Mori, E., Copeland, B. R., and Chang, C. M. (1991). Polymorphonuclear leukocytes occlude capillaries following middle cerebral artery occlusion and reperfusion in baboons. *Stroke*, 22(10):1276–1283.

Denver, P., Gault, V. A., and McClean, P. L. (2018). Sustained high-fat diet modulates inflammation, insulin signalling and cognition in mice and a modified xenin peptide ameliorates neuropathology in a chronic high-fat model. *Diabetes, Obesity and Metabolism*, 20(5):1166–1175.

Deutsch, C., Portik-Dobos, V., Smith, A. D., Ergul, A., and Dorrance, A. M. (2009). Diet-induced obesity causes cerebral vessel remodeling and increases the damage caused by ischemic stroke. *Microvascular Research*, 78(1):100–106.

Devonshire, I. M., Papadakis, N. G., Port, M., Berwick, J., Kennerley, A. J., Mayhew, J. E., and Overton, P. G. (2012). Neurovascular coupling is brain region-dependent. *NeuroImage*, 59(3):1997–2006.

Dingess, P. M., Harkness, J. H., Slaker, M., Zhang, Z., Wulff, S. S., Sorg, B. A., and Brown, T. E. (2018). Consumption of a High-Fat Diet Alters Perineuronal Nets in the Prefrontal Cortex. *Neural Plasticity*, 2018:1–8.

Dombeck, D. A., Harvey, C. D., Tian, L., Looger, L. L., and Tank, D. W. (2010). Functional imaging of hippocampal place cells at cellular resolution during virtual navigation. *Nature Neuroscience*, 13(11):1433–1440.

Du, X. L., Edelstein, D., Rossetti, L., Fantus, I. G., Goldberg, H., Ziyadeh, F., Wu, J., and Brownlee, M. (2000). Hyperglycemia-induced mitochondrial superoxide overproduction activates the hexosamine pathway and induces plasminogen activator inhibitor-1 expression by increasing Sp1 glycosylation. *Proceedings of the National Academy of Sciences of the United States of America*, 97(22):12222–12226.

El-Haschimi, K., Pierroz, D. D., Hileman, S. M., Bjørbæk, C., and Flier, J. S. (2000). Two defects contribute to hypothalamic leptin resistance in mice with diet-induced obesity. *Journal of Clinical Investigation*, 105(12):1827–1832.

Elahy, M., Lam, V., Pallebage-Gamarallage, M. M., Giles, C., Mamo, J. C., and Takechi, R. (2015). Nicotine attenuates disruption of blood-brain barrier induced by saturated-fat feeding in wild-type mice. *Nicotine and Tobacco Research*, 17(12):1436–1441.

Elmore, M. R. P., Najafi, A. R., Koike, M. A., Dagher, N. N., Spangenberg, E. E., Rice, R. A., Kitazawa, M., Matusow, B., Nguyen, H., West, B. L., and Green, K. N. (2014). Colony-

stimulating factor 1 receptor signaling is necessary for microglia viability, unmasking a microglia progenitor cell in the adult brain. *Neuron*, 82(2):380–397.

Endo, Y., Nishimura, J. I., Kobayashi, S., and Kimura, F. (1999). Chronic stress exposure influences local cerebral blood flow in the rat hippocampus. *Neuroscience*, 93(2):551–555.

Erdö, F., Denes, L., and De Lange, E. (2017). Age-associated physiological and pathological changes at the blood-brain barrier: A review.

Estato, V., Nascimento, A., Antunes, B., Gomes, F., Coelho, L., Rangel, R., Garzoni, L., Daliry, A., Bousquet, P., and Tibiriçá, E. (2017). Cerebral Microvascular Dysfunction and Inflammation Are Improved by Centrally Acting Antihypertensive Drugs in Metabolic Syndrome. *Metabolic Syndrome and Related Disorders*, 15(1):26–35.

Falagas, M. E. and Kompoti, M. (2006). Obesity and infection. *Lancet Infectious Diseases*, 6(7):438–446.

Fellin, T. and Carmignoto, G. (2004). Neurone-to-astrocyte signalling in the brain represents a distinct multifunctional unit. *Journal of Physiology*, 559(1):3–15.

Fernández-Arjona, M. d. M., Grondona, J. M., Granados-Durán, P., Fernández-Llebrez, P., and López-Ávalos, M. D. (2017). Microglia Morphological Categorization in a Rat Model of Neuroinflammation by Hierarchical Cluster and Principal Components Analysis. *Frontiers in Cellular Neuroscience*, 11.

Fernández-Klett, F., Offenhauser, N., Dirnagl, U., Priller, J., and Lindauer, U. (2010). Pericytes in capillaries are contractile in vivo, but arterioles mediate functional hyperemia in the mouse brain. *Proceedings of the National Academy of Sciences of the United States of America*, 107(51):22290–22295.

Ferreira, T. A., Blackman, A. V., Oyrer, J., Jayabal, S., Chung, A. J., Watt, A. J., Sjöström, P. J., and van Meyel, D. J. (2014). Neuronal morphometry directly from bitmap images. *Nature Methods*, 11(10):982–984.

Fjell, A. M., McEvoy, L., Holland, D., Dale, A. M., and Walhovd, K. B. (2014). What is normal in normal aging? Effects of aging, amyloid and Alzheimer's disease on the cerebral cortex and the hippocampus. *Progress in Neurobiology*, 117:20–40.

Fouda, A. Y., Fagan, S. C., and Ergul, A. (2019). Brain Vasculature and Cognition. *Arterioscleriosis, thrombosis, and vascular biology*.

Franke, D. D. and Shirwan, H. (2006). Prophylactic fenbendazole therapy does not affect the incidence and onset of type 1 diabetes in non-obese diabetic mice. *International Immunology*.

Freeman, L. R. and Granholm, A.-C. E. (2012). Vascular Changes in Rat Hippocampus following a High Saturated Fat and Cholesterol Diet. *Journal of Cerebral Blood Flow & Metabolism*, 32(4):643–653.

Frigerio, F., Frasca, A., Weissberg, I., Parrella, S., Friedman, A., Vezzani, A., and Noe', F. M. (2012). Long-lasting pro-ictogenic effects induced in vivo by rat brain exposure to serum albumin in the absence of concomitant pathology. *Epilepsia*, 53(11):1887–1897.

Fu, Z., Wu, J., Nesil, T., Li, M. D., Aylor, K. W., and Liu, Z. (2017). Long-term high-fat diet induces hippocampal microvascular insulin resistance and cognitive dysfunction. *American Journal of Physiology - Endocrinology and Metabolism*, 312(2):E89–E97.

Fuente-Martiń, E., García-Cáceres, C., Granado, M., De Ceballos, M. L., Sánchez-Garrido, M. Á., Sarman, B., Liu, Z. W., Dietrich, M. O., Tena-Sempere, M., Argente-Arizón, P., Díaz, F., Argente, J., Horvath, T. L., and Chowen, J. A. (2012). Leptin regulates glutamate and glucose transporters in hypothalamic astrocytes. *Journal of Clinical Investigation*, 122(11):3900–3913.

Füger, P., Hefendehl, J. K., Veeraraghavalu, K., Wendeln, A. C., Schlosser, C., Obermüller, U., Wegenast-Braun, B. M., Neher, J. J., Martus, P., Kohsaka, S., Thunemann, M., Feil, R., Sisodia, S. S., Skodras, A., and Jucker, M. (2017). Microglia turnover with aging and in an Alzheimer's model via long-term in vivo single-cell imaging. *Nature Neuroscience*.

Fung, A., Vizcaychipi, M., Lloyd, D., Wan, Y., and Ma, D. (2012). Central nervous system inflammation in disease related conditions: Mechanistic prospects. *Brain Research*, 1446:144–155.

Furube, E., Kawai, S., Inagaki, H., Takagi, S., and Miyata, S. (2018). Brain Region-dependent Heterogeneity and Dose-dependent Difference in Transient Microglia Population Increase during Lipopolysaccharide-induced Inflammation. *Scientific Reports*, 8(1):2203.

Gautron, L. and Elmquist, J. K. (2011). Sixteen years and counting: An update on leptin in energy balance. *Journal of Clinical Investigation*, 121(6):2087–2093.

Gemma, C. and Bickford, P. C. (2007). Interleukin-1β and caspase-1: Players in the regulation of age-related cognitive dysfunction. *Reviews in the Neurosciences*, 18(2):137–148.

Glaser, N., Ngo, C., Anderson, S., Yuen, N., Trifu, A., and O'Donnell, M. (2012). Effects of hyperglycemia and effects of ketosis on cerebral perfusion, cerebral water distribution, and cerebral metabolism. *Diabetes*, 61(7):1831–1837.

Gomez-Smith, M., Janik, R., Adams, C., Lake, E. M., Thomason, L. A., Jeffers, M. S., Stefanovic, B., and Corbett, D. (2018). Reduced Cerebrovascular Reactivity and Increased Resting Cerebral Perfusion in Rats Exposed to a Cafeteria Diet. *Neuroscience*, 371:166–177.

Gorelick, P. B. (2010). Role of inflammation in cognitive impairment: Results of observational epidemiological studies and clinical trials.

Goshen, I., Kreisel, T., Ounallah-Saad, H., Renbaum, P., Zalzstein, Y., Ben-Hur, T., Levy-Lahad, E., and Yirmiya, R. (2007). A dual role for interleukin-1 in hippocampal-dependent memory processes. *Psychoneuroendocrinology*, 32(8-10):1106–1115.

Grabert, K., Michoel, T., Karavolos, M. H., Clohisey, S., Baillie, J. K., Stevens, M. P., Freeman, T. C., Summers, K. M., and McColl, B. W. (2016). Microglial brain region-dependent diversity and selective regional sensitivities to aging. *Nature Neuroscience*, 19(3):504–516.

Granholm, A. C., Bimonte-Nelson, H. A., Moore, A. B., Nelson, M. E., Freeman, L. R., and Sambamurti, K. (2008). Effects of a saturated fat and high cholesterol diet on memory and hippocampal morphology in the middle-aged rat. *Journal of Alzheimer's Disease*, 14(2):133–145.

Grant, R. I., Hartmann, D. A., Underly, R. G., Berthiaume, A. A., Bhat, N. R., and Shih, A. Y. (2019). Organizational hierarchy and structural diversity of microvascular pericytes in adult mouse cortex. *Journal of Cerebral Blood Flow and Metabolism*, 39(3):411–425.

Gray, S. M., Aylor, K. W., and Barrett, E. J. (2017). Unravelling the regulation of insulin transport across the brain endothelial cell. *Diabetologia*, 60(8):1512–1521.

Greter, M., Lelios, I., and Croxford, A. L. (2015). Microglia Versus Myeloid Cell Nomenclature during Brain Inflammation. *Frontiers in Immunology*, 6(MAY).

Gruzdeva, O., Borodkina, D., Uchasova, E., Dyleva, Y., and Barbarash, O. (2019). Leptin resistance: Underlying mechanisms and diagnosis. *Diabetes, Metabolic Syndrome and Obesity: Targets and Therapy*, 12:191–198.

Gu, L., Kleiber, S., Schmid, L., Nebeling, F., Chamoun, M., Steffen, J., Wagner, J., and Fuhrmann, M. (2014). Long-term in vivo imaging of dendritic spines in the hippocampus reveals structural plasticity. *Journal of Neuroscience*, 34(42):13948–13953.

Guan, Z. and Fang, J. (2006). Peripheral immune activation by lipopolysaccharide decreases neurotrophins in the cortex and hippocampus in rats. *Brain, Behavior, and Immunity*, 20(1):64–71.

Guillemot-Legris, O., Masquelier, J., Everard, A., Cani, P. D., Alhouayek, M., and Muccioli, G. G. (2016). High-fat diet feeding differentially affects the development of inflammation in the central nervous system. *Journal of Neuroinflammation*, 13(1):206.

Haddad-Tóvolli, R., Dragano, N. R. V., Ramalho, A. F. S., and Velloso, L. A. (2017). Development and Function of the Blood-Brain Barrier in the Context of Metabolic Control. *Frontiers in Neuroscience*, 11(APR).

Haley, M. J., Krishnan, S., Burrows, D., de Hoog, L., Thakrar, J., Schiessl, I., Allan, S. M., and Lawrence, C. B. (2019). Acute high-fat feeding leads to disruptions in glucose homeostasis and worsens stroke outcome. *Journal of Cerebral Blood Flow and Metabolism*, 39(6):1026–1037.

Hall, C. N., Reynell, C., Gesslein, B., Hamilton, N. B., Mishra, A., Sutherland, B. A., Oâ Farrell, F. M., Buchan, A. M., Lauritzen, M., and Attwell, D. (2014). Capillary pericytes regulate cerebral blood flow in health and disease. *Nature*, 508(1):55–60.

Hammond, T. R., Dufort, C., Dissing-Olesen, L., Giera, S., Young, A., Wysoker, A., Walker, A. J., Gergits, F., Segel, M., Nemesh, J., Marsh, S. E., Saunders, A., Macosko, E., Ginhoux, F., Chen, J., Franklin, R. J., Piao, X., McCarroll, S. A., and Stevens, B. (2019). Single-Cell RNA Sequencing of Microglia throughout the Mouse Lifespan and in the Injured Brain Reveals Complex Cell-State Changes. *Immunity*.

Hanisch, U. K. (2013). Functional diversity of microglia - How heterogeneous are they to begin with? *Frontiers in Cellular Neuroscience*, 7(MAY).

Hanisch, U. K. and Kettenmann, H. (2007). Microglia: Active sensor and versatile effector cells in the normal and pathologic brain. *Nature Neuroscience*, 10(11):1387–1394.

Hargrave, S. L., Jones, S., and Davidson, T. L. (2016). The outward spiral: a vicious cycle model of obesity and cognitive dysfunction. *Current Opinion in Behavioral Sciences*, 9:40–46.

Harik, N., Harik, S. I., Kuo, N. T., Sakai, K., Przybylski, R. J., and LaManna, J. C. (1996). Time-course and reversibility of the hypoxia-induced alterations in cerebral vascularity and cerebral capillary glucose transporter density. *Brain Research*, 737(1-2):335–338.

Hariri, N. and Thibault, L. (2010). High-fat diet-induced obesity in animal models. *Nutrition Research Reviews*, 23(2):270–299.

Hassan, A. M., Mancano, G., Kashofer, K., Fröhlich, E. E., Matak, A., Mayerhofer, R., Reichmann, F., Olivares, M., Neyrinck, A. M., Delzenne, N. M., Claus, S. P., and Holzer, P. (2018). High-fat diet induces depression-like behaviour in mice associated with changes in microbiome, neuropeptide Y, and brain metabolome. *Nutritional Neuroscience*, pages 1–17.

Hatfield, J. S., Millard, W. J., and Smith, C. J. (1974). Short-term influence of intra-ventromedial hypothalamic administration of insulin on feeding in normal and diabetic rats. *Pharmacology, Biochemistry and Behavior*, 2(2):223–226.

Havrankova, J., Roth, J., and Brownstein, M. (1978). Insulin receptors are widely distributed in the central nervous system of the rat. *Nature*, 272(5656):827–829.

Hawkins, B. T. and Davis, T. P. (2005). The blood-brain barrier/neurovascular unit in health and disease. *Pharmacological Reviews*, 57(2):173–185.

He, Y., Han, D., Shi, M., Sun, Z., Xie, J., Zhu, J., and Liu, Y. (2016). Effects of high-fat diet on the morphological characteristics of cerebral microvasculature without hyperlipidemia in Wistar rat. *International Journal of Clinical and Experimental Pathology*, 9(11):11752–11759.

Heindl, S., Gesierich, B., Benakis, C., Llovera, G., Duering, M., and Liesz, A. (2018). Automated Morphological Analysis of Microglia After Stroke. *Frontiers in Cellular Neuroscience*, 12.

Heyward, F. D., Walton, R. G., Carle, M. S., Coleman, M. A., Garvey, W. T., and Sweatt, J. D. (2012). Adult mice maintained on a high-fat diet exhibit object location memory deficits and reduced hippocampal SIRT1 gene expression. *Neurobiology of Learning and Memory*, 98(1):25–32.

Hierro-Bujalance, C., Bacskai, B. J., and Garcia-Alloza, M. (2018). In Vivo imaging of microglia with multiphoton microscopy. *Frontiers in Aging Neuroscience*, 10(JUL).

Hill, R. A., Tong, L., Yuan, P., Murikinati, S., Gupta, S., and Grutzendler, J. (2015). Regional Blood Flow in the Normal and Ischemic Brain Is Controlled by Arteriolar Smooth Muscle Cell Contractility and Not by Capillary Pericytes. *Neuron*, 87(1):95–110.

Hinwood, M., Tynan, R. J., Charnley, J. L., Beynon, S. B., Day, T. A., and Walker, F. R. (2013). Chronic stress induced remodeling of the prefrontal cortex: Structural re-organization of microglia and the inhibitory effect of minocycline. *Cerebral Cortex*, 23(8):1784–1797.

Hirunpattarasilp, C., Attwell, D., and Freitas, F. (2019). The role of pericytes in brain disorders: from the periphery to the brain. *Journal of Neurochemistry*, page jnc.14725.

Holtmaat, A., Bonhoeffer, T., Chow, D. K., Chuckowree, J., De Paola, V., Hofer, S. B., Hübener, M., Keck, T., Knott, G., Lee, W. C. A., Mostany, R., Mrsic-Flogel, T. D., Nedivi, E., Portera-Cailliau, C., Svoboda, K., Trachtenberg, J. T., and Wilbrecht, L. (2009). Long-term, high-resolution imaging in the mouse neocortex through a chronic cranial window. *Nature Protocols*, 4(8):1128–1144.

Hoogland, I. C. M., Westhoff, D., Engelen-Lee, J.-Y., Melief, J., Valls Serón, M., Houben-Weerts, J. H. M. P., Huitinga, I., van Westerloo, D. J., van der Poll, T., van Gool, W. A., and van de Beek, D. (2018). Microglial Activation After Systemic Stimulation With Lipopolysaccharide and Escherichia coli. *Frontiers in Cellular Neuroscience*, 12.

Hosford, P. S. and Gourine, A. V. (2019). What is the key mediator of the neurovascular coupling response? *Neuroscience and Biobehavioral Reviews*, 96:174–181.

Huang, T. T., Leu, D., and Zou, Y. (2015). Oxidative stress and redox regulation on hippocampal-dependent cognitive functions. *Archives of Biochemistry and Biophysics*, 576:2–7.

Huber, J. D., Egleton, R. D., and Davis, T. P. (2001). Molecular physiology and pathophysiology of tight junctions in the blood -brain barrier. *Trends in Neurosciences*, 24(12):719–725.

Hudetz, A. G., Feher, G., Weigle, C. G. M., Knuese, D. E., and Kampine, J. P. (1995). Video microscopy of cerebrocortical capillary flow: Response to hypotension and intracranial hypertension. *American Journal of Physiology - Heart and Circulatory Physiology*, 268(6 37-6).

Hunter, R. L., Choi, D. Y., Kincer, J. F., Cass, W. A., Bing, G., and Gash, D. M. (2007). Fenbendazole treatment may influence lipopolysaccharide effects in rat brain. *Comparative Medicine*.

Huo, B. X., Smith, J. B., and Drew, P. J. (2014). Neurovascular coupling and decoupling in the cortex during voluntary locomotion. *Journal of Neuroscience*, 34(33):10975–10981.

Hwang, L. L., Wang, C. H., Li, T. L., Chang, S. D., Lin, L. C., Chen, C. P., Chen, C. T., Liang, K. C., Ho, I. K., Yang, W. S., and Chiou, L. C. (2010). Sex differences in high-fat diet-induced obesity, metabolic alterations and learning, and synaptic plasticity deficits in mice. *Obesity*, 18(3):463–469.

Imai, T., Hieshima, K., Haskell, C., Baba, M., Nagira, M., Nishimura, M., Kakizaki, M., Takagi, S., Nomiyama, H., Schall, T. J., and Yoshie, O. (1997). Identification and molecular characterization of fractalkine receptor CX3CR1, which mediates both leukocyte migration and adhesion. *Cell*, 91(4):521–530.

Ingalls, A. M., Dickie, M. M., and Snell, G. D. (1950). Obese, a new mutation in the house mouse. *Journal of Heredity*, 41(12):315–317.

Itoh, Y. and Suzuki, N. (2012). Control of brain capillary blood flow. *Journal of Cerebral Blood Flow and Metabolism*, 32(7):1167–1176.

Jafarian, A., Litvak, V., Cagnan, H., Friston, K. J., and Zeidman, P. (2019). Neurovascular coupling: insights from multi-modal dynamic causal modelling of fMRI and MEG. *arXiv preprint*, (arXiv:1903.07478.).

Jais, A., Solas, M., Backes, H., Ferrara, N., Karsenty, G., and Bru, J. C. (2016). Myeloid-Cell-Derived VEGF Maintains Brain Glucose Uptake and Limits Cognitive Impairment in Obesity Article Myeloid-Cell-Derived VEGF Maintains Brain Glucose Uptake and Limits Cognitive Impairment in Obesity. *Cell*, 165(4):882–895.

Jankowsky, J. L. and Patterson, P. H. (1999). Cytokine and growth factor involvement in long-term potentiation. *Molecular and Cellular Neurosciences*, 14(4-5):273–286.

Jessen, L., Clegg, D. J., and Bouman, S. D. (2010). Evaluation of the lack of anorectic effect of intracerebroventricular insulin in rats. *American Journal of Physiology-Regulatory, Integrative and Comparative Physiology*, 298(1):R43–R50.

Johnson, J. D., O'Connor, K. A., Deak, T., Stark, M., Watkins, L. R., and Maier, S. F. (2002). Prior stressor exposure sensitizes LPS-induced cytokine production. *Brain, Behavior, and Immunity*, 16(4):461–476.

Jung, S., Aliberti, J., Graemmel, P., Sunshine, M. J., Kreutzberg, G. W., Sher, A., and Littman, D. R. (2000). Analysis of Fractalkine Receptor CX3CR1 Function by Targeted Deletion and Green Fluorescent Protein Reporter Gene Insertion. *Molecular and Cellular Biology*, 20(11):4106–4114.

Kaczmarczyk, M. M., Machaj, A. S., Chiu, G. S., Lawson, M. A., Gainey, S. J., York, J. M., Meling, D. D., Martin, S. A., Kwakwa, K. A., Newman, A. F., Woods, J. A., Kelley, K. W., Wang, Y., Miller, M. J., and Freund, G. G. (2013). Methylphenidate prevents high-fat diet (HFD)-induced learning/memory impairment in juvenile mice. *Psychoneuroendocrinology*, 38(9):1553–1564.

Kaiser, T. and Feng, G. (2019). Tmem119-EGFP and Tmem119-CreERT2 Transgenic Mice for Labeling and Manipulating Microglia. *eneuro*, 6(4):ENEURO.0448–18.2019.

Kalaria, R. N. (2012). Cerebrovascular disease and mechanisms of cognitive impairment: Evidence from clinicopathological studies in humans. *Stroke*, 43(9):2526–2534.

Kanoski, S. E. and Davidson, T. L. (2010). Different Patterns of Memory Impairments Accompany Short- and Longer-Term Maintenance on a High-Energy Diet. *Journal of Experimental Psychology: Animal Behavior Processes*, 36(2):313–319.

Kanoski, S. E., Zhang, Y., Zheng, W., and Davidson, T. L. (2010). The effects of a high-energy diet on hippocampal function and blood-brain barrier integrity in the rat. *Journal of Alzheimer's Disease*, 21(1):207–219.

Karperien, A. L. (2013). FracLac for ImageJ.

Keen, R. G., Macinnis, M. L., Guilhardi, P., Chamberland, K. A., and Church, R. M. (2005). The lack of behavioral effects of fenbendazole: A medication for pinworm infection. *Contemporary Topics in Laboratory Animal Science*.

Keller, D., Erö, C., and Markram, H. (2018). Cell Densities in the Mouse Brain: A Systematic Review. *Frontiers in Neuroanatomy*, 12.

Kesby, J. P., Kim, J. J., Scadeng, M., Woods, G., Kado, D. M., Olefsky, J. M., Jeste, D. V., Achim, C. L., and Semenova, S. (2015). Spatial cognition in adult and aged mice exposed to high-fat diet. *PLoS ONE*.

Kettenmann, H., Hanisch, U.-K., Noda, M., and Verkhratsky, A. (2011). Physiology of microglia. *Physiological reviews*, 91(2):461–553.

Kim, F., Pham, M., Maloney, E., Rizzo, N. O., Morton, G. J., Wisse, B. E., Kirk, E. A., Chait, A., and Schwartz, M. W. (2008). Vascular inflammation, insulin resistance, and reduced nitric oxide production precede the onset of peripheral insulin resistance. *Arteriosclerosis, Thrombosis, and Vascular Biology*, 28(11):1982–1988.

Kishi, T., Hirooka, Y., Nagayama, T., Isegawa, K., Katsuki, M., Takesue, K., and Sunagawa, K. (2015). Calorie restriction improves cognitive decline via up-regulation of brain-derived neurotrophic factor: Tropomyosin-related kinase B in hippocampus of obesity-induced hypertensive rats. *International Heart Journal*, 56(1):110–115.

Kisler, K., Nelson, A. R., Rege, S. V., Ramanathan, A., Wang, Y., Ahuja, A., Lazic, D., Tsai, P. S., Zhao, Z., Zhou, Y., Boas, D. A., Sakadžić, S., and Zlokovic, B. V. (2017). Pericyte degeneration leads to neurovascular uncoupling and limits oxygen supply to brain. *Nature neuroscience*, 20(3):406–416.

Klein, B., Kuschinsky, W., Schrock, H., and Vetterlein, F. (1986). Interdependency of local capillary density, blood flow, and metabolism in rat brains. *American Journal of Physiology - Heart and Circulatory Physiology*, 251(6):H1333–H1340.

Kleinridders, A., Ferris, H. A., Reyzer, M. L., Rath, M., Soto, M., Manier, M. L., Spraggins, J., Yang, Z., Stanton, R. C., Caprioli, R. M., and Kahn, C. R. (2018). Regional differences in brain glucose metabolism determined by imaging mass spectrometry. *Molecular Metabolism*, 12:113–121.

Knight, E. M., Martins, I. V., Gümüsgöz, S., Allan, S. M., and Lawrence, C. B. (2014). High-fat diet-induced memory impairment in triple-transgenic Alzheimer's disease (3xTgAD) mice isindependent of changes in amyloid and tau pathology. *Neurobiology of Aging*, 35(8):1821–1832.

Kolb, H., Stumvoll, M., Kramer, W., Kempf, K., and Martin, S. (2018). Insulin translates unfavourable lifestyle into obesity. *BMC Medicine*, 16(1):232.

Kolinko, Y., Krakorova, K., Cendelin, J., Tonar, Z., and Kralickova, M. (2014). Microcirculation of the brain: Morphological assessment in degenerative diseases and restoration processes. *Reviews in the Neurosciences*.

Kozlowski, C. and Weimer, R. M. (2012). An Automated Method to Quantify Microglia Morphology and Application to Monitor Activation State Longitudinally In Vivo. *PLoS ONE*, 7(2):e31814.

Laflamme, N. and Rivest, S. (2001). Toll-like receptor 4: The missing link of the cerebral innate immune response triggered by circulating gram-negative bacterial cell wall components. *FASEB Journal*, 15(1):155–163.

Langston, R. F. and Wood, E. R. (2010). Associative recognition and the hippocampus: Differential effects of hippocampal lesions on object-place, object-context and object-place-context memory. *Hippocampus*, 20(10):1139–1153.

Lapchak, P. A., Araujo, D. M., and Hefti, F. (1993). Systemic interleukin-1β decreases brain-derived neurotrophic factor messenger RNA expression in the rat hippocampal formation. *Neuroscience*, 53(2):297–301.

Lawson, L. J., Perry, V. H., Dri, P., and Gordon, S. (1990). Heterogeneity in the distribution and morphology of microglia in the normal adult mouse brain. *Neuroscience*.

Layé, S., Parnet, P., Goujon, E., and Dantzer, R. (1994). Peripheral administration of lipopolysaccharide induces the expression of cytokine transcripts in the brain and pituitary of mice. *Molecular Brain Research*, 27(1):157–162.

Le Couteur, D. G. and Lakatta, E. G. (2010). A Vascular Theory of Aging. *The Journals of Gerontology Series A: Biological Sciences and Medical Sciences*, 65A(10):1025–1027.

Lee, S., Varvel, N. H., Konerth, M. E., Xu, G., Cardona, A. E., Ransohoff, R. M., and Lamb, B. T. (2010). CX3CR1 deficiency alters microglial activation and reduces beta-amyloid deposition in two Alzheimer's disease mouse models. *American Journal of Pathology*.

Li, C., Jiang, Z., Lu, W., Arrick, D., McCarter, K., and Sun, H. (2016). Effect of obesity on early blood-brain barrier disruption following transient focal cerebral ischemia. *Obesity Science & Practice*, 2(1):58–68.

Li, J.-W., Zong, Y., Cao, X.-P., Tan, L., and Tan, L. (2018). Microglial priming in Alzheimer's disease. *Annals of Translational Medicine*, 6(10):176–176.

Li, W., Prakash, R., Chawla, D., Du, W., Didion, S. P., Filosa, J. A., Zhang, Q., Brann, D. W., Lima, V. V., Tostes, R. C., and Ergul, A. (2013). Early effects of high-fat diet on neurovascular function and focal ischemic brain injury. *American Journal of Physiology-Regulatory, Integrative and Comparative Physiology*, 304(11):R1001–R1008.

Liang, N.-C., Hajnal, A., and Norgren, R. (2006). Sham feeding corn oil increases accumbens dopamine in the rat. *American Journal of Physiology-Regulatory, Integrative and Comparative Physiology*, 291(5):R1236–R1239.

Lin, S., Thomas, T. C., Storlien, L. H., and Huang, X. F. (2000). Development of high fat diet-induced obesity and leptin resistance in C57B1/6J mice. *International Journal of Obesity*, 24(5):639–646.

Liu, Y., Fu, X., Lan, N., Li, S., Zhang, J., Wang, S., Li, C., Shang, Y., Huang, T., and Zhang, L. (2014). Luteolin protects against high fat diet-induced cognitive deficits in obesity mice. *Behavioural Brain Research*, 267:178–188.

Lizarbe, B., Soares, A. F., Larsson, S., and Duarte, J. M. (2019). Neurochemical modifications in the hippocampus, cortex and hypothalamus of mice exposed to long-term high-fat diet. *Frontiers in Neuroscience*, 13(JAN).

Longair, M. H., Baker, D. A., and Armstrong, J. D. (2011). Simple neurite tracer: Open source software for reconstruction, visualization and analysis of neuronal processes. *Bioinformatics*, 27(17):2453–2454.

Lowe, C. J., Reichelt, A. C., and Hall, P. A. (2019). The Prefrontal Cortex and Obesity: A Health Neuroscience Perspective. *Trends in Cognitive Sciences*, 23(4):349–361.

Lugo-Hernandez, E., Squire, A., Hagemann, N., Brenzel, A., Sardari, M., Schlechter, J., Sanchez-Mendoza, E. H., Gunzer, M., Faissner, A., and Hermann, D. M. (2017). 3D visualization and quantification of microvessels in the whole ischemic mouse brain using solvent-based clearing and light sheet microscopy. *Journal of Cerebral Blood Flow and Metabolism*, 37(10):3355–3367.

Lull, M. E. and Block, M. L. (2010). Microglial Activation and Chronic Neurodegeneration. *Neurotherapeutics*, 7(4):354–365.

Lumeng, C. N. and Saltiel, A. R. (2011). Review series Inflammatory links between obesity and metabolic disease. *Life Sciences*, 121(6):2111–2117.

Luppino, F. S., De Wit, L. M., Bouvy, P. F., Stijnen, T., Cuijpers, P., Penninx, B. W., and Zitman, F. G. (2010). Overweight, obesity, and depression: A systematic review and meta-analysis of longitudinal studies.

Lynch, M. A. (2015). Neuroinflammatory changes negatively impact on LTP: A focus on IL-1β. *Brain Research*, 1621:197–204.

Madore, C., Joffre, C., Delpech, J., De Smedt-Peyrusse, V., Aubert, A., Coste, L., Layé, S., and Nadjar, A. (2013). Early morphofunctional plasticity of microglia in response to acute lipopolysaccharide. *Brain, Behavior, and Immunity*, 34:151–158.

Madore, C., Nadjar, A., Delpech, J. C., Sere, A., Aubert, A., Portal, C., Joffre, C., and Layé, S. (2014). Nutritional n-3 PUFAs deficiency during perinatal periods alters brain innate immune system and neuronal plasticity-associated genes. *Brain, Behavior, and Immunity*, 41(1):22–31.

Magezi, D. A. (2015). Linear mixed-effects models for within-participant psychology experiments: An introductory tutorial and free, graphical user interface (LMMgui). *Frontiers in Psychology*, 6(JAN).

Mainardi, M., Spinelli, M., Scala, F., Mattera, A., Fusco, S., D'Ascenzo, M., and Grassi, C. (2017). Loss of Leptin-Induced Modulation of Hippocampal Synaptic Trasmission and Signal Transduction in High-Fat Diet-Fed Mice. *Frontiers in Cellular Neuroscience*, 11.

Maness, L. M., Banks, W. A., and Kastin, A. J. (2000). Persistence of blood-to-brain transport of leptin in obese leptin-deficient and leptin receptor-deficient mice. *Brain Research*, 873(1):165–167.

Maric, T., Woodside, B., and Luheshi, G. N. (2014). The effects of dietary saturated fat on basal hypothalamic neuroinflammation in rats. *Brain, Behavior, and Immunity*, 36:35–45.

Masuda, T., Sankowski, R., Staszewski, O., Böttcher, C., Amann, L., Sagar, Scheiwe, C., Nessler, S., Kunz, P., van Loo, G., Coenen, V. A., Reinacher, P. C., Michel, A., Sure, U., Gold, R., Grün, D., Priller, J., Stadelmann, C., and Prinz, M. (2019). Spatial and temporal heterogeneity of mouse and human microglia at single-cell resolution. *Nature*.

Mato, M., Ookawara, S., Sakamoto, A., Aikawa, E., Ogawa, T., Mitsuhashi, U., Masuzawa, T., Suzuki, H., Honda, M., Yazaki, Y., Watanabe, E., Luoma, J., Yla-Herttuala, S., Fraser, I., Gordon, S., and Kodama, T. (1996). Involvement of specific macrophage-lineage cells surrounding arterioles in barrier and scavenger function in brain cortex. *Proceedings of the National Academy of Sciences*, 93(8):3269–3274.

McLean, F. H., Grant, C., Morris, A. C., Horgan, G. W., Polanski, A. J., Allan, K., Campbell, F. M., Langston, R. F., and Williams, L. M. (2018). Rapid and reversible impairment of episodic memory by a high-fat diet in mice. *Scientific Reports*, 8(1):11976.

Mendes, N. F., Kim, Y. B., Velloso, L. A., and Araújo, E. P. (2018). Hypothalamic microglial activation in obesity: A mini-review. *Frontiers in Neuroscience*, 12(NOV).

Michaelis, E. K. (2012). Selective Neuronal Vulnerability in the Hippocampus: Relationship to Neurological Diseases and Mechanisms for Differential Sensitivity of Neurons to Stress. In *The Clinical Neurobiology of the Hippocampus: An Integrative view*, pages 54–76. Oxford University Press.

Milanski, M., Degasperi, G., Coope, A., Morari, J., Denis, R., Cintra, D. E., Tsukumo, D. M., Anhe, G., Amaral, M. E., Takahashi, H. K., Curi, R., Oliveira, H. C., Carvalheira, J. B., Bordin, S., Saad, M. J., and Velloso, L. A. (2009). Saturated fatty acids produce an inflammatory response predominantly through the activation of TLR4 signaling in hypothalamus: Implications for the pathogenesis of obesity. *Journal of Neuroscience*, 29(2):359–370.

Miller, A. A. and Spencer, S. J. (2014). Obesity and neuroinflammation: A pathway to cognitive impairment. *Brain, Behavior, and Immunity*, 42:10–21.

Mittal, M., Siddiqui, M. R., Tran, K., Reddy, S. P., and Malik, A. B. (2014). Reactive oxygen species in inflammation and tissue injury. *Antioxidants and Redox Signaling*, 20(7):1126–1167.

Miyamoto, A., Wake, H., Ishikawa, A. W., Eto, K., Shibata, K., Murakoshi, H., Koizumi, S., Moorhouse, A. J., Yoshimura, Y., and Nabekura, J. (2016). Microglia contact induces synapse formation in developing somatosensory cortex. *Nature Communications*, 7(1):12540.

Molteni, R., Barnard, R. J., Ying, Z., Roberts, C. K., and Gómez-Pinilla, F. (2002). A high-fat, refined sugar diet reduces hippocampal brain-derived neurotrophic factor, neuronal plasticity, and learning. *Neuroscience*, 112(4):803–814.

Molteni, R., Wu, A., Vaynman, S., Ying, Z., Barnard, R. J., and Gómez-Pinilla, F. (2004). Exercise reverses the harmful effects of consumption of a high-fat diet on synaptic and behavioral plasticity associated to the action of brain-derived neurotrophic factor. *Neuroscience*, 123(2):429–440.

Morabito, M. V., Ravussin, Y., Mueller, B. R., Skowronski, A. A., Watanabe, K., Foo, K. S., Lee, S. X., Lehmann, A., Hjorth, S., Zeltser, L. M., LeDuc, C. A., and Leibel, R. L. (2017). Weight perturbation alters leptin signal transduction in a region-specific manner throughout the brain. *PLoS ONE*, 12(1):e0168226.

Morari, J., Anhe, G. F., Nascimento, L. F., De Moura, R. F., Razolli, D., Solon, C., Guadagnini, D., Souza, G., Mattos, A. H., Tobar, N., Ramos, C. D., Pascoal, V. D., Saad, M. J., Lopes-Cendes, I., Moraes, J. C., and Velloso, L. A. (2014). Fractalkine (CX3CL1) is involved in the early activation of hypothalamic inflammation in experimental obesity. *Diabetes*, 63(11):3770–3784.

Morioka, T., Mori, K., Motoyama, K., and Emoto, M. (2016). Ectopic Fat Accumulation and Glucose Homeostasis: Role of Leptin in Glucose and Lipid Metabolism and Mass Maintenance in Skeletal Muscle. In *Musculoskeletal Disease Associated with Diabetes Mellitus*, pages 201–213. Springer Japan, Tokyo.

Morrison, C. D., Pistell, P. J., Ingram, D. K., Johnson, W. D., Liu, Y., Fernandez-Kim, S. O., White, C. L., Purpera, M. N., Uranga, R. M., Bruce-Keller, A. J., and Keller, J. N. (2010). High fat diet increases hippocampal oxidative stress and cognitive impairment in aged mice: Implications for decreased Nrf2 signaling. *Journal of Neurochemistry*, 114(6):1581–1589.

Mumby, D. G., Gaskin, S., Glenn, M. J., Schramek, T. E., and Lehmann, H. (2002). Hippocampal damage and exploratory preferences in rats: Memory for objects, places, and contexts. *Learning and Memory*, 9(2):49–57.

Myers, M. G., Cowley, M. A., and Münzberg, H. (2008). Mechanisms of Leptin Action and Leptin Resistance. *Annual Review of Physiology*, 70(1):537–556.

Nation, D. A., Sweeney, M. D., Montagne, A., Sagare, A. P., D'Orazio, L. M., Pachicano, M., Sepehrband, F., Nelson, A. R., Buennagel, D. P., Harrington, M. G., Benzinger, T. L., Fagan, A. M., Ringman, J. M., Schneider, L. S., Morris, J. C., Chui, H. C., Law, M., Toga, A. W., and Zlokovic, B. V. (2019). Blood–brain barrier breakdown is an early biomarker of human cognitive dysfunction. *Nature Medicine*, 25(2):270–276.

Nebeling, F. C., Poll, S., Schmid, L. C., Mittag, M., Steffen, J., Keppler, K., and Fuhrmann, M. (2019). Microglia motility depends on neuronal activity and promotes structural plasticity in the hippocampus. *bioRxiv*.

Neubauer, A. C. and Fink, A. (2009). Intelligence and neural efficiency. *Neuroscience and Biobehavioral Reviews*, 33(7):1004–1023.

Ng, T., Graham, D. I., Adams, J. H., and Ford, I. (1989). Changes in the hippocampus and the cerebellum resulting from hypoxic insults: frequency and distribution. *Acta Neuropathologica*, 78(4):438–443.

Niell, C. M. and Stryker, M. P. (2008). Highly selective receptive fields in mouse visual cortex. *Journal of Neuroscience*, 28(30):7520–7536.

Niell, C. M. and Stryker, M. P. (2010). Modulation of Visual Responses by Behavioral State in Mouse Visual Cortex. *Neuron*, 65(4):472–479.

Nikolakopoulou, A. M., Zhao, Z., Montagne, A., and Zlokovic, B. V. (2017). Regional early and progressive loss of brain pericytes but not vascular smooth muscle cells in adult mice with disrupted platelet-derived growth factor receptor-β signaling. *PLOS ONE*, 12(4):e0176225.

Nimmerjahn, A., Kirchhoff, F., and Helmchen, F. (2005). Neuroscience: Resting microglial cells are highly dynamic surveillants of brain parenchyma in vivo. *Science*, 308(5726):1314–1318.

Norden, D. M. and Godbout, J. P. (2013). Review: Microglia of the aged brain: Primed to be activated and resistant to regulation. *Neuropathology and Applied Neurobiology*, 39(1):19–34.

Nortley, R., Korte, N., Izquierdo, P., Hirunpattarasilp, C., Mishra, A., Jaunmuktane, Z., Kyrargyri, V., Pfeiffer, T., Khennouf, L., Madry, C., Gong, H., Richard-Loendt, A., Huang, W., Saito, T., Saido, T. C., Brandner, S., Sethi, H., and Attwell, D. (2019). Amyloid β oligomers constrict human capillaries in alzheimer's disease via signaling to pericytes. *Science*, 365(6450):eaav9518.

Nunes-Souza, V., César-Gomes, C. J., Da Fonseca, L. J. S., Da Silva Guedes, G., Smaniotto, S., and Rabelo, L. A. (2016). Aging Increases Susceptibility to High Fat Diet-Induced Metabolic Syndrome in C57BL/6 Mice: Improvement in Glycemic and Lipid Profile after Antioxidant Therapy. *Oxidative Medicine and Cellular Longevity*.

Obadia, N., Lessa, M. A., Daliry, A., Silvares, R. R., Gomes, F., Tibiriçá, E., and Estato, V. (2017). Cerebral microvascular dysfunction in metabolic syndrome is exacerbated by ischemia–reperfusion injury. *BMC Neuroscience*, 18(1):67.

Otsu, N. (1979). A Threshold Selection Method from Gray-Level Histograms. *IEEE Transactions on Systems, Man, and Cybernetics*, 9(1):62–66.

Ouyang, S., Hsuchou, H., Kastin, A. J., Wang, Y., Yu, C., and Pan, W. (2014). Diet-induced obesity suppresses expression of many proteins at the blood-brain barrier. *Journal of Cerebral Blood Flow and Metabolism*, 34(1):43–51.

Pallebage-Gamarallage, M., Lam, V., Takechi, R., Galloway, S., Clark, K., and Mamo, J. (2012). Restoration of dietary-fat induced blood–brain barrier dysfunction by anti-inflammatory lipid-modulating agents. *Lipids in Health and Disease*, 11(1):117.

Paolicelli, R. C. and Ferretti, M. T. (2017). Function and Dysfunction of Microglia during Brain Development: Consequences for Synapses and Neural Circuits. *Frontiers in Synaptic Neuroscience*, 9(MAY).

Paris, I., Savage, J. C., Escobar, L., Abiega, O., Gagnon, S., Hui, C. W., Tremblay, M. È., Sierra, A., and Valero, J. (2018). ProMoIJ: A new tool for automatic three-dimensional analysis of microglial process motility. *Glia*, 66(4):828–845.

Park, K., Yasuda, N., Toyonaga, S., Yamada, S. M., Nakabayashi, H., Nakasato, M., Nakagomi, T., Tsubosaki, E., and Shimizu, K. (2007a). Significant association between leukoaraiosis and metabolic syndrome in healthy subjects. *Neurology*, 69(10):974–978.

Park, L., Anrather, J., Girouard, H., Zhou, P., and Iadecola, C. (2007b). Nox2-derived reactive oxygen species mediate neurovascular dysregulation in the aging mouse brain. *Journal of Cerebral Blood Flow and Metabolism*, 27(12):1908–1918.

Parnet, P., Kelley, K. W., Bluthé, R. M., and Dantzer, R. (2002). Expression and regulation of interleukin-1 receptors in the brain. Role in cytokines-induced sickness behavior. *Journal of Neuroimmunology*, 125(1-2):5–14.

Patt, S., Sampaolo, S., Théallier-Jankó, Á., Tschairkin, I., and Cervós-Navarro, J. (1997). Cerebral angiogenesis triggered by severe chronic hypoxia displays regional differences. *Journal of Cerebral Blood Flow and Metabolism*, 17(7):801–806.

Peppiatt, C. M., Howarth, C., Mobbs, P., and Attwell, D. (2006). Bidirectional control of CNS capillary diameter by pericytes. *Nature*, 443(7112):700–704.

Perry, V. H. and Holmes, C. (2014). Microglial priming in neurodegenerative disease. *Nature Reviews Neurology*, 10(4):217–224.

Phillips, S. A., Sylvester, F. A., and Frisbee, J. C. (2005). Oxidant stress and constrictor reactivity impair cerebral artery dilation in obese Zucker rats. *American Journal of Physiology-Regulatory, Integrative and Comparative Physiology*, 288(2):R522–R530.

Pi-Sunyer, F., Becker, D., Bouchard, C., Carleton, R., Colditz, G., Dietz, W., and Higgins, M. (1998). Clinical guidelines on the identification, evaluation, and treatment of overweight and obesity in adults: executive summary. Expert Panel on the Identification, Evaluation, and Treatment of Overweight in Adults. *The American Journal of Clinical Nutrition*, 68(4):899–917.

Pisauro, M. A., Dhruv, N. T., Carandini, M., and Benucci, A. (2013). Fast Hemodynamic Responses in the Visual Cortex of the Awake Mouse. *Journal of Neuroscience*, 33(46):18343–18351.

Piskunov, A., Stepanichev, M., Tishkina, A., Novikova, M., Levshina, I., and Gulyaeva, N. (2016). Chronic combined stress induces selective and long-lasting inflammatory response evoked by changes in corticosterone accumulation and signaling in rat hippocampus. *Metabolic Brain Disease*, 31(2):445–454.

Pistell, P. J., Morrison, C. D., Gupta, S., Knight, A. G., Keller, J. N., Ingram, D. K., and Bruce-Keller, A. J. (2010). Cognitive impairment following high fat diet consumption is associated with brain inflammation. *Journal of Neuroimmunology*, 219(1-2):25–32.

Pohl, J., Woodside, B., and Luheshi, G. N. (2009). Changes in hypothalamically mediated acute-phase inflammatory responses to lipopolysaccharide in diet-induced obese rats. *Endocrinology*, 150(11):4901–4910.

Polyák, Á., Ferenczi, S., Dénes, Á., Winkler, Z., Kriszt, R., Pintér-Kübler, B., and Kovács, K. J. (2014). The fractalkine/Cx3CR1 system is implicated in the development of metabolic visceral adipose tissue inflammation in obesity. *Brain, Behavior, and Immunity*.

Posey, K. A., Clegg, D. J., Printz, R. L., Byun, J., Morton, G. J., Vivekanandan-Giri, A., Pennathur, S., Baskin, D. G., Heinecke, J. W., Woods, S. C., Schwartz, M. W., and Niswender, K. D. (2009). Hypothalamic proinflammatory lipid accumulation, inflammation, and insulin resistance in rats fed a high-fat diet. *American Journal of Physiology - Endocrinology and Metabolism*, 296(5):E1003–E1012.

Price, T. O., Eranki, V., Banks, W. A., Ercal, N., and Shah, G. N. (2012). Topiramate treatment protects blood-brain barrier pericytes from hyperglycemia-induced oxidative damage in diabetic mice. *Endocrinology*, 153(1):362–372.

Pritchett, K. R. and Johnston, N. A. (2002). A Review of Treatments for the Eradication of Pinworm Infections from Laboratory Rodent Colonies.

Purves, D., Augustine, G., Fitzpatrick, D., Katz, L., LaMantia, A.-S., McNamara, J., and Williams, M. (2001). *Neuroscience. 2nd edition*.

R Core Team (2013). R: A Language and Environment for Statistical Computing. *R Foundation for Statistical Computing; Vienna, Austria*.

R Studio Team (2015). RStudio: Integrated Development Environment for R. *RStudio, Inc., Boston, MA*.

Rahner-Welsch, S., Vogel, J., and Kuschinsky, W. (1995). Regional congruence and divergence of glucose transporters (GLUT1) and capillaries in rat brains. *Journal of Cerebral Blood Flow and Metabolism*, 15(4):681–686.

Ramp, A. A., Hall, C., and Orian, J. M. (2010). Strain-related effects of fenbendazole treatment on murine experimental autoimmune encephalomyelitis. *Laboratory Animals*.

Ramsaran, A. I., Westbrook, S. R., and Stanton, M. E. (2016). Ontogeny of object-in-context recognition in the rat. *Behavioural Brain Research*.

Reaven, G. M. (2005). The Insulin Resistance Syndrome: Definition and Dietary Approaches to Treatment. *Annual Review of Nutrition*, 25(1):391–406.

Rijnsburger, M., Unmehopa, U. A., Eggels, L., Serlie, M. J., and la Fleur, S. E. (2019). One-week exposure to a free-choice high-fat high-sugar diet does not disrupt blood–brain barrier permeability in fed or overnight fasted rats. *Nutritional Neuroscience*, 22(8):541–550.

Rodríguez, E. M., Blázquez, J. L., and Guerra, M. (2010). The design of barriers in the hypothalamus allows the median eminence and the arcuate nucleus to enjoy private milieus: The former opens to the portal blood and the latter to the cerebrospinal fluid. *Peptides*, 31(4):757–776.

Rogers, J. T., Morganti, J. M., Bachstetter, A. D., Hudson, C. E., Peters, M. M., Grimmig, B. A., Weeber, E. J., Bickford, P. C., and Gemma, C. (2011). CX3CR1 deficiency leads to impairment of hippocampal cognitive function and synaptic plasticity. *Journal of Neuroscience*, 31(45):16241–16250.

Romanatto, T., Cesquini, M., Amaral, M. E., Roman, É. A., Moraes, J. C., Torsoni, M. A., Cruz-Neto, A. P., and Velloso, L. A. (2007). TNF-α acts in the hypothalamus inhibiting food intake and increasing the respiratory quotient-Effects on leptin and insulin signaling pathways. *Peptides*, 28(5):1050–1058.

Rosenegger, D. G., Tran, C. H. T., Wamsteeker Cusulin, J. I., and Gordon, G. R. (2015). Tonic local brain blood flow control by astrocytes independent of phasic neurovascular coupling. *Journal of Neuroscience*, 35(39):13463–13474.

Rummel, C., Inoue, W., Poole, S., and Luheshi, G. N. (2010). Leptin regulates leukocyte recruitment into the brain following systemic lps-induced inflammation. *Molecular Psychiatry*.

Ryu, J. K. and McLarnon, J. G. (2009). A leaky blood-brain barrier, fibrinogen infiltration and microglial reactivity in inflamed Alzheimer's disease brain. *Journal of Cellular and Molecular Medicine*, 13(9 A):2911–2925.

Saederup, N., Cardona, A. E., Croft, K., Mizutani, M., Cotleur, A. C., Tsou, C. L., Ransohoff, R. M., and Charo, I. F. (2010). Selective chemokine receptor usage by central nervous system myeloid cells in CCR2-red fluorescent protein knock-in mice. *PLoS ONE*, 5(10):e13693.

Saijo, K., Winner, B., Carson, C. T., Collier, J. G., Boyer, L., Rosenfeld, M. G., Gage, F. H., and Glass, C. K. (2009). A Nurr1/CoREST Pathway in Microglia and Astrocytes Protects Dopaminergic Neurons from Inflammation-Induced Death. *Cell*, 137(1):47–59.

Salameh, T. S., Mortell, W. G., Logsdon, A. F., Butterfield, D. A., and Banks, W. A. (2019). Disruption of the hippocampal and hypothalamic blood-brain barrier in a diet-induced obese model of type II diabetes: Prevention and treatment by the mitochondrial carbonic anhydrase inhibitor, topiramate. *Fluids and Barriers of the CNS*, 16(1):1.

Sandoval-Salazar, C., Ramírez-Emiliano, J., Trejo-Bahena, A., Oviedo-Solís, C. I., and Solís-Ortiz, M. S. (2016). A high-fat diet decreases GABA concentration in the frontal cortex and hippocampus of rats. *Biological Research*, 49(1):15.

Saunders, N. R., Dziegielewska, K. M., Møllgård, K., and Habgood, M. D. (2015). Markers for

blood-brain barrier integrity: how appropriate is Evans blue in the twenty-first century and what are the alternatives? *Frontiers in Neuroscience*, 9(OCT).

Schindelin, J., Arganda-Carreras, I., Frise, E., Kaynig, V., Longair, M., Pietzsch, T., Preibisch, S., Rueden, C., Saalfeld, S., Schmid, B., Tinevez, J. Y., White, D. J., Hartenstein, V., Eliceiri, K., Tomancak, P., and Cardona, A. (2012). Fiji: An open-source platform for biological-image analysis.

Schuster, F., Huber, G., Stölting, I., Wing, E. E., Saar, K., Hübner, N., Banks, W. A., and Raasch, W. (2018). Telmisartan prevents diet-induced obesity and preserves leptin transport across the blood-brain barrier in high-fat diet-fed mice. *Pflügers Archiv - European Journal of Physiology*, 470(11):1673–1689.

Schwaninger, R. M., Sun, H., and Mayhan, W. G. (2003). Impaired nitric oxide synthase-dependent dilatation of cerebral arterioles in type II diabetic rats. *Life sciences*, 73(26):3415–25.

Scott, M. M., Lachey, J. L., Sternson, S. M., Lee, C. E., Elias, C. F., Friedman, J. M., and Elmquist, J. K. (2009). Leptin targets in the mouse brain. *Journal of Comparative Neurology*, 514(5):518–532.

Shah, G. N., Price, T. O., Banks, W. A., Morofuji, Y., Kovac, A., Ercal, N., Sorenson, C. M., Shin, E. S., and Sheibani, N. (2013). Pharmacological inhibition of mitochondrial carbonic anhydrases protects mouse cerebral pericytes from high glucose-induced oxidative stress and apoptosis. *Journal of Pharmacology and Experimental Therapeutics*, 344(3):637–645.

Shah, R., O'Neill, S. M., Hinkle, C., Caughey, J., Stephan, S., Lynch, E., Bermingham, K., Lynch, G., Ahima, R. S., and Reilly, M. P. (2015). Metabolic effects of CX3CR1 deficiency in diet-induced obese mice. *PLoS ONE*, 10(9):e0138317.

Sipe, G. O., Lowery, R. L., Tremblay, M.-È., Kelly, E. A., Lamantia, C. E., and Majewska, A. K. (2016). Microglial P2Y12 is necessary for synaptic plasticity in mouse visual cortex. *Nature Communications*, 7(1):10905.

Sirois-Gagnon, D., Chamberland, A., Perron, S., Brisson, D., Gaudet, D., and Laprise, C. (2011). Association of common polymorphisms in the fractalkine receptor (CX3CR1) with obesity. *Obesity*.

Sirotin, Y. B., Hillman, E. M., Bordier, C., and Das, A. (2009). Spatiotemporal precision and hemodynamic mechanism of optical point spreads in alert primates. *Proceedings of the National Academy of Sciences of the United States of America*, 106(43):18390–18395.

Sloan, H. L., Austin, V. C., Blamire, A. M., Schnupp, J. W., Lowe, A. S., Allers, K. A., Matthews, P. M., and Sibson, N. R. (2010). Regional differences in neurovascular coupling in rat brain as determined by fMRI and electrophysiology. *NeuroImage*, 53(2):399–411.

Smith, A. G., Sheridan, P. A., Harp, J. B., and Beck, M. A. (2007). Diet-Induced Obese Mice Have Increased Mortality and Altered Immune Responses When Infected with Influenza Virus. *The Journal of Nutrition*, 137(5):1236–1243.

Sobesky, J. L., Barrientos, R. M., De May, H. S., Thompson, B. M., Weber, M. D., Watkins, L. R., and Maier, S. F. (2014). High-fat diet consumption disrupts memory and primes elevations in hippocampal IL-1β, an effect that can be prevented with dietary reversal or IL-1 receptor antagonism. *Brain, Behavior, and Immunity*, 42:22–32.

Sobesky, J. L., D'Angelo, H. M., Weber, M. D., Anderson, N. D., Frank, M. G., Watkins, L. R., Maier, S. F., and Barrientos, R. M. (2016). Glucocorticoids Mediate Short-Term High-Fat Diet Induction of Neuroinflammatory Priming, the NLRP3 Inflammasome, and the Danger Signal HMGB1. *eneuro*, 3(4):ENEURO.0113–16.2016.

Sorop, O., Olver, T. D., van de Wouw, J., Heinonen, I., van Duin, R. W., Duncker, D. J., and Merkus, D. (2017). The microcirculation: a key player in obesity-associated cardiovascular disease. *Cardiovascular Research*, 113(9):1035–1045.

Soto, I., Graham, L. C., Richter, H. J., Simeone, S. N., Radell, J. E., Grabowska, W., Funkhouser, W. K., Howell, M. C., and Howell, G. R. (2015). APOE Stabilization by Exercise Prevents Aging Neurovascular Dysfunction and Complement Induction. *PLoS Biology*, 13(10):1–33.

Souza, A. C. P., Souza, C. M., Amaral, C. L., Lemes, S. F., Santucci, L. F., Milanski, M., Torsoni, A. S., and Torsoni, M. A. (2019). Short-term high-fat diet consumption reduces hypothalamic expression of the nicotinic acetylcholine receptor α7 subunit (α7nAChR) and affects the anti-inflammatory response in a mouse model of sepsis. *Frontiers in Immunology*, 10(MAR).

Spanswick, S. C. and Dyck, R. H. (2012). Object/Context Specific Memory Deficits following Medial Frontal Cortex Damage in Mice. *PLoS ONE*, 7(8):e43698.

Speakman, J. R. (2019). Use of high-fat diets to study rodent obesity as a model of human obesity.

Spencer, S. J., Basri, B., Sominsky, L., Soch, A., Ayala, M. T., Reineck, P., Gibson, B. C., and Barrientos, R. M. (2019). High-fat diet worsens the impact of aging on microglial function and morphology in a region-specific manner. *Neurobiology of Aging*, 74:121–134.

Stowell, R. D., Sipe, G. O., Dawes, R. P., Batchelor, H. N., Lordy, K. A., Bidlack, J. M., Brown, E., Sur, M., Majewska, A. K., Grayson O., S., Ryan P., D., Hanna N, B., A., K., Lordy, Jean M., B., Edward, B., Mriganka, S., and Ania K., M. (2019). Noradrenergic signaling in wakeful states inhibits microglial surveillance and synaptic plasticity in the mouse visual cortex. *bioRxiv*.

Stranahan, A. M., Norman, E. D., Lee, K., Cutler, R. G., Telljohann, R. S., Egan, J. M., and Mattson, M. P. (2008). Diet-induced insulin resistance impairs hippocampal synaptic plasticity and cognition in middle-aged rats. *Hippocampus*, 18(11):1085–1088.

Stratoulias, V., Venero, J. L., Tremblay, M., and Joseph, B. (2019). Microglial subtypes: diversity within the microglial community. *The EMBO Journal*, 38(17).

Suzuki, M., Kawagoe, T., Nishiguchi, S., Abe, N., Otsuka, Y., Nakai, R., Asano, K., Yamada, M., Yoshikawa, S., and Sekiyama, K. (2018). Neural Correlates of Working Memory Maintenance in Advanced Aging: Evidence From fMRI. *Frontiers in Aging Neuroscience*, 10.

Sweeney, M. D., Ayyadurai, S., and Zlokovic, B. V. (2016). Pericytes of the neurovascular unit: Key functions and signaling pathways. *Nature Neuroscience*, 19(6):771–783.

Sweeney, M. D., Kisler, K., Montagne, A., Toga, A. W., and Zlokovic, B. V. (2018). The role of brain vasculature in neurodegenerative disorders.

Sweeney, P. and Yang, Y. (2015). An excitatory ventral hippocampus to lateral septum circuit that suppresses feeding. *Nature Communications*, 6(1):10188.

Takechi, R., Pallebage-Gamarallage, M. M., Lam, V., Giles, C., and Mamo, J. C. (2013). Nutraceutical agents with anti-inflammatory properties prevent dietary saturated-fat induced disturbances in blood–brain barrier function in wild-type mice. *Journal of Neuroinflammation*, 10(1):842.

Takimoto, M. and Hamada, T. (2014). Acute exercise increases brain region-specific expression of MCT1, MCT2, MCT4, GLUT1, and COX IV proteins. *Journal of Applied Physiology*, 116(9):1238–1250.

Tay, T. L., Savage, J. C., Hui, C. W., Bisht, K., and Tremblay, M. È. (2017). Microglia across the lifespan: from origin to function in brain development, plasticity and cognition. *Journal of Physiology*, 595(6):1929–1945.

Thaler, J. P., Yi, C. X., Schur, E. A., Guyenet, S. J., Hwang, B. H., Dietrich, M. O., Zhao, X., Sarruf, D. A., Izgur, V., Maravilla, K. R., Nguyen, H. T., Fischer, J. D., Matsen, M. E., Wisse,

B. E., Morton, G. J., Horvath, T. L., Baskin, D. G., Tschop, M. H., and Schwartz, M. W. (2012). Obesity is associated with hypothalamic injury in rodents and humans. *Journal of Clinical Investigation*, 122(1):153–162.

Thévenaz, P., Ruttimann, U. E., and Unser, M. (1998). A pyramid approach to subpixel registration based on intensity. *IEEE Transactions on Image Processing*, 7(1):27–41.

Thirumangalakudi, L., Prakasam, A., Zhang, R., Bimonte-Nelson, H., Sambamurti, K., Kindy, M. S., and Bhat, N. R. (2008). High cholesterol-induced neuroinflammation and amyloid precursor protein processing correlate with loss of working memory in mice. *Journal of Neurochemistry*, 106(1):475–485.

Todorov, M. I., Paetzold, J. C., Schoppe, O., Tetteh, G., Efremov, V., Völgyi, K., Düring, M., Dichgans, M., Piraud, M., Menze, B., and Ertürk, A. (2019). Automated analysis of whole brain vasculature using machine learning. *bioRxiv*.

Torres-Platas, S. G., Comeau, S., Rachalski, A., Bo, G., Cruceanu, C., Turecki, G., Giros, B., and Mechawar, N. (2014). Morphometric characterization of microglial phenotypes in human cerebral cortex. *Journal of Neuroinflammation*, 11(1):12.

Toth, P., Tarantini, S., Tucsek, Z., Ashpole, N. M., Sosnowska, D., Gautam, T., Ballabh, P., Koller, A., Sonntag, W. E., Csiszar, A., and Ungvari, Z. (2014). Resveratrol treatment rescues neurovascular coupling in aged mice: role of improved cerebromicrovascular endothelial function and downregulation of NADPH oxidase. *American Journal of Physiology-Heart and Circulatory Physiology*, 306(3):H299–H308.

Tracy, A. L., Wee, C. J., Hazeltine, G. E., and Carter, R. A. (2015). Characterization of attenuated food motivation in high-fat diet-induced obesity: Critical roles for time on diet and reinforcer familiarity. *Physiology and Behavior*.

Trost, A., Lange, S., Schroedl, F., Bruckner, D., Motloch, K. A., Bogner, B., Kaser-Eichberger, A., Strohmaier, C., Runge, C., Aigner, L., Rivera, F. J., and Reitsamer, H. A. (2016). Brain and retinal pericytes: Origin, function and role. *Frontiers in Cellular Neuroscience*, 10(FEB).

Tucsek, Z., Toth, P., Sosnowska, D., Gautam, T., Mitschelen, M., Koller, A., Szalai, G., Sonntag, W. E., Ungvari, Z., and Csiszar, A. (2014a). Obesity in Aging Exacerbates Blood-Brain Barrier Disruption, Neuroinflammation, and Oxidative Stress in the Mouse Hippocampus: Effects on Expression of Genes Involved in Beta-Amyloid Generation and Alzheimer's Disease. *The Journals of Gerontology Series A: Biological Sciences and Medical Sciences*, 69(10):1212–1226.

Tucsek, Z., Toth, P., Tarantini, S., Sosnowska, D., Gautam, T., Warrington, J. P., Giles, C. B., Wren, J. D., Koller, A., Ballabh, P., Sonntag, W. E., Ungvari, Z., and Csiszar, A. (2014b). Aging Exacerbates Obesity-induced Cerebromicrovascular Rarefaction, Neurovascular Uncoupling, and Cognitive Decline in Mice. *The Journals of Gerontology Series A: Biological Sciences and Medical Sciences*, 69(11):1339–1352.

Valdearcos, M., Douglass, J. D., Robblee, M. M., Dorfman, M. D., Stifler, D. R., Bennett, M. L., Gerritse, I., Fasnacht, R., Barres, B. A., Thaler, J. P., and Koliwad, S. K. (2017). Microglial Inflammatory Signaling Orchestrates the Hypothalamic Immune Response to Dietary Excess and Mediates Obesity Susceptibility. *Cell Metabolism*, 26(1):185–197.e3.

Valdearcos, M., Robblee, M. M., Benjamin, D. I., Nomura, D. K., Xu, A. W., and Koliwad, S. K. (2014). Microglia Dictate the Impact of Saturated Fat Consumption on Hypothalamic Inflammation and Neuronal Function. *Cell Reports*, 9(6):2124–2139.

Valladolid-Acebes, I., Fole, A., Martín, M., Morales, L., Victoria Cano, M., Ruiz-Gayo, M., and Olmo, N. D. (2013). Spatial memory impairment and changes in hippocampal morphology are triggered by high-fat diets in adolescent mice. Is there a role of leptin? *Neurobiology of Learning and Memory*, 106:18–25.

Van Heek, M., Compton, D. S., France, C. F., Tedesco, R. P., Fawzi, A. B., Graziano, M. P., Sybertz, E. J., Strader, C. D., and Davis, H. R. (1997). Diet-induced obese mice develop peripheral, but not central, resistance to leptin. *Journal of Clinical Investigation*, 99(3):385–390.

Vannucci, S. J., Clark, R. R., Koehler-Stec, E., Li, K., Smith, C. B., Davies, P., Maher, F., and Simpson, I. A. (1998). Glucose transporter expression in brain: Relationship to cerebral glucose utilization. *Developmental Neuroscience*, 20(4-5):369–379.

Velloso, L. a. and Schwartz, M. W. (2011). Altered hypothalamic function in diet-induced obesity. *International Journal of Obesity*, 35(12):1455–1465.

Vento, P. J., Swartz, M. E., Martin, L. B., and Daniels, D. (2008). Food intake in laboratory rats provided standard and fenbendazole- supplemented diets. *Journal of the American Association for Laboratory Animal Science*.

Villar, D., Cray, C., Zaias, J., and Altman, N. H. (2007). Biologic effects of fenbendazole in rats and mice: A review.

Wang, J., Obici, S., Morgan, K., Barzilai, N., Feng, Z., and Rossetti, L. (2001). Overfeeding rapidly induces leptin and insulin resistance. *Diabetes*, 50(12):2786–2791.

Wei, H. S., Kang, H., Rasheed, I. Y. D., Zhou, S., Lou, N., Gershteyn, A., McConnell, E. D., Wang, Y., Richardson, K. E., Palmer, A. F., Xu, C., Wan, J., and Nedergaard, M. (2016). Erythrocytes Are Oxygen-Sensing Regulators of the Cerebral Microcirculation. *Neuron*, 91(4):851–862.

Wei, W., Pham, K., Gammons, J. W., Sutherland, D., Liu, Y., Smith, A., Kaczorowski, C. C., and O'Connell, K. M. (2015). Diet composition, not calorie intake, rapidly alters intrinsic excitability of hypothalamic AgRP/NPY neurons in mice. *Scientific Reports*, 5(1):16810.

Weigle, D. S., Duell, P. B., Connor, W. E., Steiner, R. A., Soules, M. R., and Kuijper, J. L. (1997). Effect of fasting, refeeding, and dietary fat restriction on plasma leptin levels. *Journal of Clinical Endocrinology and Metabolism*, 82(2):561–565.

Weiss, H. R., Buchweitz, E., Murtha, T. J., and Auletta, M. (1982). Quantitative regional determination of morphometric indices of the total and perfused capillary network in the rat brain. *Circulation Research*, 51(4):494–503.

Williams, K. W., Margatho, L. O., Lee, C. E., Choi, M., Lee, S., Scott, M. M., Elias, C. F., and Elmquist, J. K. (2010). Segregation of acute leptin and insulin effects in distinct populations of arcuate proopiomelanocortin neurons. *Journal of Neuroscience*, 30(7):2472–2479.

Wilson, J. A. and Clark, J. J. (2004). Obesity: impediment to postsurgical wound healing. *Advances in skin & wound care*, 17(8):426–435.

Winkler, E. A., Bell, R. D., and Zlokovic, B. V. (2011). Central nervous system pericytes in health and disease. *Nature Neuroscience*, 14(11):1398–1405.

Winkler, E. A., Nishida, Y., Sagare, A. P., Rege, S. V., Bell, R. D., Perlmutter, D., Sengillo, J. D., Hillman, S., Kong, P., Nelson, A. R., Sullivan, J. S., Zhao, Z., Meiselman, H. J., Wenby, R. B., Soto, J., Abel, E. D., Makshanoff, J., Zuniga, E., De Vivo, D. C., and Zlokovic, B. V. (2015). GLUT1 reductions exacerbate Alzheimer's disease vasculo-neuronal dysfunction and degeneration. *Nature Neuroscience*, 18(4):521–530.

Winzell, M. S. and Ahren, B. (2004). The High-Fat Diet-Fed Mouse: A Model for Studying Mechanisms and Treatment of Impaired Glucose Tolerance and Type 2 Diabetes. *Diabetes*, 53(Supplement 3):S215–S219.

Wolburg, H. and Lippoldt, A. (2002). Tight junctions of the blood-brain barrier: Development, composition and regulation. *Vascular Pharmacology*, 38(6):323–337.

Wu, A., Ying, Z., and Gomez-Pinilla, F. (2004a). The interplay between oxidative stress and brain-derived neurotrophic factor modulates the outcome of a saturated fat diet on synaptic plasticity and cognition. *European Journal of Neuroscience*, 19(7):1699–1707.

Wu, E. X., Tang, H., and Jensen, J. H. (2004b). High-resolution MR imaging of mouse brain microvasculature using the relaxation rate shift index Q. *NMR in Biomedicine*, 17(7):507–512.

Xia, S. F., Xie, Z. X., Qiao, Y., Li, L. R., Cheng, X. R., Tang, X., Shi, Y. H., and Le, G. W. (2015). Differential effects of quercetin on hippocampus-dependent learning and memory in mice fed with different diets related with oxidative stress. *Physiology and Behavior*, 138:325–331.

Xu, W. L., Atti, A. R., Gatz, M., Pedersen, N. L., Johansson, B., and Fratiglioni, L. (2011). Midlife overweight and obesity increase late-life dementia risk: A population-based twin study. *Neurology*, 76(18):1568–1574.

Yaffe, K., Kanaya, A., Lindquist, K., Simonsick, E. M., Harris, T., Shorr, R. I., Tylavsky, F. A., and Newman, A. B. (2004). The metabolic syndrome, inflammation, and risk of cognitive decline. *Journal of the American Medical Association*.

Yamamoto, M., Guo, D.-H., Hernandez, C. M., and Stranahan, A. M. (2019). Endothelial Adora2a Activation Promotes Blood–Brain Barrier Breakdown and Cognitive Impairment in Mice with Diet-Induced Insulin Resistance. *The Journal of Neuroscience*, 39(21):4179–4192.

Yamashiro, K., Tanaka, R., Tanaka, Y., Miyamoto, N., Shimada, Y., Ueno, Y., Urabe, T., and Hattori, N. (2014). Visceral fat accumulation is associated with cerebral small vessel disease. *European Journal of Neurology*, 21(4):667–673.

Yemisci, M., Gursoy-Ozdemir, Y., Vural, A., Can, A., Topalkara, K., and Dalkara, T. (2009). Pericyte contraction induced by oxidative-nitrative stress impairs capillary reflow despite successful opening of an occluded cerebral artery. *Nature Medicine*, 15(9):1031–1037.

Yeomans, M. R. (2017). Adverse effects of consuming high fat–sugar diets on cognition: implications for understanding obesity. *Proceedings of the Nutrition Society*.

Yi, C. X., Gericke, M., Krüger, M., Alkemade, A., Kabra, D. G., Hanske, S., Filosa, J., Pfluger, P., Bingham, N., Woods, S. C., Herman, J., Kalsbeek, A., Baumann, M., Lang, R., Stern, J. E., Bechmann, I., and Tschöp, M. H. (2012). High calorie diet triggers hypothalamic angiopathy. *Molecular Metabolism*, 1(1-2):95–100.

Yoo, D. Y., Yim, H. S., Jung, H. Y., Nam, S. M., Kim, J. W., Choi, J. H., Seong, J. K., Yoon, Y. S., Kim, D. W., and Hwang, I. K. (2016). Chronic type 2 diabetes reduces the integrity of

the blood-brain barrier by reducing tight junction proteins in the hippocampus. *The Journal of veterinary medical science*, 78(6):957–62.

Young, K., Rothers, J., Castaneda, S., Ritchie, J., Pottenger, A., and Morrison, H. (2018). Sex and regional differences in microglia morphology and complement receptor 3 are independent of constitutive neuroinflammatory protein concentrations in healthy mice. *PeerJ Preprints*.

Yu, C. G., Singh, R., Crowdus, C., Raza, K., Kincer, J., and Geddes, J. W. (2014). Fenbendazole improves pathological and functional recovery following traumatic spinal cord injury. *Neuroscience*.

Zeller, K., Rahner-Welsch, S., and Kuschinsky, W. (1997). Distribution of Glut1 glucose transporters in different brain structures compared to glucose utilization and capillary density of adult rat brains. *Journal of Cerebral Blood Flow and Metabolism*, 17(2):204–209.

Zhang, L., Wu, J., Duan, X., Tian, X., Shen, H., Sun, Q., and Chen, G. (2016). NADPH Oxidase: A Potential Target for Treatment of Stroke. *Oxidative Medicine and Cellular Longevity*, 2016:1–9.

Zhang, X., Zhang, G., Zhang, H., Karin, M., Bai, H., and Cai, D. (2008). Hypothalamic IKKβ/NF-κB and ER Stress Link Overnutrition to Energy Imbalance and Obesity. *Cell*, 135(1):61–73.

Zhang, Y., Proenca, R., Maffei, M., Barone, M., Leopold, L., and Friedman, J. M. (1994). Positional cloning of the mouse obese gene and its human homologue. *Nature*, 372(6505):425–432.

Zhou, J., Mao, L., Xu, P., and Wang, Y. (2018). Effects of (-)-Epigallocatechin Gallate (EGCG) on Energy Expenditure and Microglia-Mediated Hypothalamic Inflammation in Mice Fed a High-Fat Diet. *Nutrients*, 10(11):1681.

Zhou, Y. and Rui, L. (2013). Leptin signaling and leptin resistance. *Frontiers of Medicine*, 7(2):207–222.

Zhu, X., Hill, R. A., and Nishiyama, A. (2008). NG2 cells generate oligodendrocytes and gray matter astrocytes in the spinal cord. *Neuron Glia Biology*, 4(1):19–26.

Zlokovic, B. V. (2008). The Blood-Brain Barrier in Health and Chronic Neurodegenerative Disorders. *Neuron*, 57(2):178–201.

Zuloaga, K. L., Johnson, L. A., Roese, N. E., Marzulla, T., Zhang, W., Nie, X., Alkayed, F. N., Hong, C., Grafe, M. R., Pike, M. M., Raber, J., and Alkayed, N. J. (2016). High fat diet-induced diabetes in mice exacerbates cognitive deficit due to chronic hypoperfusion. *Journal of Cerebral Blood Flow and Metabolism*, 36(7):1257–1270.

Appendix A

Appendix

A.1 *In Vivo* Microglial Changes

A.1.1 Components of the Inflammation Index

Figure legends are identical for all figures and tables presented in this subsection of the appendix.

Figure Legends A.1 - A.7

Analysis of LPS and Dietary Effects (A) The effect of LPS treatment split by region. **(B)** Dietary and regional differences at the 14 day timepoint. **(C)** Changes over 8 weeks of dietary manipulation (brackets and numbers in **A, B** indicate p values of corrected pairwise dietary comparisons. In **C** D-1 refers to measurements taken a day before the beginning of dietary treatment, and hours are relative to the the start of dietary manipulation. ', *, **, ***, indicates p < .10, .05, .01, and .001 respectively. LPS N = 333 cells (HFD: 198; Hippocampus: 135). N = 16 mice (HFD:10, Hippocampus: 6). Day 14 N = 300 cells (HFD: 167; Hippocampus: 114). N = 22 mice (HFD: 12, Hippocampus: 10). Timecourse N = 3992 cells (HFD: 2138; Hippocampus: 1365). N = 28 mice (HFD: 14; Hippocampus: 11)).

Table Legends A.1 - A.7

Analysis Statistics. Analyses were run using LMMs to investigate the changes in response to LPS treatment, two weeks of HFD feeding, and the 8 week dietary timecourse (numDF and denDF refer to degrees of freedom. F and p values are rounded to 4 decimal places. **Red text** indicates significance. **Green text** indicates trend level. **Background shading** indicates size of p value where darker is larger. Sig shows significance indicator. Factor indicates factors in the model. Measure indicates the model run. Colons indicate interaction effects).

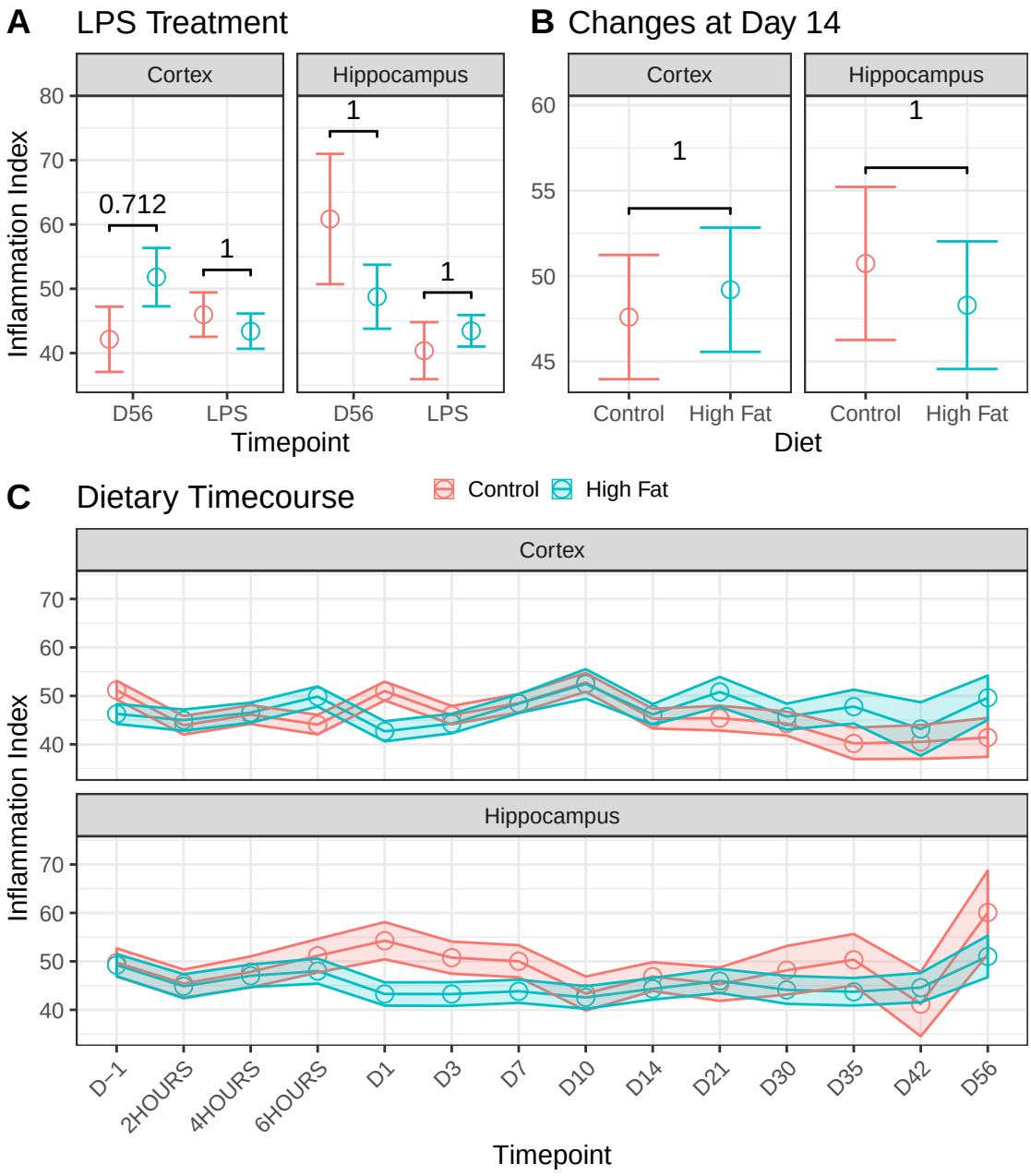

Figure A.1: Analysis of LPS and Dietary Effects on Soma Area.

numDF	denDF	F-value	P-Value	Factor	Sig	Measure
1	9	0.2093	0.6581	Diet		LPS
1	9	0.0007	0.9795	Diet:Region		
1	9	0.0334	0.8591	Region		
1	313	2.6413	0.1051	LPS Condition		
1	313	1.0506	0.3062	LPS Condition:Diet		
1	313	3.4808	0.0630	LPS Condition:Diet:Region	'	
1	313	0.4665	0.4951	LPS Condition:Region		
1	15	0.0077	0.9314	Diet		D14
1	15	0.3419	0.5674	Diet:Region		
1	15	0.0834	0.7766	Region		
1	22	0.2098	0.6514	Diet		Timecourse
1	22	2.0049	0.1708	Diet:Region		
1	22	0.0963	0.7592	Region		
13	3911	2.6941	0.0009	Timepoint	***	
13	3911	2.9171	0.0003	Timepoint:Diet	***	
13	3911	0.9557	0.4934	Timepoint:Diet:Region		
13	3911	1.8427	0.0319	Timepoint:Region	*	

Table A.1: Soma Area Analysis Statistics.

numDF	denDF	F-value	P-Value	Factor	Sig	Measure
1	9	2.5263	0.1464	Diet		LPS
1	9	3.0351	0.1155	Diet:Region		
1	9	0.3630	0.5617	Region		
1	313	0.0241	0.8767	LPS Condition		
1	313	0.1092	0.7413	LPS Condition:Diet		
1	313	0.0259	0.8723	LPS Condition:Diet:Region		
1	313	0.0552	0.8144	LPS Condition:Region		
1	15	1.6261	0.2216	Diet		D14
1	15	0.0550	0.8177	Diet:Region		
1	15	0.1624	0.6926	Region		
1	22	1.4183	0.2464	Diet		Timecourse
1	22	0.2939	0.5932	Diet:Region		
1	22	0.0023	0.9619	Region		
13	3911	0.6479	0.8149	Timepoint		
13	3911	1.5341	0.0972	Timepoint:Diet	'	
13	3911	0.6286	0.8320	Timepoint:Diet:Region		
13	3911	0.9511	0.4982	Timepoint:Region		

Table A.2: Maximum Branch Length Analysis Statistics.

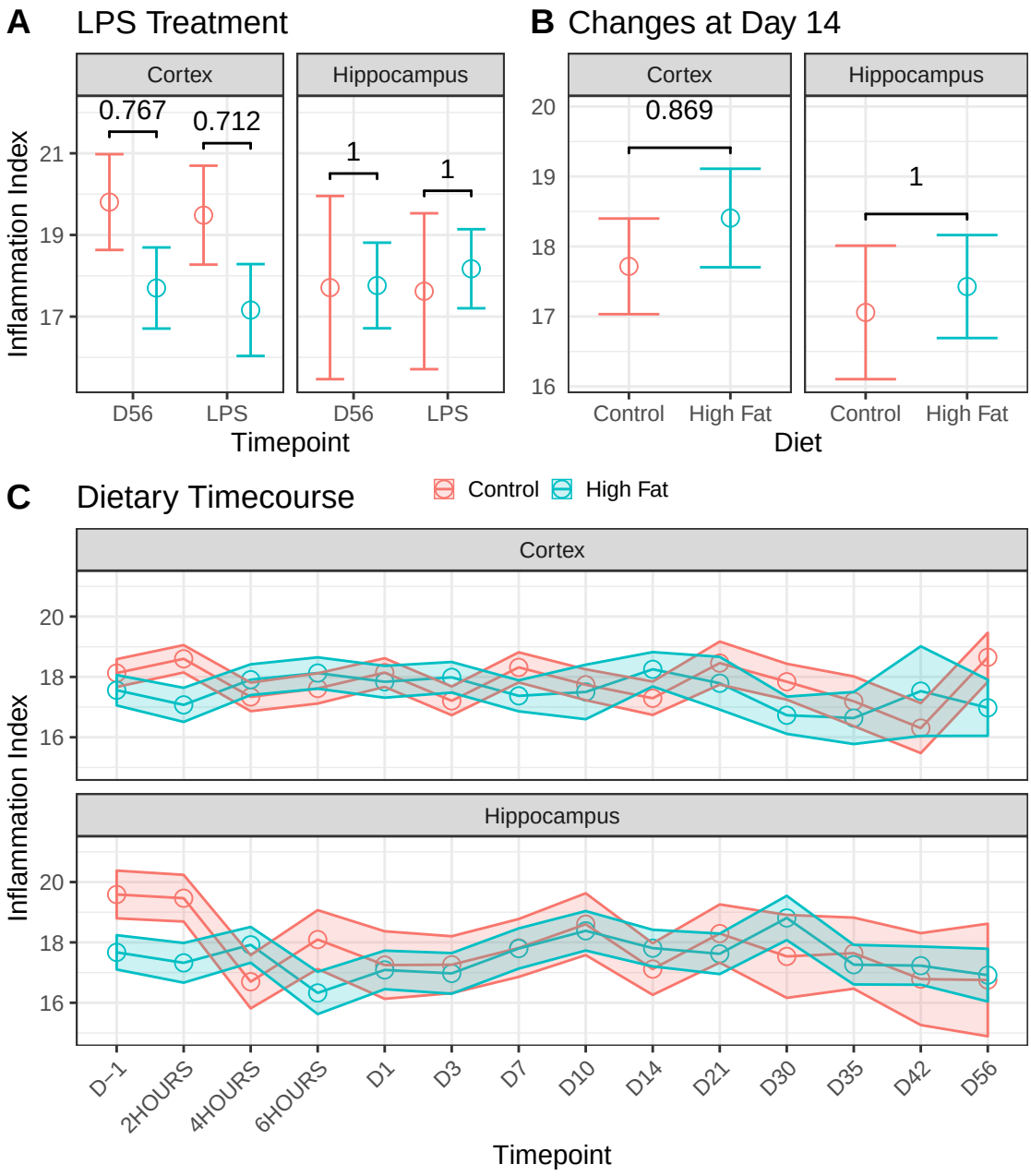

Figure A.2: Analysis of LPS and Dietary Effects on Maximum Branch Length.

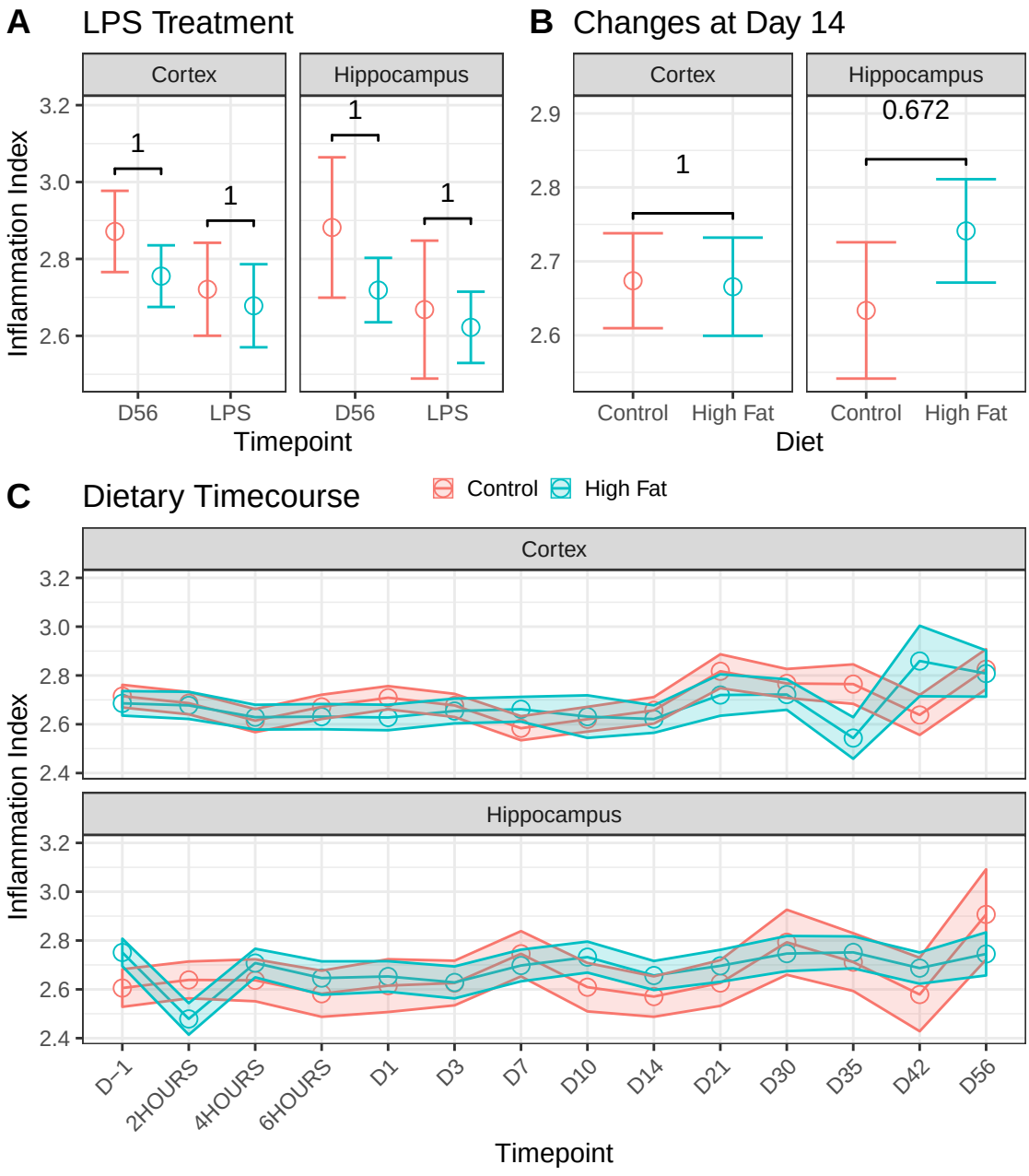

Figure A.3: Analysis of LPS and Dietary Effects on the Log-log Regression Coefficient.

numDF	denDF	F-value	P-Value	Factor	Sig	Measure
1	9	0.7780	0.4007	Diet		LPS
1	9	0.0260	0.8755	Diet:Region		
1	9	0.3521	0.5675	Region		
1	313	3.8150	0.0517	LPS Condition	'	
1	313	0.2941	0.5880	LPS Condition:Diet		
1	313	0.0194	0.8893	LPS Condition:Diet:Region		
1	313	0.0469	0.8286	LPS Condition:Region		
1	15	0.0178	0.8955	Diet		D14
1	15	0.7930	0.3873	Diet:Region		
1	15	0.5752	0.4600	Region		
1	22	0.2502	0.6219	Diet		Timecourse
1	22	1.1647	0.2922	Diet:Region		
1	22	0.5890	0.4510	Region		
13	3911	0.9051	0.5470	Timepoint		
13	3911	0.7973	0.6637	Timepoint:Diet		
13	3911	0.8616	0.5941	Timepoint:Diet:Region		
13	3911	1.0786	0.3727	Timepoint:Region		

Table A.3: Log-log Regression Coefficient Analysis Statistics.

numDF	denDF	F-value	P-Value	Factor	Sig	Measure
1	9	0.2188	0.6511	Diet		LPS
1	9	0.3811	0.5523	Diet:Region		
1	9	0.5156	0.4909	Region		
1	313	4.6902	0.0311	LPS Condition	*	
1	313	0.1180	0.7315	LPS Condition:Diet		
1	313	0.4926	0.4833	LPS Condition:Diet:Region		
1	313	0.0712	0.7898	LPS Condition:Region		
1	15	0.1253	0.7283	Diet		D14
1	15	0.7343	0.4050	Diet:Region		
1	15	0.3598	0.5576	Region		
1	22	0.0107	0.9187	Diet		Timecourse
1	22	0.8227	0.3742	Diet:Region		
1	22	0.5085	0.4833	Region		
13	3911	1.0960	0.3570	Timepoint		
13	3911	0.8500	0.6066	Timepoint:Diet		
13	3911	1.0212	0.4270	Timepoint:Diet:Region		
13	3911	1.3235	0.1907	Timepoint:Region		

Table A.4: Log-log Regression Intercept Analysis Statistics.

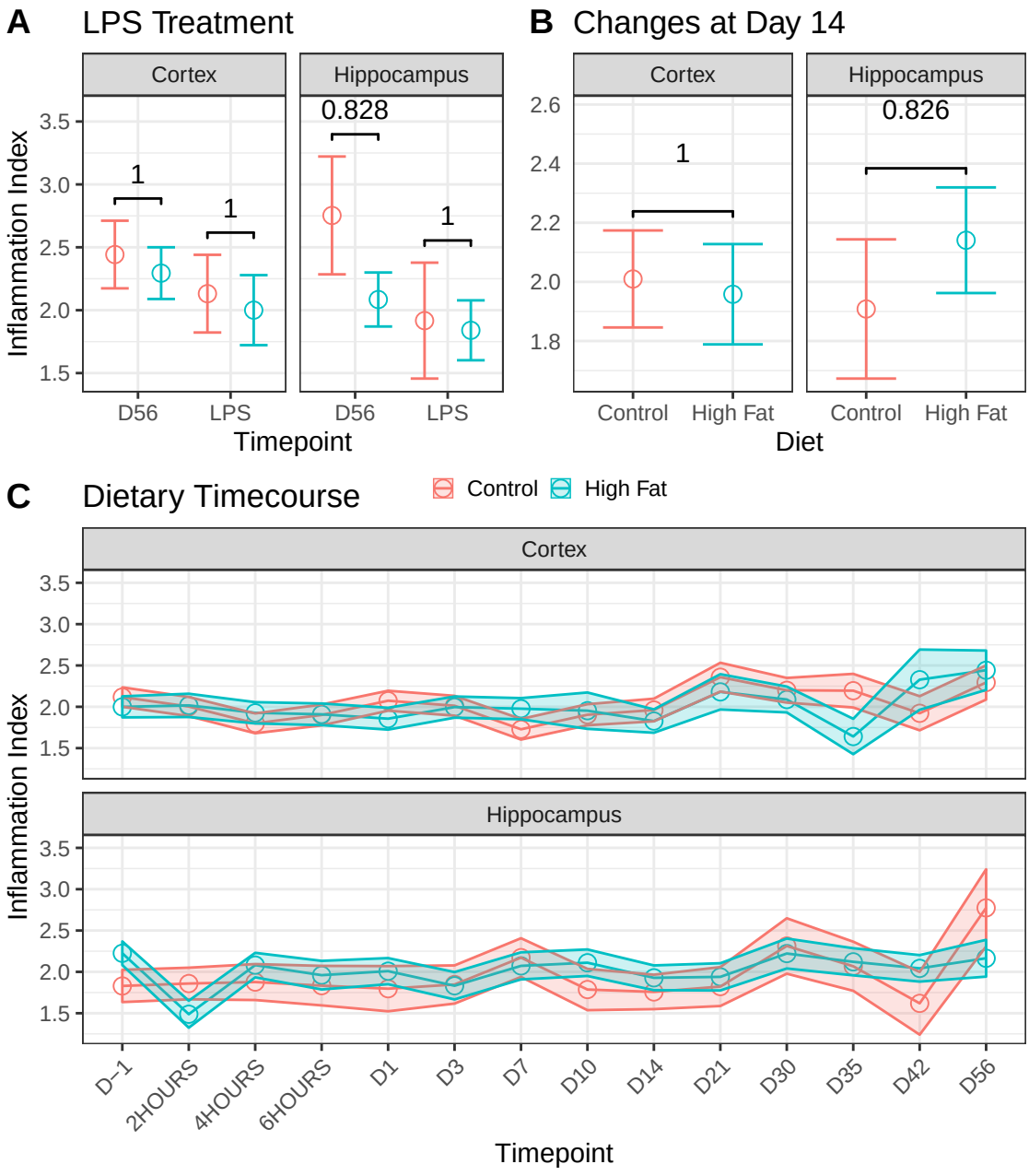

Figure A.4: Analysis of LPS and Dietary Effects on the Log-log Regression Intercept.

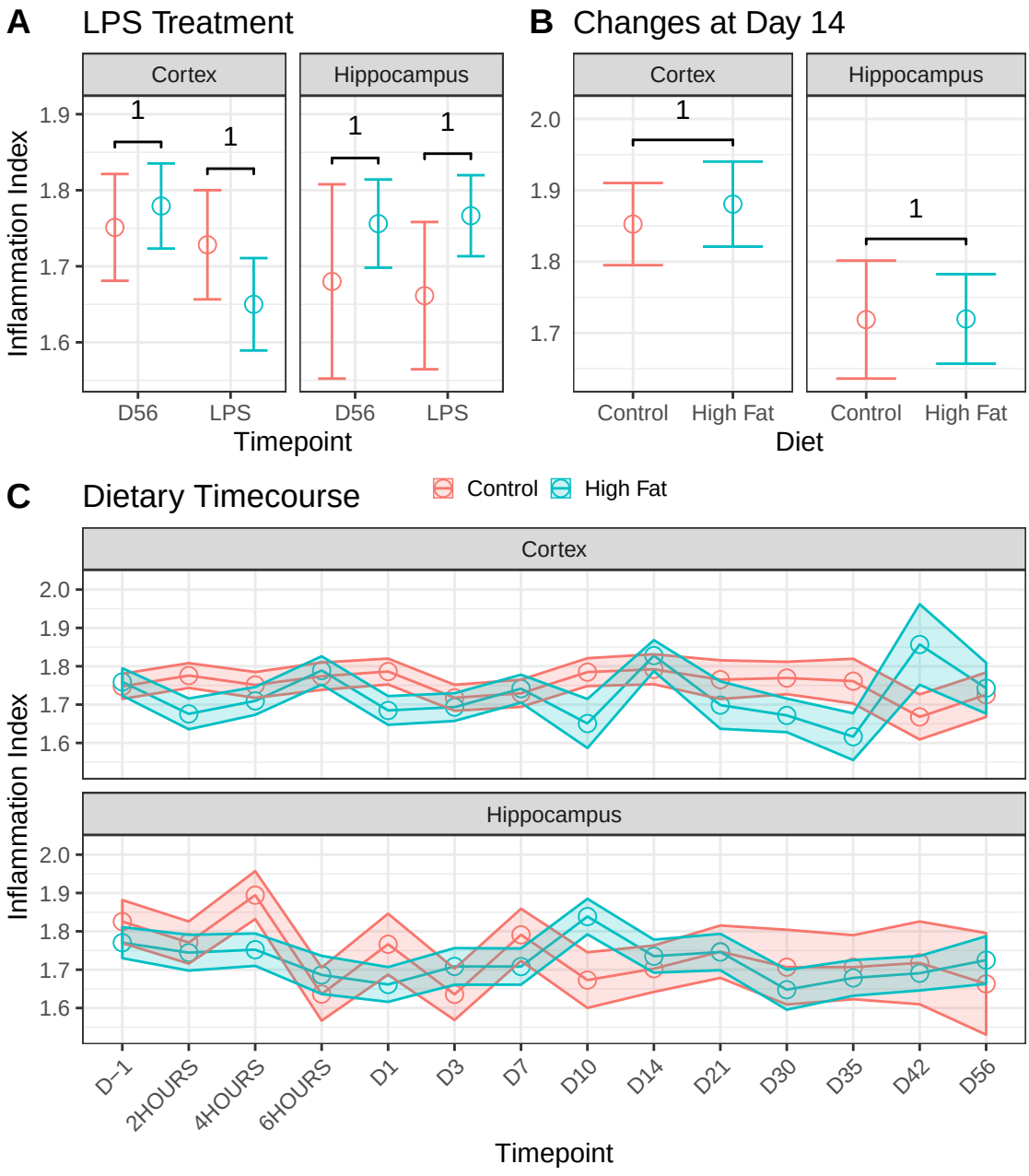

Figure A.5: Analysis of LPS and Dietary Effects on the Coefficient of Variation for All Radii.

numDF	denDF	F-value	P-Value	Factor	Sig	Measure
1	9	0.1178	0.7394	Diet		LPS
1	9	1.5718	0.2415	Diet:Region		
1	9	0.0077	0.9321	Region		
1	313	0.6768	0.4113	LPS Condition		
1	313	0.0336	0.8547	LPS Condition:Diet		
1	313	0.4733	0.4920	LPS Condition:Diet:Region		
1	313	0.9552	0.3292	LPS Condition:Region		
1	15	0.0971	0.7596	Diet		D14
1	15	0.0542	0.8190	Diet:Region		
1	15	2.6152	0.1267	Region		
1	22	5.1753	0.0330	Diet	*	Timecourse
1	22	0.3553	0.5572	Diet:Region		
1	22	0.6840	0.4171	Region		
13	3911	1.1177	0.3380	Timepoint		
13	3911	1.0950	0.3579	Timepoint:Diet		
13	3911	1.1573	0.3050	Timepoint:Diet:Region		
13	3911	1.3653	0.1679	Timepoint:Region		

Table A.5: Coefficient of Variation for All Radii Analysis Statistics.

numDF	denDF	F-value	P-Value	Factor	Sig	Measure
1	9	0.1991	0.6660	Diet		LPS
1	9	0.0055	0.9426	Diet:Region		
1	9	0.0487	0.8303	Region		
1	313	0.6215	0.4311	LPS Condition		
1	313	0.2232	0.6370	LPS Condition:Diet		
1	313	0.1519	0.6970	LPS Condition:Diet:Region		
1	313	0.6401	0.4243	LPS Condition:Region		
1	15	0.4256	0.5240	Diet		D14
1	15	0.1444	0.7092	Diet:Region		
1	15	0.7164	0.4106	Region		
1	22	3.9870	0.0584	Diet	'	Timecourse
1	22	0.8001	0.3807	Diet:Region		
1	22	0.0139	0.9072	Region		
13	3911	0.8332	0.6249	Timepoint		
13	3911	1.3706	0.1652	Timepoint:Diet		
13	3911	0.7067	0.7585	Timepoint:Diet:Region		
13	3911	0.7954	0.6658	Timepoint:Region		

Table A.6: Mean Radius from Circle's Centre Analysis Statistics.

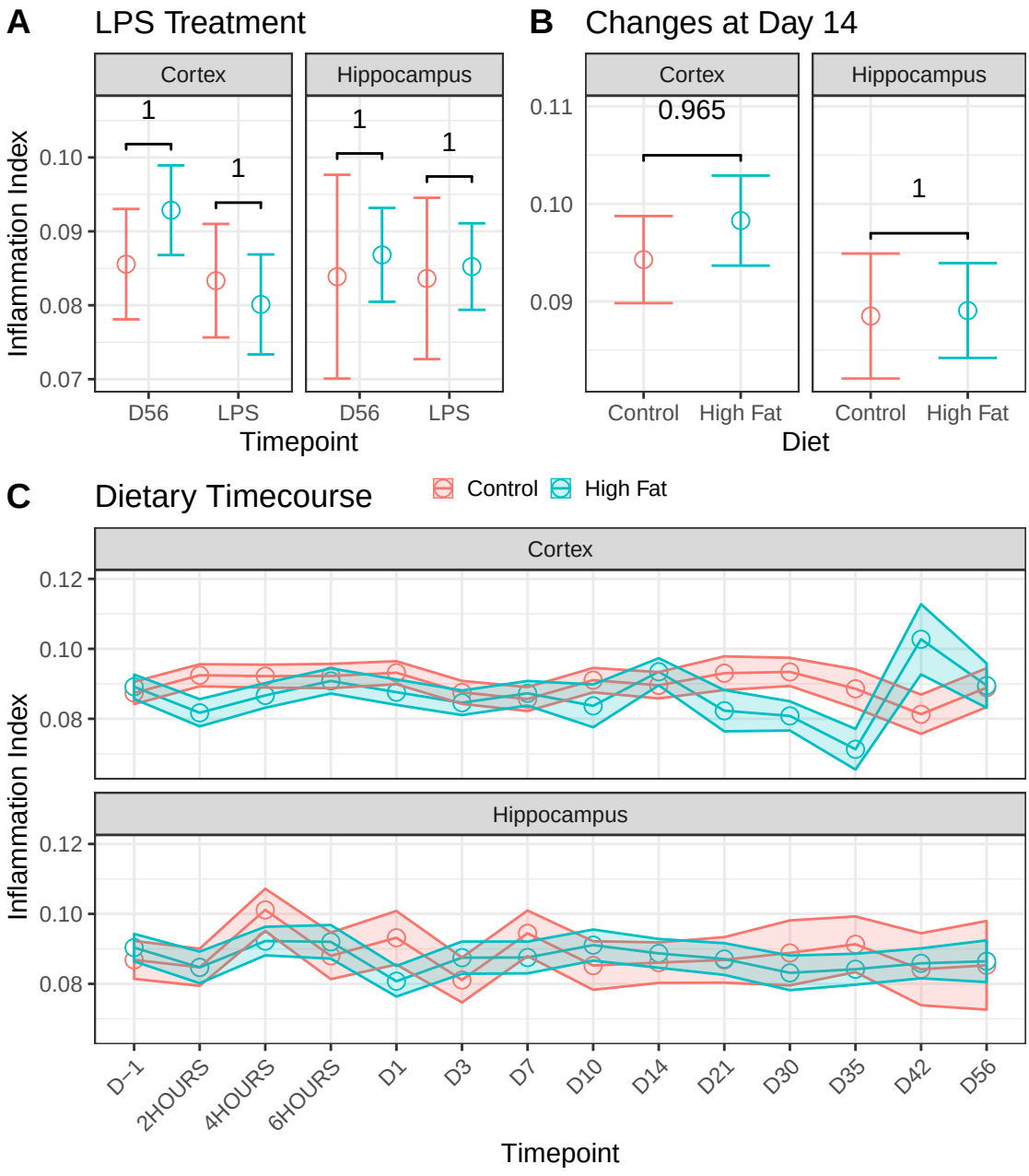

Figure A.6: Analysis of LPS and Dietary Effects on the Mean Radius from Circle's Centre.

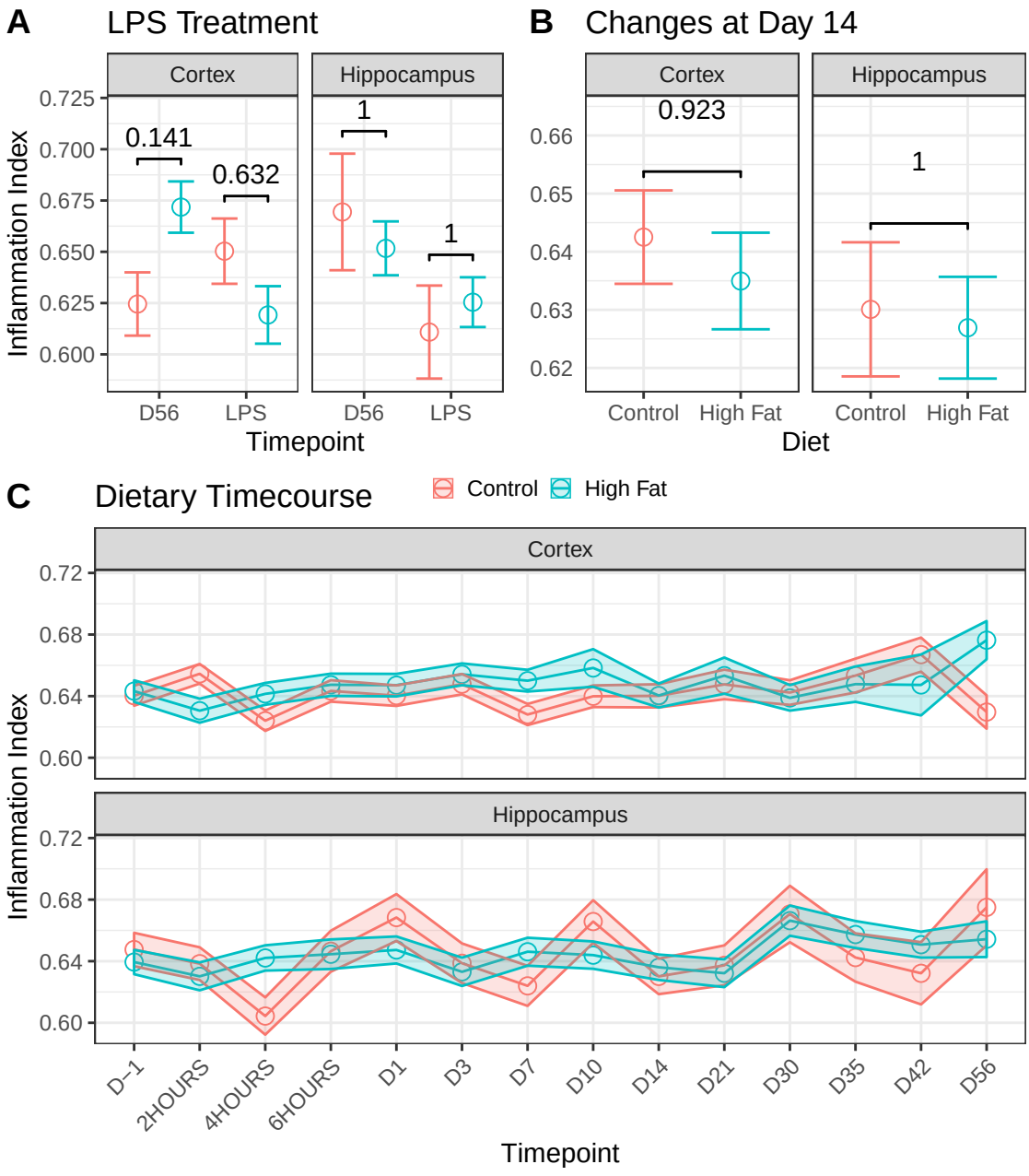

Figure A.7: Analysis of LPS and Dietary Effects on Lacunarity.

numDF	denDF	F-value	P-Value	Factor	Sig	Measure
1	9	0.0428	0.8407	Diet		LPS
1	9	0.0266	0.8740	Diet:Region		
1	9	0.7324	0.4143	Region		
1	313	3.6518	0.0569	LPS Condition	'	
1	313	5.6239	0.0183	LPS Condition:Diet	*	
1	313	5.1902	0.0234	LPS Condition:Diet:Region	*	
1	313	0.0488	0.8253	LPS Condition:Region		
1	15	0.0074	0.9327	Diet		D14
1	15	0.0731	0.7906	Diet:Region		
1	15	1.3231	0.2680	Region		
1	22	1.1549	0.2942	Diet		Timecourse
1	22	0.3854	0.5411	Diet:Region		
1	22	0.8739	0.3600	Region		
13	3911	1.3258	0.1893	Timepoint		
13	3911	2.2496	0.0062	Timepoint:Diet	**	
13	3911	1.3094	0.1989	Timepoint:Diet:Region		
13	3911	1.3402	0.1813	Timepoint:Region		

Table A.7: Lacunarity Analysis Statistics.

A.1.2 Motility Indices

Table legends are identical for all tables in this subsection so will be defined once here.

Table Legends A.8 - A.10

Analysis Statistics. Analyses were run using LMMs to investigate changes in the motility indices (numDF and denDF refer to degrees of freedom. F and p values are rounded to 4 decimal places. **Red text** indicates significance. **Green text** indicates trend level. **Background shading** indicates size of p value where darker is larger. Sig shows significance indicator. Factor indicates factors in the model. Measure indicates the motility index analysed. Colons indicate interaction effects).

numDF	denDF	F-value	P-Value	Factor	Sig	Measure
1	11	1.0596	0.3254	Diet		MI
1	11	0.5038	0.4926	Diet:Region		
1	11	0.8831	0.3675	Region		
1	75	13.8916	0.0004	LPS Condition	***	
1	75	0.0921	0.7624	LPS Condition:Diet		
1	75	0.4459	0.5063	LPS Condition:Diet:Region		
1	75	0.0160	0.8998	LPS Condition:Region		
1	11	0.9144	0.3595	Diet		RI
1	11	0.3080	0.5900	Diet:Region		
1	11	0.7948	0.3917	Region		
1	75	13.5153	0.0004	LPS Condition	***	
1	75	0.0740	0.7864	LPS Condition:Diet		
1	75	0.5781	0.4495	LPS Condition:Diet:Region		
1	75	0.0421	0.8379	LPS Condition:Region		
1	11	1.1863	0.2994	Diet		EI
1	11	0.7301	0.4111	Diet:Region		
1	11	0.9618	0.3478	Region		
1	75	14.1446	0.0003	LPS Condition	***	
1	75	0.1117	0.7392	LPS Condition:Diet		
1	75	0.3330	0.5657	LPS Condition:Diet:Region		
1	75	0.0031	0.9559	LPS Condition:Region		
1	11	0.0796	0.7831	Diet		SI
1	11	0.1281	0.7272	Diet:Region		
1	11	0.5801	0.4623	Region		
1	75	1.1636	0.2842	LPS Condition		
1	75	0.8198	0.3681	LPS Condition:Diet		
1	75	0.4275	0.5152	LPS Condition:Diet:Region		
1	75	0.1720	0.6796	LPS Condition:Region		
1	11	1.6067	0.2311	Diet		II
1	11	0.3467	0.5679	Diet:Region		
1	11	0.3147	0.5860	Region		
1	75	3.6496	0.0599	LPS Condition	'	
1	75	0.5863	0.4462	LPS Condition:Diet		
1	75	0.9995	0.3207	LPS Condition:Diet:Region		
1	75	2.2974	0.1338	LPS Condition:Region		
1	11	0.8230	0.3837	Diet		CMS
1	11	0.3904	0.5448	Diet:Region		
1	11	0.7953	0.3916	Region		
1	75	14.4335	0.0003	LPS Condition	***	
1	75	0.0449	0.8328	LPS Condition:Diet		
1	75	0.5516	0.4600	LPS Condition:Diet:Region		
1	75	0.0131	0.9091	LPS Condition:Region		

Table A.8: Statistics for the Effect of LPS on Motility Indices.

numDF	denDF	F-value	P-Value	Factor	Sig	Measure
1	23	1.6378	0.2134	Diet		MI
1	23	0.2403	0.6286	Diet:Region		
1	23	8.4033	0.0081	Region	**	
14	1035	1.0967	0.3560	Timepoint		
14	1035	1.0586	0.3919	Timepoint:Diet		
14	1035	0.9017	0.5567	Timepoint:Diet:Region		
14	1035	0.8185	0.6494	Timepoint:Region		
1	23	1.6253	0.2151	Diet		RI
1	23	0.2440	0.6260	Diet:Region		
1	23	8.1403	0.0090	Region	**	
14	1035	1.1473	0.3115	Timepoint		
14	1035	1.0805	0.3710	Timepoint:Diet		
14	1035	0.9385	0.5162	Timepoint:Diet:Region		
14	1035	0.8533	0.6106	Timepoint:Region		
1	23	1.6441	0.2125	Diet		EI
1	23	0.2358	0.6318	Diet:Region		
1	23	8.6410	0.0074	Region	**	
14	1035	1.0509	0.3994	Timepoint		
14	1035	1.0394	0.4107	Timepoint:Diet		
14	1035	0.8690	0.5931	Timepoint:Diet:Region		
14	1035	0.7868	0.6844	Timepoint:Region		
1	23	2.7547	0.1105	Diet		SI
1	23	1.9180	0.1794	Diet:Region		
1	23	0.6180	0.4398	Region		
14	1035	0.7816	0.6901	Timepoint		
14	1035	2.9135	0.0002	Timepoint:Diet	***	
14	1035	1.4106	0.1407	Timepoint:Diet:Region		
14	1035	1.0346	0.4156	Timepoint:Region		
1	23	5.1674	0.0327	Diet	*	II
1	23	0.0319	0.8598	Diet:Region		
1	23	20.3449	0.0002	Region	***	
14	1035	1.3593	0.1662	Timepoint		
14	1035	0.7671	0.7058	Timepoint:Diet		
14	1035	0.8730	0.5885	Timepoint:Diet:Region		
14	1035	0.5356	0.9130	Timepoint:Region		
1	23	1.4671	0.2381	Diet		CMS
1	23	0.2590	0.6156	Diet:Region		
1	23	8.9328	0.0066	Region	**	
14	1035	1.0928	0.3596	Timepoint		
14	1035	1.0433	0.4069	Timepoint:Diet		
14	1035	0.8993	0.5592	Timepoint:Diet:Region		
14	1035	0.8129	0.6557	Timepoint:Region		

Table A.9: Statistics for the Effects of Dietary Timecourse Treatment on Motility Indices.

numDF	denDF	F-value	P-Value	Factor	Sig	Measure
1	18	0.0466	0.8315	Diet		MI
1	18	3.5421	0.0761	Diet:Region	'	
1	18	0.8381	0.3720	Region		
1	18	0.1181	0.7351	Diet		RI
1	18	3.6694	0.0714	Diet:Region	'	
1	18	1.0196	0.3260	Region		
1	18	0.0078	0.9306	Diet		EI
1	18	3.2284	0.0892	Diet:Region	'	
1	18	0.6428	0.4331	Region		
1	18	0.0641	0.8030	Diet		SI
1	18	0.8182	0.3776	Diet:Region		
1	18	1.3313	0.2637	Region		
1	18	1.3715	0.2568	Diet		II
1	18	2.3618	0.1417	Diet:Region		
1	18	1.7949	0.1970	Region		
1	18	0.0723	0.7910	Diet		CMS
1	18	3.8156	0.0665	Diet:Region	'	
1	18	0.8563	0.3670	Region		

Table A.10: Statistics for the Effects of Two Weeks of HFD on Motility Indices.

A.2 *In Vivo* Neurovascular and Blood Supply Changes

A.2.1 V1 Neurovascular Coupling

The Effect of Locomotion

Legend Figure A.8;

The Effect of Locomotion on V1 Neurovascular Coupling. The effect of locomotion on values for peak, time to peak, time to onset, time to offset, AUC, and composite measure values, for visual stimulus data collected from V1. Peak values are displayed as percentages of the baseline. Timings are in seconds. **'Loco'** refers to trials with locomotion both during and preceding stimulus presentation, **'No Loco'** refers to trials where no locomotion was present in either window. The baseline period was the second preceding stimulus presentation. Timings are relative to the beginning of stimulus trials, where stimulus presentation occurs from 5 to 10 seconds. **Horizontal lines** indicate locomotion group means. **Solid lines** indicate significant ($p < .05$) differences. N = 17 (HFD: 8) animals; 148 sessions; 2135 ('Loco':1146) stimulus presentations.

Dietary Timecourse

Legend A.9;

V1 Visual Stimulus Peak Values. Peak values as a proportion of baseline. **'Loco'** refers to trials with locomotion both during and preceding stimulus presentation, **'No Loco'** refers to trials where no locomotion was present in either window. The baseline period was the second preceding stimulus presentation. **Thick borders** indicate diet by time interactions. **Grey backgrounds** indicate diet by time by locomotion interactions. N = 17 (HFD: 8) animals; 148 sessions; 2135 ('Loco':1146) stimulus presentations.

Legend A.10;

V1 Visual Stimulus AUC Values. Area under the curve measurements. **'Loco'** refers to trials with locomotion both during and preceding stimulus presentation, **'No Loco'** refers to trials where no locomotion was present in either window. The baseline period was the second preceding stimulus presentation. **Thick borders** indicate diet by time interactions. **Grey backgrounds** indicate diet by time by locomotion interactions. N = 17 (HFD: 8) animals; 148 sessions; 2135 ('Loco':1146) stimulus presentations.

A.2.2 Resting Data

Regional Differences

Legend A.11;

Regional Differences In Resting Values. Differences in resting values restricted to the final three imaging timepoints (D42, D49, D56) between regions (**'V1'** refers to primary visual cortex, **'CA1'** refers to hippocampal CA1. Periods of rest were epochs where no locomotion or visual stimulation occurred, or had occurred in the preceding one or five seconds respectively. **Horizontal lines** indicate regional group means. **Solid lines** indicate significant ($p < .05$) differences. N = 18 (HFD: 10, CA1: 11) animals; 50 sessions; 845 resting epochs).

Dietary Timecourse

Legend A.12;

Resting Values Over The Dietary Timecourse. Epochs of rest were periods where no locomotion or visual stimulation occurred, or had occurred in the preceding one or five seconds respectively. **Thick borders** indicate diet by time interactions. **Grey backgrounds** indicate diet by time by region interactions. * and ' indicates $p < .05$ and $< .10$ respectively. N = 29 (HFD: 14) animals; 259 sessions; 4460 resting epochs).

Legend A.13;

Ratio of Resting Values to $CMRO_2$ Over The Dietary Timecourse. Ratio of SO_2 and HbT to $CMRO_2$ at rest. Epochs of rest were periods where no locomotion or visual stimulation occurred, or had occurred in the preceding one or five seconds respectively. **Thick borders** indicate diet by time interactions. **Grey backgrounds** indicate diet by time by region interactions. ** indicates $p < .01$. N = 29 (HFD: 14) animals; 259 sessions; 4460 resting epochs)

A.2.3 $CMRO_2$ Peak Aligned Data

Regional Differences

Legend A.14;

Regional Differences in CPA Data. Differences in CPA data by region for peak, time to peak, time to onset, time to offset, AUC, and composite measure values. Peak values are displayed as percentages of the baseline. Timings are in seconds. T2p for $CMRO_2$ was not analysed as all $CMRO_2$ peaks were set to occur at 3 seconds. **'V1'** refers to primary visual cortex, **'CA1'** refers

to hippocampal CA1. Data was cut around detected peaks in $CMRO_2$ signal. Times are relative to trial start (3s before $CMRO_2$ peak). **Horizontal lines** indicate regional group means. **Solid lines** indicate significant ($p < .05$) differences. N = 21 (HFD: 11, CA1: 11) animals; 57 sessions; 2720 CPA events.

Dietary Timecourse

Legend A.15;

CPA Peak Values. Peak values as a proportion of baseline (Data was cut around detected peaks in $CMRO_2$ signal. **Thick borders** indicate diet by time interactions. **Grey backgrounds** indicate diet by time by region interactions. * and ** indicates $p < .05$ and $< .01$ respectively. N = 29 (HFD: 14) animals; 281 sessions; 13506 CPA events).

Legend A.16;

CPA AUC Values. Data was cut around detected peaks in $CMRO_2$ signal. **Thick borders** indicate diet by time interactions. **Grey backgrounds** indicate diet by time by region interactions. * and ** indicates $p < .05$ and $< .01$ respectively. N = 29 (HFD: 14) animals; 281 sessions; 13506 CPA events.

Behavioural Correlations

Legend A.17;

Peak Value Correlations with NOCR. Analysis of CPA data at day 14, with NOCR performance included as a factor. Peak values as percent of baseline are plotted on the y-axis. Novelty index is plotted on the x-axis (CPA data is cut around detected peaks in $CMRO_2$ signal. Novelty index reflects the difference between the proportion of exploration time spent exploring novel versus familiar objects. **Dotted line** indicates zero point where no difference exists in proportion of exploration time spent with novel versus familiar objects. Plotted lines represent the estimated marginal mean +/- 95% confidence intervals. These are predictions of the trend extracted from the relevant LMM. **Text boxes** indicate the slope of the trends by diet groups, and the p value of diet by performance interaction. * next to slope values indicates it is significantly different from zero. N = 11 (HFD: 6); 11 sessions; 374 CPA events).

Legend A.18;

AUC Value Correlations with NOCR. Analysis of CPA data at day 14, with NOCR performance included as a factor. AUC values are plotted on the y-axis. Novelty index is plotted on the x-axis (CPA data is cut around detected peaks in $CMRO_2$ signal. Novelty index reflects the difference

between the proportion of exploration time spent exploring novel versus familiar objects. **Dotted line** indicates zero point where no difference exists in proportion of exploration time spent with novel versus familiar objects. Plotted lines represent the estimated marginal mean +/- 95% confidence intervals. These are predictions of the trend extracted from the relevant LMM. **Text boxes** indicate the slope of the trends by diet groups, and the p value of diet by performance interaction. * next to slope values indicates it is significantly different from zero. N = 11 (HFD: 6); 11 sessions; 374 CPA events).

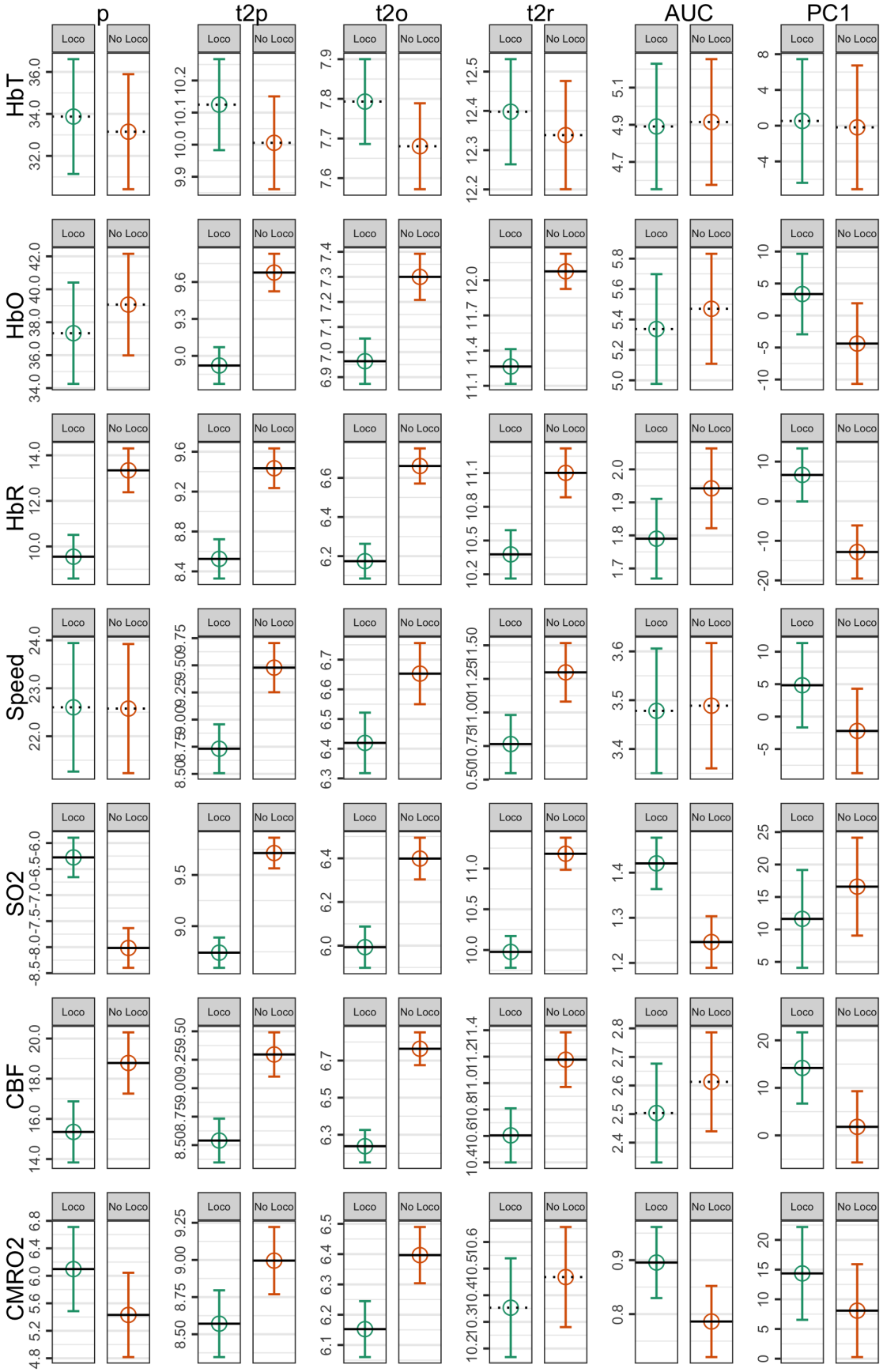

Figure A.8: The Effect of Locomotion on V1 Neurovascular Coupling.

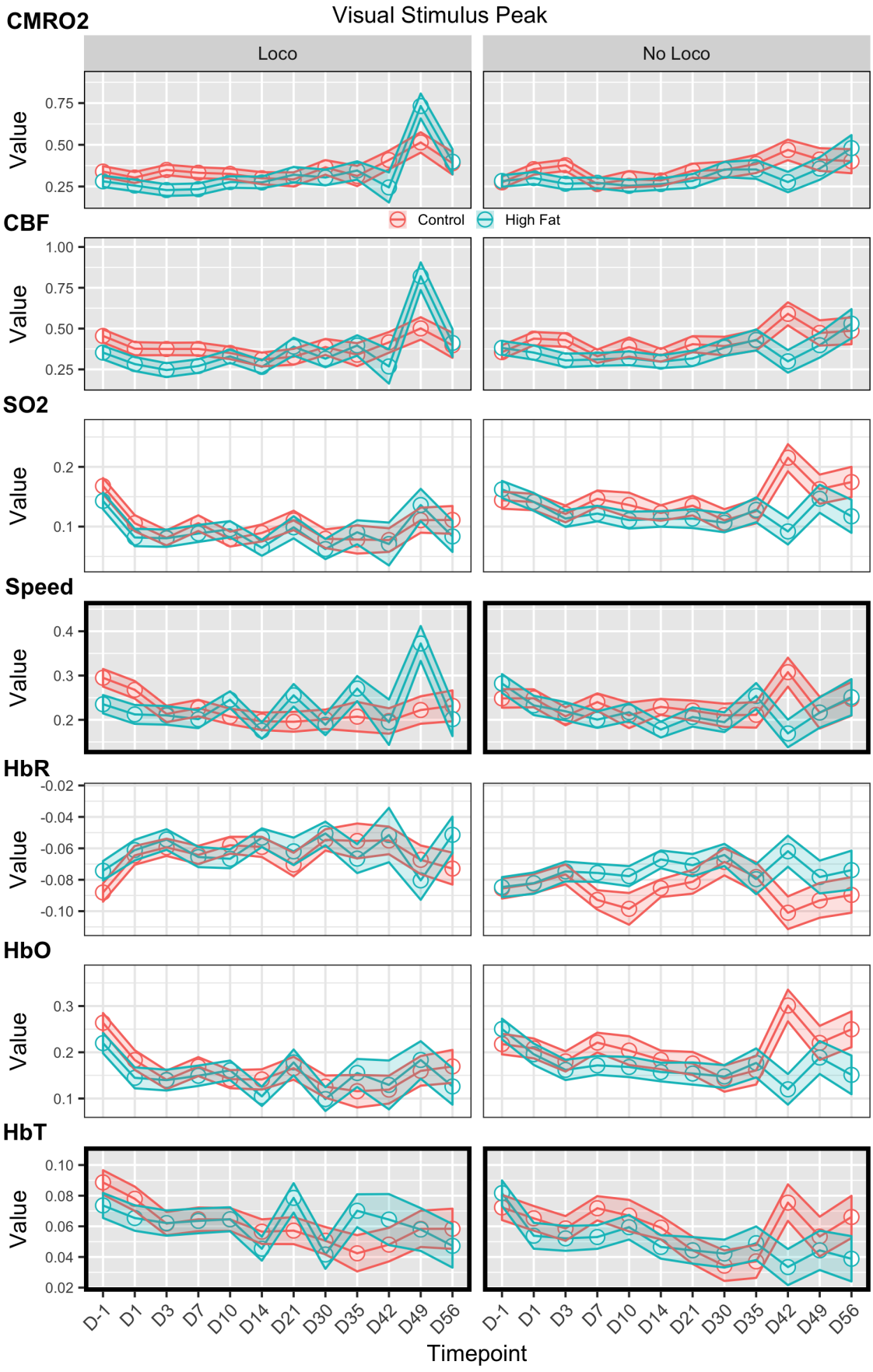

Figure A.9: V1 Visual Stimulus Peak Values.

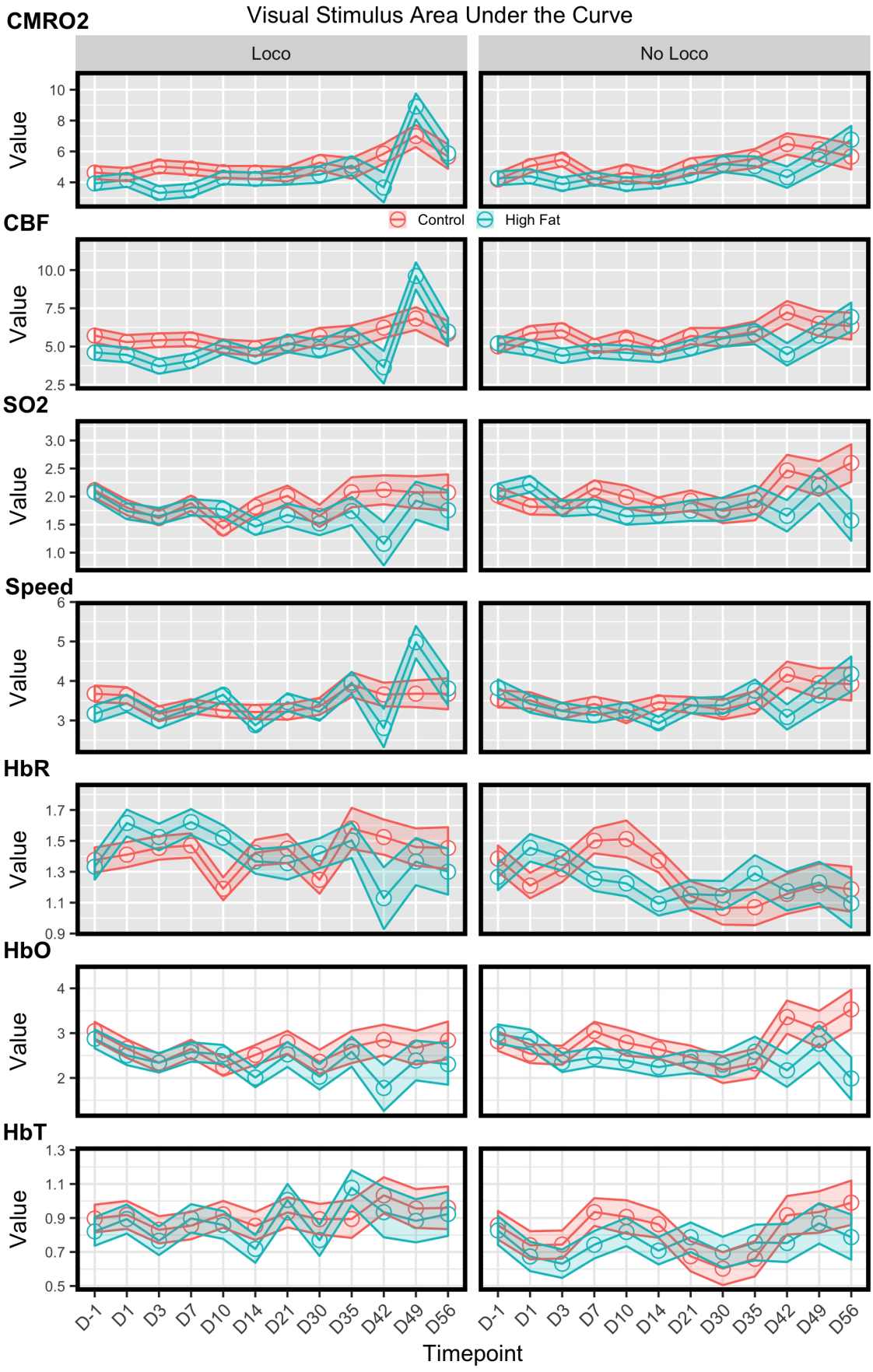

Figure A.10: V1 Visual Stimulus AUC Values.

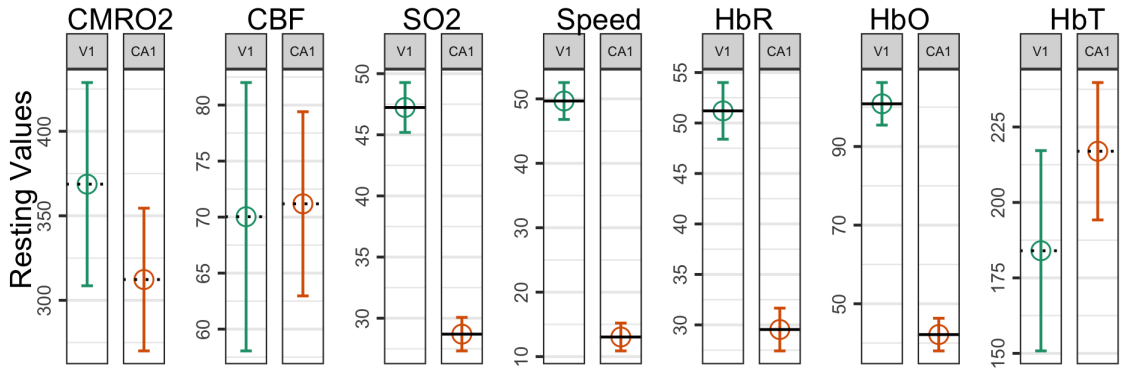

Figure A.11: Regional Differences in Resting Values.

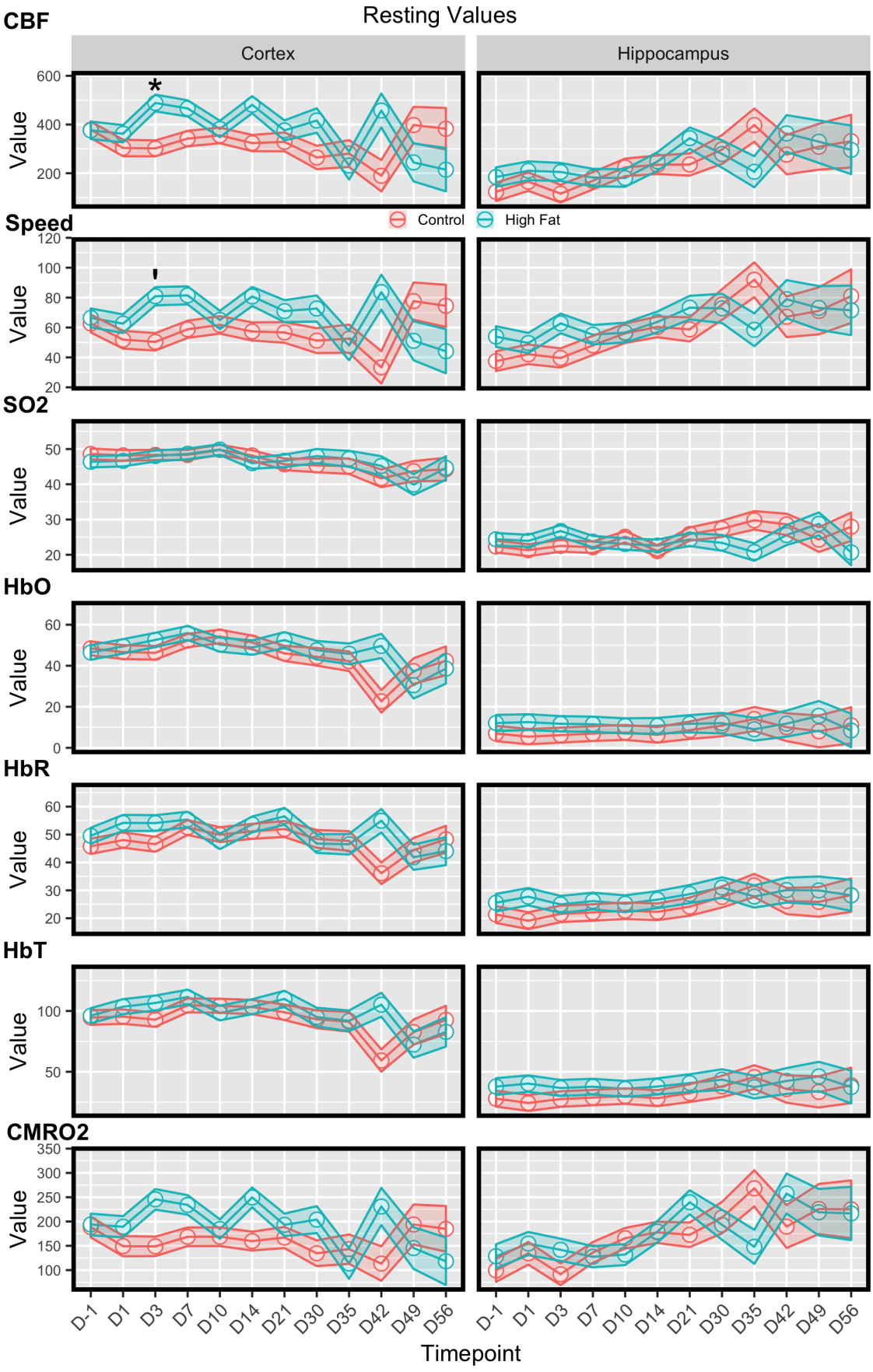

Figure A.12: Resting Values Over the Dietary Timecourse.

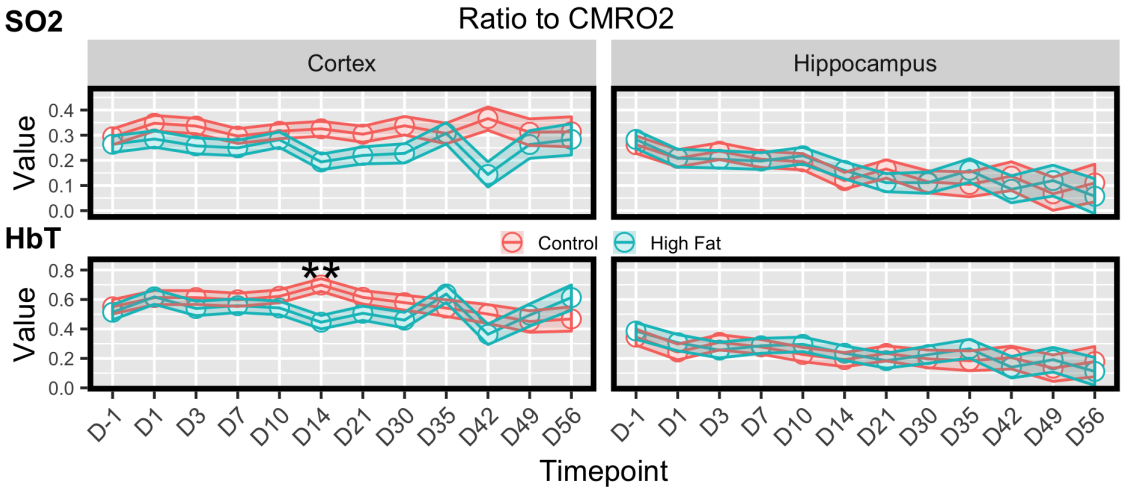

Figure A.13: Ratio of Resting Values to $CMRO_2$ Over the Dietary Timecourse.

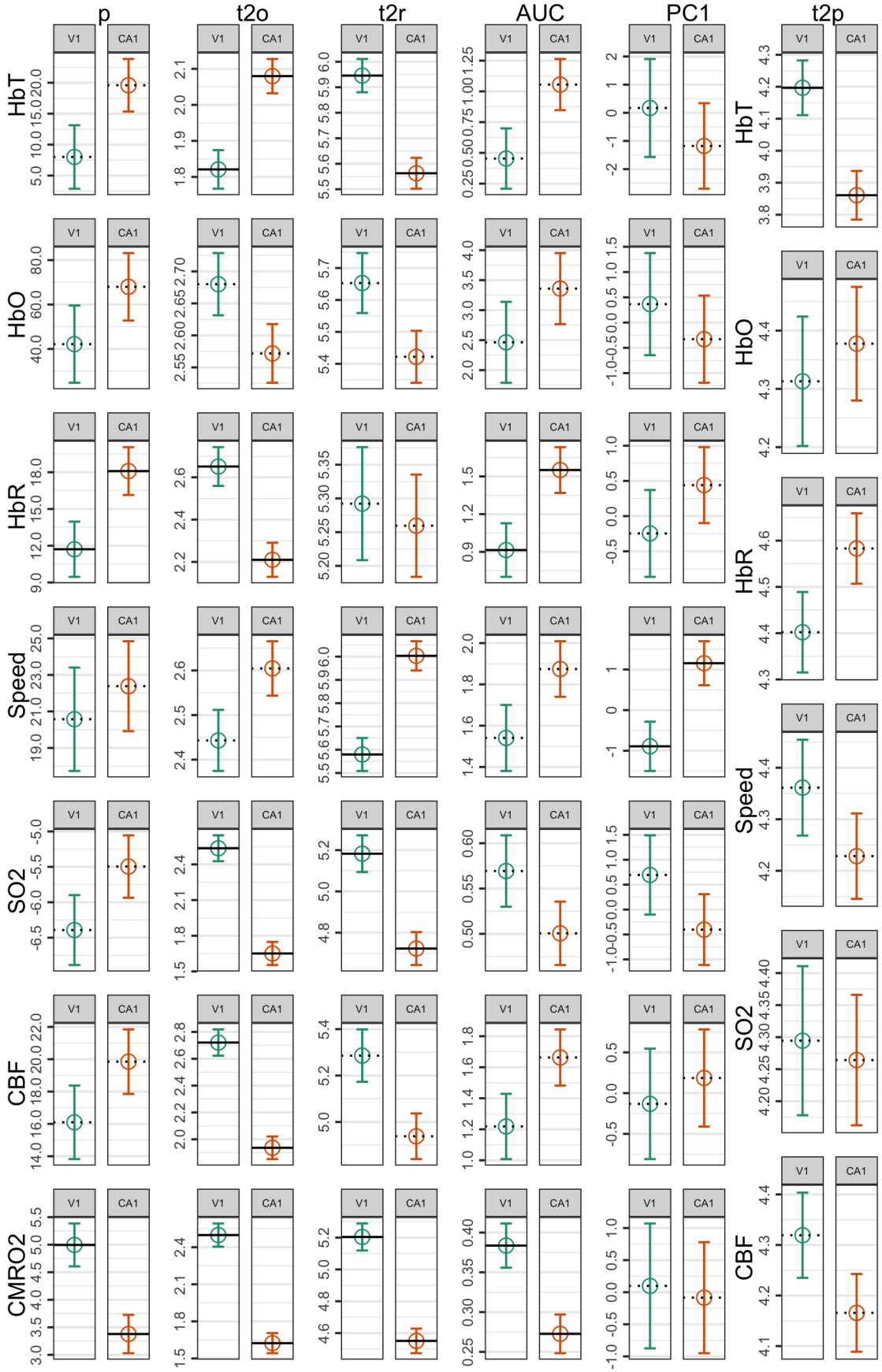

Figure A.14: Regional Differences in CPA Data.

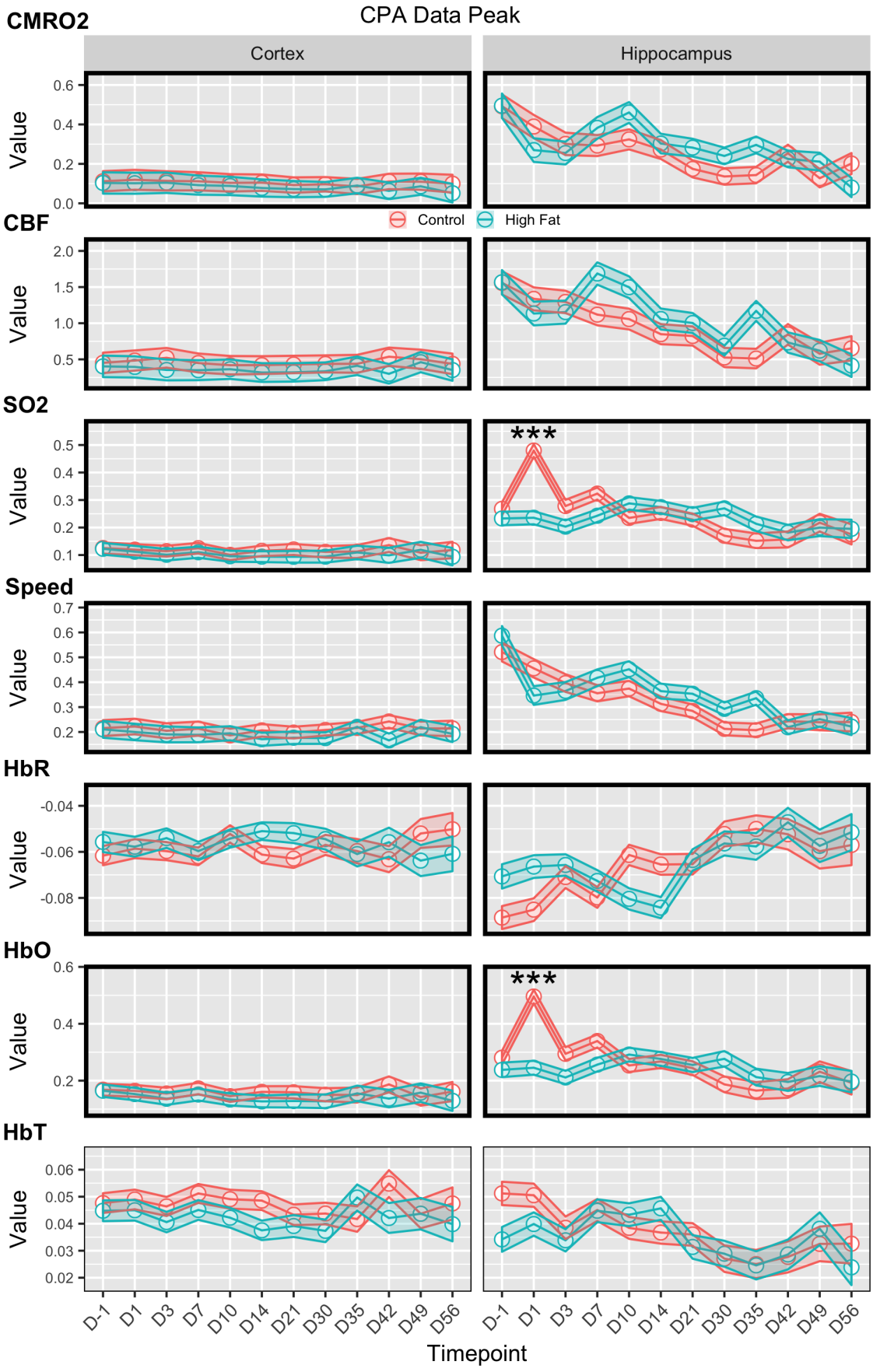

Figure A.15: CPA Peak Values.

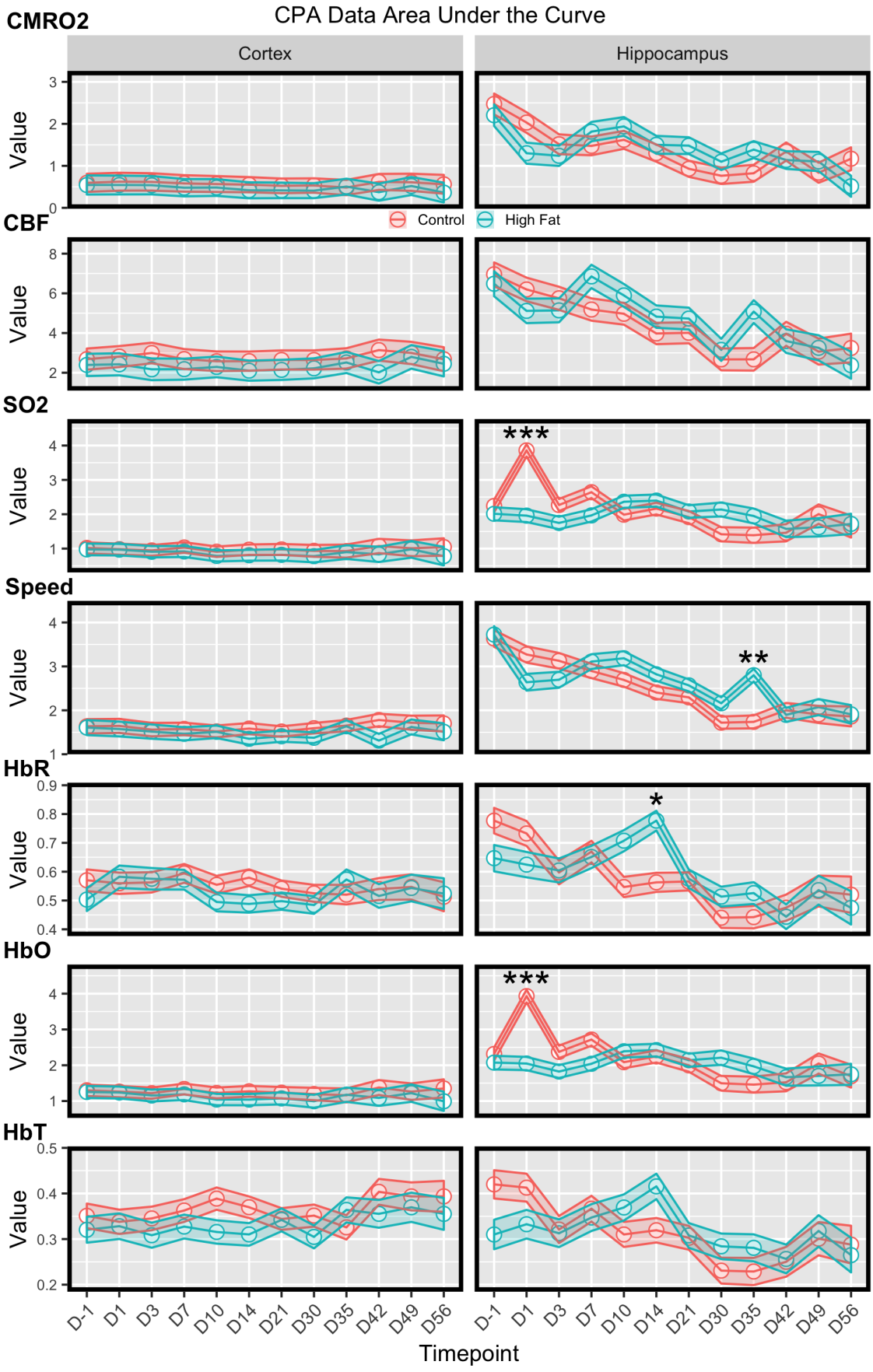

Figure A.16: CPA AUC Values.

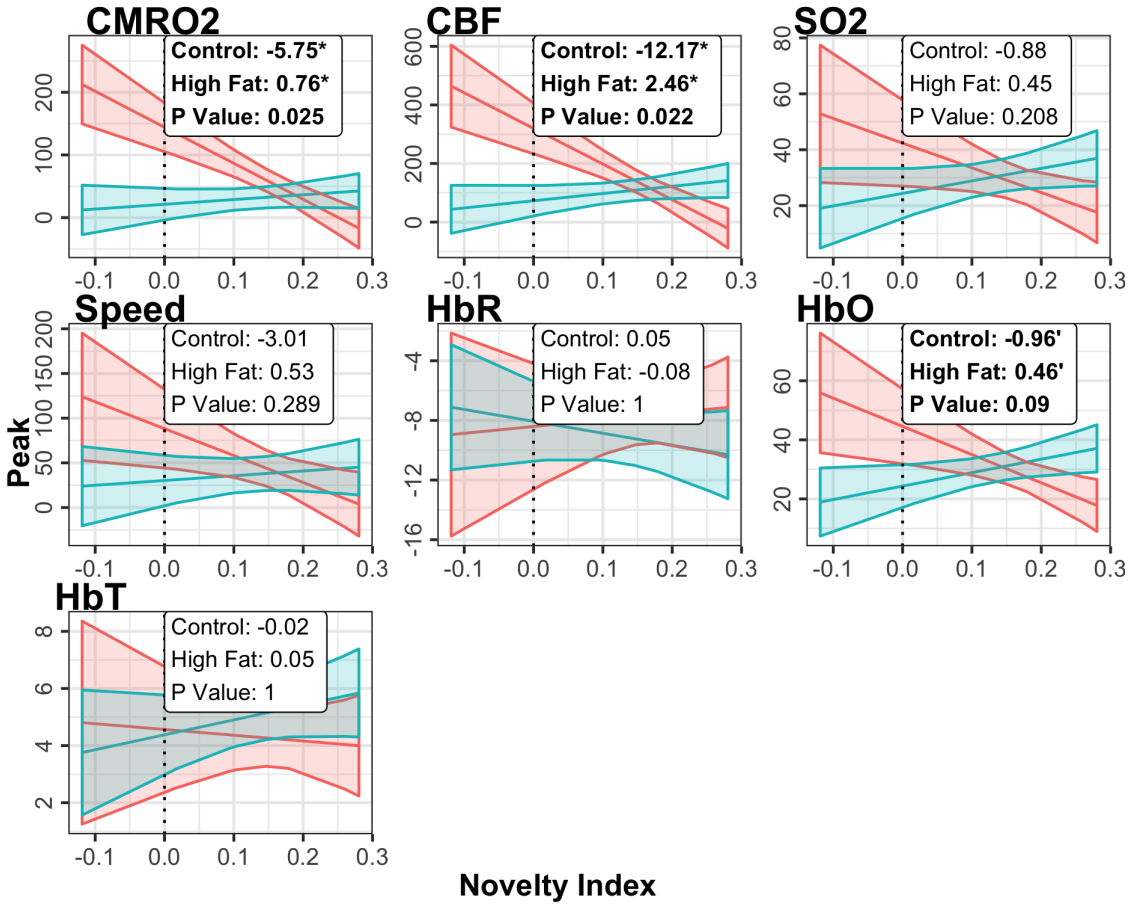

Figure A.17: Peak Value Correlations with NOCR..

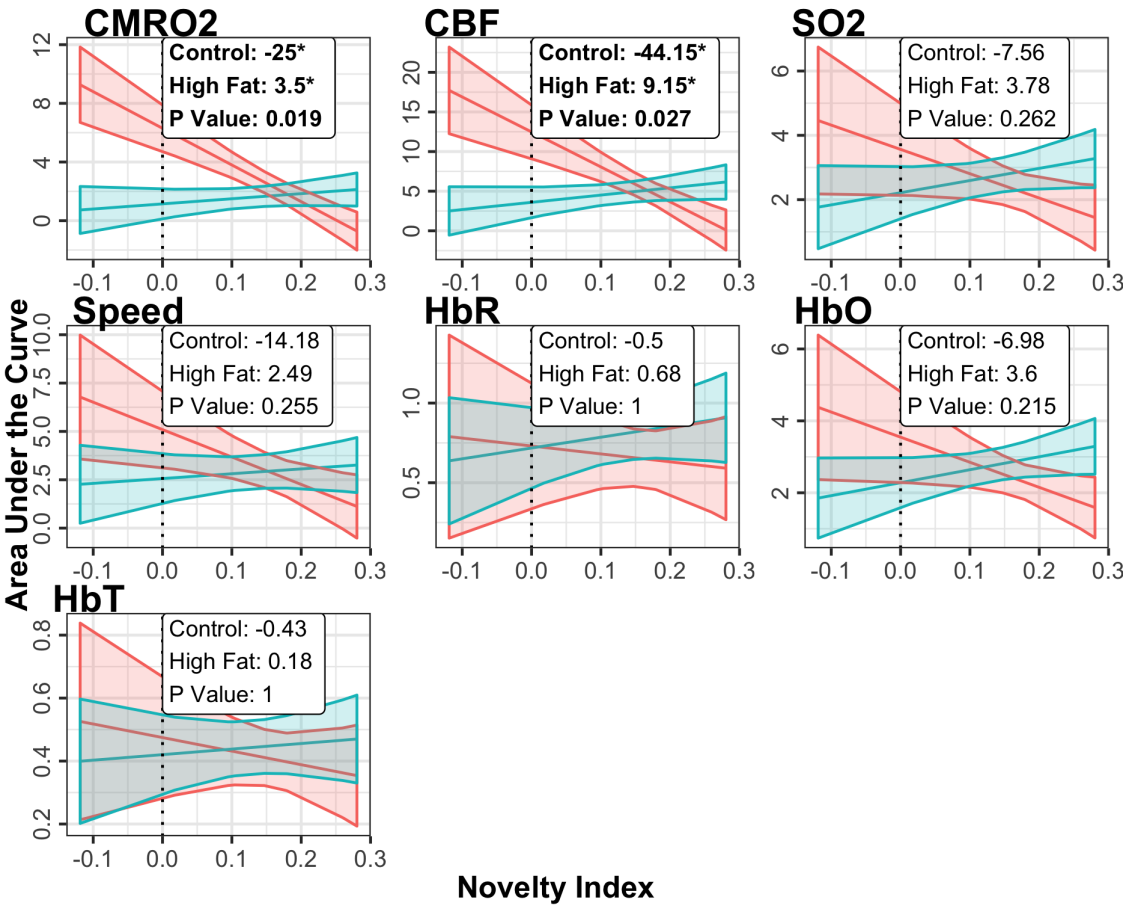

Figure A.18: AUC Value Correlations with NOCR.